MAGMATISM, METAMORPHISM, AND DEFORMATION IN THE MOUNTAIN HOME METAMORPHIC COMPLEX, BLUE MOUNTAINS PROVINCE, OREGON, AND ITS ROLE IN LATE JURASSIC DEFORMATION IN THE WESTERN NORTH AMERICAN CORDILLERA.

by

BRYAN SCOTT ANDERSON

JOSHUA J. SCHWARTZ, CHAIR
HAROLD STOWELL
KENNETH JOHNSON
DELORES ROBINSON

A THESIS

Submitted in partial fulfillment of the requirements
for the degree of Master of Science
in the Department of Geological Sciences
in the Graduate School of
The University of Alabama

TUSCALOOSA, ALABAMA

2013

ABSTRACT

Orogenesis in the Blue Mountains Province (BMP) of NE Oregon involved the accretion of various tectonostratigraphic terranes in concert with syn-tectonic magmatism. Timescales of deformation, metamorphism and magmatism in this region of the Cordillera are poorly constrained, hindering detailed understanding of the timing of tectonic events and the magmatic and metamorphic processes accompanying them.

The Mountain Home Metamorphic Complex (MHMC) is a sequence of medium-grade metavolcanic and metasedimentary rocks that borders the Wallowa and Baker terranes of the BMP. The MHMC is intruded by two groups of plutons distinguished based on their respective presence and absence of crystal-plastic deformational textures. This study utilizes U-Pb zircon dating on both crystal-plastically deformed and undeformed pluton suites to bracket the timing of metamorphism and deformation in the MHMC. The whole rock geochemistry of the MHMC was compared to the adjacent Baker and Wallowa terranes to assists in determining the relationship between these terranes and the MHMC. In addition, the petrogenesis of plutonic and metamorphic rocks in the MHMC is determined by Lu-Hf isotopic ratios of zircons.

Two distinct plutonic suites are present in the MHMC: 1) deformed hornblende (±clinopyroxene) gabbro, hornblende tonalite and trondhjemite (Group 1), and 2) undeformed biotite-hornblende tonalite, biotite-hornblende quartz diorite, and hornblende gabbronorite (Group 2). $^{206}Pb/^{238}U$ zircon ages for Group 1 plutons range from 159.46 ± 0.67 to 149.5 ± 1.6 Ma; whereas Group 2 plutons yield ages ranging from 149.4 ± 2.1 Ma to 145.66 ± 0.50 Ma. These ages bracket deformation to between 149.5 to 149.4 Ma, which contrasts with the timing

of previously documented tectonic events in the BMP.

Epsilon Hf values in the MHMC range from +16.3 to +10.2 in Group 1 plutons and +13.8 to +4.2 in Group 2 plutons. These values exclude correlation between the MHMC and the Baker terrane, but not the Wallowa terrane. On a large scale, the MHMC is metamorphosed to amphibolite facies, a significantly higher grade than any other regional scale metamorphism in the BMP.

The timing of deformation constrained in this study does not correspond with any of the previously proposed deformational models for the BMP. The geographically closest known deformational event that corresponds with the timing of deformation in the MHMC is the 150 ±1 Ma Nevadan Orogeny of the Klamath Mountains. The unique timescale of deformation and higher grade metamorphism imply that the MHMC does not belong to the Baker or Wallowa terranes, but may be a new terrane in the BMP.

LIST OF ABBREVIATIONS AND SYMBOLS

BMP	Blue Mountains Province
MHMC	Mountain Home Metamorphic Complex
NCP	North Cascades Province
LILE	Large ion lithophile element
N-MORB	Normal mid-ocean ridge basalt
LREE	Light rare earth element
HREE	Heavy rare earth element
MREE	Middle rare earth element
HFSE	High field strength element
REE	Rare earth elements
εHf_i	Epsilon hafnium initial
2σ	Two sigma
HNO_3	Nitric acid
HF	Hydrofluoric acid

N	Normality
HCl	Hydrochloric acid
GPS	Global positioning system
USGS	United States Geological Society
Pb*	Radiogenic lead
t	Time in years
e	Euler's number
λ	Radioactive decay constant
i	Initial
n	Number of samples
LA-ICPMS	Laser ablation inductively coupled mass spectrometry
TIMS	Thermal ionization mass spectrometry
SIMS	Secondary ion mass spectrometer
XRF	X-ray fluorescence
ICP-OES	Inductively coupled plasma optical emission spectroscopy
ICP-AES	Inductively coupled plasma atomic emission spectroscopy
CL	Cathodoluminescence

SEM	Scanning electron microprobe
SEI	Secondary electron imaging
SHRIMP	Sensitive high resolution ion microprobe
SHRIMP-RG	Sensitive high resolution ion microprobe-reverse geometry
CHUR	Chondritic uniform reservoir
ppm	Parts per million
Km^2	Square kilometers
My	Million years
By	Billion years
Ga	Gigaannum
Ma	Megaannum
Kbar	Kilobar
μm	Micrometer
amp	Amperes
Å	Angstrom
Km	Kilometer
Am	Amphibole

Bt	Biotite
Chl	Chlorite
Cpx	Clinopyroxene
Grt	Garnet
Ms	Muscovite
Op	Opaque mineral
Opx	Orthopyroxene
Pl	Plagioclase feldspar
Qtz	Quartz
St	Staurolite

ACKNOWLEDGEMENTS

I would first like to thank my adviser, Dr. Joshua Schwartz, for his guidance, patience, time, and assistance. Thanks and love to my wife, Jestina Hansen, for unending support, editorial assistance, logic, and her help in sharing our family commitments and lives; this could not have been done without her. A great debt goes to Mark Ferns, whose 2001 map of the area served as the basis for much of this project and whose advice helped to direct my efforts while in the field. Thanks also to Ryan Jeffcoats, who may only have signed on to be a field assistant but whose steadfast nature proved the perfect foil to my distractible personality, whose people skills built relationships with landowners, and who was invaluable in the lab. Thanks to Scott Milo and Raya Greenberger, who helped process my samples. I appreciate Dr. Joe Wooden of the USGS SHRIMP-RG lab on Stanford University for the use of his excellent lab and his early help understanding my U-Pb data. Thanks, also, to Dr. Paul Mueller for the use of his (also) excellent lab and advice. I am grateful to Ken Johnson who performed part of the whole rock geochemistry analyses for this project. I would also like to thank my other committee members, Dr. Harold Stowell and Dr. Delores Robinson, for their assistance with this project. Last, but not least I would like to thank my daughter, Kyrie, whose very existence changed this project from science for fun into a project that needed to be completed.

CONTENTS

LIST OF TABLES

LIST OF FIGURES

1. INTRODUCTION

The growth of continents has been attributed to the collision of island arc terranes onto continental margins (de Witt, 1998). The processes by which mafic to intermediate, intra-oceanic terranes such as island arcs are accreted and transformed into a more felsic continental crust is the result of intracrustal differentiation (e.g. Taylor and McLennan, 1995) and possibly the delamination of fractionated mafic roots (DeBari and Sleep, 1991, Condie and Chomiak, 1996). However, the timing for the collision and suturing of oceanic and continental terranes to each other and to the western North American continent is not well understood.

The western North American Cordillera consists of a series of island-arc and related terranes accreted onto the Laurentian margin (Figure 1). The relationship between the timing of island arc accretion, deformation and metamorphism, and the plutons that stitch them is well known in the Klamath Mountains of northern California (e.g., Snoke and Barnes, 2007). In the Klamaths, accreted terranes are cut by plutons and overlain by volcanic and sedimentary rocks. This region experienced two orogenic events in Middle and Late Jurassic time, resulting in significant regional deformation (Hacker *et al.*, 1995; Wright and Fahan, 1988). The first event is known as the Middle Jurassic Siskiyou orogeny at ~169-161 Ma (Coleman *et al*., 1988; Barnes *et al.*, 2006; Snoke and Barnes, 2006). This event involved regional greenschist-facies metamorphism with local amphibolite-facies metamorphism, usually located near intrusive units (Wright and Fahan, 1988). The second deformational event is known as the Nevadan orogeny and it occurred around

150 ± 1 Ma (Harper and Wright, 1984; Chamberlain *et al.*, 2006). It occurred predominantly in the Northern Sierra Nevadas and reached amphibolite facies metamorphism (Hacker *et al.*, 1995; Schwartz *et al*., 2011a). However, due to burial underneath Tertiary volcanic rocks, sedimentary rocks, and basalts, the northern extent of the deformational events associated with the Klamath Mountains is unclear as are the location and nature of the boundary between the accreted terranes of the Klamaths and those of the Blue Mountain province to the north.

The Blue Mountains Province (BMP) of northeastern Oregon (Figure 1) is a series of deformed island-arc and related sedimentary terranes, which were amalgamated to each other in late Middle Jurassic to Late Jurassic time (159-154 Ma: Schwartz *et al.*, 2010; Schwartz *et al.*, 2011a) and accreted onto the North American craton in an arc-continent collision event between 141 and 124 Ma (Getty *et al.*,1993; Selverstone *et al.*, 1992; McKay *et al.*, in review). Like the Klamath Mountains of northern California and southern Oregon, the BMP shows evidence of regional deformation and metamorphism.

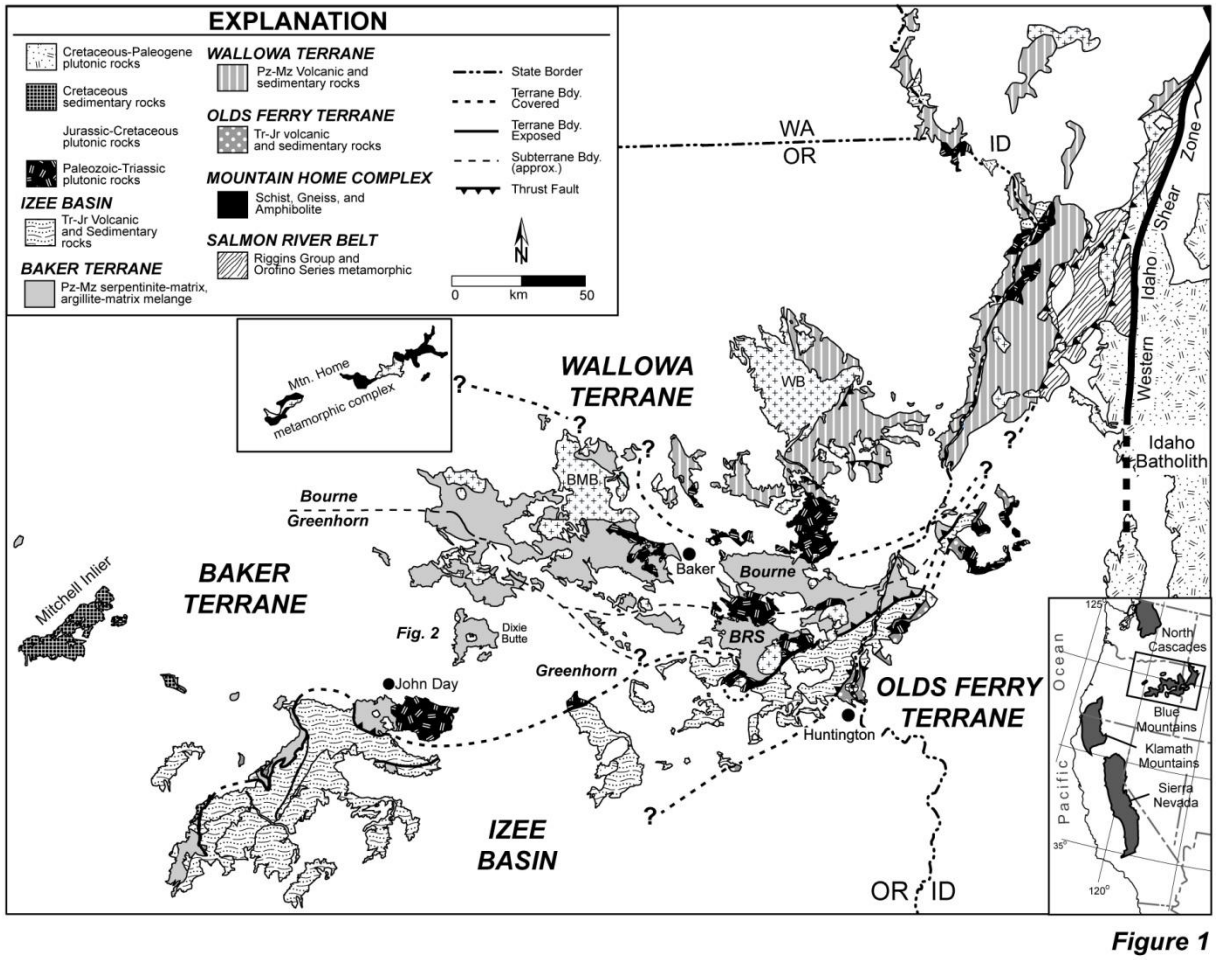

Figure 1

Figure 1. The terranes of the Blue Mountains Province, with the Mountain Home Metamorphic Complex indicated by the black box in the upper left (after Lamaskin *et al.*, 2009). The lower right box shows the Northwestern Cordillera, with the Blue Mountains Province delineated in the inset and magnified as the main figure.

The Mountain Home Metamorphic Complex (MHMC), located on the northwestern edge of the BMP, exhibits evidence of regional deformation as well as pre- to syn-deformational garnet growth in metamorphic units. The MHMC also contains zircon bearing plutonic units that locally crosscut deformational fabrics. The MHMC consists of two suites of plutons (one older and deformed, the other younger and undeformed), which intrude into schistose metamorphic rocks. The younger, undeformed suite of plutons is also referred to as the Carney Butte Stock (Ferns *et al.*, 2001). Both metamorphic rocks and plutons are surrounded and partially overlain by Miocene Columbia River basalts and Tertiary volcanic rocks. Avé Lallemant's (1995) structural work suggests that the deformation in the Wallowa terrane (in which Avé Lallemant includes the MHMC area) is the result of Late Jurassic deformation, based on crosscutting by post-tectonic plutonic intrusive rocks at143 Ma, but the timing of deformation in the MHMC remains unconfirmed by modern geochronological methods.

This study combines new U-Pb geochronologic and Lu-Hf isotopic analysis of zircon with both new and existant field mapping of largely intrusive rocks in the MHMC to constrain and relate its deformational and metamorphic history to that of the BMP. This study's findings are supported using whole rock major and trace element analyses.

1a. Late Jurassic tectonism in the North American Cordillera

From the Permian through Cretaceous periods, the terranes of the North American Cordillera were a series of offshore island arc chains (Dickinson, 2004).These island arcs extended from what is now Baja California to Alaska. The Cordilleran provinces most likely to have been associated with the arcs that would later become the BMP are the modern day Klamath Mountains and the North Cascades Province (NCP) due to their geographic proximity.

1b. Terranes and magmatism in the BMP

The Blue Mountains Province is subdivided into the Wallowa and Olds Ferry terranes (island arcs), the Izee terrane (sedimentary and volcaniclastic rocks), and the Baker terrane, which consists of two subterranes, the Bourne and the Greenhorn (mélange and other accretionary features) (Schwartz *et al.*, 2010; Ferns and Brooks, 1995; Schwartz *et al.*, 2011a) (Figure 1). The Wallowa, Olds Ferry, and associated terranes amalgamated into one large, deformed block, during the Late Jurassic (Schwartz *et al.*, 2011a) before accreting onto the North American craton beginning in the Early Cretaceous, from ~141-124 Ma (Getty *et al.*, 1993; McKay *et al.*, in review).

Three episodes of Middle Jurassic to Early Cretaceous magmatism are recognized in the BMP: 162-154 Ma, 148 to 141 Ma, and 125-111 Ma (Schwartz *et al.*, 2011a). The first episode (162 to 154 Ma) resulted in plutons emplaced into the Wallowa terrane and Greenhorn subterrane, ranging in composition from gabbro to quartz diorite (Unruh *et al.*, 2008; Schwartz *et al.*, 2011b). The second magmatic event (148 to 141 Ma) resulted in relatively aluminous and sodic tonalite-trondhjemite-granodioritic plutons emplaced across the Baker and Wallowa terranes. The final pulse of magmatism in the BMP consisted of two distinct belts that span the Wallowa, Baker, and Izee-Olds Ferry terranes; one belt is a series of metaluminous hornblende-biotite tonalites emplaced between 124 and 120 Ma, and the other is a series of peraluminous tonalites and trondhjemites emplaced between 125 and 111 Ma (Johnson and Schwartz, 2009; Schwartz *et al.*, 2011a). The BMP block was rotated ~ 60° clockwise during the post-Cretaceous period (Wilson and Cox, 1980). It has been postulated that the rotation of the BMP could have

accompanied back arc rifting in the Early Cretaceous or may reflect regional dextral shearing in the BMP area in the Late Cretaceous (Wilson and Cox, 1980).

i. *The Wallowa Terrane*

The Wallowa terrane occupies the northernmost portion of the BMP. Volcanic and sedimentary rocks in the Wallowa terrane vary in age from Permian to Early Jurassic (LaMaskin *et al.,* 2009). The terrane includes volcaniclastic and volcanic rocks (ranging primarily from Early Permian to Late Triassic), sedimentary rocks (Triassic and Jurassic in age), and plutonic rocks (Jurassic to Early Cretaceous) (Avé Lallemant, 1995; Vallier, 1995). Two main pulses of magmatism occurred in the Wallowa terrane: silicic arc magmatism occurred from ~265.4-248.8 Ma, followed by deformation and erosion of the Wallowa arc, and finally by ~229.4-229.1 mafic to intermediate magmatism (Kurz *et al.*, 2012), based on U-Pb zircon dating of the Cougar Creek Complex. Some sporadic volcanism continued until the end of the Middle Jurassic (161 Ma) (Avé Lallemant, 1995 after Vallier *et al.*, 1977; Follo, 1994; White and Vallier, 1994). The Wallowa terrane was regionally metamorphosed to greenschist facies conditions but does reach amphibolite-facies conditions in some localities, such as the Cougar Creek Complex (Vallier, 1995).

The plutonic units of the Wallowa terrane show compositional diversity. The terrane is exposed primarily in two places: along the Snake River in the Hells Canyon region, and in the Wallowa Mountains (Figure 1). The Snake River roughly parallels the boundary between the BMP and the Laurentian craton. Plutons intrude the area and the adjacent Wallowa terrane and include the Round Valley, Wolf Creek/Deep Creek, Cougar Creek, Sheep Creek, and Oxbow complexes.

The interior of the Wallowa Mountains is dominated by the Wallowa Batholith, a series of biotite and hornblende bearing plutons ranging from tonalite to granodiorite (Petcovic and Grunder, 2003). $^{206}Pb/^{238}U$ (SHRIMP-RG) ages were determined to range from 140.2 ± 1.4 Ma to 122.9 ± 1.7 Ma, with the units emplaced after 125.6 Ma having Sr/Y > 40, La/Yb > 17, and LREE enrichment relative to HREEs (Johnson *et al.*, 2011).

The southern end of the Wallowa Mountains is composed of the Sparta Complex. The southernmost igneous units of the terrane, primarily the Sparta Complex, include both mafic to ultramafic rocks (older than 215 Ma, ^{206}Pb-^{238}U of zircon, Walker, 1995) and high SiO_2 trondhjemites (253+/-1Ma, ^{206}Pb-^{238}U of zircon, Walker, 1995) whereas the aforementioned complexes (Round Valley, Wolf Creek/Deep Creek, etc.) paralleling the eastern edge of the BMP range in composition from gabbroic to trondhjemitic. Also present along the edge of the BMP are various mylonites and shear zones often associated with up to amphibolite grade metamorphism. This later stage of deformation may have resulted from docking of the BMP onto the continental craton (Avé Lallemant, 1995).

The smaller Cornucopia Stock is located to the south of the Wallowa batholith and is made up of a biotite trondhjemite, three two-mica and magmatic cordierite bearing trondhjemites, and a hornblende and biotite bearing tonalite. Johnson *et al.* (1997) established the cooling age of the stock as 116.8 ± 1.2 Ma ($^{40}Ar/^{39}Ar$ step heating of biotite). They further constrained the geochemistry of the Cornucopia Stock to also have (La/Yb) between 7.6 and 11.8 with LREE enrichment and HREE depletion. The Fish Lake Complex has not been studied to the extent of its nearby plutons, but Johnson *et al.* (2012) establish its emplacement age at 157.5 ± 1.3 Ma. This complex is composed of a series of small two-pyroxene gabbroic bodies (± relict

olivine) characterized by cumulate geochemical signatures. Schwartz (personal communication) found that the εHf_i values of zircons from various plutons in the Wallowa terrane range from +14 to +9 (2σ weighted averages).

ii. *The Olds Ferry Terrane*

The Olds Ferry terrane is an accreted island arc that is lithologically similar to the Wallowa terrane, but chronologically distinct. The Olds Ferry island arc contains volcanic rocks of Late Triassic to Early Jurassic age (Tumpane, 2010) and plutonic rocks of mostly Middle Triassic to Late Triassic age (Iron Mountain and Brownlee pluton). Unlike the Wallowa terrane, the Olds Ferry terrane is poorly exposed with a less well defined age. The Huntington and Weatherby Formations are considered by some to be part of the Olds Ferry terrane (Dorsey and LaMaskin, 2007). These formations are composed of clastic sedimentary rock, limestone, and keratophyre rocks, generally defined as a felsic tuff or flow characterized by phenocrysts of quartz and albite as well as a high Na to K ratio. Albitized volcanic rocks are best recognized by the preservation of volcanic textures such as groundmass and post-emplacement growth rims. These keratophyre rocks are in basins up to 7 km thick, which overlay the plutonic rocks of the arc. Regional metamorphism of the Olds Ferry terrane did not exceed greenschist facies conditions (Tumpane, 2010; Brooks and Vallier, 1978).

iii. *The Izee Terrane*

The Izee terrane is a Triassic to Jurassic sedimentary sequence that primarily outcrops in the southern region of the BMP. It is mainly composed of clastic sedimentary rocks, although some correlate with the limestone and volcanic rocks of the Huntington and Weatherby

Formations (Dickinson, 1979; Avé Lallemant, 1995). Dorsey and LaMaskin (2007) cast doubt on the definition of the Izee as a separate terrane by correlating its Jurassic age sediments with other sediments such as the Coon Hollow Formation of the Wallowa terrane (LaMaskin *et al*., 2011) across the BMP. They speculate that the Izee is not a terrane but may be a regional overlap assemblage of largely Jurassic sedimentary rocks which unconformably overlies the Baker and Olds Ferry terranes of the BMP. The area known as the Izee terrane may be an unusually thick (~12 to 15 km) overlap basin of the Olds Ferry arc (Schwartz *et al*., 2011a). Late Jurassic deformation in the Izee terrane is manifested in brittle to semi-brittle deformation zones along the terrane boundary with the Baker and Olds Ferry terranes (Schwartz *et al.,* 2011a). The Izee terrane is metamorphosed in only a few locations, and not higher than greenschist facies (Dorsey and LaMaskin, 2007).

iv**.** *The Baker Terrane*

The Baker terrane is an accretionary complex located between the Wallowa and Olds Ferry terranes. It is composed of three subterranes: the Bourne, the Greenhorn, and the Burnt River Schist. The Bourne subterrane is dominated by the Permian to Early Jurassic Elkhorn Ridge Argillite, which consists primarily of disrupted chert and argillite with lesser amounts of tuffaceous argillite, limestone and conglomerate (Schwartz *et al.*, 2010; Schwartz *et al.,* 2011b). The Greenhorn subterrane is a serpentinite-matrix mélange containing large blocks of chert-argillite breccias, volcaniclastic breccias, keratophyre, meta-plutonic rocks, and some amphibolitic rocks (Schwartz *et al.,* 2011b). Whereas the Bourne subterrane is uniformly lower greenschist facies in metamorphism, the Greenhorn subterrane ranges from upper greenschist-facies to lower amphibolite-facies (Schwartz *et al.,* 2010).

The Burnt River Schist was only recently determined to be its own subterrane (Schwartz *et al.,* 2010), and recent work has established it to be isotopically distinct (Mailloux *et al.,* 2009). It is a heterogeneous subterrane dominated by siliceous phyllite and slatey argillite. It also contains marble, metaplutonic rocks (ranging from felsic to mafic), and keratophyre rocks. Metamorphism in the Burnt River Schist is greenschist facies, but a higher greenschist facies than the Greenhorn subterrane, and near plutons, contact metamorphism reaches hornblende to hornblende-pyroxene hornfels facies (Ashley, 1995).

Igneous rocks in the Baker terrane include the Bald Mountain Batholith and the Dixie Butte meta-andesite complex, which intrude the Bourne and Greenhorn subterranes, respectively. The oldest units in the Dixie Butte complex consist of volcanic and volcaniclastic rocks as well as tuffaceous sediments. Intruded into these rocks and sediments are deformed gabbroic to trondhjemitic plutons (162 to 157 Ma, metamorphosed to greenschist facies). Two pulses of magmatism are present: a suite of 148-145 Ma post-kinematic tonalitic to dacitic plutons intrude 162-157 Ma lavas and plutons (Schwartz *et al.*, 2011b). The pre-deformational plutons have εHf_i values ranging from +10.1 to +12.3 (2σ weighted average). The post-deformational plutons have εHf_i values ranging from +10.5 to +7.8 (2σ weighted average, Schwartz *et al.,* 2011b). Geochemical analyses show the Middle Jurassic (162-157 Ma) plutons in the Dixie Butte complex to have flat to slightly enriched light rare earth element (REE) abundances, low Sr (<400) and low Sr/Y values (<40). The Late Jurassic (148-145 Ma) plutons show depleted heavy REE abundances with steep LREE profiles, high Sr (>600 ppm) and high Sr/Y values (>40), with one exception being distinguished by its lower Sr/Y (Schwartz *et al*., 2011b). The Middle Jurassic rock types are gabbro, hornblende ± biotite diorite, and biotite-hornblende trondhjemite. There are four Late Jurassic plutons defined: three undeformed biotite-hornblende tonalities and

one porphyritic biotite-hornblende dacite (Schwartz *et al.*, 2011b). The emplacement ages of the two magmatic pulses combined with the degree of deformation define a greenschist facies metamorphic and deformational period lasting from 159 to 154 Ma (Schwartz *et al.*, 2011b).

1c. Existing tectonic models

There are several proposed models for deformation in the BMP, each one delineated from the others by the timing of deformation and metamorphism. One model, put forth by Getty *et al.* (1993) and Snee *et al.* (1995), defines the deformation and metamorphism of the eastern BMP as resulting from contractional deformation in the Salmon River Suture Zone at 128 Ma. Another model is that the metamorphism is related to the amalgamation of the BMP via arc-arc collision between the Wallowa and Olds Ferry island arc terranes (Avé Lallemant, 1995 and Schwartz *et al.*,2011b) from 159 – 154 Ma. The third possible model is that the deformation is related to the emergence of a doubly vergent thrust belt in the Bourne subterrane of the Baker terrane and associated basin formation in Late Triassic time as a result of the incipient collision of the Wallowa and Olds Ferry island arcs (Dorsey and LaMaskin, 2007). Finally, Kurz *et al*. (2012) and Avé Lallemant (1995) propose that a sinistral deformational event occurred in the Middle Triassic. Each of these models includes a specific time of deformation for the BMP region. Deformation styles in these models also vary, with the first three models involving orthogonal east-west deformation restoring ~60° of post-contractional clockwise rotation (Wilson and Cox, 1980), and the last model involving north-south sinistral deformation. This study brackets the timing of metamorphism and deformation style in the MHMC to help establish which model, if any, is applicable to the BMP area.

1d. Previous works on the MHMC

Zen (1985) observed magmatic epidote in a sample taken from a pluton near Heppner, OR and from this determined the paleopressure of intrusion to be above 8 kbar. The epidote that was analyzed is likely from the small outlier to the southwest of the MHMC, as that outlier is the only magmatic epidote bearing plutonic complex known to be in the area. Bishop (1995a) also studied paleopressure in the metasediments of the MHMC's southwestern outlier. Whereas she identified them as the schistose rocks of Rhea Creek, Bishop also linked them with the southwesternmost outcrops of the metasedimentary rocks of the MHMC proper. She used compositional variations in amphiboles (mainly Na/K/Ca) to estimate the paleopressure and paleotemperature (using tetrahedral Al). Bishop (1995a) found that the southwestern outlier's metasedimentary rocks, similar to the biotite-garnet bearing Schist of Yellow Jacket Road of the MHMC, had metamorphic growth pressures between 3 and 4 kbars, as well as blue grunerite in the graphite bearing metasedimentary rocks.

i. *Trauba (1975)*

Trauba (1975) recognized the presence of two suites of plutons temporally separated by a regional metamorphic event. He established the easternmost rocks as possessing a metamorphic assemblage dominated by albite, chlorite, epidote, quartz, and biotite. Trauba identified a metamorphic assemblage ranging from quartz, biotite, muscovite, sodic feldspar, and garnet (400 m from any intrusive) to quartz, biotite, plagioclase, muscovite, sillimantite, staurolite, and garnet in the pelitic schist of the central region. Trauba (1975) mainly used petrography and limited geochemical analysis, structural analysis, and field mapping to determine the mineralogy, units, and microtectonic history of the MHMC.

ii. *Ferns et al. (2001)*

Ferns *et al.* (2001) was the first to include the Tonalite of Granite Meadows in the post-deformation suite of plutons. Ferns *et al.* (2001) found that the Tonalite of Granite Meadows was mainly composed of plagioclase with minor biotite, quartz, and orthoclase as well as apatite, iron oxide, and rutile as accessory phases.

iii. *Avé Lallemant (1995)*

Avé Lallemant (1995) incorporated the MHMC into the Wallowa terrane based on broad structural similarities. He defined four major deformational events across the BMP (D_1 through D_4). The D_1 deformational event is found in the Baker terrane but not the MHMC. D_2 is a major deformational event in the Wallowa terrane (where fold axial planes and axial–plane cleavages strike NE-SW) and in the MHMC (where fold axes and mineral lineations are N-S trending). D_3 is a lesser event in the Wallowa characterized by steep axial planes which strike NE-SW to N-S, nearly perpendicular to D_2 . D_4 is an event with E-W trending fold axes; there is only minor evidence of this event in the SW-most corner of the MHMC.

Avé Lallemant (1995) established that in areas that experienced the D_2 deformation event in the MHMC, the fold axes and lineations (largely amphibole lineations) trend generally north-south, and the fold axial planes approach (class-2) similar fold geometry. Avé Lallemant (1995) supported this conclusion with microscopic analysis of the axial orientations of constituent minerals as well as asymmetrical pressure shadows, grain deformation, rotated minerals in pressure shadows, and the rotation of porphyroblasts. This D_2 event is estimated to have occurred between 161 and 143 Ma, based on dating of the folded sedimentary units and

post-tectonic plutonic rocks that cut the deformational structures in the Bald Mountain batholith (Walker, 1989). Unfortunately, none of the locations Avé Lallemant's (1995) age constraints are based on are within 100 to 150 km of any part of the MHMC.

Avé Lallemant's (1995) D_3 deformational event did not involve a large amount of strain and resulted in parallel (class 1-b) folding with steep axial plains oriented almost perpendicular to those of D_2. The D_3 event occurred after (and may simply be a later stage in) D_2 deformation. D_4 type deformation was insignificant and found only in subhorizontal kink folds with east-west trending fold axis located in the southwest corner of the MHMC. Avé Lallemant's (1995) data indicate that major principal compressive strain axes of samples within the MHMC were fairly consistent with each other, but contrasted with those of the rest of the Wallowa.

The study concluded that D_2 deformation in the Wallowa and MHMC was the result of the collision between the Wallowa-MHMC and the amalgamated Baker-Izee-Olds Ferry terranes, although only limited evidence of D_2 deformation in the Baker terrane was found (primarily in the Burnt River Canyon and along the contact between the Baker and Izee terranes). In Avé Lallemant's (1995) analysis of the six sites from the MHMC, the analyses from the greenschist facies area have a nearly horizontal (north by northeast trending) orientation for their major principle compressive strain axes, whereas the amphibolite facies analysis areas are differentiated by having major principle compressive strain axes with much greater dips. These orientations agree with Trauba's (1975) more geographically comprehensive structural dataset.

iv. *Vallier (1995)*

Vallier (1995) performed whole rock major element geochemistry analysis and trace element geochemistry (with partial REE suites) analysis on several samples from the MHMC, including the Trondhjemite of Pearson Creek, the Amphibolite Gneiss, the Norite of Carney Butte, and two samples from the outlier to the southwest of the MHMC (one gabbro and the other granodiorite). The Amphibolite Gneiss has a very low LREE content with a La_n/Lu_n ratio which implies a tholeiitic protolith. The Trondhjemite of Pearson Creek had a Na_2O content of 4.19, a K_2O content of 0.12, and a FeO_{tot}/MgO vs Ce_n/Yb_n and REE pattern that follow a tholeiitic trend. The Norite of Carney Butte was found to be strongly depleted in HFSE and total REE. The gabbroic sample from the outlier to the southwest of the MHMC was also found to be noritic and geochemically similar (in major element, trace element, and REE) to the Norite of Carney Butte. The other unit analyzed from the MHMC's southwestern outlier was a granodiorite which bears a geochemical similarity (primarily in trace element and REE composition as well as in K_2O content) to the Tonalite of Granite Meadows.

Vallier (1995) performed strontium isotope analysis on samples located in the Trondhjemite of Pearson Creek, the Amphibolite Gneiss, and the Norite of Carney Butte ($^{87}Sr/^{86}Sr$ of 0.70418, 0.70367, and 0.70406, respectively). These isotopic ratios indicate derivation from a depleted mantle source, supporting an intraoceanic island arc origin.

1e. Objectives and tools

In this study, U-Pb zircon dating is used on both deformed and undeformed pluton suites to bracket the timing of metamorphism and deformation in the MHMC. Whole rock

geochemistry is used to categorize the units and better understand the chemical and potentially pressure conditions under which these rocks formed and developed. The geochemical signatures of the MHMC are compared to the adjacent Baker and Wallowa terranes to assist in determining the relationship between the MHMC and the two other terranes. Lutetium-Hafnium isotopic analysis of zircons are used to understand the petrogenesis of the plutonic and metamorphic rocks in the MHMC. Once the timescales of deformation, plutonism, and metamorphism and its degree in the MHMC are established, the MHMC's relationship with the Wallowa and Baker terranes can be determined, and the geologic history of the MHMC can be related to orogenic events in the western North American Cordillera.

2. METHODS

2a. Field methods

Rock orientations were measured on foliations along with trend and plunge of lineations. Seldom exposed lithologic contacts were marked with a GPS location. All sample locations were located with a GPS. Units were observed in hand sample with a 10x magnifying lens and compositional, deformational, and textural relationships were recorded.

Geochronological samples were first crushed in a Bico jaw crusher, and then more finely ground in a Bico disk mill. This coarse powder was then density separated on a Gemini water table. The densest separate was run through the water table again. The densest resulting portion was then separated with a 250 μm sieve. A hand magnet was used to remove most iron filings. The sample was then run through a Franz electromagnetic separator set to tilt 10° forward and 10° downhill to the side. Separates were collected at 0.1 amp, 0.5 amp, 1.0 amp, 1.5 amp. All sample fractions were retained. Samples were then density separated in methylene iodide (S.G. 3.3) and cleaned with acetone. The denser portion was then handpicked for zircons, which were subsequently mounted in epoxy. The grain mount was polished halfway through the zircons and sputter coated in carbon so that the zircons could be imaged with a scanning electron microscope (SEM), both with Secondary Electron Imaging (SEI), and Cathodoluminescence, at the Stanford University-USGS SHRIMP-RG facility.

2b. U-Th-Pb geochronology in zircons

The U-Th-Pb isotopic system is in fact three isotopic systems. Thorium is a 4+ valence REE with an ionic radius of 0.94 Ångstroms (Å). It is most common as a trace element, although it does concentrate in monazite, zircon, and to a lesser extent apatite and sphene. It is not particularly mobile under most conditions. Uranium, on the other hand, has two common valence states: 4+ and 6+. The 4+ cation has an ionic radius of 0.89Å and that of the 6+ cation is 0.73Å or 0.86 Å (for its 6-fold and 8-fold coordination, respectively). The radius of U^{4+} in 8-fold coordination is 1.00 Å; The radius of Th^{4+} in 8-fold radius is 1.05 Å. The U^{6+} ion is commonly known as the uranyl ion and occurs as a result of oxidation of the 4+ ion. The 6+ ion is soluble and hence is quite mobile at the earth's surface.

The U-Th-Pb systems primary advantage over other systems is that all three parents decay to different isotopes of the same daughter element, Pb. The parent isotopes involved are ^{238}U, ^{235}U, and ^{232}Th. All three decay via both alpha and beta decay, releasing several alpha particles in the process. ^{232}Th decays to ^{208}Pb with a decay constant of $4.948 \times 10^{-11} y^{-1}$, ^{238}U decays to ^{206}Pb with a decay constant of $1.551 \times 10^{-10} y^{-1}$, and ^{235}U decays to ^{207}Pb with a decay constant of $9.849 \times 10^{-10} y^{-1}$. All three daughter products are measured with respect to ^{204}Pb, which is non-radiogenic. Because the relative abundances of ^{235}U and ^{238}U are a constant 1/137.88 ratio, the standard decay equations for ^{235}U to ^{207}Pb and ^{238}U to ^{206}Pb can be combined into one equation with only one unknown (time) directly dependant on the ratio of $^{207}Pb^*/^{206}Pb^*$.

$$\frac{207Pb^*}{206Pb^*} = \frac{1 * \left(e^{\lambda_{235U}t} - 1\right)}{137.88 * (e^{\lambda_{238U}t} - 1)}$$

This is known as the Pb-Pb system, and the system enables measurement of the age without knowing the amount of either parent. Because both parents are different isotopes of the same element, the parent isotopes will behave the same chemically, further increasing the robustness of this system. Thorium does not necessarily behave similarly to either isotope of uranium, somewhat limiting its usefulness unless high Th minerals are being studied exclusively. The ability to determine the age of a mineral without the use of the parent elements is particularly useful if there is reason to suspect the parent may have been removed from the system, but the daughter has not, allowing a geochronologic date that 'sees through' open system behavior. This is especially useful when oxidizing conditions drastically increase the solubility of uranium and it becomes mobilized.

Zircon is a particularly good mineral for study in the U-Th-Pb system. It is very resistant to metamorphism and chemical weathering, preferentially concentrates U and Th while excluding Pb. It also has a hardness of 7.5 on Moh's scale, making zircon one of the most resilient minerals to form in a magma and certainly the most common resistant mineral. The preferential exclusion of the non-radiogenic daughter and inclusion of the parent isotopes results in an excellent geochronometer.

The Concordia diagram takes advantage of the very high parent to non-radiogenic daughter ratios. Due to the constant ratio of ^{238}U / ^{235}U (137.88:1), ^{238}U is the predominant radiogenic isotope, but because ^{235}U is also present, they can both be used to produce a graphical representation of the agreement between the two decay systems at any point in earth's history; this is the Concordia line.

The Concordia line is a curve because the ratio of ^{238}U to ^{235}U has changed throughout time as the shorter half life of ^{235}U compared to ^{238}U (704 Ma and 4.46 Ga, respectively) results in an more rapidly decreasing supply of ^{235}U on earth and the approaching 'death' of this geochronologic system. The Concordia diagram uses both the parent and daughter isotopes and a well chosen specimen can be treated as a closed system. The use of the SHRIMP (Sensitive High Resolution Ion Micro-Probe) to study only very small portions of a single specimen refines this closed system even more. If a sample has not behaved as a closed system, (i.e. Pb or U has been added or lost) then the sample would begin to move along a cord off the Concordia curve, removing it from the line itself and making its open system behavior readily apparent. Pb loss is the most likely outcome of open system behavior in zircons due to the preferential exclusion of Pb from the zircon.

U-Pb ages can be determined using either TIMS (Thermal Ionization Mass Spectrometry), LA-ICPMS (Laser Ablation Inductively Coupled Mass Spectrometry), or the SHRIMP. The TIMS has a much higher signal intensity and precision of measurement. However, it requires dissolution of the sample and hence the destruction of the sample and any spatial information such as multiple growth periods (zonation). The SHRIMP uses less sample material and produces lower signal intensity, but it is possible to identify regions of multiple growth phases in zircon and sample only discreet portions of the specimen.

The SHRIMP is a unique type of Secondary Ion Mass Spectrometer (SIMS) analysis. It uses an oxygen based primary ion beam and a mass spectrometer for geochronological analysis. This type of beam source allows for an unusually small analysis location (~25 μm in diameter and ~2 μm in depth). It also allows for the synchronous analysis of the trace element composition of the sample when used in conjunction with a standard.

2c. Lu-Hf: petrogenetic tracers for zircons

The Lu-Hf isotopic decay system can be used both for the dating of mineral crystallization and as a tracer of petrogenetic derivation if the minerals ages are already known. The parent ^{176}Lu decays to ^{176}Hf via beta decay. The associated decay constant has been recently revised as 1.86 x $10^{-11}y^{-1}$ by direct scintillation counting (Nir-El and Lavi, 1998) and by correlation with U-Pb using Lu-rich minerals of known age (Scherer *et al.,* 2001). Earlier studies had determined it to be either $1.94x10^{-11}y^{-1}$ as determined from eucrite achondrite meteorites (Patchett and Tatsumoto, 1980a; Tatsumoto *et al.*, 1981) or $1.93x10^{-11}y^{-1}$, originally from direct measurement of gamma ray activity (Sguigna *et al.*, 1982). Regardless, the half life of ^{176}Lu is approximately 35 Ga. The isotopes of Hf (174, 176, 177, 178, 179, and 180) are all stable. There are only 2 naturally occurring isotopes of Lu: ^{175}Lu, which is stable, and ^{176}Lu, which is radiogenic. Natural Lu includes 2.6% ^{176}Lu (Kinny and Maas, 2003). The decay equation for the Lu-Hf system is:

$$\left(\frac{176Hf}{177Hf}\right)_t = \left(\frac{176Hf}{177Hf}\right)_i + \left(\frac{176Lu}{177Hf}\right)_t * (e^{\lambda t} - 1)$$

As long as the age of the mineral is known, the radiogenic decay of ^{176}Lu to ^{176}Hf can be corrected for and the initial ratio of the radiogenically-derived isotopes of Hf to non-daughter Hf isotopes can be determined. The petrogenesis as derived from the ratio of Lu to Hf is commonly quantified in terms of epsilon (εHf_i) where a negative epsilon value denotes an evolved signature and a positive epsilon is a more primitive signature with respect to CHUR.

$$\varepsilon_{Hf} = \left\{ \left[\frac{\left(\frac{176Hf}{177Hf}\right)_{sample}}{\left(\frac{176Hf}{177Hf}\right)_{CHUR}} \right] - 1 \right\} * 1000$$

This system is particularly useful in the study of zircons. Zircons commonly incorporate 0.5-2.0 weight % Hf (Hoskin and Schaltegger, 2003) and a very small quantity of Lu relative to that of Hf (Lu/Hf <0.0005; Kinny and Maas, 2003). This means that zircon growth contains the epsilon Hf value of the melt from which it crystallized at the time of crystal growth, which can be calculated as long as the age of the zircons is known. The age of zircons can be determined rather precisely using the U-Pb isotopic system. This technique is made even more useful by the use of SIMS in the study of U-Pb. Lu-Hf ratios can also be measured using LA-ICPMS of a grain mount prepared for SIMS work. This allows a zircon sample to be prepared for SIMS, an U-Pb age determined, and then an εHf_i value determined from the same location on the zircon.

Any mass spectrometry analysis of Lu-Hf must be corrected for isobaric interference. This correction is rendered necessary because ^{176}Hf, ^{176}Lu, and ^{176}Yb all have the same mass. The fractionation of ^{176}Hf, ^{176}Lu, and ^{176}Yb is also an issue. Unfortunately, ^{176}Lu and ^{176}Yb can constitute a significant portion of the signal associated with mass 176. The fractionation problem for ^{176}Hf is minimized by measuring several other isotopes, specifically ^{179}Hf, and ^{177}Hf. The ratio of $^{179}Hf/^{177}Hf$ is a constant (0.73250) (Patchett and Tatsumoto, 1980), hence mass bias of any given analysis is calculable. The fractionation of ^{176}Yb can be solved by measuring ^{173}Yb and ^{171}Yb, the ratio of which is 1.132338 (Vervoort *et al.*, 2004). However, the amount of ^{171}Yb in the sample is so low that often the use of the ^{176}Hf mass bias function is used instead of that of ^{176}Yb for the sake of accuracy. Lu only has two isotopes (176 and 175) so a ratio is not useful, but the amount of ^{176}Lu is much lower than that of either ^{176}Hf or ^{176}Yb, so the impact is negligible and any mass bias is assumed to be the same as that of ^{176}Yb. The isobaric interference between ^{176}Yb and ^{176}Hf is corrected for by measuring ^{171}Yb and assuming the

$^{176}Yb/^{171}Yb$ ratio is a constant 0.901691 (Vervoort *et al.*, 2004). The isobaric impact of ^{176}Lu is determined by measuring ^{175}Lu and assuming a $^{176}Lu/^{175}Lu$ of 0.02653 (Patchett, 1983).

In mass spectrometry analysis, corrections must be made for fractionation effects. Fractionation is defined as two isotopes behaving differently based on the difference in their masses. Low atomic mass elements will fractionate at temperatures that occur naturally at the earth's surface. This is because the relative difference in mass between two isotopes of a light element is greater than between two isotopes of a heavy element. Fractionation of heavy elements only becomes an issue at the very high temperatures of a mass spectrometer ion source, either the filament of a TIMS or the laser to sample interaction site. In the case of the LA-ICPMS, as the laser ablates the sample initially the lighter isotopes are preferentially liberated. As ablation continues the heavier isotopes are liberated, but there may remain a disproportionate amount of light isotopes in the resulting sample gas. The ratio is corrected for by normalizing the signal value to a standard.

The Lu-Hf system is useful in determining petrogenesis because Hf is preferentially incorporated into silicate melts as a result of partial melting of mantle material while Lu remains in the restite. This is important because the ratio of ^{176}Hf to ^{177}Hf at the time of plutonic emplacement establishes the degree to which the magma is isotopically distinct from the mantle from which it is derived. As such, different crustal blocks or terranes will have differing ranges of $^{176}Hf/^{177}Hf$ contained in their constituent plutons, which can be used to differentiate between them. In this case, the possibility of an isotopic difference between the MHMC and the surrounding terranes would contribute to the determination of to which, if any, of the surrounding terrains the MHMC belongs.

2d. Major element geochemistry: ICP-OES

Inductively coupled plasma optical emission spectrometry (ICP-OES) is also known as inductively coupled plasma atomic emission spectroscopy (ICP-AES). The ICP portion of the machine produces high temperature argon plasma via electromagnetic excitation (Jarvis and Jarvis, 1992). The sample is introduced to the plasma via solution nebulization. The sample reacts with the plasma and releases electromagnetic radiation in various wavelengths correlating to the reacting element at an intensity dependant on the quantity of the element present.

In this study, the samples were powdered (see ICPMS section) and dissolved, then analyzed using an ICP-OES primarily for major element oxides and some trace element composition. With the exception of the powdering step, these analyses were performed at the University of Houston-Downtown by Dr. Kenneth Johnson. One sample (08MH03) was analyzed by x-ray fluorescence (XRF) at the University of Alabama.

In this study, major element geochemistry is combined with the trace element geochemistry to define changes in magmatic origin through time. It is used to compare the geochemical signatures of the Wallowa and Baker terranes to those of the MHMC and to help define the relationship of the MHMC to these surrounding terranes.

2e. Trace element geochemistry

i. *Whole Rock*

Samples were powdered using an aluminosilicate ring and puck mill (shatterbox). This powder was then dissolved for whole rock analysis in varying solutions applied in several steps: 1) a mix of concentrated HNO_3 and concentrated HF (both optima purity), after which samples

were heated on a hot plate and subsequently dried down; 2) concentrated HNO_3, followed by heating and drying; 3) a repeat of concentrated HNO_3, followed by heating and drying; 4) 12N HCl (trace element grade) and another drying period, and finally; 5) 2% HNO_3 and 0.5% HF. Samples were then run through the ICPMS while still in acid solution.

The inductively coupled plasma mass spectrometer (ICP-MS) includes a similar mechanism to that of the ICP-OES. During ICP-MS analysis, the sample is introduced to an argon plasma source excited by an electromagnetic coil. The resulting excited sample plasma is used as an ion source to a quadrupole mass spectrometer. The quadrupole uses a series of electromagnets to dynamically direct various isotopes into the collector, unlike a magnetic sector mass spectrometer which would use a static electromagnet and a flight tube for its mass differentiation.

In this study, all sample preparations were performed at the University of Alabama in the Department of Geological Sciences. The ICP-MS was used exclusively to obtain trace element data.

ii. *Zircon*

Sensitive High Resolution Ion Microprobe-Reverse Geometry (SHRIMP-RG) trace element data were collected simultaneously with U-Pb data and on the exact same analysis locations. A summary of the analyses that were performed on each unit is provided in Table 1. An R-33 standard was analyzed after every four unknowns. The elements collected were rare earth elements (REEs), although the entire suite of stable REEs was not collected. REEs not collected included Lu, Tb, and Tm. For comparison with whole rock REE data, trace element compositions of melt in equilibrium with zircon were determined using the zircon/liquid partition

coefficients of Sano et al. (2002). All data were collected at the U.S. Geological Survey Stanford Microprobe Laboratory using the SHRIMP-RG. Trace element geochemistry is used to establish geochemical distinctions in a single population of zircons or to compare chemical conditions in several magmas as recorded at the time of zircon crystallization.

Table 1. Summary of analyses performed on each unit in the MHMC. Note that while sample MTJ-2 of the Trondhjemite of Pearson Creek was geochronologically analyzed, it was not successfully analyzed for Lu-Hf. Samples that do not indicate IC-MS, ICP-OES, XRF, or zircon data (unless otherwise noted zircon analyses include trace elements, Lu-Hf, and U-Pb) were studied only in thin section for petrography.

Unit	Sample Name	ICP-MS	ICP-OES	XRF	Zircon
Schist of Yellow Jacket Road					
	SYR-4				
Garnet bearing	SYR-5				
	SYR-6				
	SYR-7				
	SYR-8				
	SYR-9				
Amphibole	PCSS-1				
Bearing	PCSS-3				
	PCSS-4				
Neither	SHT-1				
Serpentinized Peridotite					
	MGB-6				
Keratophyre of Pearson Creek					
Eastern	PCS-1				
Exposure	PCS-2				
	PCS-3	x	x		
	PCS-4	x	x		
	PCS-5	x	x		
	PCS-6	x	x		
	PCS-7	x	x		
Central	MGB-5				
Exposure	UMV-1	x	x		
	UMV-2				
	UMV-3		x		
Trondhjemite of Pearson Creek					
Pluton	MTJ-1				
	MTJ-2		x		x
	MTJ-4	x	x		
Mafic Dike	MTJ-3		x		

Table 1, continued. Summary of analyses performed on each unit in the MHMC. Note that while sample MTJ-2 of the Trondhjemite of Pearson Creek was geochronologically analyzed, it was not successfully analyzed for Lu-Hf. Samples that do not indicate IC-MS, ICP-OES, XRF, or zircon data (unless otherwise noted zircon analyses include trace elements, Lu-Hf, and U-Pb) were studied only in thin section for petrography.

Unit	Sample Name	ICP-MS	ICP-OES	XRF	Zircon
Metagabbro					
Typical	MGB-3/MGB-4	x	x		
	WBC-2				
	WBC-3				
Fine Grained	MGB-1				
	MGB-2	x	x		
Porphyritic	CAG-1	x	x		
Xenolithic	DSC-1	x	x		
Tonalite of California Gulch					
	TONA-1	x	x		x
	MEG-4	x	x		
Amphibolite Gneiss					
Most Migmatitic	GTON-1				
	GTON-2				
	TON-3	x	x		
	MEG-3				
	MEG-2				
Gneissic	ASM-4	x	x		
	ASM-3				
	ASM-2				
	MGB-4-2				
	ASM-1				
Most Schistose	MEG-1				
Trondhjemite of Johnson Creek					
	JOC-1	x	x		x
Diorite of Alexander Creek					
	DAC-1	x	x		x
	10DAC1b				
Norite of Carney Butte					
	08MH03a			x	x
	08MH03b				

Table 1, continued. Summary of analyses performed on each unit. Note that while sample MTJ-2 of the Trondhjemite of Pearson Creek was geochronologically analyzed, it was not successfully analyzed for Lu-Hf. Samples that do not indicate IC-MS, ICP-OES, XRF, or zircon data (unless otherwise noted zircon analyses include trace elements, Lu-Hf, and U-Pb) were studied only in thin section for petrography.

Unit	Sample Name	ICP-MS	ICP-OES	XRF	Zircon
Tonalite of Granite Meadows					
Pluton	TGM-1	x	x	x	x
	GRM-2		x		
	GRM-6	x	x		
Mafic Enclaves	GRM-1	x	x		
	GRM-3		x		
	GRM-4	x	x		
	GRM-5	x	x		
Dike south of DAC	UTON-1				
	UTON-2		x		
Dike on Table Mtn	WBC-5				
	TBM-1				
	PCSS-2				
Gabbronorite of Ridenor Canyon					
	GNR-3		x		
	GNR-5		x		x

3. RESULTS

3a. Geology of the Mountain Home Metamorphic Complex

In the MHMC, both metamorphic rocks and plutons are surrounded and partially overlain by Miocene Columbia River Basalts and Tertiary volcanic rocks. Deformed units in the MHMC include the Trondhjemite of Johnson Creek, the Amphibolite Gneiss, the Tonalite of California Gulch, the Metagabbro, the Hornblendite, the Trondhjemite of Pearson Creek, the Pearson Creek Keratophyre, and the Schist of Yellow Jacket Road. Undeformed units in the MHMC include the Gabbronorite of Ridenor Canyon, the Tonalite of Granite Meadows, the Norite of Carney Butte, and the Diorite of Alexander Creek (Figure 2).

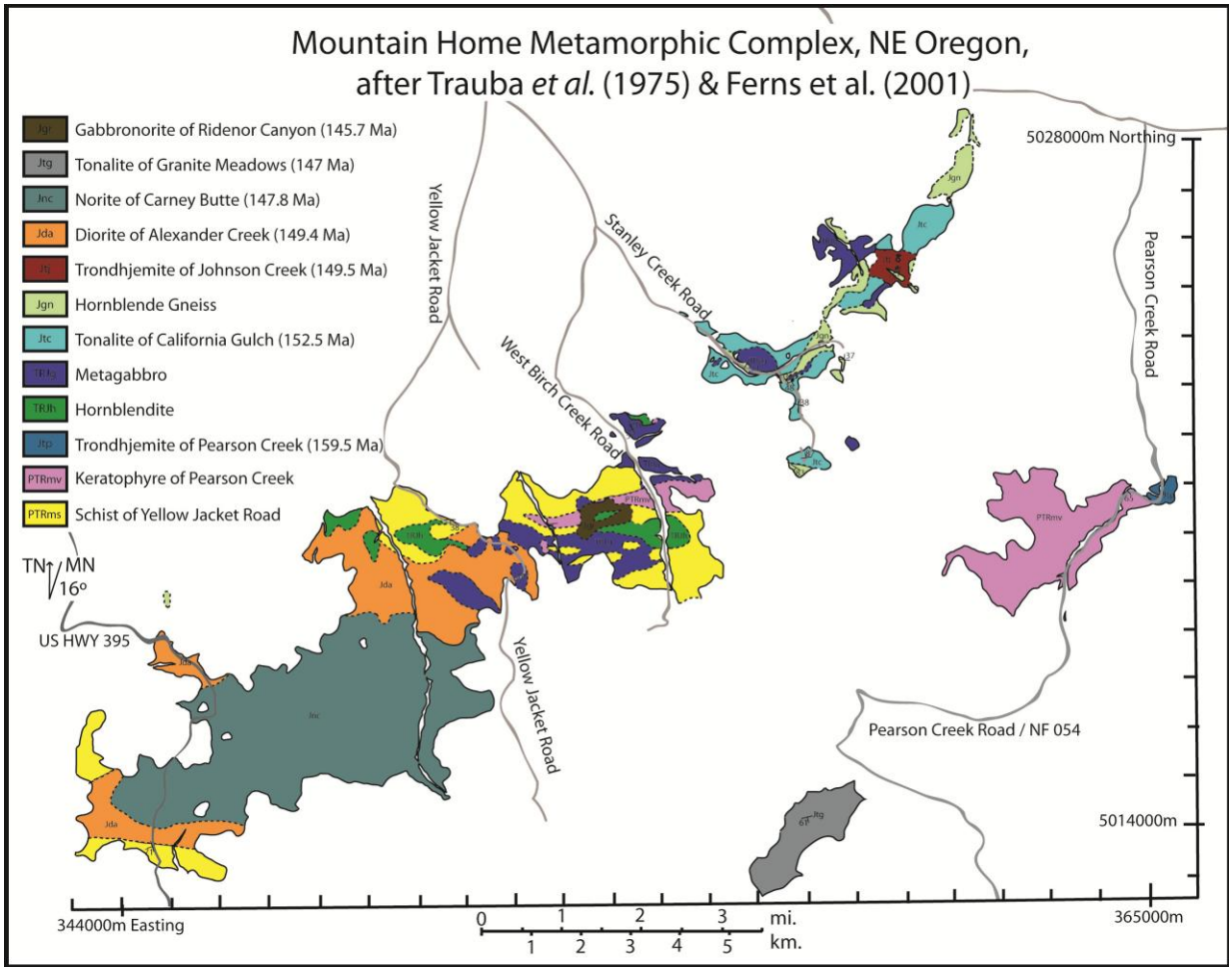

Figure 2. Map of the pre-Tertiary geologic units in the MHMC (geology is modified from Trauba, 1975; Ferns *et al.*, 2001). Unit ages are rounded from $^{206}Pb/^{238}U$ ages presented in this study (Section 3b).

3b. Deformed units of the MHMC

i. *Metasedimentary Units in the MHMC*

The Schist of Yellow Jacket Road unit is predominantly composed of fine-grained biotite garnet schist. Its mineralogy is consistently dominated by quartz, plagioclase, and usually biotite or less commonly muscovite, both of which define the foliation (Figure 3). Whereas the schist's texture and bulk mineralogy are generally consistent across its exposure, the mineralogy of its ubiquitous porphyroblasts differs with location. Although garnet is the predominant porphyroblast in the unit, some areas of the MHMC either lack garnet or also include other porphyroblasts including either staurolite or sillimanite. Graphite is ubiquitous in all samples. The area southeast of the Ridenor Canyon pluton contains both hornblende porphyroblasts (usually in clumps) and fine grained hornblende as the mineral that defines schistosity, rather than biotite or muscovite.

Porphyroblast mineralogy often varies with degree of metamorphism. The outcrop along Yellow Jacket Road contains copious garnet porphyroblasts as well as several igneous dikes. Garnet size and degree of preservation is often directly correlated to proximity to the dikes. Most garnets in the Yellow Jacket Road area are two stage, as indicated by two zones of minimal inclusion density separated by a zone of inclusions, and do not include tracks of host rock inclusions; therefore, they are pre or syn-tectonic. They are also usually surrounded by sigmoidal pressure shadows.

The area to the northwest of Table Mountain at the southern end of West Birch Creek (Figure 2) has been mapped as hornsfelsed keratophyre (Trauba, 1975), but this study finds that it is the Schist of Yellow Jacket Road. Significantly more amphibole is present than in the other

keratophyre outcroppings, and this area lacks the felty texture common to the keratophyre's groundmass. No garnet or biotite is found in the southern exposures, but they are present further north, near the Hornblendite. Metamorphic hornblende defines the schistosity and is sometimes altered to chlorite. Clumps of metamorphic hornblende are also commonly found in this area; they are often associated with or surrounding opaque minerals. Symmetric strain shadows are also found around these hornblende clumps, forming augens. Chlorite occasionally defines foliation, but is most likely a post deformational alteration product.

Cleavage is well-defined and parallels foliation and bedding. The Schist of Yellow Jacket Road is the most commonly folded unit in the MHMC (Figure 3). It only appears in the central and southwest portions of the MHMC where it is metamorphosed and usually contains dikes of other units. Its deformed nature is clear in all areas by its schistosity, the growth and rotation of porphyroblasts, the strained nature of the quartz in thin section, and the clearly apparent presence of folding.

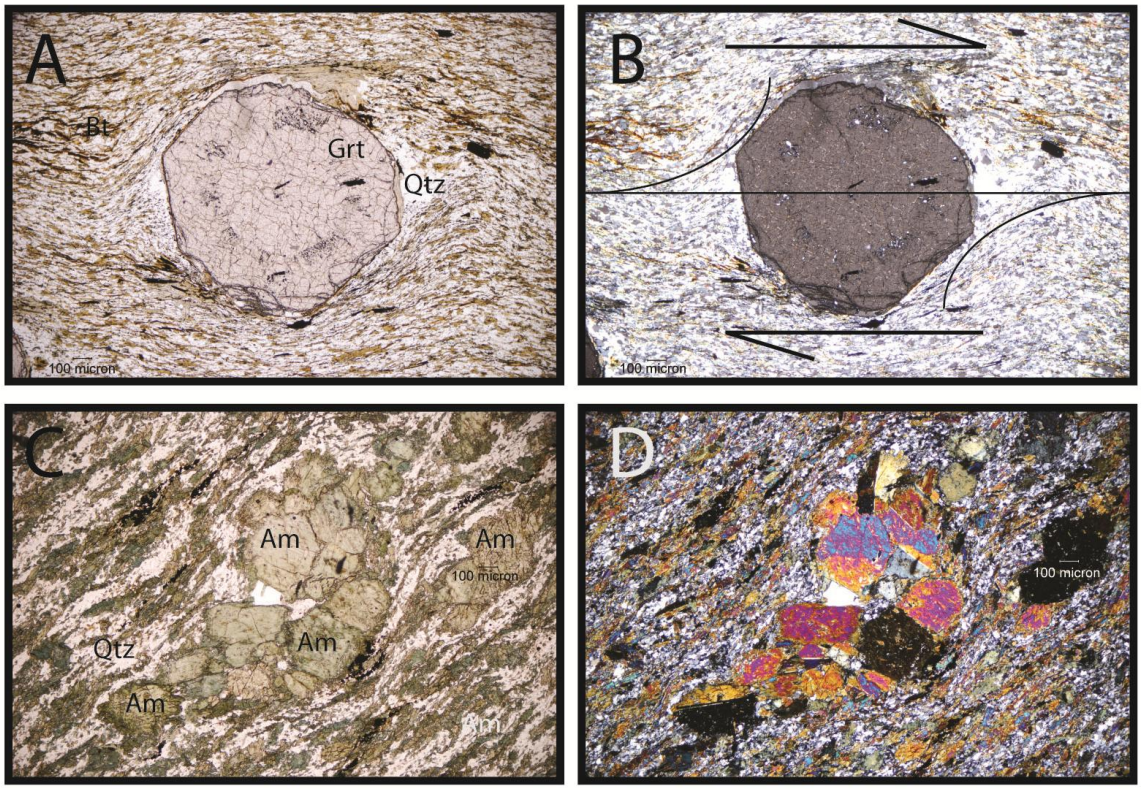

Figure 3. Selected photomicrographs of the metasedimentary unit found in the MHMC. A) Plain polarized photomicrograph focused on a garnet exhibiting sigmoidal rotation. B) Crossed polarized light image of A. Sigmoidal pressure shadow and direction of garnet rotation marked in black. C) Plain polarized photomicrograph of a rotated amphibole clot in a matrix of quartz and plagioclase with foliation defined by amphiboles. D) Crossed polarized light image of C.

ii. *The Keratophyre*

The Pearson Creek Keratophyre (Figure 2) crops out in both the easternmost exposure of the MHMC and in the central region. It is consistently foliated and resistant to weathering. Whereas the keratophyre's age is unknown, it is intruded by, and therefore older than, the Trondhjemite of Pearson Creek (Figure 2). It is also intrafolded with the Schist of Yellow Jacket Road and contact metamorphosed by the Metagabbro in the central region of the MHMC (Trauba, 1975). Furthermore, it is cut by the younger Ridenor Canyon pluton. The main exposure along Pearson Creek varies in hand specimen from blocky to schistose. This variation between schistose and blocky texture is consistent throughout the unit.

The keratophyre in the MHMC is consistently identifiable in hand specimen by its sugary texture and in thin section by its felted groundmass (Figure 4 and Appendix A). In the Pearson Creek exposure, phenocrysts include generally altered plagioclase, but can also include blue-green hornblende, spheres of strain-resistant blue quartz, sphene, and occasionally zircon. Depending on the location, this exposure also includes muscovite or biotite primarily defining schistosity, but in some samples the biotite occurs in radiating clots. In the western exposure, phenocrysts are primarily twinned plagioclase and recrystallized quartz. Staurolite and sigmoidally-rotated garnets were also observed. The deformed nature of this unit's western exposure is apparent from the rotation and growth of metamorphic minerals (including garnet and staurolite) and the deformation of plagioclase and quartz. In contrast, the eastern exposure's deformation is characterized by its foliation and strained quartz.

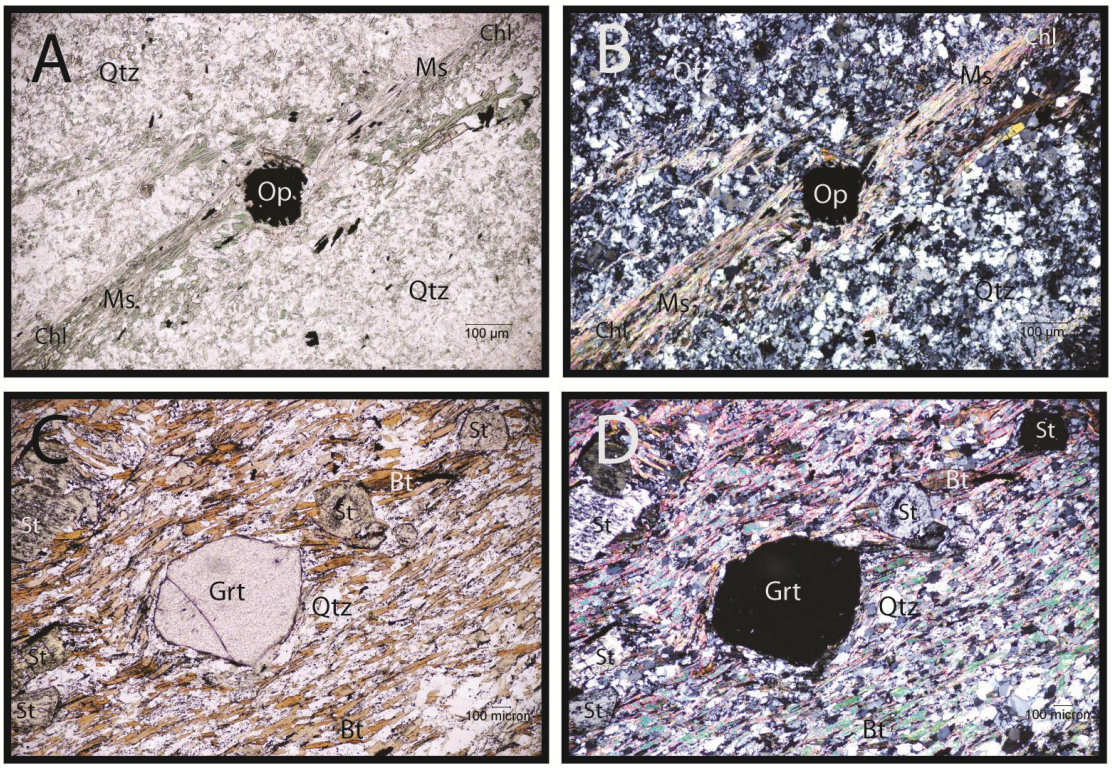

Figure 4. Selected photomicrographs of the Pearson Creek Keratophyre. A) Plain polarized photomicrograph focused on an opaque exhibiting sigmoidal rotation in a foliation plane. This image also shows the standard mineralogy of the greenschist facies exposure of the Pearson Creek Keratophyre. B) Crossed polarized light image of A. C) Plain Polarized photomicrograph of a garnet and staurolite in a biotite schist version (amphibolite facies) of the Pearson Creek Keratophyre. D) Crossed polarized light image of C.

iii. *The Amphibolite Gneiss*

The Amphibolite Gneiss varies across its exposure from amphibolite schist to gneiss, and even to a migmatite in some locations. The Amphibolite Gneiss' protolith is not well understood, but where present in the central area of the MHMC, its schistose nature leaves it resembling the Schist of Yellow Jacket Road more than the nearby igneous plutons (with some exceptions). The gneiss varies in mineralogical and textural composition between similarity to the Metagabbro and to the Schist of Yellow Jacket Road. Protolith identification is further complicated by the intrusion of the Tonalite of California Gulch (Figure 2). Quartz, plagioclase, and hornblende are usually present. The only other amphibole observed in the unit is actinolite, but Trauba (1975) has also reported finding tremolite in the unit. In this study, the only actinolite-bearing samples were collected from the more texturally schistose areas. Whereas hornblende is lacking, biotite is present. The proportion of hornblende to biotite increases in the region between Stanley Creek and California Gulch. Garnet is present in several locations, but it is usually in zones of finer grained textures and in association with higher quartz content.

Clinopyroxene or orthopyroxene are less than 5% of modal mineralogy but do not occur together (Figure 5). The schistosity in the southernmost outcrop of the Amphibolite Gneiss is defined entirely by amphibole and the unit contains rotated porphyroblast cavities, which have been filled in with paragonite (likely retrograde, see Appendix A). Evaluating the textures with the mineralogy reveals the potential that the southern part of the gneiss is either derived from, or shares a protolith with, the Schist of Yellow Jacket Road. This study does not find textural evidence that the gneiss is derived from igneous units, but Trauba (1975) reported it as gneiss with a mixed protolith of metasedimentary, metavolcanic, and meta-plutonic rocks; this may be true in its northern exposures.

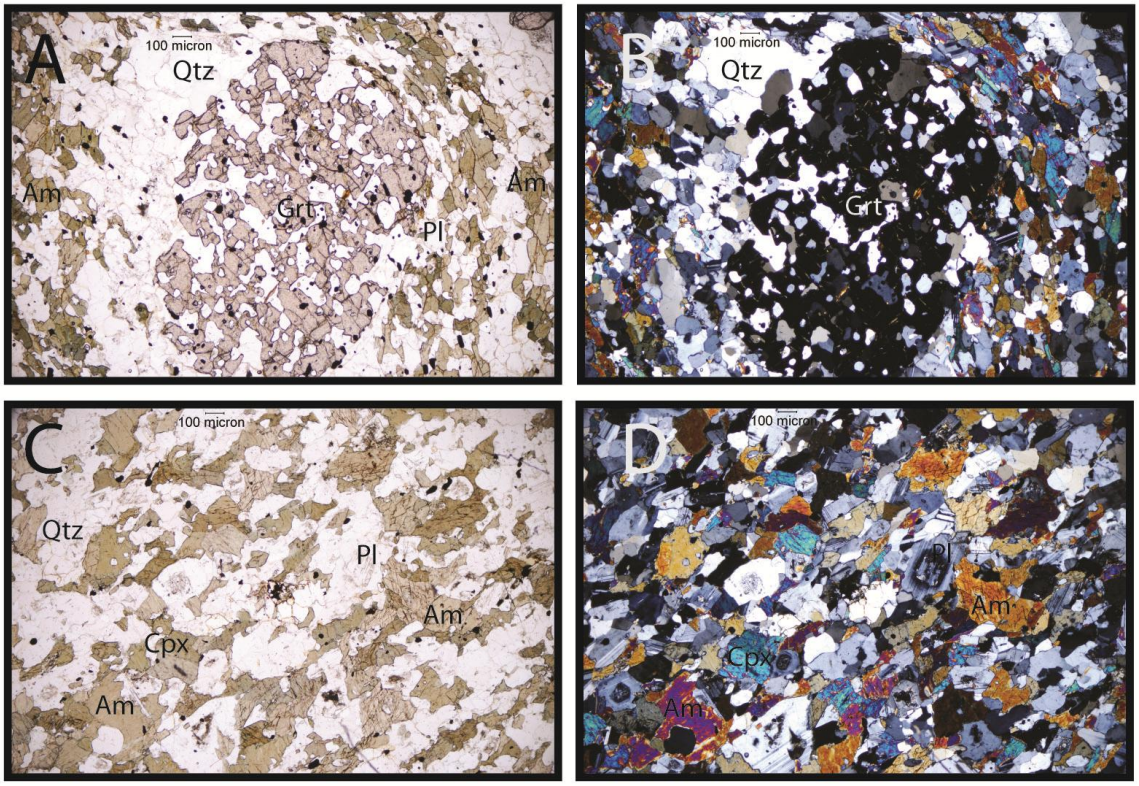

Figure 5.Selected photomicrographs of the Amphibolite Gneiss of the MHMC. A) Plain polarized photomicrograph of a garnet surrounded by a quartz and plagioclase leucosome. B) Crossed polarized light image of A. C) Plain polarized photomicrograph of the general texture of the Amphibolite Gneiss, in this case clinopyroxene bearing. D) Crossed polarized light image of C.

iv. *The Trondhjemite of Pearson Creek*

The Trondhjemite of Pearson Creek is exposed over a small area (~0.4 km^2) where it intrudes the Pearson Creek Keratophyre (Figure 2). It is dominated by quartz and heavily sericitized plagioclase, but minor blue-green hornblende is also present. The trondhjemite is weakly foliated, and shows significant amounts of microstructural deformation in thin section such as strained quartz and microfracturing followed by later zoned growth in plagioclase (see Figure 6 and Appendix A). The trondhjemite intrudes the Pearson Creek exposure of the Pearson Creek Keratophyre and does not contact another pre-Tertiary unit in the MHMC. It is significantly more felsic than the other deformed plutonic units including the Johnson Creek Trondhjemite, despite their similar mineralogies.

This unit's limited geographic extent (~0.4 km^2) precludes much variation with distance, but it does contain a sizable mafic dike that cuts the pluton along the unit's only road cut. The dike represents the only mafic igneous rock in the eastern MHMC. This dike is mainly composed of hornblende with some quartz, plagioclase, orthopyroxenes, and opaques. The dike's hornblende is distinguished from that of the pluton by being ubiquitously brown. The dike does not display any detectable foliation.

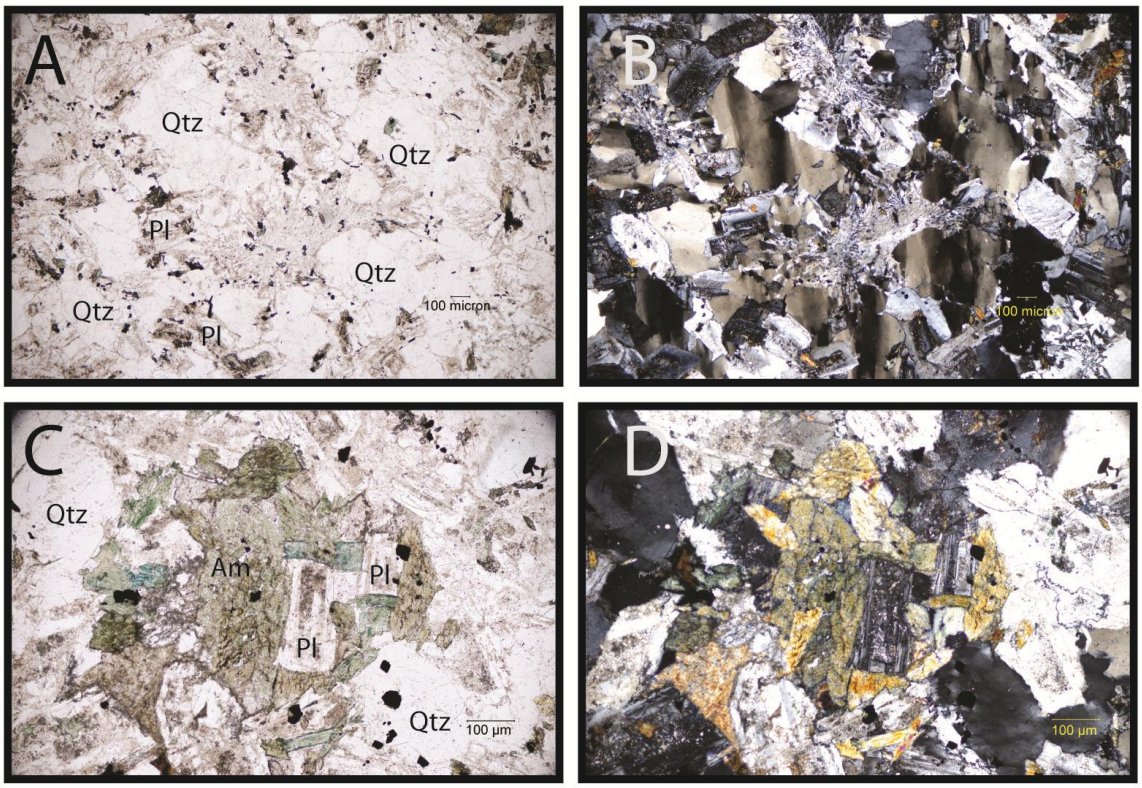

Figure 6. Selected photomicrographs of the Trondhjemite of Pearson Creek. A) Plain polarized photomicrograph showing the typical texture of the unit: deformed quartz and plagioclase filled with alteration and vermicular intergrowths of quartz. While this is the typical texture, the quartz in this image is displaying the strongest case of dynamic recrystallization yet found in the unit. B) Crossed polarized light image of A. C) Plain polarized photomicrograph of an amphibole clump surrounded by quartz and plagioclase. The amphiboles are typically prismatic and in this case are associated with an example of a heavily altered plagioclase feldspar core overgrown by later plagioclase. D) Crossed polarized light image of C.

v. *The Hornblendite*

On a large scale the unit identified as Hornblendite by Trauba (1975), which this study identifies as a metaigneous rock, is important for its relationship to the other predeformational plutonic units. This unfoliated unit intrudes the Schist of Yellow Jacket Road and may have been included in the much younger Diorite of Alexander Creek as several large xenoliths. In the northernmost part of the central MHMC, the Hornblendite is intruded by the younger Metagabbro and is incorporated into the Metagabbro as xenoliths.

The Hornblendite is clearly deformed. Plagioclase shows deformation twinning and undulose extinction (Figure 7). Quartz shows bulging and general dynamic recrystallization. However, foliation is not observed. Only five small outcrops were mapped across the central MHMC. Trauba (1975) reported the unit to usually consist of >95% blue-green hornblende, but its mineralogy is more variable with up to 25% clinopyroxene, up to 45% chlorite + clays, and minor plagioclase. The hornblende is brown in the coarse grained, pyroxene bearing areas, and zoned (brown cores with green rims) in the medium grained, pyroxene-free areas.

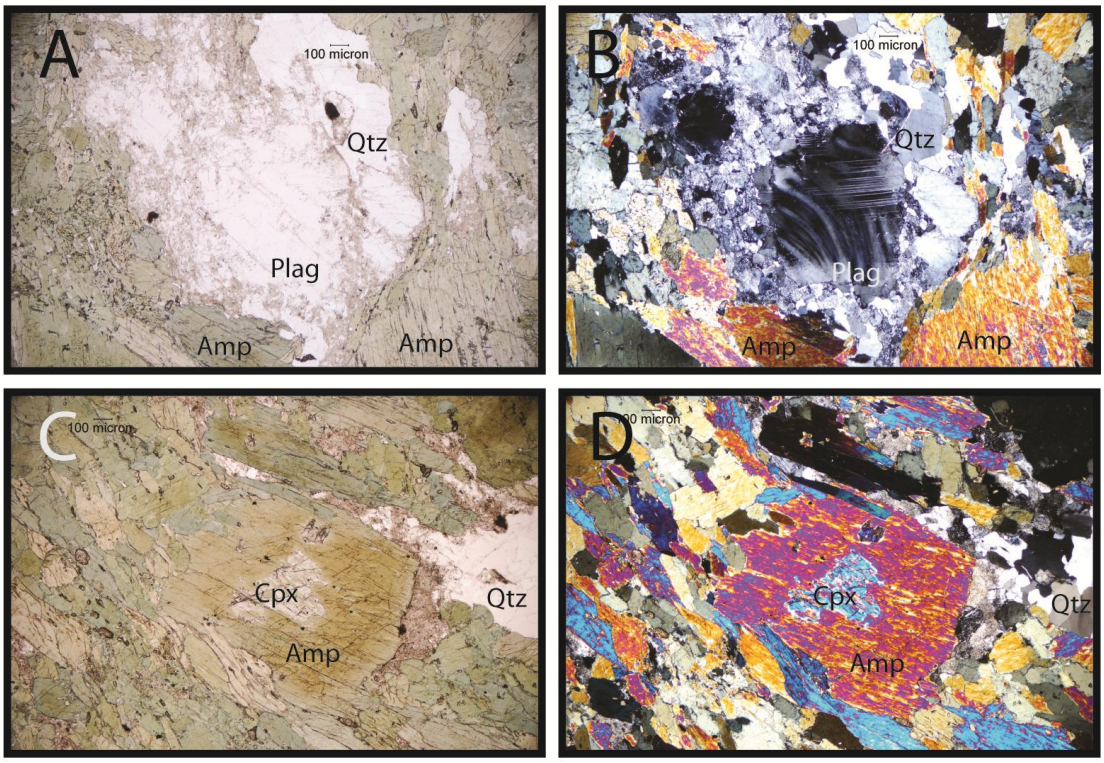

Figure 7.Selected photomicrographs of the Hornblendite of the MHMC. A) Plain polarized photomicrograph focused on a plagioclase showing both deformation twinning and strong undulose extinction. This image also shows the standard mineralogy of the more felsic rich areas of the pluton. B) Crossed polarized light image of A. C) Plain polarized photomicrograph of a clinopyroxene-cored amphibole surrounded by smaller amphiboles and flattened quartz. D) Crossed polarized light image of C.

vi. *The Metagabbro*

The Metagabbro (Figure 2, 8, and 9) is the most laterally extensive deformed unit, but it is composed of four separate texturally defined groups: 1) medium-grained Metagabbro composed of generally equal parts plagioclase and amphibole (Figure 8), 2) xenolithic gabbro containing greater than 50% xenoliths of any version of the Metagabbro (Figure 9), 3) fine-grained Metagabbro, and 4) porphyritic Metagabbro characterized by relatively large plagioclase porphryoclasts in a fine-grained groundmass matrix (Figure 8). These descriptions are only a general guide to this heterogeneous unit. The sample mapped as "typical" is, in fact, primarily plagioclase with equal parts amphibole and resorbed clinopyroxene.

The textural groups also differ in mineralogical makeup; although all are dominated by plagioclase and amphibole, the typical texture variably contains clinopyroxene, the xenolithic texture variably contains biotite, clinopyroxene, and quartz; the fine grained texture contains significant opaques; the groundmass of the porphyritic texture contains fine-grained brown hornblende, plagioclase, quartz, and variable amounts of clinopyroxene and biotite (Figures 8 and 9). Hornblende is the dominant amphibole throughout the Metagabbro. In the typical textured areas, hornblende ranged from blue green grains to brown grains. Trauba (1975) also reported finding actinolite, tremolite, and hornblende. He also found that the presence of hornblende was correlative to textural evidence of reheating. Brown hornblendes are only present in fresh samples of the porphyritic variation. The fine grained Metagabbro contains zoned hornblendes with brown cores and green rims.

Overall the unit is foliated, but the degree of foliation varies greatly with location. While its contacts are usually hidden, it intrudes the Schist of Yellow Jacket Road and the Amphibolite

Gneiss (Trauba, 1975) and is incorporated as xenoliths into the Tonalite of California Gulch and Trondhjemite of Johnson Creek. In hand specimen, it is usually identified by the scarcity or lack of quartz or biotite unless the sample was collected close to a contact.

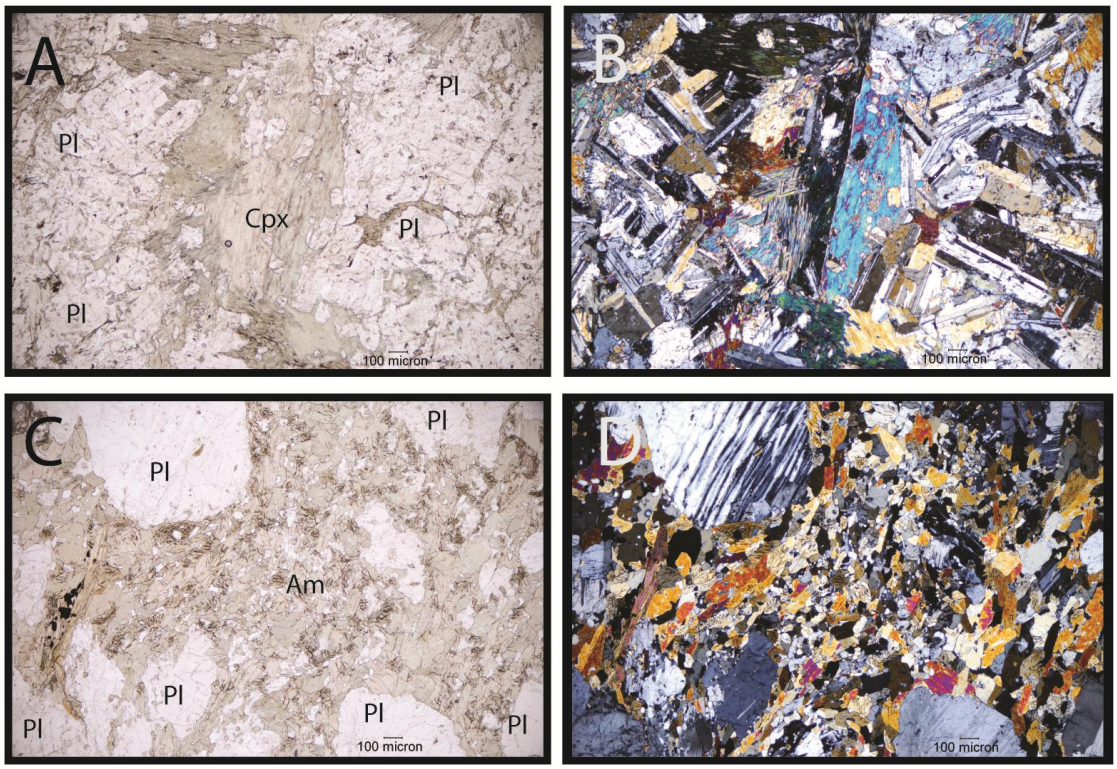

Figure 8.Selected photomicrographs of two of the Metagabbro varieties found in the MHMC: the 'typical' and the porphyritic. A) Plain polarized photomicrograph of the "typical" Metagabbro's usual texture; primarily plagioclase (sometimes showing undulatory extinction) with varying proportions of clinopyroxene and amphibole. B) Crossed polarized light image of A. C) Plain polarized photomicrograph of the porphyritic variety of the Metagabbro. Texture is typical: porphyroclasts of undulose plagioclase feldspar in an amphibole (with some deformed biotite) dominated matrix. Composition varies somewhat in this unit, with pyroxene content (in the matrix) increasing to the north, the occasional absence of biotite altogether, and the occasional presence of substantial quartz (up to 15%). D) Crossed polarized light image of C.

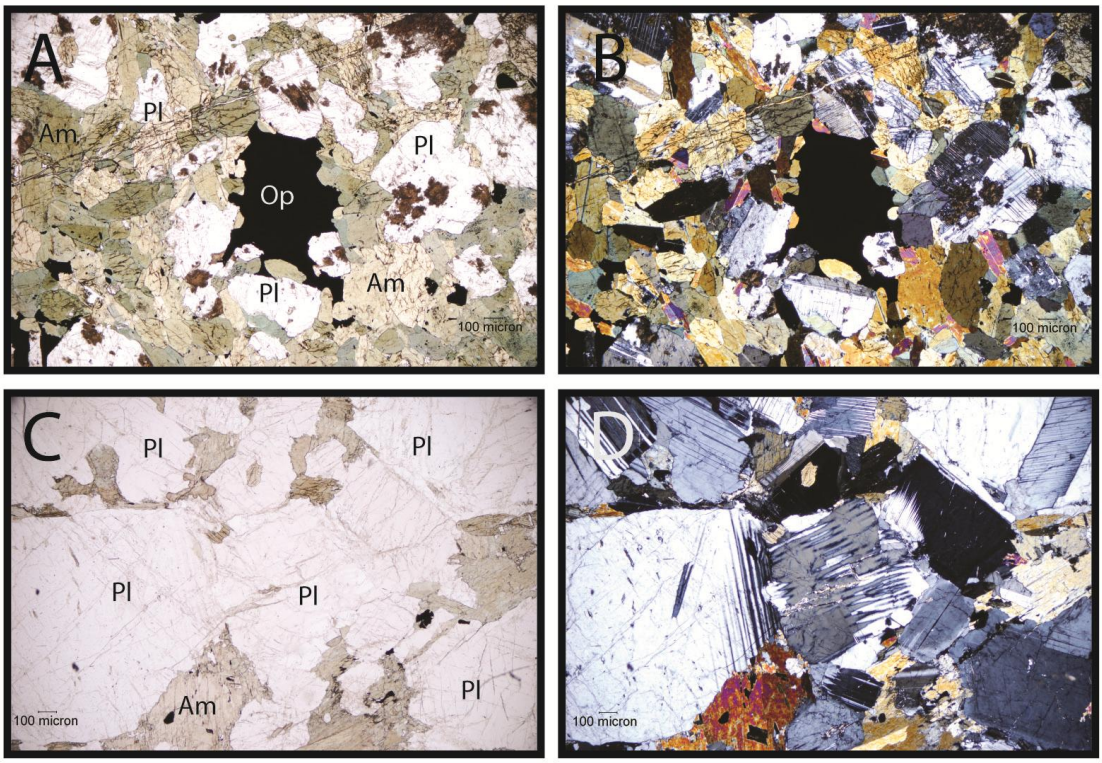

Figure 9. Selected photomicrographs of two of the Metagabbro varieties found in the MHMC: the fine-grained and the xenolithic. A) Plain polarized photomicrograph of the fine grained varieties usual texture: a mix of small (usually elongate) green amphibole and subhedral, complexly twinned plagioclase with the occasional undulose extinction as well as well as resorbed early stage opaques. B) Crossed polarized light image of A. C) Plain polarized photomicrograph of the xenolithic variety of the Metagabbro. The texture consists of moderately coarse grained rock composed almost entirely of plagioclase (first) and amphibole (second). Plagioclase feldspar contains substantial signs of deformation including undulose extinction and pressure twinning. D) Crossed polarized light image of C.

vii. *The Tonalite of California Gulch*

The Tonalite of California Gulch is a plagioclase, quartz, and hornblende dominated rock which displays well developed foliation. It is easily distinguished from the Metagabbro by the presence of biotite and substantial quartz content (~20-40 modal % for the tonalite versus 0-15 modal % for the metagabbro, Figure 10). Opaques compose up to 5% of the modal mineralogy and some are euhedral. Amphibole is entirely hornblende: resorbed, brown to blue-green, and often simply twinned. Trauba (1975) reported tremolite in the western exposures. In some locations, clinopyroxene is found as cores in amphibole as well, but it is not very common. Foliation is well developed in the tonalite and lineation is locally present (Trauba, 1975). The tonalite incorporated xenoliths of the Metagabbro and was later intruded by the Trondhjemite of Johnson Creek. The relationship between the tonalite and the Amphibolite Gneiss is unclear, although Trauba (1975) reported finding tonalite injected into the gneiss.

The Tonalite of California Gulch is the most laterally extensive unit in the northern portion of the MHMC, and is the youngest of the deformed plutonic units with the exception of the Trondhjemite of Johnson Creek. Its size and timing of intrusion may have contributed to the increased degree of metamorphism of less refractory units near its exposure, possibly resulting in metamorphism of the Amphibolite Gneiss. Although the tonalite is a well foliated igneous rock, it does not display characteristic gneissic banding and cannot, therefore, be termed an orthogneiss.

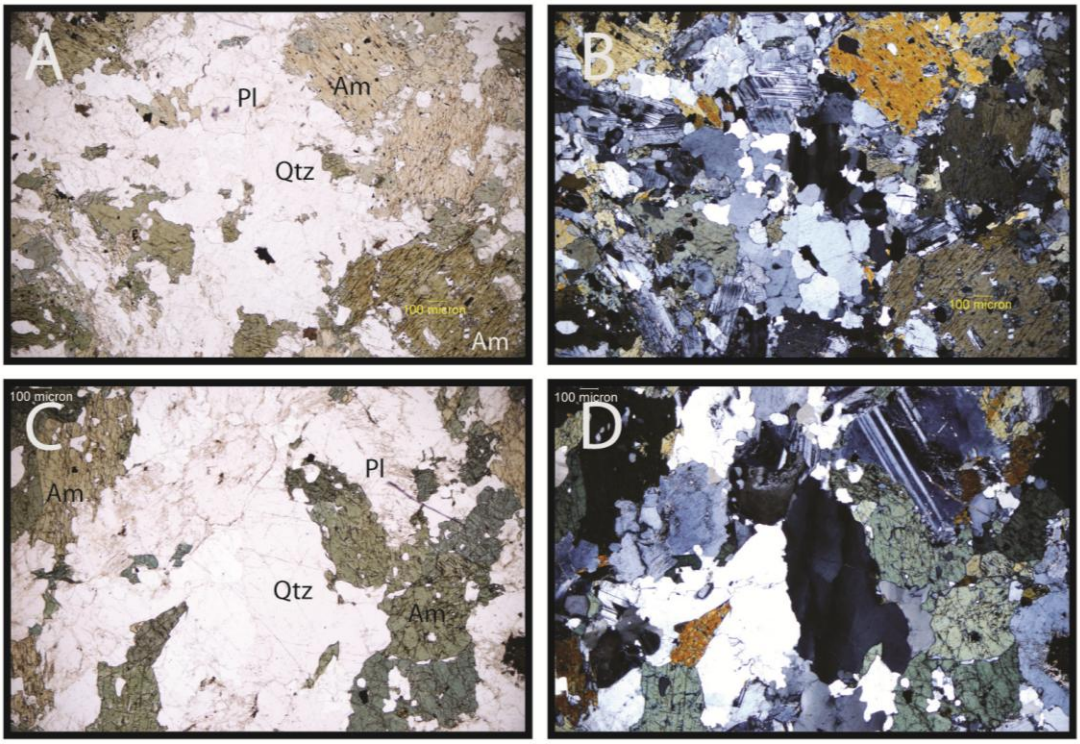

Figure 10. Selected photomicrographs of the Tonalite of California Gulch. A) Plain polarized photomicrograph with plagioclase showing deformation twinning, and amphibole showing substantial microfracturing and embayment. B) Crossed polarized light image of A. C) Plain polarized photomicrograph of a coarser grained sample, again showing dynamically recrystallized quartz, plagioclase, and amphibole. D) Crossed polarized light image of C.

viii. *The Trondhjemite of Johnson Creek*

The Trondhjemite of Johnson Creek is dominated by deformed quartz and plagioclase. Blue-green hornblende, biotite, and uncommon opaques are approximately 10% of the overall rock. Mineralogically, the trondhjemite is very similar to the Tonalite of California Gulch. The main difference between the two in terms of modal mineralogy is 15% to 20% more hornblende or plagioclase in the tonalite and trondhjemite, respectively (Figure 11, Trauba 1975, and Appendices A and B). In hand specimen, this rock is clearly foliated; in thin section, it is even more clearly deformed with bulging quartz, flattening, and dynamic recrystallization as well as plagioclase microfracturing followed by growth nucleated on the relict grains and showing later deformation twinning (see Figure 11 and Appendix B). Only a very limited single exposure, 1 km at its widest point, of the trondhjemite was identified in the field.

The trondhjemite is the youngest of the predeformational units (based on Pb/U geochronology) and it stitches the Amphibolite Gneiss, the Metagabbro, and the California Gulch Tonalite. It is also one of only two felsic predeformational units. Excluding the significantly older Trondhjemite of Pearson Creek, this illustrates the increasing degree of evolution of this plutonic complex as well as the progression of pluton emplacement eastward (post-rotation direction) through time.

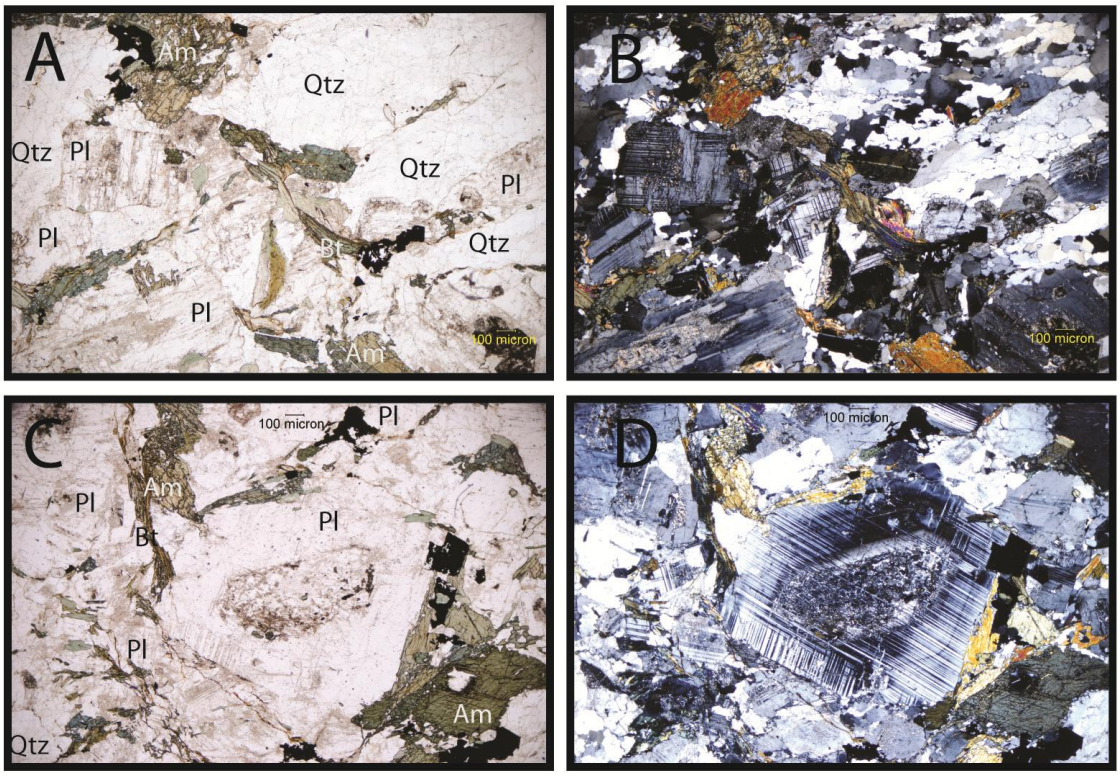

Figure 11. Selected photomicrographs of the Trondhjemite of Johnson Creek. A) Plain polarized photomicrograph showing the deformation of the unit. This image is centered on a deformed biotite but also illustrates the degree of dynamic recrystallization in the quartz. B) Crossed polarized light image of A. C) Plain polarized photomicrograph focused on plagioclase feldspar and growth centered on an earlier relict grain. This image also illustrates the condition of amphibole in the trondhjemite. D) Crossed polarized light image of C.

3c. Undeformed units of the MHMC

i. *The Diorite of Alexander Creek*

This unit is one of the largest units in the MHMC and the first to postdate the MHMC's major deformational event. Foliation is present along the edges of the pluton, but development varies locally. It exists only on the periphery of the younger Norite of Carney Butte, but on the northern exposure it incorporates several of the oldest units in the MHMC: the Hornblendite, the Metagabbro, and the Schist of Yellow Jacket Road. Several of the intrusive dikes found in the Yellow Jacket Road exposure of the Schist of Yellow Jacket Road may in fact be dikes related to the Diorite of Alexander Creek. This unit is very similar to the Norite of Carney Butte and the contact between the two is gradational (Trauba, 1975). The intrusive nature of the contact between the Alexander Creek pluton and the Schist of Yellow Jacket Road is well exposed along a road-cut by Highway 395 where the contact can be walked from one end where dikes of tonalite transition into diorite, then into pluton plus xenoliths, and into xenolith-free pluton at the other end. Interestingly, garnets are only found in the schist near the intrusive dikes in the location at the southernmost exposure of the MHMC, but are generally ubiquitous in the schist's other exposures. The mineralogy of the diorite consists of biotite, zoned hornblende (brown cores with green rims), plagioclase, clinopyroxene, and mica (Figure 12). Trauba (1975) also reported clear amphibole (tremolite) with vermicular quartz inclusions as cores in some hornblende grains.

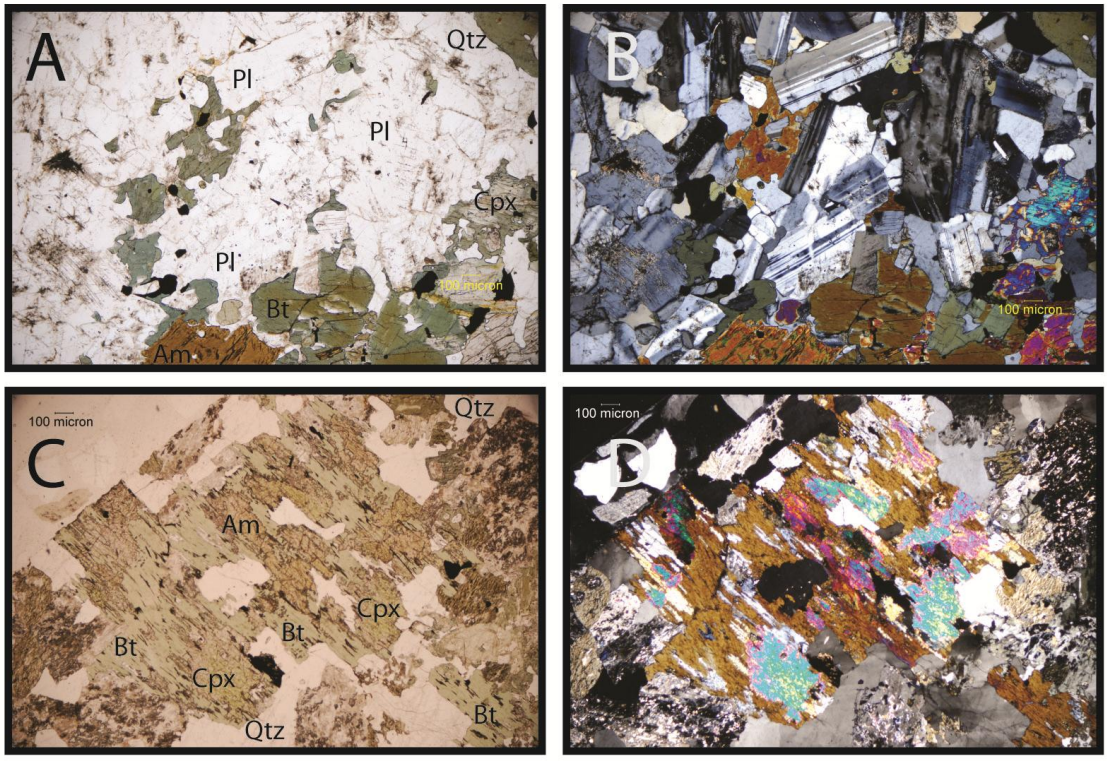

Figure 12. Selected photomicrographs of the Diorite of Alexander Creek, the first unit to be emplaced of the undeformed Carney Butte Stock. A) Plain polarized photomicrograph showing the general texture of the diorite. This illustrates the difference between early plagioclase, shown in the upper right quadrant of the thin section, with its larger grains and undulose extinction and the late plagioclase with its smaller grains and crisp albite law twinning. This image also demonstrates the unstrained nature and prevalence of biotite and amphibole in this pluton as well as that of an unusually well preserved clinopyroxene. B) Crossed polarized light image of A. C) Plain polarized photomicrograph showing a more typical version of the relationships between clinopyroxene which has altered to amphibole and biotite as well as the prevalence of white mica alteration in this unit. Although amphibole is only present on the periphery of the clinopyroxene-biotite reaction in this image, it has been found cannibalizing biotite in other locations. D) Crossed polarized light image of C.

ii. *The Norite of Carney Butte*

This is the largest unit in the MHMC. It only contacts one non-Tertiary unit, the Diorite of Alexander Creek. This contact is intrusive as the younger norite intrudes the older diorite. The norite is unfoliated in hand specimen and undeformed in thin section. The unit is minerologically homogenous and dominated by plagioclase followed by green hornblende, orthopyroxene, clinopyroxene, biotite, and quartz, none of which show any signs of deformation or alteration (Figure 13) in the samples collected. Trauba (1975) reported finding actinolite as well as tremolite and cummingtonite–rimming augite and hypersthenes, respectively.

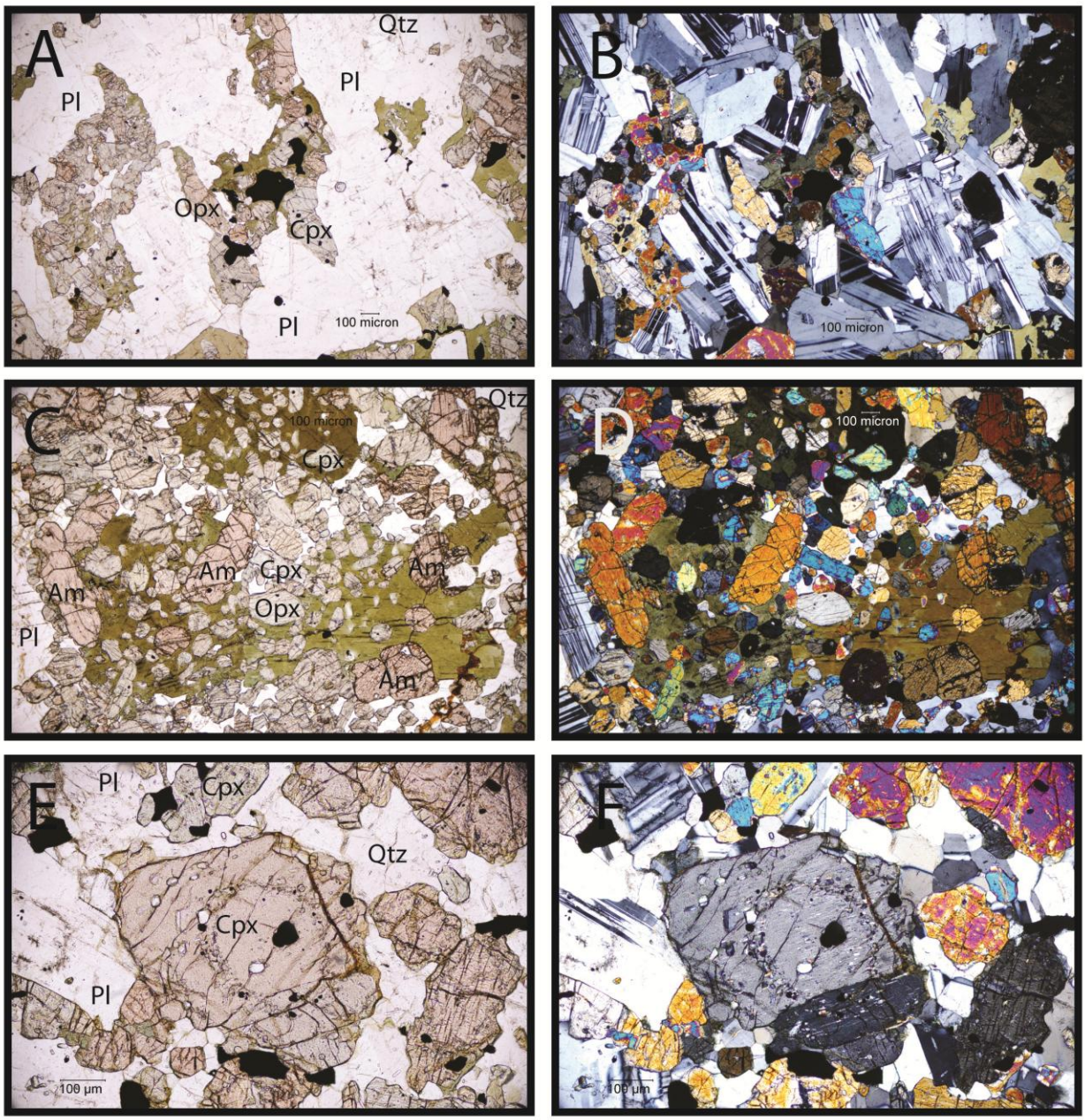

Figure 13. Selected photomicrographs of the Norite of Carney Butte, the second unit to be emplaced of the undeformed Carney Butte Stock. A) Plain polarized photomicrograph illustrating the relationship between blebs of resorbed opaques and the mafic minerals in this unit. It also shows the prevalent state of plagioclase in this rock. B) Crossed polarized light image of A. C) Plain polarized photomicrograph of both types of pyroxene and amphibole subsumed into a larger (and relatively fast growing) biotite. This also illustrates the subhedral nature of some orthopyroxene and amphibole in this unit. D) Crossed polarized light image of C. E) Plain polarized photomicrograph of a subhedral clinopyroxene containing a zone of inclusions. It also shows the interstitial nature of quartz in this pluton. F) Crossed polarized light image of E.

iii. *The Tonalite of Granite Meadows*

The Tonalite of Granite Meadows does not contact any other MHMC unit; thus, its relationship to the other units is unknown. It is the most felsic unit of the post deformational period and second youngest in the MHMC. It contains mafic enclaves that include plagioclase and pyroxene-cored amphiboles. This tonalite contains the highest proportion of biotite of any of the other plutonic units. It is weakly foliated and is the easternmost unit of the Carney Butte Stock. Other primary minerals in the tonalite consist of hornblende, clinopyroxene, and both orthoclase and plagioclase feldspars (Figure 14).

The Tonalite of Granite Meadows is the most coarse-grained and felsic of the plutons that compose the Carney Butte Stock. While it does post date the main deformational event that is present in so much of the rest of the MHMC, it is also the most clearly foliated of the Carney Butte Stock plutons. Foliation is defined by aligned biotite; however, there is no evidence for subsolidus dynamic recrystallization. It is dominated by feldspar, but also contains nearly equal amounts (~20% modal) of quartz, altered hornblende, and undeformed biotite.

The Tonalite of Granite Meadows is the only unit in the MHMC that contains orthoclase. Clinopyroxene is only found in mafic enclaves and even then is strongly resorbed and armored in hornblende. Hornblende is found throughout the unit and is always in some state of resorption. When it is found by itself, hornblende is usually zoned with a brown core and a blue-green rim; when found as a corona on clinopyroxene it is generally blue-green. It consistently shows signs of fracturing as well. Orthoclase and plagioclase feldspars are present in both mafic enclaves (all of which are somewhat incorporated into the main body) and perthite is sporadically present in both enclaves and main body. Both are present interstitially and in larger grains.

Larger grains show signs of deformation such as undulose extinction and deformation twinning, likely due to deformation of the earliest forming minerals before the pluton's final emplacement. Biotite occasionally shows evidence of deformation but is limited to the occasional undulose extinction. Feldspars found interstitially show no significant signs of deformation. Quartz is only found interstitially and is generally undeformed. Ferns *et al.* (2001) described this unit as hypidiomorphic and while subhedral grains are common, these are usually the feldspars; other minerals are largely either too resorbed or interstitial to possess a substantial amount of their original crystalline shape.

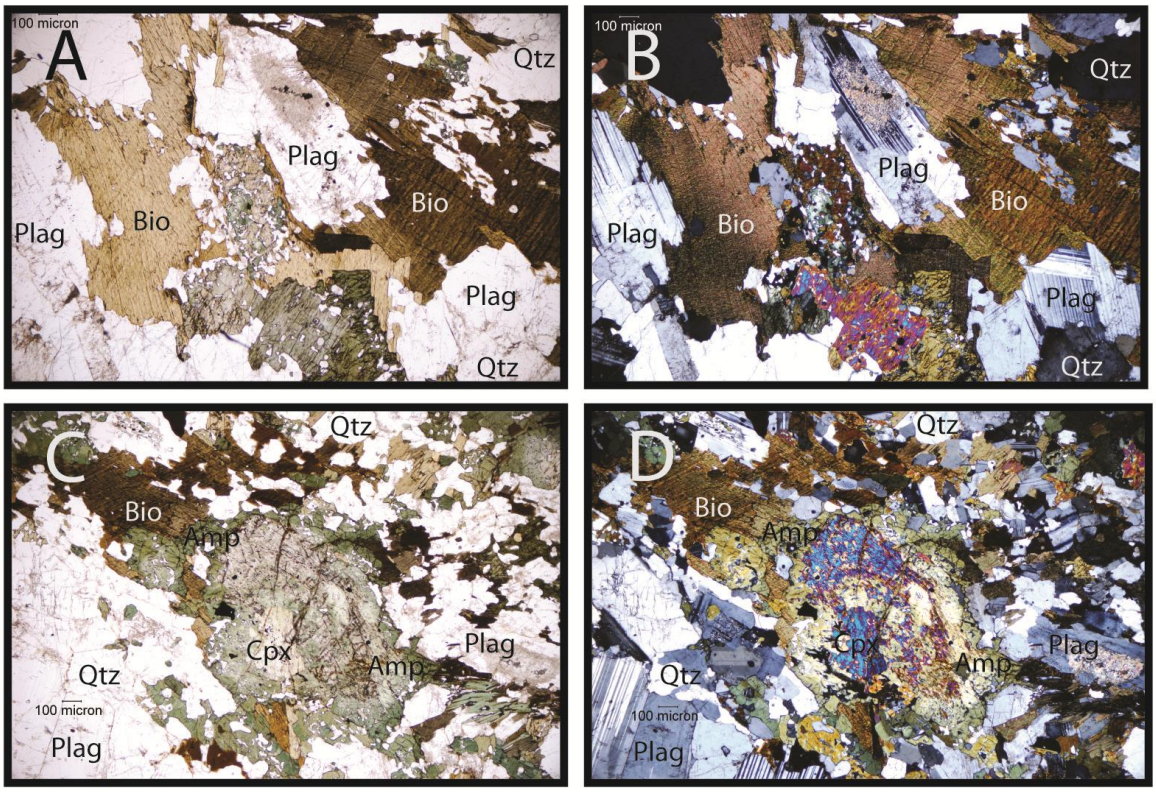

Figure 14. Selected photomicrographs of the Tonalite of Granite Meadows, the third unit emplaced of the undeformed Carney Butte Stock. A) Plain polarized photomicrograph of a biotite and amphibole clot representing the standard mineralogy of the pluton. B) Crossed polarized light image of A. C) Plain polarized photomicrograph of a clinopyroxene cored amphibole in a mafic enclave of the tonalite. D) Crossed polarized light image of C.

iv. *The Gabbronorite of Ridenor Canyon*

The Ridenor Canyon Pluton stitches the Schist of Yellow Jacket Road, the Metagabbro, and amphibolite-facies keratophyre units. It is the youngest unit in the MHMC and it is compositionally heterogeneous across its ≤ 1.5 km expanse. The unit ranges from a fine-grained plagioclase cumulate to a coarse-grained hornblende/pyroxene cumulate, but three distinct outcrop types are present (Figure 15). One is a medium grained pyroxene cumulate containing euhedral clinopyroxene and brown hornblende with interstitial quartz but no plagioclase. The second is a fine grained plagioclase cumulate that contains plagioclase and quartz as well as either brown hornblende but no pyroxene or both orthopyroxene and clinopyroxene with no amphibole. The third is a coarse grained pyroxene and hornblende cumulate. Amphibole and pyroxene grains are large, anhedral, filled with inclusions, and bounded by smaller grains of the same set of minerals. Near the center of the pluton, the only pyroxene present is orthopyroxene, while closer to West Birch Creek (Figure 2) there is only clinopyroxene. The unit is largely undeformed, although the larger grains of amphibole do contain substantial fracturing. While xenoliths are not generally recognized in the main body of the pluton, small xenoliths of metasediment are present near the edges. Also present in the pluton is a medium-grained rock primarily composed of subhedral to euhedral clinopyroxenes and amphiboles as well as interstitial quartz. This sample does not fit well into the other categories based on texture, but its mineralogy identified it as pyroxene-amphibole cumulate. Trauba (1975) also reported observing several grains of augite with rims of tremolite/actinolite.

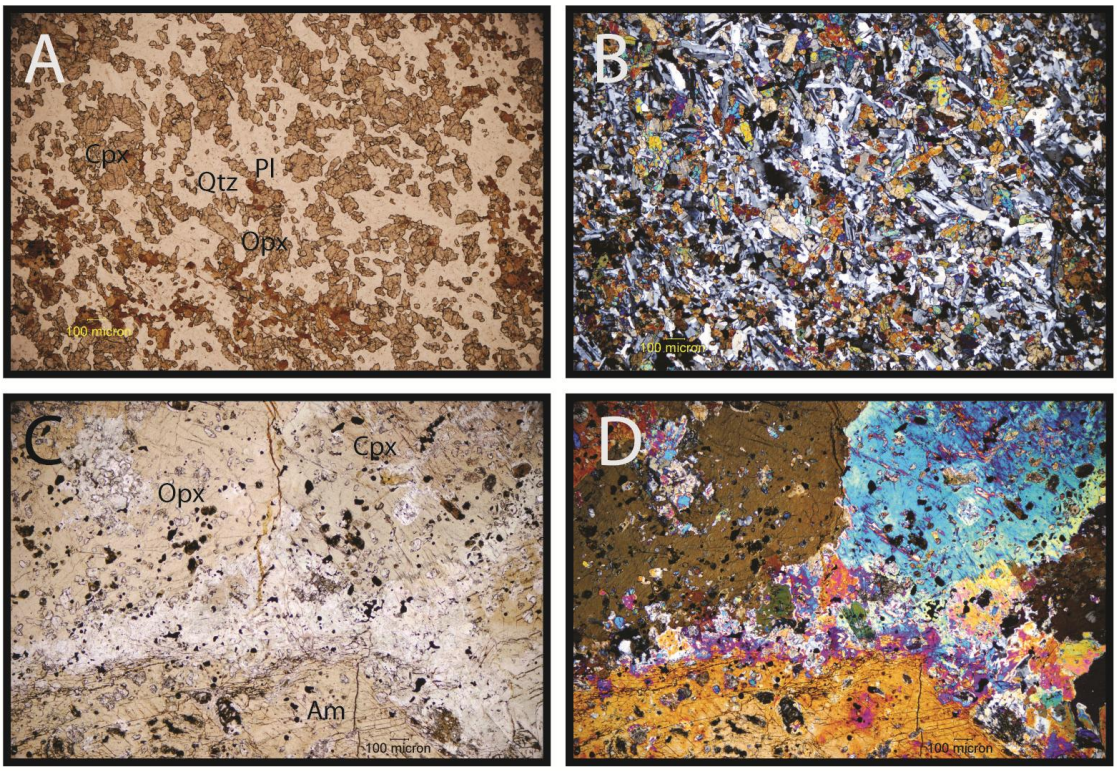

Figure 15. Selected photomicrographs of the Gabbronorite of Ridenor Canyon, fourth and final unit to be emplaced of the undeformed Carney Butte Stock. A) Plain polarized photomicrograph focused on the fine grained texture found throughout the pluton. B) Crossed polarized light image of A. C) Plain polarized photomicrograph of an amphibole, clinopyroxene, and an orthopyroxene in the pyroxene and amphibole cumulate (course grained) variety of the Ridenor Canyon pluton. D) Crossed polarized light image of C.

3d. U-Pb zircon geochronology

Zircons of the Trondhjemite of Pearson Creek are square in profile and show textural evidence for multiple phases of magmatic growth. These zircons show three distinct growths: a largely homogenous core surrounded by a zone of interior growth, and a thin rim of very different composition than the rest of the zircon filling fractures in the crystals (Figure 16). Twelve zircon grains from the Trondhjemite of Pearson Creek were analyzed; eight were in agreement on age, and four were not. Of those not in agreement, one yielded a strongly discordant age of 335 ±1.6 Ma. The other three yielded weakly discordant ages ranging from 163.3 to 162.3 Ma. Excluding these four grains as outliers yields an error-weighted average age of 159.46 ± 0.67Ma (n=8, MSWD of 1.8) (Figure 17, Table 2).

The Tonalite of California Gulch zircon grains are mostly anhedral fragments. Interior zonation is generally sector or patchy zoning, but there is some oscillatory zonation as well. They also display the occasional twinning cross in the rim growth rather than in the cores. Whereas most of the zircons showed complex zonation, analysis spots were preferentially chosen from the least complex zones (usually cores). Thirteen analyses were performed on twelve grains. One subeuhedral grain contained both a clearly defined core and separate rim, so both were analyzed (Figure 16). Of the thirteen total analyses only the core of the grain analyzed twice was not in agreement with the others and its analysis resulted in an age younger than that of the grain's rim. U/Pb analysis dates the tonalite at 152.45 ± 0.96 Ma (twelve analyses with an MSWD of 1.7) (Figure 17, Table 2).

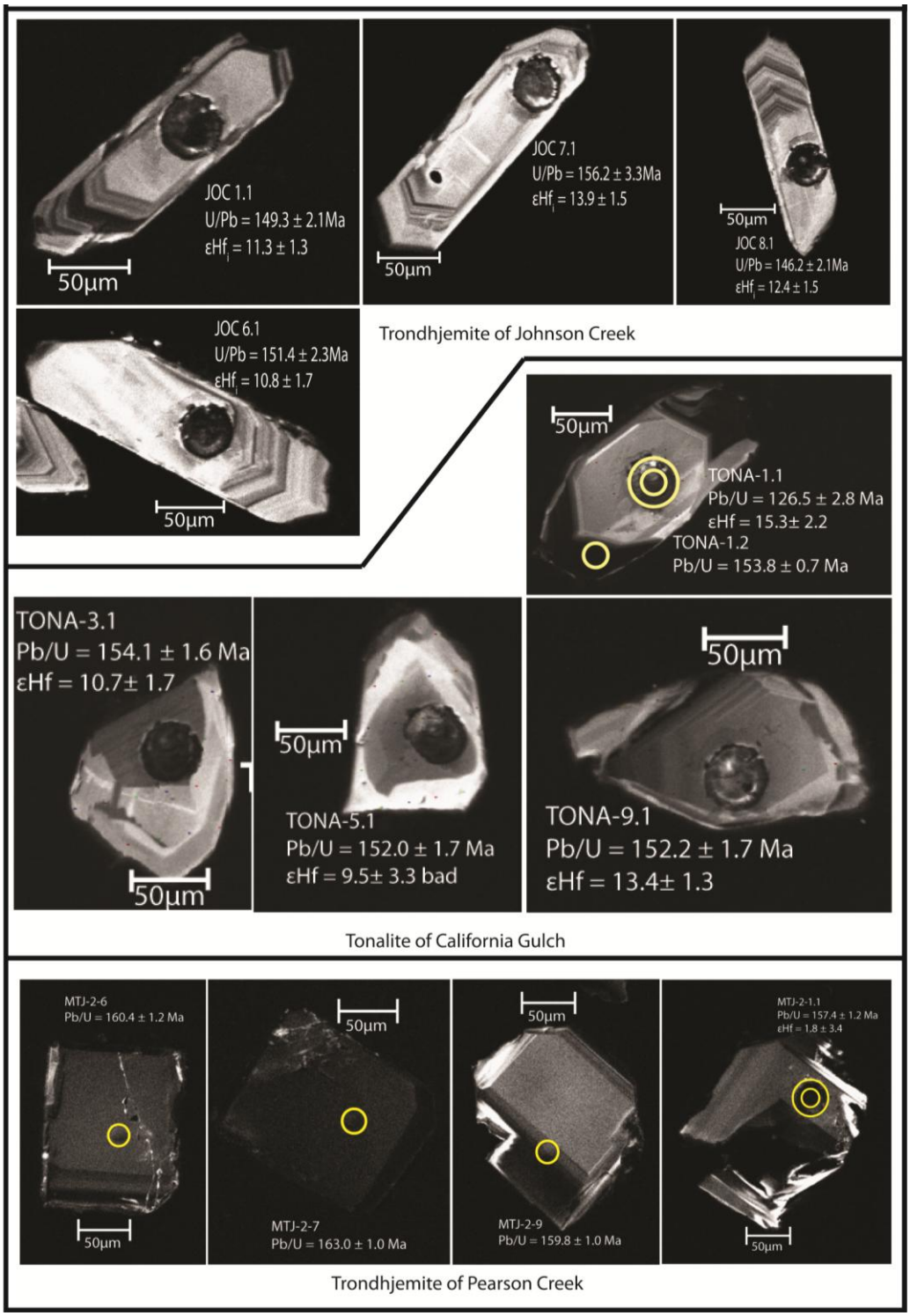

Figure 16. CL images of representative zircons from deformed plutons in the MHMC. Small yellow circles represent the 25µm diameter pit and location of SHRIMP analysis for U-Pb and trace element composition; the larger yellow circles represent the 50 µm diameter pit of an LA-ICP-MS Hf isotope analysis. All uncircled pits have a SHRIMP analysis at its center and an LA-ICP-MS analysis on the same location.

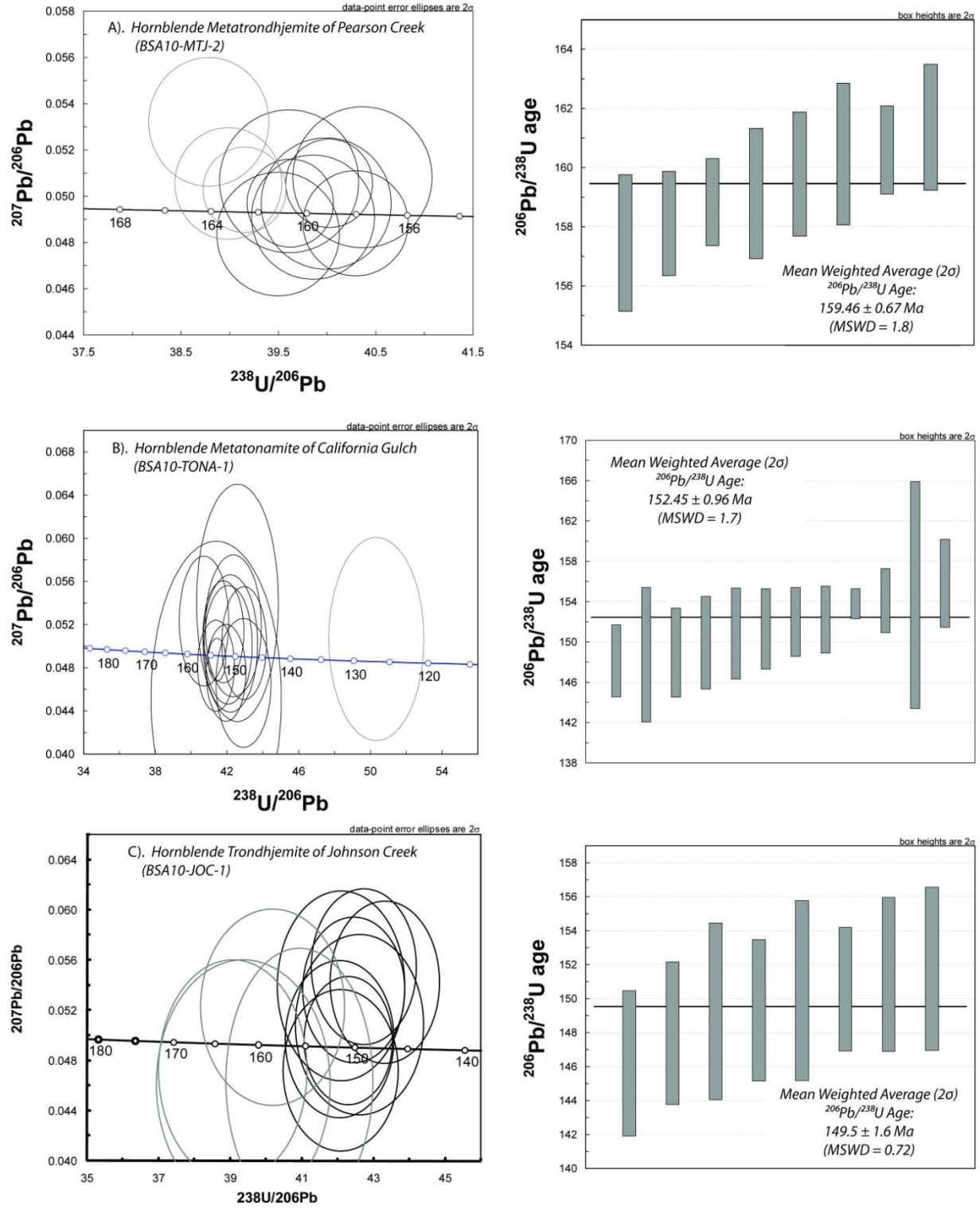

Figure 17. Tera-Wasserburg diagrams (on the left of each portion) and mean weighted averages of nonexcluded analyses (on the right of each portion) of zircons from the deformed plutonic units of the MHMC. Excluded analyses are in grey.

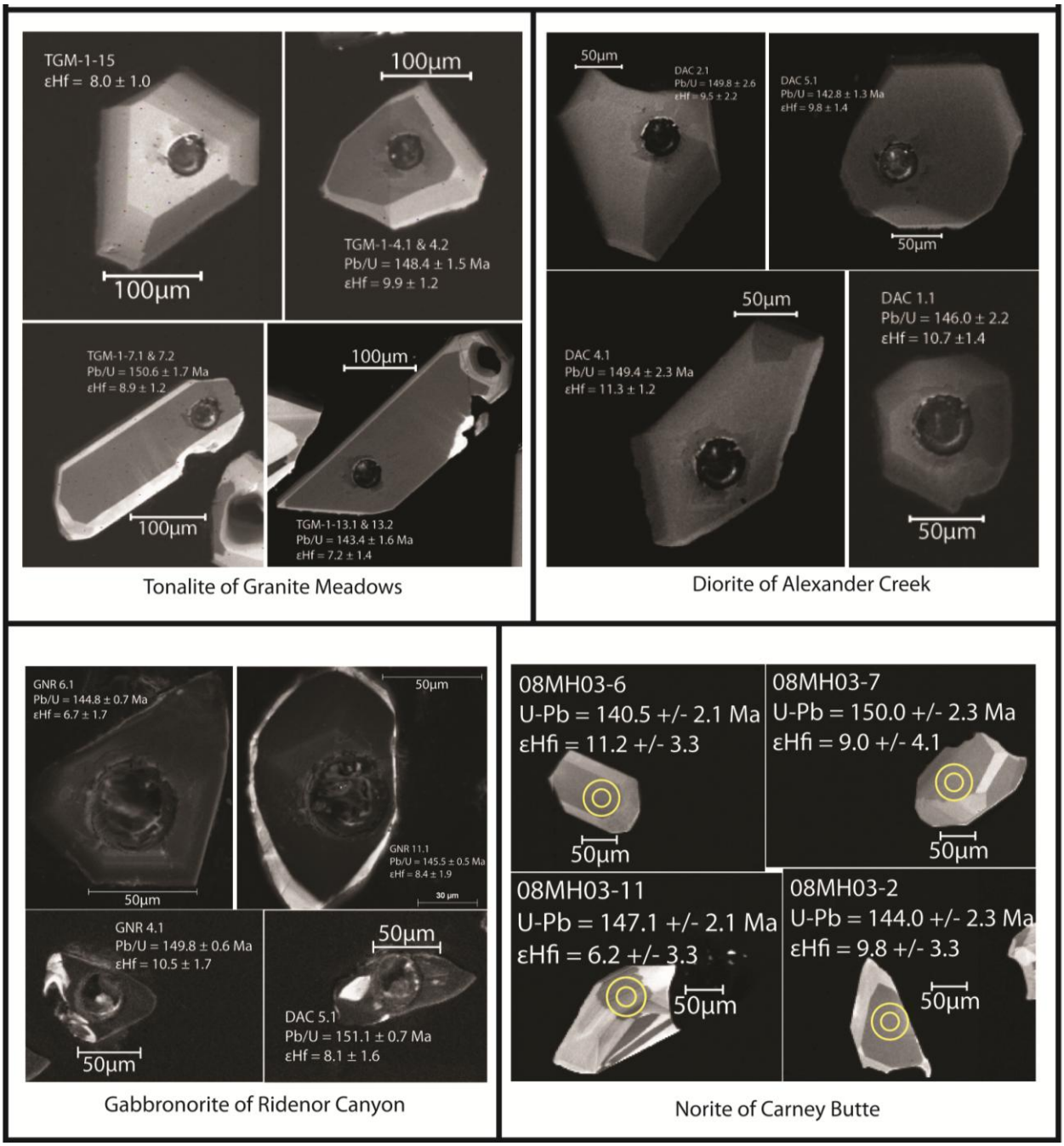

Figure 18. CL images of representative zircons from undeformed plutons of the Carney Butte Stock. Small yellow circles represent the 25µm diameter pit and location of SHRIMP analysis for U-Pb and trace element composition; the larger yellow circles represent the 50 µm diameter pit of an LA-ICP-MS Hf isotope analysis. All uncircled pits have a SHRIMP analysis at its center and an LA-ICP-MS analysis on the same location.

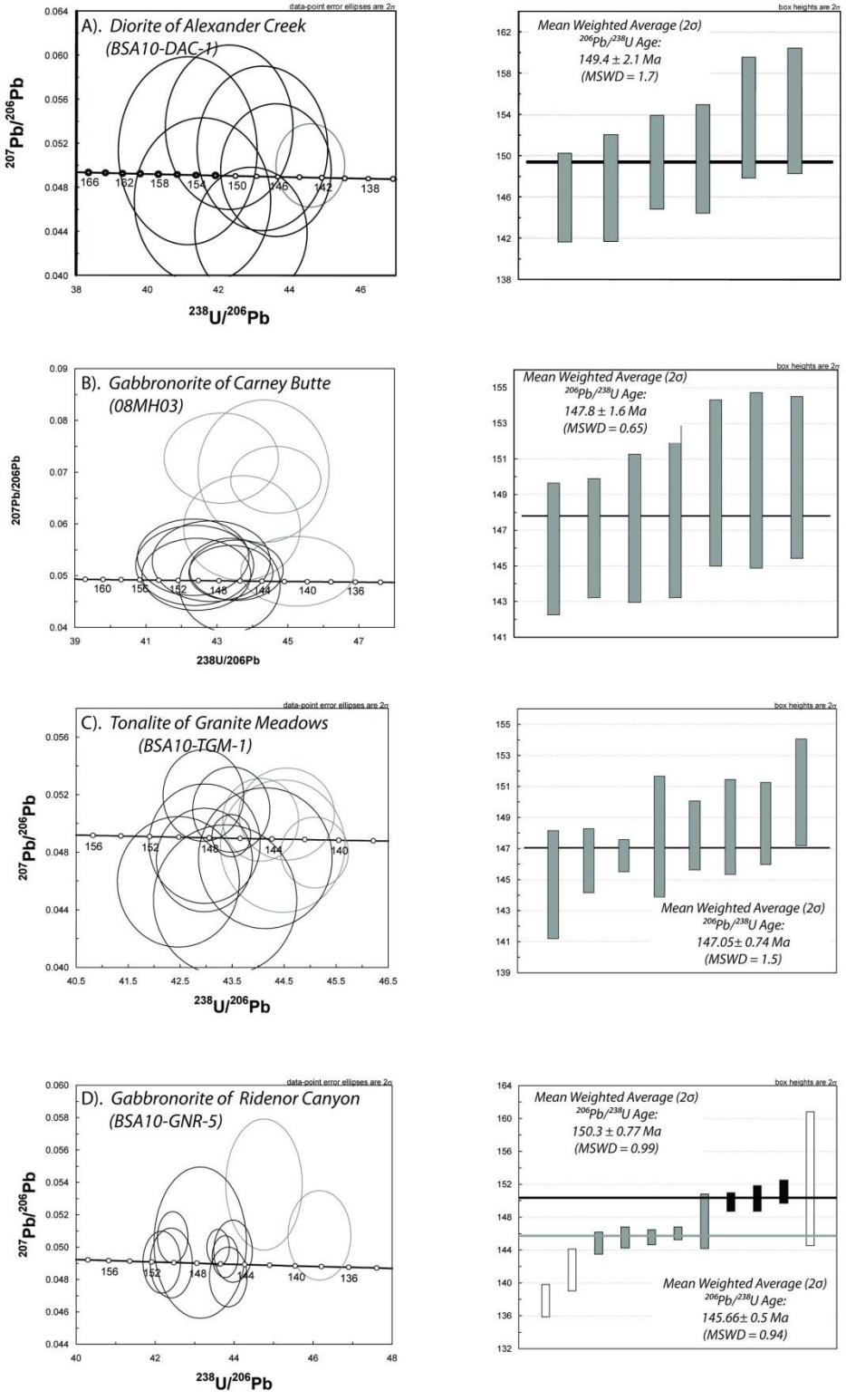

Figure 19. Tera-Wasserburg diagrams (left) and mean weighted averages of nonexcluded analyses (right) of zircons from the undeformed plutonic units of the Carney Butte Stock. Excluded analyses are in grey.

Table 2. U-Pb zircon SHRIMP mean weighted average ages for a sampling of seven plutonic units in the MHMC.

	Concentrations					Atomic Ratios[i]								
Analysis	U (ppm)	Th (ppm)	Th/U	Pb*[ii] (ppm)	f 206[iii] (%)	$^{238}U/^{206}Pb$[iv]	error (1σ)	$^{207}Pb/^{206}Pb$[iv]	error (1σ)	$^{206}Pb/^{238}U$[v]	error (1σ)	$^{206}Pb/^{238}U$[vi] (1σ)	error (1σ)	Weighted Average[vii] (2σ)
Trondhjemite of Pearson Creek														
MTJ-2.1	409.65	338.76	1.21	8.53	0.20	40.36	0.72	0.0508	2.45	0.0247	0.0002	157.44	1.16	**159.46 ±0.67**
MTJ-2.2	516.76	499.39	1.03	10.89	-0.12	39.50	0.65	0.0484	2.26	0.0253	0.0002	161.36	1.07	**MSWD = 1.8**
~~**MTJ-2.3**~~	~~1136.72~~	~~1486.90~~	~~0.76~~	~~23.96~~	~~0.12~~	~~39.15~~	~~0.44~~	~~0.0503~~	~~1.50~~	~~0.0255~~	~~0.0001~~	~~162.38~~	~~0.73~~	
MTJ-2.4	1050.45	1287.16	0.82	22.08	0.17	40.02	0.45	0.0506	1.55	0.0249	0.0001	158.83	0.73	
MTJ-2.5	697.29	729.26	0.96	14.60	-0.05	40.29	0.55	0.0488	1.90	0.0248	0.0001	158.11	0.88	
MTJ-2.6	398.48	279.72	1.42	8.36	0.17	39.61	0.74	0.0506	2.49	0.0252	0.0002	160.45	1.20	
~~**MTJ-2.7**~~	~~670.99~~	~~550.09~~	~~1.22~~	~~14.42~~	~~0.15~~	~~38.99~~	~~0.58~~	~~0.0505~~	~~1.95~~	~~0.0256~~	~~0.0002~~	~~163.02~~	~~0.95~~	
~~**MTJ-2.8**~~	~~510.40~~	~~427.39~~	~~1.19~~	~~11.01~~	~~0.49~~	~~38.78~~	~~0.65~~	~~0.0532~~	~~2.14~~	~~0.0257~~	~~0.0002~~	~~163.31~~	~~1.08~~	
MTJ-2.9	512.62	324.77	1.58	10.99	-0.02	39.86	0.65	0.0491	2.23	0.0251	0.0002	159.78	1.05	
MTJ-2.10	1052.44	1155.82	0.91	22.21	0.05	39.62	0.46	0.0497	1.56	0.0252	0.0001	160.59	0.74	
MTJ-2.11	450.05	325.23	1.38	9.67	0.06	39.99	0.68	0.0497	2.34	0.0250	0.0002	159.12	1.10	
~~**MTJ-2.12**~~	~~498.84~~	~~49.56~~	~~10.07~~	~~23.34~~	~~0.09~~	~~18.68~~	~~0.48~~	~~0.0539~~	~~1.42~~	~~0.0535~~	~~0.0003~~	~~335.88~~	~~1.61~~	
Tonalite of California Gulch														
~~**TONA-1.1**~~	~~65.64~~	~~26.34~~	~~2.49~~	~~1.11~~	~~0.26~~	~~50.33~~	~~2.15~~	~~0.0507~~	~~7.59~~	~~0.0198~~	~~0.0004~~	~~126.49~~	~~2.77~~	**152.45 ± 0.96**
TONA-1.2	947.81	390.02	2.43	19.94	-0.05	41.44	0.48	0.0488	1.66	0.0241	0.0001	153.78	0.75	**MSWD = 1.7**
TONA-2.1	16.79	3.17	5.30	0.34	-0.50	41.40	3.59	0.0452	13.17	0.0243	0.0009	154.63	5.62	
TONA-3.1	201.55	50.48	3.99	4.11	-0.12	41.39	1.01	0.0482	3.58	0.0242	0.0003	154.09	1.58	
TONA-4.1	103.76	21.46	4.84	2.18	0.40	40.72	1.38	0.0523	4.70	0.0245	0.0003	155.80	2.19	
TONA-5.1	176.75	78.72	2.25	3.56	0.28	41.80	1.11	0.0513	3.76	0.0239	0.0003	151.96	1.71	
TONA-6.1	44.15	10.09	4.38	0.86	0.63	42.58	2.19	0.0540	8.32	0.0233	0.0005	148.70	3.34	
TONA-7.1	124.47	47.06	2.65	2.52	0.13	42.06	1.30	0.0501	4.48	0.0237	0.0003	151.27	2.00	
TONA-8.1	99.77	23.43	4.26	1.96	-0.30	42.92	1.46	0.0466	5.23	0.0234	0.0004	148.92	2.21	
TONA-9.1	172.93	63.42	2.73	3.56	-0.20	41.94	1.08	0.0475	3.86	0.0239	0.0003	152.18	1.67	
TONA-10.1	142.22	31.05	4.58	2.88	0.16	42.96	1.18	0.0503	4.25	0.0232	0.0003	148.11	1.78	
TONA11.1	94.27	36.44	2.59	1.89	0.36	42.35	1.51	0.0519	5.17	0.0235	0.0004	149.91	2.30	
TONA-12.1	92.44	33.53	2.76	1.93	0.15	42.18	1.47	0.0502	5.17	0.0237	0.0004	150.81	2.26	

Table 2, Continued. U-Pb zircon SHRIMP mean weighted average ages for a sampling of seven plutonic units in the MHMC.

	Concentrations					Atomic Ratios[i]								
Analysis	U (ppm)	Th (ppm)	Th/U	Pb*[ii] (ppm)	f 206[iii] (%)	$^{238}U/^{206}Pb$[iv]	error (1σ)	$^{207}Pb/^{206}Pb$[iv]	error (1σ)	$^{206}Pb/^{238}U$[v]	error (1σ)	$^{206}Pb/^{238}U$[vi] (1σ)	error (1σ)	Weighted Average[vii] (2σ)
Trondhjemite of Johnson Creek														
JOC-1.1	99.13	35.07	2.83	2.10	0.58	42.44	1.37	0.0536	4.43	0.0234	0.0003	149.29	2.08	**149.5 ± 1.6**
JOC-2.1	149.68	56.38	2.65	2.96	0.07	42.29	1.19	0.0496	4.22	0.0236	0.0003	150.55	1.82	**MSWD = 0.72**
~~**JOC-3.1**~~	~~40.42~~	~~8.99~~	~~4.50~~	~~0.82~~	~~-0.40~~	~~39.36~~	~~2.52~~	~~0.0461~~	~~8.78~~	~~0.0255~~	~~0.0007~~	~~162.37~~	~~4.14~~	
JOC-4.1	82.15	23.94	3.43	1.61	0.62	42.09	1.73	0.0540	5.72	0.0236	0.0004	150.45	2.65	
~~**JOC-5.1**~~	~~69.10~~	~~17.87~~	~~3.87~~	~~1.42~~	~~0.38~~	~~40.18~~	~~2.04~~	~~0.0522~~	~~6.10~~	~~0.0248~~	~~0.0005~~	~~157.86~~	~~3.26~~	
JOC-6.1	96.53	27.78	3.48	1.96	0.08	42.04	1.48	0.0497	5.14	0.0238	0.0004	151.42	2.27	
~~**JOC-7.1**~~	~~48.99~~	~~15.08~~	~~3.25~~	~~1.02~~	~~-0.36~~	~~40.93~~	~~2.04~~	~~0.0463~~	~~9.38~~	~~0.0245~~	~~0.0005~~	~~156.17~~	~~3.28~~	
JOC-8.1	107.42	33.30	3.23	2.07	0.66	43.31	1.43	0.0542	4.86	0.0229	0.0003	146.18	2.14	
~~**JOC-9.1**~~	~~47.39~~	~~11.56~~	~~4.10~~	~~0.98~~	~~-0.26~~	~~39.07~~	~~2.16~~	~~0.0472~~	~~7.61~~	~~0.0257~~	~~0.0006~~	~~163.36~~	~~3.57~~	
JOC-10.1	73.73	21.91	3.37	1.41	0.23	42.60	1.72	0.0509	5.79	0.0234	0.0004	149.24	2.60	
JOC-11.1	115.24	37.96	3.04	2.24	0.82	42.72	1.39	0.0555	4.58	0.0232	0.0003	147.94	2.10	
JOC-12.1	82.21	25.26	3.25	1.67	-0.23	42.08	1.57	0.0472	5.58	0.0238	0.0004	151.75	2.41	
Diorite of Alexander Creek														
DAC-1.1	96.97	25.62	3.78	1.87	0.08	43.62	1.46	0.0496	4.96	0.0229	0.0003	146.02	2.16	**149.4 ± 2.1**
DAC-2.1	64.76	30.50	2.12	1.28	0.56	42.31	1.73	0.0535	5.71	0.0235	0.0004	149.77	2.64	**MSWD = 1.7**
DAC-3.1	68.83	18.36	3.75	1.35	0.32	43.24	1.74	0.0515	5.92	0.0231	0.0004	146.93	2.60	
DAC-4.1	87.88	27.99	3.14	1.72	-0.65	42.91	1.51	0.0439	5.57	0.0235	0.0004	149.45	2.28	
~~**DAC-5.1**~~	~~256.34~~	~~65.25~~	~~3.93~~	~~4.93~~	~~0.14~~	~~44.59~~	~~0.89~~	~~0.0500~~	~~3.11~~	~~0.0224~~	~~0.0002~~	~~142.79~~	~~1.29~~	
DAC-6.1	55.55	25.87	2.15	1.12	-0.29	41.54	1.89	0.0468	6.57	0.0241	0.0005	153.77	2.94	
DAC-7.1	52.00	25.99	2.00	1.07	0.27	41.13	1.94	0.0513	6.79	0.0242	0.0005	154.43	3.05	

Table 2, Continued. U-Pb zircon SHRIMP mean weighted average ages for a sampling of seven plutonic units in the MHMC.

	Concentrations					Atomic Ratios[i]								
Analysis	U (ppm)	Th (ppm)	Th/U	Pb*[ii] (ppm)	f 206[iii] (%)	$^{238}U/^{206}Pb$[iv]	error (1σ)	$^{207}Pb/^{206}Pb$[iv]	error (1σ)	$^{206}Pb/^{238}U$[v]	error (1σ)	$^{206}Pb/^{238}U$[vi] (1σ)	error (1σ)	Weighted Average[vii] (2σ)
Norite of Carney Butte														
08MHO3-1	n.d.	n.d.	n.d.	1.21	0.48	42.84	1.58	0.0528	6.03	0.0232	0.0004	148.05	2.40	**147.8 ± 1.6**
~~**08MHO3-2**~~	~~n.d.~~	~~n.d.~~	~~n.d.~~	~~1.25~~	~~1.30~~	~~43.71~~	~~1.53~~	~~0.0592~~	~~6.96~~	~~0.0226~~	~~0.0004~~	~~143.96~~	~~2.32~~	**MSWD = 0.65**
08MHO3-3	n.d.	n.d.	n.d.	1.34	0.57	42.33	1.51	0.0536	5.64	0.0235	0.0004	149.67	2.32	
~~**08MHO3-4**~~	~~n.d.~~	~~n.d.~~	~~n.d.~~	~~2.20~~	~~2.47~~	~~44.66~~	~~1.16~~	~~0.0685~~	~~3.86~~	~~0.0218~~	~~0.0003~~	~~139.26~~	~~1.67~~	
~~**08MHO3-5**~~	~~n.d.~~	~~n.d.~~	~~n.d.~~	~~1.37~~	~~2.99~~	~~43.12~~	~~1.52~~	~~0.0727~~	~~4.89~~	~~0.0225~~	~~0.0004~~	~~143.42~~	~~2.27~~	
~~**08MHO3-6**~~	~~n.d.~~	~~n.d.~~	~~n.d.~~	~~1.37~~	~~0.25~~	~~45.27~~	~~1.44~~	~~0.0509~~	~~5.41~~	~~0.0220~~	~~0.0003~~	~~140.49~~	~~2.06~~	
08MHO3-7	n.d.	n.d.	n.d.	1.40	0.15	42.42	1.48	0.0503	5.65	0.0235	0.0004	149.97	2.26	
08MHO3-8	n.d.	n.d.	n.d.	2.40	0.20	43.40	1.11	0.0506	4.24	0.0230	0.0003	146.57	1.67	
08MHO3-9	n.d.	n.d.	n.d.	1.23	0.37	42.37	1.60	0.0520	6.07	0.0235	0.0004	149.81	2.45	
~~**08MHO3-10**~~	~~n.d.~~	~~n.d.~~	~~n.d.~~	~~1.15~~	~~2.68~~	~~44.32~~	~~1.70~~	~~0.0702~~	~~8.01~~	~~0.0220~~	~~0.0004~~	~~140.03~~	~~2.57~~	
08MHO3-11	n.d.	n.d.	n.d.	1.70	-0.10	43.36	1.34	0.0482	7.69	0.0231	0.0003	147.13	2.07	
08MHO3-12	n.d.	n.d.	n.d.	1.97	0.26	43.55	1.24	0.0510	4.66	0.0229	0.0003	145.98	1.84	
Tonalite of Granite Meadows														
TGM-1.1	1703.51	390.58	4.36	33.19	0.02	43.48	0.35	0.0492	1.22	0.0230	0.0001	146.53	0.52	**147.05 ± 0.74**
TGM-2.1	124.83	74.98	1.66	2.43	-0.54	43.36	1.30	0.0447	4.78	0.0232	0.0003	147.76	1.94	**MSWD = 1.5**
TGM-3.1	382.90	210.33	1.82	7.51	0.37	42.95	0.74	0.0519	2.50	0.0232	0.0002	147.84	1.11	
TGM-4.1	202.80	123.89	1.64	3.97	-0.05	42.97	1.02	0.0486	3.49	0.0233	0.0002	148.38	1.53	
TGM-5.1	142.68	90.62	1.57	2.79	-0.17	44.14	1.19	0.0476	4.20	0.0227	0.0003	144.66	1.74	
TGM-6.1	407.99	224.52	1.82	8.18	0.25	43.48	0.70	0.0510	2.37	0.0229	0.0002	146.20	1.03	
TGM-7.1	163.33	99.34	1.64	3.22	-0.39	42.47	1.13	0.0459	4.03	0.0236	0.0003	150.62	1.72	
TGM-8.1	263.04	152.32	1.73	5.17	-0.20	42.97	0.88	0.0475	3.09	0.0233	0.0002	148.60	1.32	
~~**TGM-9.1**~~	~~430.14~~	~~236.70~~	~~1.82~~	~~8.40~~	~~0.17~~	~~44.05~~	~~0.68~~	~~0.0503~~	~~2.34~~	~~0.0227~~	~~0.0002~~	~~144.47~~	~~0.99~~	
~~**TGM-10.1**~~	~~557.67~~	~~291.15~~	~~1.92~~	~~10.69~~	~~-0.11~~	~~45.09~~	~~0.59~~	~~0.0480~~	~~2.10~~	~~0.0222~~	~~0.0001~~	~~141.58~~	~~0.84~~	
~~**TGM-11.1**~~	~~345.37~~	~~188.49~~	~~1.83~~	~~7.03~~	~~0.22~~	~~44.55~~	~~0.84~~	~~0.0507~~	~~2.58~~	~~0.0224~~	~~0.0002~~	~~142.80~~	~~1.21~~	
~~**TGM-12.1**~~	~~1697.90~~	~~369.69~~	~~4.59~~	~~32.29~~	~~-0.01~~	~~45.12~~	~~0.35~~	~~0.0488~~	~~1.25~~	~~0.0222~~	~~0.0001~~	~~141.33~~	~~0.51~~	
~~**TGM-13.1**~~	~~163.21~~	~~102.97~~	~~1.58~~	~~3.15~~	~~-0.06~~	~~44.47~~	~~1.10~~	~~0.0484~~	~~3.88~~	~~0.0225~~	~~0.0003~~	~~143.44~~	~~1.60~~	

Table 2, Continued. U-Pb zircon SHRIMP mean weighted average ages for a sampling of seven plutonic units in the MHMC.

	Concentrations					Atomic Ratios[i]								
Analysis	U (ppm)	Th (ppm)	Th/U	Pb*[ii] (ppm)	f 206[iii] (%)	$^{238}U/^{206}Pb$[iv]	error (1σ)	$^{207}Pb/^{206}Pb$[iv]	error (1σ)	$^{206}Pb/^{238}U$[v]	error (1σ)	$^{206}Pb/^{238}U$[vi] (1σ)	error (1σ)	Weighted Average[vii] (2σ)
Gabbro-norite of Ridenor Canyon														
Population 1														
GNR-2.1	798.27	209.08	3.82	16.14	0.00	42.41	0.52	0.0490	1.80	0.0236	0.0001	150.25	0.79	**150.3 ± 0.77**
GNR-4.1	1504.48	733.59	2.05	29.63	0.20	42.45	0.37	0.0506	1.27	0.0235	0.0001	149.82	0.57	**MSWD = 0.99**
GNR-5.1	987.00	415.00	2.38	19.59	0.00	42.17	0.46	0.0491	1.59	0.0237	0.0001	151.09	0.70	
Population 2														
GNR-1.1	172.94	34.74	4.98	3.40	0.16	43.14	1.11	0.0503	3.80	0.0231	0.0003	147.48	1.66	**145.66 ± 0.5**
GNR-3.1	992.51	317.20	3.13	19.03	-0.10	43.85	0.44	0.0482	1.56	0.0228	0.0001	145.50	0.65	**MSWD = 0.94**
GNR-6.1	965.16	246.98	3.91	18.51	0.10	43.97	0.45	0.0497	1.58	0.0227	0.0001	144.82	0.67	
GNR-10.1	2869.57	1180.47	2.43	55.60	0.13	43.60	0.27	0.0500	0.92	0.0229	0.0001	146.02	0.39	
GNR-11.1	2170.66	1072.14	2.02	42.34	0.06	43.77	0.31	0.0494	1.07	0.0228	0.0001	145.53	0.45	
Baddeleyite														
~~**GNR-9.1**~~	~~254.12~~	~~64.68~~	~~3.93~~	~~5.13~~	~~0.63~~	~~44.76~~	~~0.70~~	~~0.0539~~	~~2.23~~	~~0.0222~~	~~0.0002~~	~~141.56~~	~~1.28~~	
~~**GNR-8.1**~~	~~493.99~~	~~155.46~~	~~3.18~~	~~9.77~~	~~0.24~~	~~46.16~~	~~0.88~~	~~0.0507~~	~~3.07~~	~~0.0216~~	~~0.0002~~	~~137.82~~	~~0.98~~	
~~**GNR-12.1**~~	~~33.08~~	~~11.60~~	~~2.85~~	~~0.90~~	~~11.96~~	~~36.74~~	~~2.38~~	~~0.1444~~	~~6.08~~	~~0.0240~~	~~0.0006~~	~~152.66~~	~~4.07~~	

[i] Errors are reported at 1σ level and refer to last digits.
[ii] Radiogenic 206Pb.
[iii] Fraction of total 206Pb that is common 206Pb.
[iv] Uncorrected ratios.
[v] 207Pb corrected ratios using age-appropriate Pb isotopic composition of Stacey and Kramers (1975).
[vi] 207Pb corrected age; spot analyses with strikethrough were excluded in age calculation due to open system behavior and/or analytical problems.

Trondhjemite of Johnson Creek zircons show significant zonation, but are euhedral with unzoned cores containing the occasional twinning cross (Figure 16; Appendix B). The rims contain repeated narrow growth zones. Twelve zircon grains from the Trondhjemite of Johnson Creek were analyzed; four grains have ages that did not agree with the other eight (Table 2). Analyses are from both rims of grains (6 analyses: 2.1, 3.1, 4.1, 9.1, 11.1, and 12.1) and cores of other grains (another 6 analyses: 1.1, 5.1, 6.1, 7.1, 8.1, and 10.1). No correlation exists between the ages of the zircons and the region of the zircons analyzed. Whereas the four grains with ages older than that of the general population did not correspond to a sampling location, they did contain anomalously low amounts of uranium (40.4 to 69.1 ppm), thorium (9 to 17.9 ppm), and radiogenic ^{206}Pb (0.8 to 1.4 ppm) relative to the majority of the population (ranges of 73.7-149.7 ppm, 21.9-56.4ppm, and 1.4-3 ppm, respectively). The analyses of the majority yield results with an error-weighted average age of 149.5 ± 1.6 Ma (eight concordant grains with an MSWD of 0.72) (Figure 17, Table 2).

The Diorite of Alexander Creek zircons are largely rounded and show a core and one or two periods of further growth (Figure 18). The cores are strongly irregular in shape. A few have some sector zoning and others have rim zonation (with a few thick zones), but generally the zircons vary so little in terms of composition that it is difficult to discern. Seven analyses were performed on seven grains of zircon, with only one anomalous age (142.8 ± 1.3Ma) that had corresponding anomalously high U (256.3 ppm), Th (65.3 ppm), and ^{206}Pb* (4.9 ppm) relative to those of the general zircon population (52-97 ppm, 18.3-30.5 ppm, and 1.07-1.87 ppm, respectively). The diorite is 149.4 ± 2.1 Ma in age (6 concordant zircons with an MSWD of 1.7) (Figure 19, Table 2).

In the Norite of Carney Butte, twelve zircon grains were analyzed (one analysis per grain); five grains demonstrated ages in disagreement with those of the larger population. The five outlier grains showed significantly younger ages than the main zircon population. The outlier grains range in age from ~144 to ~139.3 Ma, in contrast to the 147.8 ± 1.6 Ma (seven grains with an MSWD of 0.65) age of the main population. The differing age population does not correspond to any geochemical or textural population or trait observed. While morphologically complex, these zircons show no more than two growth zones. These zircons are largely fragmentary and anhedral, although one is subhedral-rounded and another is half of a euhedral-tabular crystal (Figure 18). Most contain a homogeneous core, although their shapes vary with patchy or sector zoning.

Zircons in the undeformed plutons of the MHMC are characterized by less complex growth zoning than those in deformed plutons (Figures 16 and 18). The zircons of the Tonalite of Granite Meadows are composed of euhedral to subhedral grains that show multiple morphologies ranging from tabular (a few may be acicular) to more rounded or stubby. They are fairly simple in terms of zonation, usually showing only a homogeneous core with a single growth rim. A few have thin, oscillating rims that do not vary much in composition. Thirteen analyses were taken from thirteen zircon grains. Five of these grains showed ages that did not agree with those of the general population of zircons. The five anomalous aged grains do not correspond to any other geochemical or textural grouping, although they are all significantly younger than the general zircon population (~147 Ma). Pb/U analysis dates this tonalite at 147.05 +/- 0.74 Ma (n=8, MSWD of 1.5) (Figure 19, Table 2).

The zircons of the Gabbronorite of Ridenor Canyon are primarily anhedral although some subhedral grains are present. Most of these grains have been largely resorbed. In terms of

composition, these grains show two to three preserved zonation events. What zoning is present is sector zoning, although a few have thin growth zones around a resorbed and compositionally distinct core. Zircons are not abundant in this sample and the grains are small (~60µm by 100µm). Eleven grains from the Gabbronorite of Ridenor Canyon were analyzed. Three grains are baddeleyite and are not included in any age calculations or interpretations. Of the remaining eight zircon grains two age populations are present: an older group with an age of 150.3 ± 0.77 Ma (n=3, MSWD of 0.99) and a younger population of age 145.66 ± 0.50 Ma (n=4, MSWD of 0.94) (Figure 18 and 19, Table 2). There is no clear morphological, textural, or geochemical distinction between the two age populations.

In all, seven plutonic units have Pb/U age data (Table 2). Deformed plutons range in age from 159.46 ± 0.67 Ma to 149.5 ± 1.6 Ma. Undeformed plutons range in age from 149.4 ± 2.1 Ma to 145.66 ± 0.50 Ma. At least twelve grains were analyzed from each unit except for the Diorite of Alexander Creek, although some analyses indicate an open system behavior and are excluded from the final mean weighted average ages. A summary of Pb/U age data, rock types, deformation, and cross-cutting unit relationships in the MHMC is provided in Table 3.

Table 3. A summary of Pb/U age data, rock types, deformation, and cross-cutting unit relationships in the MHMC.

Unit Name	Rock Type	Age (Ma)	Basis for Age	Relationship to Other Units
Schist of Yellow Jacket Road	Biotite-Garnet Schist	Probably older than the Hornblendite	Uncertain, Constrained by intrusive contact	Intruded by Metagabbro, possibly Hornblendite, and interfolded with Keratophyre
Keratophyre of Pearson Creek	Hornblende-Chlorite Schist	Older than 159.46	Uncertain, Constrained by intrusive contact	Intruded by Trondhjemite of Pearson Creek
Trondhjemite of Pearson Creek	Hornblende Trondhjemite	159.46 ± 0.67	U-Pb - Zircon	Intrudes the Keratophyre of Pearson Creek
Hornblendite	Hornblendite to Pyroxenite Cumulate	Older than Metagabbro	Uncertain, Constrained by intrusive contact	Intruded by the Metagabbro
Metagabbro	Quartz-Hornblende Gabbro	Older than 152.45	Uncertain, Constrained by intrusive contact	Intruded by the Tonalite of California Gulch
Tonalite of California Gulch	Biotite Bearing, Hornblende Tonalite	152.45 ± 0.96	U-Pb - Zircon	Intrudes Metagabbro and intruded by Trondhjemite of Johnson Creek
Amphibolite Gneiss	Variable	between Metagabbro and 149.5	Intrusive contact	Intruded by Trondhjemite of Johnson Creek and intercalated with Metagabbro
Trondhjemite of Johnson Creek	Hornblende Trondhjemite	149.5 ± 1.6	U-Pb - Zircon	Intrudes the Amphibolite Gneiss
End of Deformational Period				
Diorite of Alexander Creek	Biotite-Bearing, Quartz-Hornblende Diorite	149.4 ± 2.1	U-Pb - Zircon	Intrudes the Schist of Yellow Jacket Road, Metagabbro, and Hornblendite
Norite of Carney Butte	Hornblende Norite	147.8 ± 1.6	U-Pb - Zircon	Intrudes the Diorite of Alexander Creek
Tonalite of Granite Meadows	Hornblende Tonalite to Hornblende Granodiorite	147.05 ± 0.74	U-Pb - Zircon	Geochemically and minerologically similar dikes intrude the Schist of Yellow Jacket Road
Gabbronorite of Ridenor Canyon	Hornblende Gabbronorite	145.66 ± 0.50	U-Pb - Zircon	Intrudes the Schist of Yellow Jacket Road, the Keratophyre of Pearson Creek, the Hornblendite, and the Metagbbro

3e. Hf_i analysis

The seven zircon separates analyzed for Pb/U ages were also analyzed for Hf isotopic content (see Table 4 for full Hf analysis results and Table 5 for Hf analysis results summary). The Trondhjemite of Pearson Creek showed significant isobaric interference and did not yield any acceptable analyses of its zircons. These values exclude any analyses that show significant isobaric interference. At least 15 grains were analyzed from each separate of zircons for this data set. Appendix C shows a table of other εHf_i analysis values necessary for the calculation of percent correction due to isobaric interference.

Table 4. Zircon Lu-Hf isotopic data for seven igneous units of the MHMC.

Zircon Spot	Hf (V)	$^{176}Hf/^{177}Hf$	Error (1σ)	$^{176}Lu/^{177}Hf$	Error (1σ)	Tchur	Tdm (1)	ε(0)	ε(t)	Error (2 σ)	Maximum ε Range
Trondhjemite of Pearson Creek											**n.a.**
MTJ-2-1	1.70	0.2828	4.90E-05	1.10E-02	7.80E-05	0.04	0.91	-0.64	**1.78**	**3.51**	
MTJ-2-2	1.61	0.2828	7.70E-05	1.41E-02	4.40E-05	-0.05	0.94	0.67	**2.75**	**5.48**	
MTJ-2-3	1.39	0.2829	5.70E-05	1.20E-02	9.00E-05	-0.23	0.72	3.25	**5.56**	**4.08**	
MTJ-2-13	1.81	0.2830	3.40E-05	8.99E-03	8.70E-05	-0.43	0.46	7.00	**9.63**	**2.45**	
Tonalite of California Gulch											**18.57 - 8.84**
TONA 1.1_2	0.88	0.2831	3.10E-05	2.08E-03	1.00E-04	-0.58	0.17	12.06	**15.25**	**2.24**	
TONA 2.1_2	0.98	0.2830	2.80E-05	1.88E-03	1.80E-04	-0.37	0.35	7.64	**10.84**	**2.04**	
TONA 3.1_2	1.01	0.2830	2.30E-05	2.26E-03	1.60E-05	-0.36	0.36	7.50	**10.66**	**1.66**	
TONA 4.1_2	0.91	0.2831	2.60E-05	1.06E-03	2.90E-05	-0.54	0.18	11.63	**14.93**	**1.87**	
TONA 5.1_2		0.2830	4.60E-05	4.26E-03	2.80E-05	-0.34	0.42	6.61	**9.58**	**3.29**	
TONA 6.1_2	0.88	0.2830	3.50E-05	1.67E-03	2.00E-05	-0.34	0.36	7.25	**10.48**	**2.51**	
TONA 7.1_2	1.02	0.2831	2.60E-05	1.02E-03	1.80E-05	-0.52	0.20	11.03	**14.33**	**1.87**	
TONA 8.1_2	0.97	0.2831	1.80E-05	1.96E-03	4.40E-05	-0.53	0.21	10.96	**14.16**	**1.31**	
TONA 9.1_2	0.95	0.2831	2.30E-05	1.17E-03	2.30E-05	-0.47	0.24	10.11	**13.39**	**1.66**	
TONA 10.1_2	0.99	0.2830	2.70E-05	6.38E-04	6.40E-05	-0.35	0.33	7.67	**11.01**	**1.95**	
TONA 11.1_2	0.81	0.2830	2.00E-05	1.55E-03	1.10E-05	-0.33	0.37	7.00	**10.24**	**1.44**	
TONA 12.1_2	0.92	0.2831	2.50E-05	8.94E-04	5.30E-05	-0.58	0.14	12.52	**15.83**	**1.81**	
TONA 13_2	0.88	0.2832	3.20E-05	1.40E-03	2.20E-05	-0.62	0.12	13.01	**16.27**	**2.30**	
TONA 14_2	0.88	0.2830	2.10E-05	1.77E-03	7.70E-05	-0.43	0.29	9.09	**12.31**	**1.53**	
TONA 15_2	0.86	0.2831	2.50E-05	2.13E-03	1.10E-04	-0.46	0.27	9.58	**12.76**	**1.82**	
Trondhjemite of Johnson Creek											**15.4 - 9.22**
JOC 1.1_2	1.11	0.2830	1.70E-05	2.06E-03	9.00E-05	-0.39	0.33	8.17	**11.29**	**1.26**	
JOC 2.1_2	1.25	0.2830	1.80E-05	1.66E-03	1.00E-05	-0.35	0.36	7.36	**10.52**	**1.31**	
JOC 3.1_2	1.32	0.2830	1.60E-05	1.70E-03	6.70E-05	-0.37	0.34	7.85	**11.01**	**1.18**	
JOC 4.1_2	1.21	0.2830	1.90E-05	2.03E-03	2.90E-05	-0.39	0.33	8.13	**11.26**	**1.39**	
JOC 5.1_2	1.08	0.2830	1.60E-05	2.30E-03	3.50E-05	-0.36	0.36	7.32	**10.42**	**1.18**	
JOC 6.1_2	1.09	0.2830	2.40E-05	2.28E-03	3.50E-05	-0.38	0.35	7.74	**10.84**	**1.74**	
JOC 7.1_2	1.08	0.2831	2.00E-05	1.82E-03	3.80E-05	-0.51	0.22	10.75	**13.90**	**1.46**	
JOC-8.1_2	1.06	0.2830	2.10E-05	2.08E-03	2.90E-05	-0.45	0.28	9.26	**12.39**	**1.53**	
JOC-9.1_2	1.20	0.2830	1.70E-05	1.65E-03	4.30E-05	-0.41	0.30	8.70	**11.86**	**1.25**	
JOC-10.1_2	1.13	0.2830	2.30E-05	2.00E-03	5.10E-05	-0.36	0.36	7.39	**10.52**	**1.68**	
JOC-11.1_2	1.15	0.2831	2.10E-05	1.77E-03	1.80E-05	-0.51	0.22	10.61	**13.76**	**1.53**	
JOC-12.1_2	1.14	0.2830	1.60E-05	2.20E-03	4.30E-05	-0.36	0.35	7.53	**10.64**	**1.18**	
JOC-13_2	1.14	0.2830	2.20E-05	2.03E-03	5.50E-05	-0.39	0.33	8.13	**11.26**	**1.61**	
JOC-14_2	1.29	0.2830	2.30E-05	1.71E-03	3.60E-05	-0.44	0.28	9.26	**12.42**	**1.67**	
JOC-15_2	1.12	0.2831	1.90E-05	2.11E-03	8.50E-05	-0.56	0.19	11.60	**14.72**	**1.40**	

Table 4, Continued. Zircon Lu-Hf isotopic data for seven igneous units of the MHMC.

Zircon Spot	Hf (V)	$^{176}Hf/^{177}Hf$	Error (1σ)	$^{176}Lu/^{177}Hf$	Error (1σ)	Tchur	Tdm (1)	ε(0)	ε(t)	Error (2 σ)	Maximum ε Range
Diorite of Alexander Creek											**15.47 - 6.52**
DAC 1.1_2	1.09	0.2830	1.90E-05	3.85E-04	7.80E-06	-0.35	0.34	7.57	**10.77**	**1.44**	
DAC 2.1_2	0.98	0.2830	3.00E-05	4.11E-04	4.20E-06	-0.29	0.38	6.33	**9.53**	**2.22**	
DAC 3.1_2	0.97	0.2829	2.70E-05	3.07E-04	9.90E-07	-0.24	0.42	5.34	**8.54**	**2.00**	
DAC 4.1_2	0.89	0.2830	1.60E-05	2.90E-04	3.60E-06	-0.37	0.31	8.10	**11.31**	**1.23**	
DAC 5.1_2	0.94	0.2830	1.90E-05	2.83E-04	5.70E-06	-0.30	0.38	6.54	**9.75**	**1.44**	
DAC 6.1_2	0.83	0.2830	2.70E-05	4.98E-04	1.50E-06	-0.36	0.32	7.89	**11.07**	**2.00**	
DAC 7.1_2	0.93	0.2831	2.30E-05	7.63E-04	1.30E-05	-0.49	0.22	10.61	**13.77**	**1.72**	
DAC 7.1_2	0.93	0.2831	2.30E-05	7.63E-04	1.30E-05	-0.49	0.22	10.61	**13.77**	**1.72**	
DAC 8_2	0.98	0.2830	2.00E-05	4.76E-04	2.30E-06	-0.29	0.38	6.37	**9.55**	**1.51**	
DAC 9_2	0.86	0.2830	2.30E-05	3.53E-04	4.20E-06	-0.36	0.32	7.96	**11.16**	**1.72**	
DAC 10_2	0.87	0.2831	2.30E-05	3.35E-04	1.50E-05	-0.46	0.24	10.01	**13.21**	**1.72**	
DAC 11_2	0.95	0.2829	2.10E-05	4.38E-04	4.40E-06	-0.23	0.43	5.13	**8.32**	**1.58**	
DAC 12_2	0.89	0.2829	2.50E-05	3.49E-04	7.10E-06	-0.25	0.42	5.48	**8.68**	**1.86**	
DAC 13_2	0.95	0.2830	1.80E-05	4.28E-04	6.80E-06	-0.38	0.31	8.24	**11.43**	**1.37**	
DAC 14_2	0.94	0.2830	2.50E-05	8.37E-04	7.00E-06	-0.33	0.36	7.11	**10.26**	**1.86**	
DAC 15_2	0.96	0.2830	2.30E-05	2.39E-04	1.30E-05	-0.38	0.30	8.38	**11.59**	**1.72**	
Norite of Carney Butte											**17.2 - 1.6**
08MH03 2	2.16	0.2830	9.21E-05	9.96E-04		-309.68	360.66	6.65	**9.84**	**3.26**	
08MH03 3	2.24	0.2829	1.47E-04	6.54E-04		-166.48	478.41	3.62	**6.84**	**5.20**	
08MH03 4	2.20	0.2830	7.58E-05	2.02E-03		-314.94	374.90	6.55	**9.64**	**2.68**	
08MH03 5	2.18	0.2829	9.65E-05	6.42E-04		-250.26	405.77	5.43	**8.66**	**3.41**	
08MH03 6	1.95	0.2830	9.29E-05	5.62E-04		-365.91	304.39	7.95	**11.19**	**3.28**	
08MH03 7	2.17	0.2829	1.16E-04	6.89E-04		-264.34	394.40	5.73	**8.95**	**4.10**	
08MH03 8	1.96	0.2829	9.23E-05	1.45E-03		-272.40	401.02	5.77	**8.92**	**3.26**	
08MH03 10	2.25	0.2829	1.20E-04	9.41E-04		-119.94	523.52	2.58	**5.78**	**4.23**	
08MH03 11	2.12	0.2829	9.45E-05	1.00E-03		-141.43	506.03	3.04	**6.23**	**3.34**	
08MH03 12	2.24	0.2830	1.12E-04	1.07E-03		-388.01	294.48	8.30	**11.49**	**3.98**	
08MH03 13	2.07	0.2830	9.20E-05	1.08E-03		-279.59	388.16	5.99	**9.17**	**3.25**	
08MH03 14	2.14	0.2831	1.26E-04	1.02E-03		-446.37	243.14	9.56	**12.75**	**4.44**	
08MH03 15	2.08	0.2830	1.06E-04	5.32E-04		-339.38	326.79	7.39	**10.63**	**3.73**	
08MH03 16	2.20	0.2830	1.57E-04	7.01E-04		-312.35	353.13	6.76	**9.99**	**5.54**	
08MH03 17	2.02	0.2829	1.28E-04	1.11E-03		-241.00	421.93	5.16	**8.34**	**4.52**	
08MH03 18	2.30	0.2829	1.19E-04	6.87E-04		-224.66	428.67	4.87	**8.09**	**4.22**	

Table 4, Continued. Zircon Lu-Hf isotopic data for seven igneous units of the MHMC.

Zircon Spot	Hf (V)	$^{176}Hf/^{177}Hf$	Error (1σ)	$^{176}Lu/^{177}Hf$	Error (1σ)	Tchur	Tdm (1)	ε(0)	ε(t)	Error (2 σ)	Maximum ε Range
Tonalite of Granite Meadows											**13 - 5.79**
TGM-1.1	1.64	0.2830	1.90E-05	8.24E-04	9.40E-06	-0.34	0.35	7.39	**10.55**	**1.38**	
TGM-2.2	1.51	0.2830	2.00E-05	8.58E-04	4.50E-06	-0.39	0.31	8.35	**11.50**	**1.45**	
TGM-3.2	1.89	0.2830	1.50E-05	6.33E-04	1.90E-05	-0.28	0.40	6.05	**9.22**	**1.10**	
TGM-4.2	1.65	0.2830	1.60E-05	8.95E-04	2.70E-06	-0.31	0.37	6.72	**9.87**	**1.17**	
TGM-5.2	1.63	0.2829	1.60E-05	8.88E-04	3.20E-05	-0.25	0.43	5.30	**8.46**	**1.17**	
TGM-6.2	1.85	0.2830	1.30E-05	8.49E-04	2.80E-06	-0.28	0.40	5.94	**9.10**	**0.96**	
TGM-7.2	1.61	0.2829	1.60E-05	1.02E-03	2.90E-05	-0.27	0.41	5.76	**8.90**	**1.17**	
TGM-8.2	1.70	0.2829	1.70E-05	8.30E-04	1.10E-05	-0.19	0.48	4.14	**7.29**	**1.24**	
TGM-9.2	1.57	0.2829	1.70E-05	8.49E-04	3.30E-06	-0.26	0.42	5.59	**8.74**	**1.24**	
TGM-10.2	2.03	0.2830	1.40E-05	4.71E-04	3.70E-06	-0.31	0.36	6.86	**10.05**	**1.03**	
TGM-11.2	1.74	0.2830	1.70E-05	7.88E-04	8.10E-06	-0.30	0.38	6.47	**9.63**	**1.24**	
TGM-13.2	1.66	0.2829	1.90E-05	8.26E-04	2.80E-06	-0.19	0.48	4.03	**7.19**	**1.38**	
TGM-14.2	1.63	0.2830	1.10E-05	7.53E-04	2.90E-05	-0.33	0.35	7.21	**10.38**	**0.82**	
TGM-15.2	1.71	0.2829	1.40E-05	5.39E-04	5.20E-06	-0.22	0.45	4.81	**7.99**	**1.03**	

Table 2. Lu-Hf LA-ICP-MS isotopic analysis (continued)

Zircon Spot	Hf (V)	$^{176}Hf/^{177}Hf$	Error (1σ)	$^{176}Lu/^{177}Hf$	Error (1σ)	Tchur	Tdm (1)	ε(0)	ε(t)	Error (2 σ)	Maximum ε Range
Gabbro-norite of Ridenor Canyon											**13.55 - 2.4**
Age Population 1											
GNR 2.1_2	0.82	0.2830	2.70E-05	1.59E-03	3.40E-05	-0.34	0.36	7.18	**10.26**	**1.93**	**12.19 - 6.54**
~~GNR 4.1_2~~	~~0.87~~	~~0.2830~~	~~2.40E-05~~	~~2.25E-03~~	~~1.60E-05~~	~~-0.36~~	~~0.36~~	~~7.50~~	~~**10.52**~~	~~**1.71**~~	
GNR 5.1_2	0.84	0.2829	2.20E-05	1.91E-03	3.20E-05	-0.24	0.45	5.06	**8.11**	**1.57**	
Age Population 2											
GNR 1.1_2	0.81	0.2829	2.50E-05	7.74E-04	5.60E-06	-0.23	0.44	5.06	**8.22**	**1.78**	**13.55 - 2.44**
GNR 3.1_2	0.88	0.2828	3.20E-05	1.57E-03	4.10E-06	-0.08	0.59	1.63	**4.71**	**2.28**	
~~GNR 6.1_2~~	~~0.92~~	~~0.2829~~	~~2.40E-05~~	~~2.21E-03~~	~~3.30E-06~~	~~-0.18~~	~~0.51~~	~~3.64~~	~~**6.67**~~	~~**1.71**~~	
GNR 10.1_2	0.61	0.2830	4.00E-05	1.03E-03	3.60E-05	-0.35	0.34	7.57	**10.71**	**2.85**	
GNR 11.1_2	0.67	0.2829	2.70E-05	1.92E-03	3.20E-05	-0.25	0.44	5.30	**8.36**	**1.93**	
Age unknown											
GNR 13_2	1.52	0.2829	2.10E-05	8.38E-04	3.30E-05	-0.25	0.43	5.30	**8.46**	**1.50**	**12.85 - 2.42**
~~GNR 14_2~~		~~0.2815~~	~~1.70E-05~~	~~8.98E-04~~	~~1.80E-05~~	~~2.05~~	~~2.39~~	~~-45.05~~	~~**-41.92**~~	~~**1.22**~~	
~~GNR 15_2~~	~~1.06~~	~~0.2829~~	~~2.40E-05~~	~~2.26E-03~~	~~2.60E-05~~	~~-0.13~~	~~0.55~~	~~2.69~~	~~**5.71**~~	~~**1.71**~~	
GNR 16_2	0.85	0.2828	2.50E-05	1.11E-03	4.70E-06	-0.10	0.56	2.19	**5.32**	**1.78**	
GNR 17_2	0.85	0.2828	2.50E-05	1.72E-03	1.10E-05	-0.05	0.61	1.13	**4.20**	**1.78**	
GNR 18_2	0.93	0.2829	2.40E-05	7.75E-04	2.80E-05	-0.23	0.44	4.92	**8.08**	**1.71**	
GNR 19_2	0.60	0.2829	4.40E-05	1.35E-03	1.70E-05	-0.14	0.53	2.90	**6.01**	**3.13**	
GNR 20_2	0.73	0.2830	4.60E-05	1.37E-03	3.20E-05	-0.30	0.39	6.47	**9.58**	**3.27**	

Table 5. Summary and MWA of εHf_i data from LA-ICP-MS analysis of zircons for seven igneous units of the MHMC. The MSWD given is for the Hf data.

Unit	Age ($^{206}Pb/^{238}U$)	εHf_i (MWA)	Error (2σ)	MSWD	Number of analyses
Trondhjemite of Pearson Creek	159.5	n.a.	n.a.	n.a.	n.a.
Tonalite of California Gulch	152.5	13	1.3	5.1	12
Gabbronorite of Ridenor Canyon (population 1)	150.3	7.8	3.4	4	4
Trondhjemite of Johnson Creek	149.5	11.47	0.64	2.5	14
Diorite of Alexander Creek	149.4	10.85	0.88	4.1	16
Norite of Carney Butte	147.8	9.22	0.91	0.9	16
Tonalite of Granite Meadows	147	9.25	0.66	4	14
Gabbronorite of Ridenor Canyon (population 2)	145.7	9.5	3.4	2.6	3
Gabbronorite of Ridenor Canyon (population unknown)	n.a.	6.8	2.1	4.3	6
All accepted Hf analyses		10.33	0.46	6.9	84

3f. Whole rock major element geochemistry

All units analyzed for Pb/U and Hf isotopes were also analyzed for major element composition along with several other units including the Pearson Creek Keratophyre, the Metagabbro, the Amphibolite Gneiss, dikes and mafic enclaves (Tables 1, 6, 7, and 8). Major element composition results are presented in Table 5. Geochemically, three zones are present: the greenschist grade rocks of the eastern exposure, the amphibolite grade rocks of the north and central areas, and the Carney Butte Stock.

Whereas silicate content varies across the entire MHMC, it is consistently lowest in the deformed units with the exception of the two trondhjemites. The trondhjemites have SiO_2 contents in the 63 to 70% range, the tonalites have SiO_2 in the mid 50-60% range, and the norites, gabbros, and non-trondhjemitic deformed plutonic units have SiO_2 values below the mid 50% range (Figures 20, 21, and 22; Tables 6, 7, and 8). The greenschist grade rocks of the eastern exposure have Al_2O_3 values ranging from 13.6% to 15.5%. The amphibolite grade rocks have Al_2O_3 values ranging from 17 to 27.5%. The Carney Butte Stock ranges in Al_2O_3 from 17.4 to 22.7%. The pyroxene cumulate Trauba (1975) mapped as the Gabbronorite of Ridenor Canyon has an Al_2O_3 value between 6 and 6.8%.

The Gabbronorite of Ridenor Canyon shows the highest concentration of Mg and Fe for the Carney Butte Stock (12.2-21.2% MgO and 8-13% Fe_2O_3 for the pyroxenite and 8.2-8.6% MgO and 8.3-10.4% Fe_2O_3 for the main body), but also the most heterogeneous in composition. In the entire MHMC, it is comparable with the fine-grained version of the deformed Metagabbro: 7.5% MgO and 13.2% Fe_2O_3. The Trondhjemite of Pearson Creek unit is between 71 and 78% SiO_2, ~4.9% Na_2O, and ~ 3% CaO while its K_2O content doesn't exceed 0.24%. It is compositionally similar to the Pearson Creek Keratophyre, which it intrudes. The Tonalite of

Granite Meadows is compositionally homogeneous and even the mafic enclaves found within it are chemically similar to the bulk of the pluton. The entire plutonic body contains the highest proportion of K_2O, 1.47% to 1.78% for the bulk of the pluton, 1.32 to 1.96% for the mafic enclaves. The mafic enclaves differ from the rest of the tonalite in their respectively higher Ca (6.27-8.9% versus 6.52-6.56%) and Fe^{+3} (6.52-8.26% versus 5.31-5.67%), slightly higher Mg (4.14-6.02% versus 3.44-3.56%), and generally lower Si (53.35-58.72 versus 59.26-60.28).

Table 6. Whole rock major elemental abundances for plutonic and volcanic units in the easternmost exposure of the MHMC.

Unit	Metavolcanic							Trondhjemite of Pearson Creek		
	East					West		Pluton		Mafic Dike
Sample Name	PCS-3	PCS-4	PCS-5	PCS-6	PCS-7	UMV-1	UMV-3	MTJ-2	MTJ-4	MTJ-3
SiO2	70.27	69.58	70.99	69.09	69.22	73.43	65.57	71.18	73.84	46.86
TiO2	0.50	0.47	0.47	0.46	0.44	0.62	0.71	0.54	0.45	0.84
Al2O3	14.56	14.32	14.41	14.31	13.78	14.33	14.42	14.14	13.62	15.48
Fe2O3	3.35	4.05	3.47	5.96	4.42	2.76	6.83	3.36	2.95	9.68
MnO	0.06	0.04	0.08	0.09	0.27	0.08	0.07	0.08	0.05	0.19
MgO	1.32	1.31	1.47	2.77	3.17	0.64	3.62	1.00	0.78	11.03
CaO	3.75	3.31	4.58	1.23	3.54	1.12	1.97	3.25	3.07	10.30
Na2O	4.47	4.04	3.76	0.83	3.60	5.77	2.04	4.85	4.93	3.07
K2O	0.19	0.15	0.25	1.37	0.07	0.64	2.26	0.24	0.21	0.13
P2O5	0.11	0.12	0.11	0.12	0.07	0.14	0.12	0.10	0.07	0.13
LOI	1.14	1.21	1.29	3.94	1.96	0.41	2.03	1.24	0.86	2.82
Total	99.73	98.58	100.88	100.16	100.54	99.95	99.64	99.99	100.83	100.53
Pb	1.66	0.80	2.42	7.30	4.28	2.17	n.d.	n.d.	0.98	1.25
Th	1.29	1.33	1.21	1.21	1.49	3.29	n.d.	n.d.	1.87	0.34
U	0.48	0.35	0.44	0.35	0.44	0.46	n.d.	n.d.	0.57	0.15
La	8.64	10.04	9.04	9.12	9.60	18.42	n.d.	n.d.	11.71	4.32
Ce	20.84	22.08	20.43	21.06	21.92	40.21	n.d.	n.d.	27.15	10.73
Pr	3.04	3.00	2.85	2.95	3.07	5.54	n.d.	n.d.	3.89	1.69
Nd	14.63	13.77	13.07	13.67	14.30	24.97	n.d.	n.d.	18.67	8.70
Sm	3.96	3.64	3.44	3.41	3.80	5.72	n.d.	n.d.	5.26	2.39
Eu	1.18	1.10	1.08	1.10	1.08	1.73	n.d.	n.d.	1.23	0.88
Gd	4.47	4.02	3.83	4.14	4.06	4.85	n.d.	n.d.	6.27	2.49
Tb	0.83	0.76	0.72	0.77	0.73	0.84	n.d.	n.d.	1.15	0.42
Dy	5.69	5.29	5.05	5.33	5.05	5.30	n.d.	n.d.	8.06	2.85
Ho	1.20	1.10	1.08	1.11	1.05	0.97	n.d.	n.d.	1.72	0.58
Er	3.46	3.08	3.06	3.13	3.08	2.45	n.d.	n.d.	5.20	1.68
Tm	0.46	0.43	0.43	0.43	0.44	0.35	n.d.	n.d.	0.75	0.23
Yb	2.80	2.51	2.59	2.47	2.81	2.13	n.d.	n.d.	5.03	1.51
Lu	0.35	0.30	0.32	0.28	0.37	0.29	n.d.	n.d.	0.72	0.21
Sc	13.51	13.00	12.57	11.22	16.46	13.59	n.d.	n.d.	17.46	35.82
Cs	0.14	0.08	0.24	0.35	0.03	0.58	n.d.	n.d.	1.42	0.59
Ba	142.18	98.09	102.56	677.66	95.11	403.62	n.d.	n.d.	197.58	62.78
Rb	3.45	2.47	4.13	15.23	0.45	6.38	n.d.	n.d.	2.57	1.58
Sr	217.20	188.29	228.45	53.48	225.98	221.39	n.d.	n.d.	170.48	304.11
Sc	13.25	13.16	12.90	12.16	16.78	13.78	20.64	18.98	17.06	31.82
V	30.73	25.45	29.15	20.92	76.31	21.92	155.01	25.02	21.09	176.72
Cr	1.03	1.49	1.15	2.47	31.48	2.16	133.86	1.13	1.54	460.15
Ni	0.00	b.d.	b.d.	b.d.	15.58	b.d.	77.63	0.32	0.00	152.95
Cu	11.36	21.71	18.49	18.69	10.46	25.70	33.59	13.27	11.22	19.18
Zn	35.47	207.84	51.02	48.45	68.78	59.31	180.92	40.80	16.89	90.54
Ba	129.50	84.28	100.38	642.94	93.03	372.91	829.16	150.69	185.05	51.04
Sr	213.93	179.42	239.27	58.27	234.83	217.97	186.25	183.62	177.68	282.34
Y	28.56	28.11	28.56	30.36	27.99	36.25	22.04	41.21	40.29	9.27
Zr	125.92	118.52	117.44	117.65	128.55	157.10	125.00	122.68	145.72	36.91
Nb	n.d.	n.d.	n.d.	n.d.	n.d.	n.d.	n.d.	n.d.	n.d.	n.d.
Be	0.65	0.61	0.60	0.58	0.57	0.80	0.89	0.71	0.53	0.97

Table 7. Whole rock major elemental abundances for deformed plutonic and metamorphic units in the north or central exposure of the MHMC.

Unit	Metagabbro				Tonalite of California Gulch		Amphibolite Schist		Trondhjemite of Johnson Creek		
	Porphyritic	Xenolithic	Fine Grained	Typical							Tonalite dike
Sample Name	CAG-1	DSC-1	MGB-2	MGB-3	MEG-4	TONA-1	ASM-4	TON-3	JOC-1	JOC-1	UTON-2
SiO2	47.28	46.87	41.77	45.40	56.61	53.29	47.06	51.44	63.90	63.84	63.25
TiO2	0.25	0.37	1.34	0.17	0.49	0.82	0.70	0.45	0.40	0.38	0.39
Al2O3	24.18	28.48	20.47	27.51	16.98	19.21	18.97	17.50	18.10	18.04	17.77
Fe2O3	6.06	4.44	13.22	4.15	9.24	9.59	11.08	7.72	4.11	3.93	5.90
MnO	0.11	0.07	0.16	0.07	0.19	0.17	0.19	0.15	0.10	0.09	0.12
MgO	5.14	3.90	7.51	4.39	4.81	4.63	6.84	7.27	1.73	1.66	1.42
CaO	14.08	15.62	12.32	14.41	9.09	9.39	12.26	12.75	5.94	5.99	3.81
Na2O	1.58	1.23	1.92	2.14	2.70	2.53	2.03	1.36	4.09	4.00	3.96
K2O	0.24	0.11	0.21	0.10	0.33	0.13	0.42	0.22	0.46	0.54	1.35
P2O5	0.01	0.03	0.04	0.01	0.02	0.09	0.06	0.05	0.13	0.12	0.26
LOI	0.99	1.09	1.25	1.62	1.04	0.98	1.22	1.08	1.18	1.18	1.91
Total	99.92	102.22	100.21	99.98	101.51	100.84	100.83	99.99	100.13	99.79	100.14
Pb	1.70	2.41	0.81	1.78	2.21	1.38	1.08	2.33	3.44	n.d.	14.00
Th	0.16	0.18	0.06	0.05	0.38	0.15	0.70	0.39	0.47	n.d.	4.29
U	0.06	0.15	0.02	0.02	0.17	0.07	0.20	0.20	0.22	n.d.	1.34
La	0.73	2.15	2.25	1.01	3.60	3.15	5.09	2.85	5.07	n.d.	21.43
Ce	1.67	5.94	7.70	2.45	9.32	8.56	12.06	7.01	11.48	n.d.	43.37
Pr	0.28	0.98	1.49	0.35	1.57	1.45	1.75	1.13	1.74	n.d.	5.55
Nd	1.52	5.06	8.93	1.79	8.20	8.11	8.09	5.76	8.44	n.d.	21.70
Sm	0.50	1.51	2.98	0.48	2.55	2.73	2.16	1.72	2.03	n.d.	3.70
Eu	0.25	0.46	1.13	0.37	0.95	0.96	0.79	0.58	0.74	n.d.	1.27
Gd	0.77	1.61	3.62	0.61	3.23	3.67	2.46	2.17	1.99	n.d.	2.07
Tb	0.15	0.27	0.60	0.11	0.58	0.67	0.45	0.39	0.34	n.d.	0.43
Dy	1.08	1.68	3.91	0.72	4.06	4.74	3.17	2.71	2.21	n.d.	2.93
Ho	0.23	0.33	0.80	0.15	0.89	1.02	0.69	0.57	0.44	n.d.	0.58
Er	0.71	0.91	2.22	0.45	2.62	3.11	2.09	1.73	1.25	n.d.	1.61
Tm	0.11	0.12	0.31	0.06	0.39	0.45	0.32	0.25	0.18	n.d.	0.25
Yb	0.74	0.85	1.95	0.41	2.66	2.99	2.20	1.67	1.21	n.d.	1.68
Lu	0.11	0.12	0.27	0.06	0.40	0.45	0.33	0.26	0.17	n.d.	0.25
Sc	33.12	22.93	45.25	8.50	40.47	35.81	59.75	43.75	9.23	n.d.	3.89
Cs	1.07	0.12	0.13	0.04	0.19	0.08	0.57	0.54	0.50	n.d.	1.23
Ba	84.17	53.31	47.11	42.15	91.67	59.87	126.00	99.32	275.79	n.d.	526.98
Rb	5.24	2.65	1.05	1.02	4.10	1.11	4.85	3.75	9.78	n.d.	46.41
Sr	176.26	476.80	474.43	368.95	240.64	181.66	272.31	133.85	428.96	n.d.	525.87
Sc	28.55	20.76	44.22	21.22	37.58	37.36	48.76	45.65	8.59	8.32	4.97
V	158.86	123.63	399.80	67.26	211.13	240.24	299.85	231.11	56.52	55.11	16.04
Cr	71.88	71.28	26.34	37.53	51.31	12.33	71.49	91.96	8.41	8.44	9.91
Ni	21.35	25.36	0.00	35.46	1.79	0.00	17.55	30.08	0.00	0.00	b.d.
Cu	6.28	8.35	34.80	3.94	13.90	20.77	18.17	12.19	9.50	9.34	16.58
Zn	54.01	37.77	97.93	31.98	77.19	85.19	80.35	63.52	63.09	60.38	90.35
Ba	77.48	48.51	41.65	44.21	82.69	61.67	118.25	94.34	247.10	274.50	497.46
Sr	166.99	452.45	458.36	393.71	230.06	208.05	251.65	156.83	417.33	429.74	521.68
Y	5.64	7.98	18.21	5.54	20.26	23.90	15.59	13.41	12.71	11.54	16.18
Zr	9.02	14.24	26.90	5.66	36.08	45.73	23.59	27.33	105.00	103.46	134.32
Nb	n.d.	n.d.	n.d.	n.d.	n.d.	n.d.	n.d.	n.d.	n.d.	n.d.	n.d.
Be	0.36	0.51	2.04	0.22	0.63	1.19	1.02	0.65	0.52	0.51	0.41

Table 8. Whole rock major elemental abundances for the undeformed plutonic units of the Carney Butte Stock in the MHMC. The major element and (non-REE) trace element data is reported in weight percent.

Unit	Diorite of Alexander Creek	Norite of Carney Butte	Tonalite of Granite Meadows							Gabbronorite of Ridenor Canyon				
			Pluton			Mafic Enclave				Plagioclase cumulate			Pyroxene Cumulate	
Sample Name	DAC-1a	08MH03 (XRF)	GRM-2	GRM-6	TGM-1	GRM-1	GRM-3	GRM-4	GRM-5	GNR-3	GNR-5	GNR-5	GNR-2	GNR-4
SiO2	54.52	52.89	59.26	59.43	60.28	58.72	57.17	53.68	53.35	50.16	47.07	46.16	56.77	50.73
TiO2	0.93	0.94	0.66	0.62	0.62	0.72	0.81	1.03	0.82	0.67	0.47	0.45	0.56	0.81
Al2O3	17.82	17.50	17.69	18.10	17.97	17.72	17.52	18.98	17.89	17.40	22.72	21.36	6.05	6.81
Fe2O3	7.93	9.13	5.67	5.37	5.31	6.76	6.52	7.93	8.26	10.37	8.51	8.25	7.94	12.98
MnO	0.13	0.16	0.10	0.09	0.09	0.12	0.12	0.16	0.18	0.19	0.15	0.15	0.18	0.24
MgO	5.63	6.53	3.56	3.45	3.44	4.27	4.14	5.08	6.02	8.22	8.59	8.21	12.19	15.07
CaO	8.33	9.09	6.56	6.53	6.52	7.24	6.27	8.06	8.90	12.63	11.78	11.28	14.76	10.57
Na2O	3.33	3.22	3.78	4.01	3.81	3.67	3.69	3.88	3.84	2.22	1.06	0.92	0.98	0.91
K2O	0.50	0.34	1.57	1.47	1.78	1.52	1.96	1.92	1.32	0.11	0.16	0.15	0.52	0.19
P2O5	0.20	0.20	0.16	0.15	0.14	0.17	0.19	0.30	0.17	0.01	0.01	0.01	0.04	0.01
LOI	1.06	n.d.	0.69	0.91	0.67	0.76	1.56	1.21	1.09	0.28	1.54	1.54	1.27	1.30
Total	100.37	n.d.	99.70	100.13	100.63	101.67	99.95	102.23	101.84	102.27	102.07	98.48	101.26	99.63
Pb	3.43	2.25	n.d.	6.11	5.76	6.61	n.d.	6.52	6.36	n.d.	n.d.	n.d.	n.d.	0.54
Th	0.97	0.44	n.d.	2.36	1.85	1.37	n.d.	1.41	0.84	n.d.	n.d.	n.d.	n.d.	0.16
U	0.37	0.17	n.d.	0.79	1.17	0.78	n.d.	0.75	0.53	n.d.	n.d.	n.d.	n.d.	0.06
La	7.62	4.16	n.d.	13.82	10.67	12.79	n.d.	15.46	12.51	n.d.	n.d.	n.d.	n.d.	1.11
Ce	17.79	9.80	n.d.	29.15	24.74	28.27	n.d.	30.77	27.11	n.d.	n.d.	n.d.	n.d.	3.27
Pr	2.52	1.39	n.d.	3.79	3.41	3.84	n.d.	3.95	3.63	n.d.	n.d.	n.d.	n.d.	0.61
Nd	11.64	7.00	n.d.	16.20	14.90	16.77	n.d.	16.77	16.30	n.d.	n.d.	n.d.	n.d.	3.75
Sm	2.59	1.83	n.d.	3.07	2.94	3.33	n.d.	3.18	3.56	n.d.	n.d.	n.d.	n.d.	1.44
Eu	0.90	0.70	n.d.	0.90	0.80	0.97	n.d.	0.88	1.04	n.d.	n.d.	n.d.	n.d.	0.50
Gd	2.29	1.94	n.d.	2.40	2.43	2.62	n.d.	2.43	3.01	n.d.	n.d.	n.d.	n.d.	2.08
Tb	0.40	0.27	n.d.	0.42	0.42	0.47	n.d.	0.43	0.52	n.d.	n.d.	n.d.	n.d.	0.36
Dy	2.60	1.84	n.d.	2.78	2.80	3.05	n.d.	2.79	3.43	n.d.	n.d.	n.d.	n.d.	2.53
Ho	0.52	0.45	n.d.	0.55	0.55	0.60	n.d.	0.55	0.68	n.d.	n.d.	n.d.	n.d.	0.53
Er	1.47	1.35	n.d.	1.55	1.55	1.68	n.d.	1.49	1.88	n.d.	n.d.	n.d.	n.d.	1.53
Tm	0.22	0.18	n.d.	0.22	0.23	0.25	n.d.	0.22	0.28	n.d.	n.d.	n.d.	n.d.	0.21
Yb	1.46	1.24	n.d.	1.48	1.48	1.67	n.d.	1.42	1.78	n.d.	n.d.	n.d.	n.d.	1.33
Lu	0.22	0.17	n.d.	0.21	0.21	0.24	n.d.	0.21	0.26	n.d.	n.d.	n.d.	n.d.	0.19
Sc	24.11	25.75	n.d.	15.51	14.20	20.18	n.d.	21.26	28.39	n.d.	n.d.	n.d.	n.d.	83.93
Cs	0.79	n.d.	n.d.	1.73	1.78	1.77	n.d.	1.85	0.94	n.d.	n.d.	n.d.	n.d.	0.02
Ba	255.85	n.d.	n.d.	603.66	680.46	514.54	n.d.	566.31	380.53	n.d.	n.d.	n.d.	n.d.	40.47
Rb	11.30	5.60	n.d.	39.30	44.84	41.48	n.d.	53.55	31.26	n.d.	n.d.	n.d.	n.d.	1.37
Sr	559.59	n.d.	n.d.	577.25	522.30	558.80	n.d.	596.27	593.71	n.d.	n.d.	n.d.	n.d.	61.35
Sc	22.05	n.d	14.49	14.80	14.10	19.02	14.27	20.86	27.30	47.43	39.43	40.08	88.89	86.83
V	191.67	222.40	113.40	109.28	111.29	130.87	151.01	181.04	176.32	330.56	500.26	485.32	262.72	416.70
Cr	57.52	129.00	45.18	42.40	50.01	73.67	48.97	54.52	84.29	85.12	60.68	90.12	893.05	525.05
Ni	32.23	51.60	21.31	26.60	28.81	29.36	28.21	30.94	51.95	37.54	34.71	30.47	17.88	41.05
Cu	23.13	46.40	16.42	15.00	15.18	20.20	22.64	26.21	20.19	17.43	11.54	12.57	12.87	37.99
Zn	92.87	96.60	68.39	64.27	63.93	75.42	79.70	96.14	100.89	74.16	69.81	70.45	58.24	95.81
Ba	234.83	156.00	539.44	546.88	629.50	477.07	589.02	536.88	348.71	61.84	55.18	48.58	257.07	39.57
Sr	509.18	522.80	557.38	567.45	551.65	547.65	536.70	602.71	591.29	343.65	441.85	408.50	80.56	73.67
Y	12.18	12.60	13.31	14.36	13.81	14.13	11.49	13.48	16.00	10.98	7.32	5.41	14.11	9.53
Zr	50.54	67.00	103.50	86.85	43.31	64.68	99.36	39.22	43.12	16.67	8.91	10.16	49.68	19.85
Nb	n.d.	4.00	n.d.	n.d	5.40 (XRF)	n.d	n.d	n.d.	n.d.	n.d.	n.d.	n.d.	n.d.	n.d.
Be	1.33	n.d.	0.91	0.84	0.84	0.93	1.13	1.46	1.15	0.93	0.67	0.64	0.72	1.10

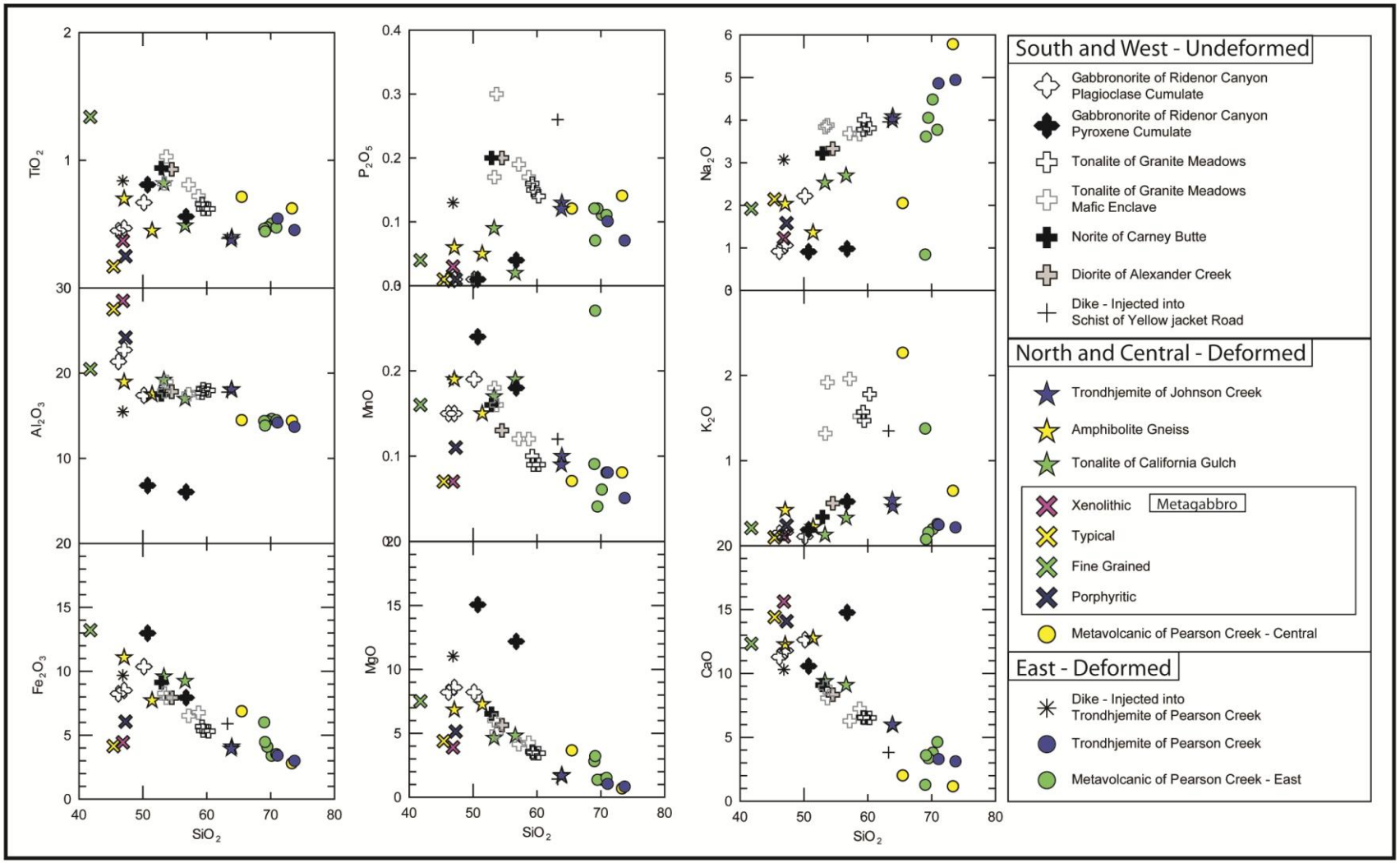

Figure 20. Whole rock major element Harker diagrams for the major units in the MHMC. Diagrams are based on the data presented in Table 3.

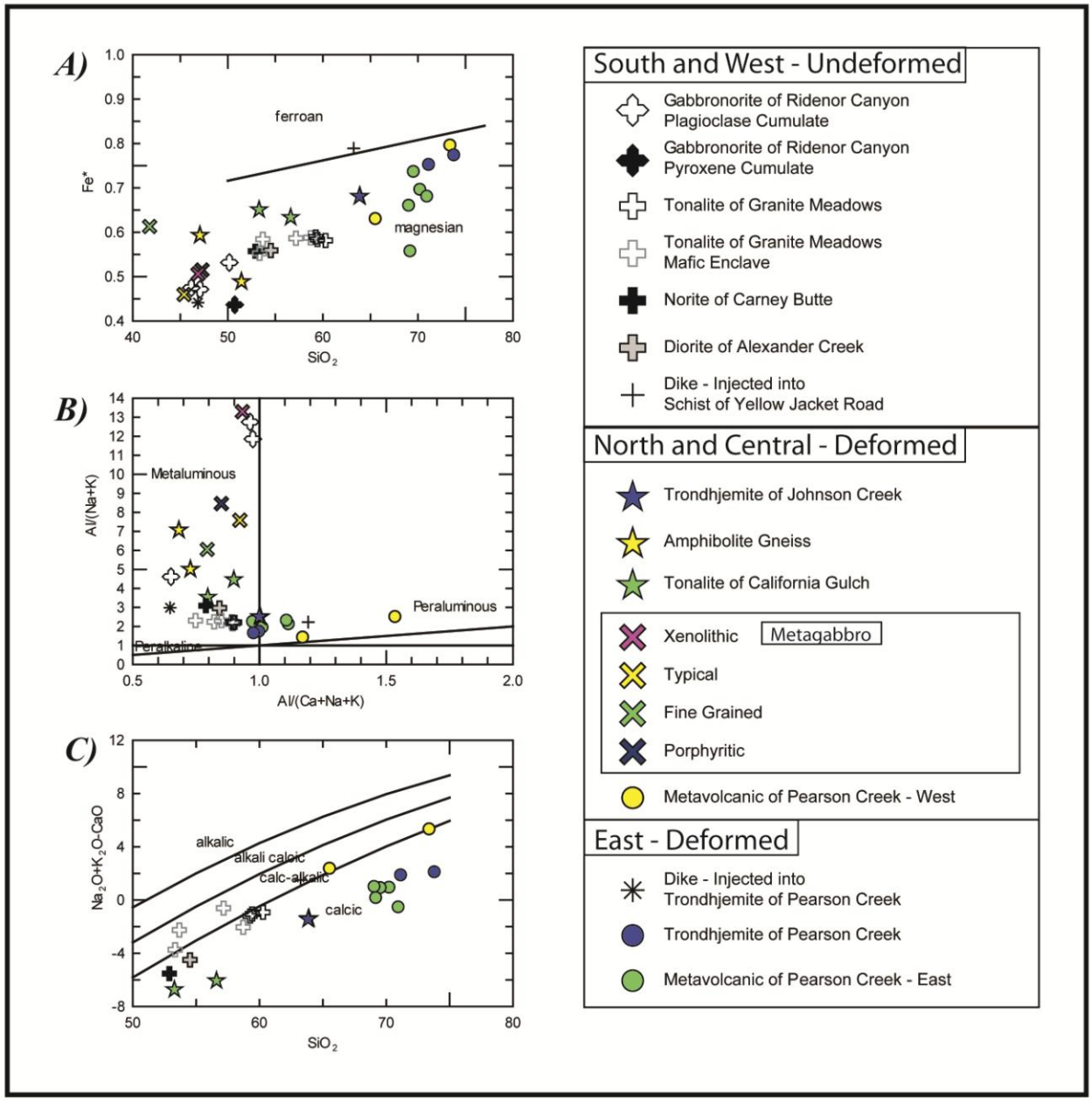

Figure 21. Whole rock major element geochemical diagrams for igneous rocks in the MHMC. A).Variation of Fe* as a function of SiO_2 (Frost *et al.*,2001). B) Shand's index for granitoids. C) MALI (Modified Alkali Lime Index) as a function of SiO_2 (Frost *et al.*,2001).

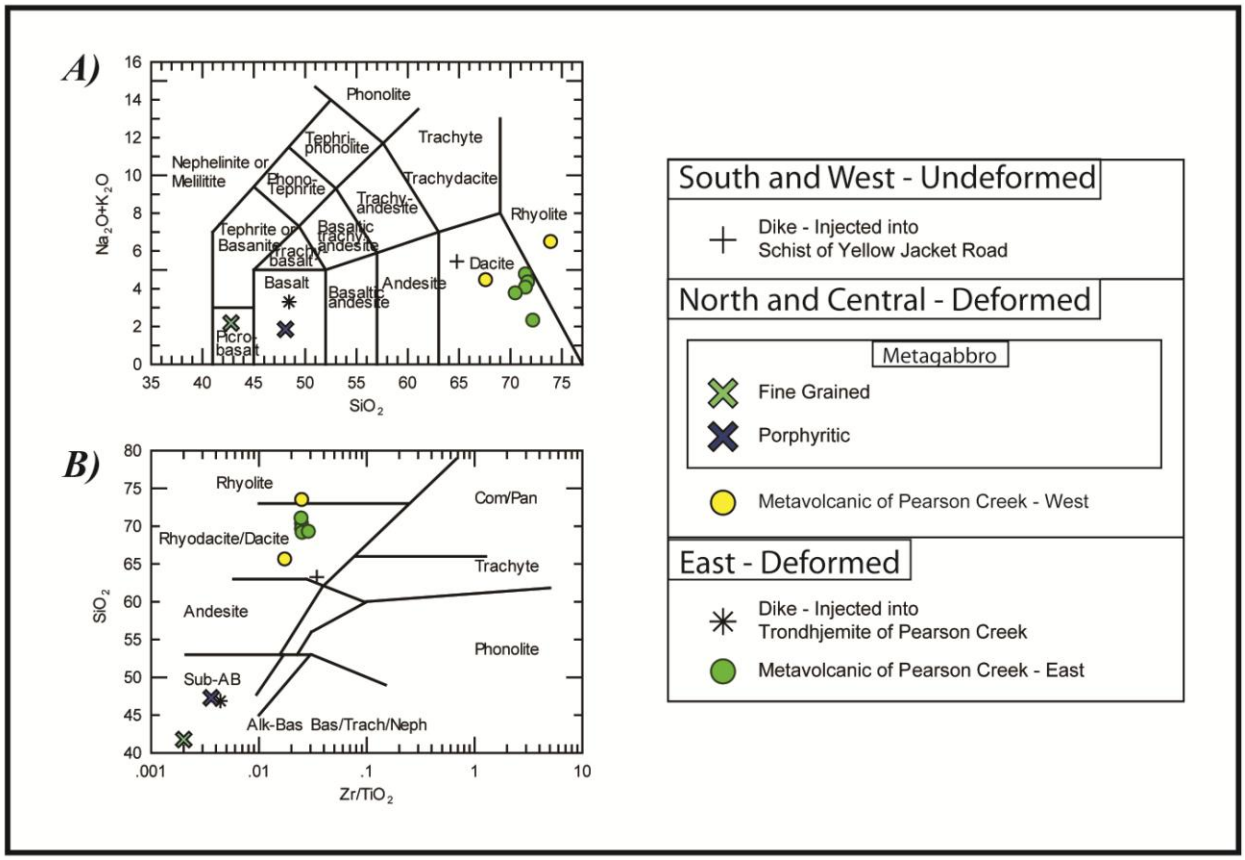

Figure 22. Two whole rock major element geochemical diagrams for the extrusive (or likely to have been extruded) units of the MHMC; the Pearson Creek Keratophyre and two of the Metagabbro variations. A)The total alkali versus SiO_2 diagram of Le Bas *et al.*, (1986). B) SiO_2 versus Zr/TiO_2 diagram of Winchester and Floyd (1977).

The whole rock major element geochemical signatures of the analyzed samples reveal several large scale trends when plotted (Figure 21). The igneous units of the Pearson Creek exposure, the Pearson Creek Keratophyre and the Trondhjemite of Pearson Creek, are magnesian, aluminous, calc-alkaline to arc tholeitic and the keratophyre ranges from rhyolitic to dacitic with some variation for degree of metamorphism (Figure 21). The two Pearson Creek Keratophyre samples taken from the central region of the MHMC (UMV-1 and UMV-2) both plot as calc-alkalic as opposed to the calcic nature of the other keratophyre samples (Figure 22). The fine grained and possibly extrusive deformed units from the north and central region (Metagabbro, both fine-grained and porphyritic varieties) range from the basaltic to picrobasaltic in composition (SiO_2 of 41.77% to 47.28, see Figure 22). All of the deformed north and central units are magnesian, metaluminous, and calcic.

The undeformed units, the Diorite of Alexander Creek, Norite of Carney Butte, Tonalite of Granite Meadows, and Gabbronorite of Carney Butte, are also magnesian and metaluminous; however, the Diorite of Alexander Creek and the Norite of Carney Butte are calcic basaltic andesite. The Tonalite of Granite Meadows is calcic and magnesian, but the mafic enclaves within it range into calc-alkalic. The Gabbronorite of Carney Butte is quite heterogeneous in composition, but both varieties of it are always magnesian and calcic. Two dikes, one intruding the Trondhjemite of Pearson Creek and the other intruding the Schist of Yellow Jacket Road, plot as metaluminous, magnesian, calc-alkalic basalt and peralkaline, ferroan, calc-alkaline dacite, respectively (Figures 21 and 22).

In major element Harker diagrams, the only oddity of the MHMC is the unusual Al_2O_3 range of the units sampled. The undeformed units are generally greater than 15% Al_2O_3 and so are the deformed units of the central and northern regions. The only units that do not exceed

15% are the samples from the Pearson Creek region (> 13.78% Al_2O_3) and the pyroxene cumulates of the Gabbronorite of Ridenor Canyon that range from 6-7% Al_2O_3 for pyroxene cumulates to 17-23% Al_2O_3 for plagioclase cumulates. Except for the Gabbronorite, the undeformed units have a higher P_2O_3 content than the deformed units (Figure 20).

In the deformed units, only the rocks of the Pearson Creek exposure and the Trondhjemite of Johnson Creek exceed 57 wt. % SiO_2 and those are 69-73 wt. % and ~64 wt. % SiO_2, respectively. The Carney Butte Stock contains 53-60% SiO_2, except for the mafic gabbronorite. While most of the MHMC units follow simple trends in SiO_2 content (negative correlation with Mg, Mn, Fe^{3+}, Ca, Ti, and Al, positive with Na, and humped with P_2O), two units do not. The gabbronorite is one, again most likely due to its mineralogical heterogeneity, and the other is the Metagabbro. The Metagabbro is lower in MgO, MnO, Fe_2O_3, and TiO_2, and higher in Al_2O_3 than would be expected based on the trend followed by the rest of the MHMC. The single Metagabbro sample that does fit the trend is the fine grained variety.

3g. Whole rock rare earth and trace element geochemistry

Whole rock results for trace element and rare earth element (REE) compositions are presented in Figures 23, 24, and 25 as well as Tables 6, 7, and 8. Two samples of the Gabbronorite of Ridenor Canyon (GNR) show high chromium (893 and 525 ppm), as does the mafic dike in the Trondhjemite of Pearson Creek (460 ppm), although that sample also contains high nickel (153 ppm) and higher strontium (282 ppm) than the GNR samples (18 to 41 ppm and 81 to 74 ppm, respectively). Most samples contain high strontium (Sr). In the deformed eastern zone, Sr is 178-235 ppm; in the deformed north and central zone, Sr is 157-459 ppm; and in the Carney Butte Stock, Sr is 344-603 ppm. Three samples had lower Sr, the high chromium GNR samples (74-81 ppm Sr) and one of the keratophyre samples (58 ppm). Vanadium (Figure 24

and Tables 6, 7, and 8), zirconium (Figure 25 and Tables 6, 7, and 8), and barium (Tables 6, 7, and 8) also distinguish several of the sample regions. The Tonalite of Granite Meadows and the keratophyre unit are fairly homogeneous. The Gabbronorite of Ridenor Canyon is again fairly heterogeneous. Europium, cerium, neodymium, and lanthanum levels vary between units in all three geochemical zones.

Overall, the light REE's show two distinct trends with respect to SiO_2, corresponding to the undeformed units and the deformed units (Figure 23). The heavy REEs in the underformed unit have the same range of SiO2. The single unusually HREE enriched unit in the MHMC is the Trondhjemite of Pearson Creek. The only LREE enriched deformed unit is the Pearson Creek Keratophyre sample taken from the central region of the MHMC, which experienced amphibolite facies metamorphic conditions. The Tonalite of California Gulch is also a little enriched in LREEs relative to the rest of the MHMC.

i. *Whole Rock Transition (Trace) Elements*

The yttrium (Y) and scandium (Sc) Harker diagrams fit the expected trends of positive for mafic units and negative for felsic units and so does the V Harker diagram, except for the deformed amphibolite facies units (Figure 24; Tables 6 and 7). The deformed amphibolite facies units show a variety of trends. Only the fine grained Metagabbro is consistent with the trend of the rest of the units. The other Metagabbro samples and the dike from the Trondhjemite of Pearson Creek are all relatively low in V relative to the trend. The undeformed Gabbronorite of Ridenor Canyon, both plagioclase and pyroxene cumulates, is high in V. The undeformed units plot slightly off of trend in the Sc Harker diagram, with the exception of the Gabbronorite of Ridenor Canyon, which follows the trend.

Uranium, Th, and to a lesser extent, Pb all show separate fractionation trends for the undeformed units and the deformed units (Figure 25). The mafic enclaves and the tonalitic dike in the Schist of Yellow Jacket Road correspond to the main plutons of the undeformed suite to make a clear trend. The Pearson Creek Keratophyre fits the deformed unit trend, except for the sample taken in the central region of the MHMC. Zr shows a consistent linear trend when compared to the SiO_2 content of the units.

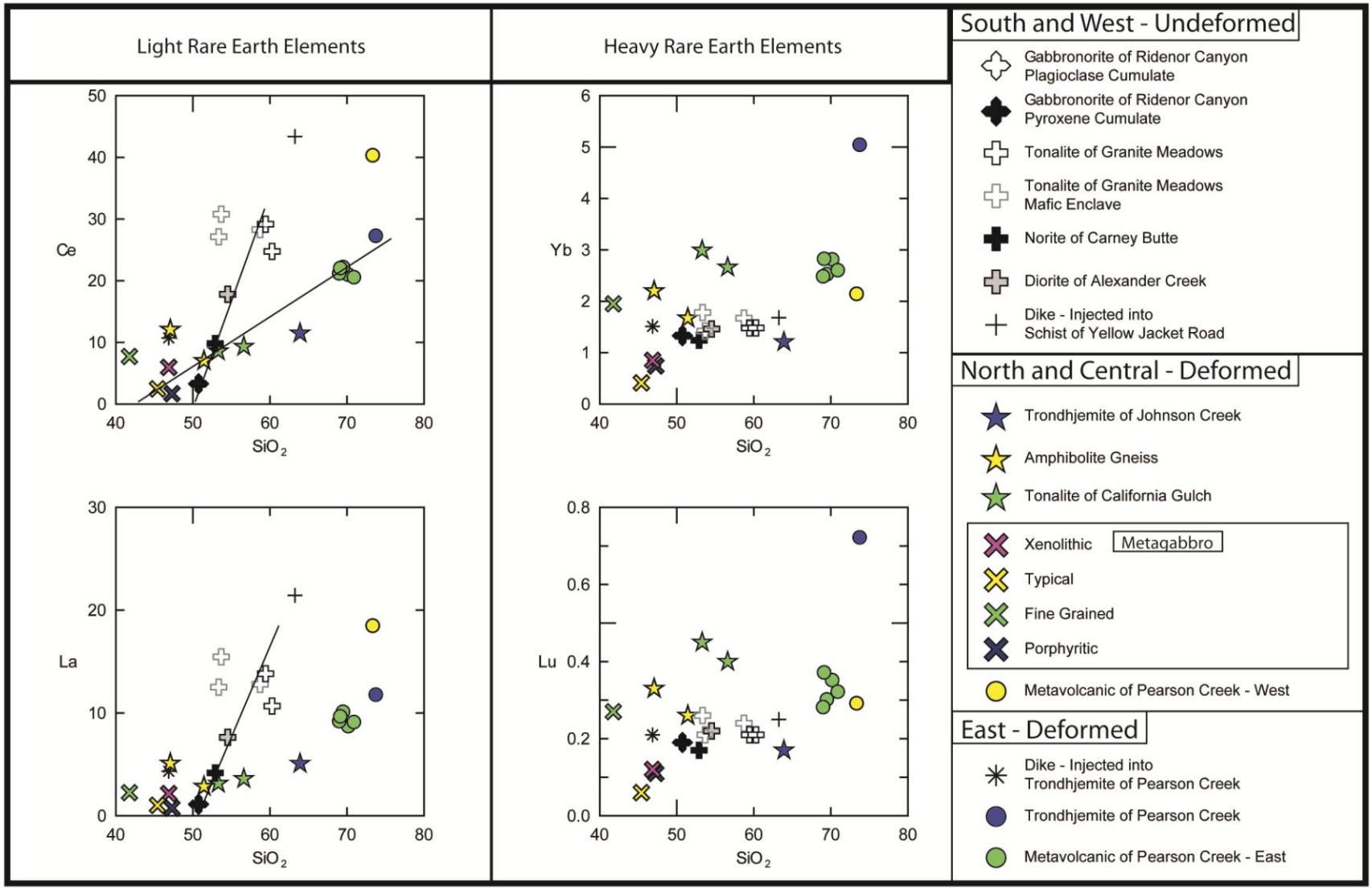

Figure 23. Whole rock rare earth element Harker diagrams displaying trends in the light REEs and heavy REEs. The lines represent apparent trends in this data, specifically LREE enrichment in the Carney Butte Stock relative to the deformed units of the MHMC.

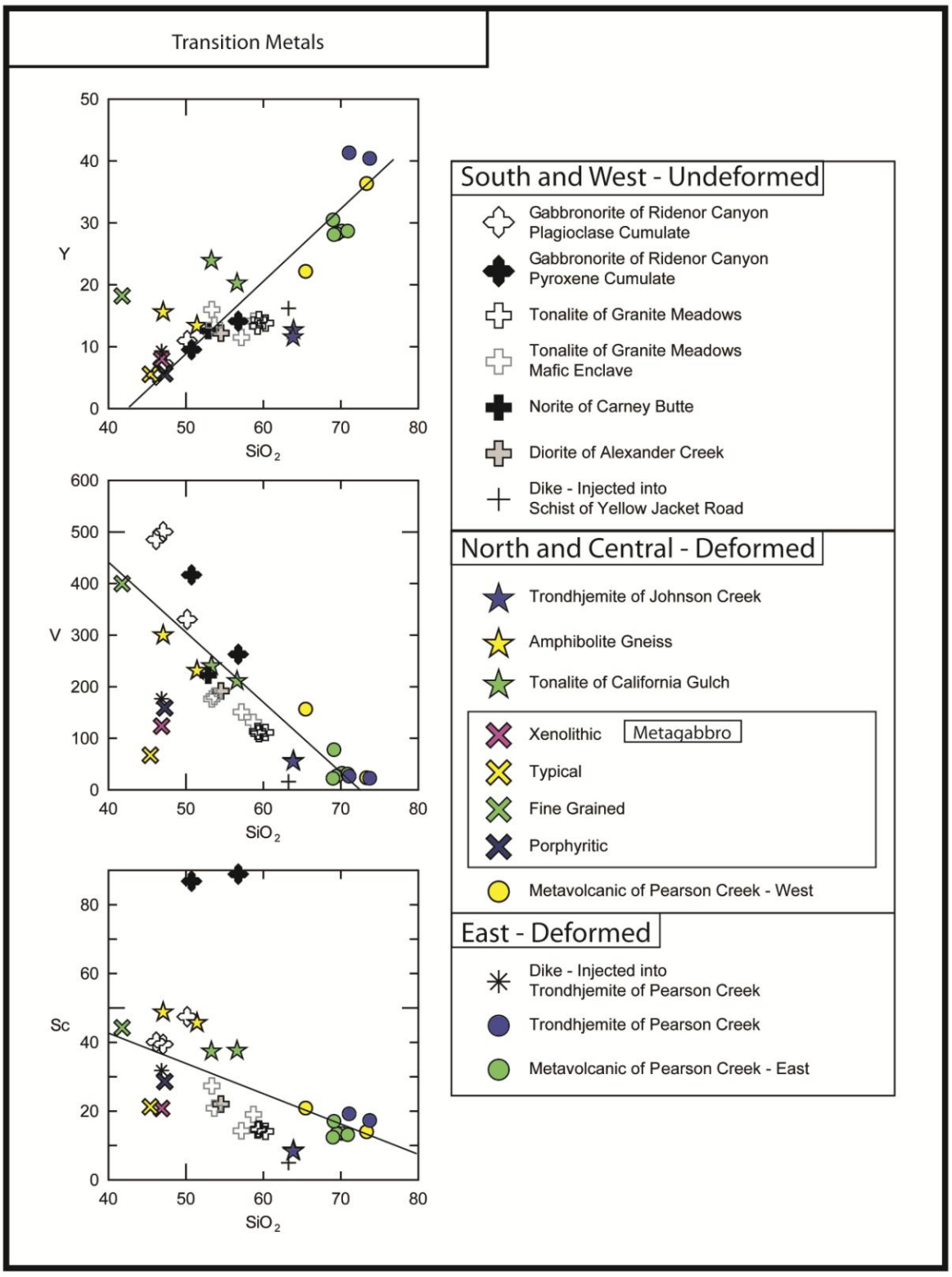

Figure 24. Whole rock transition metal Harker diagrams displaying trends in Y, V, and Sc with respect to SiO_2. The lines represent general trends in the data.

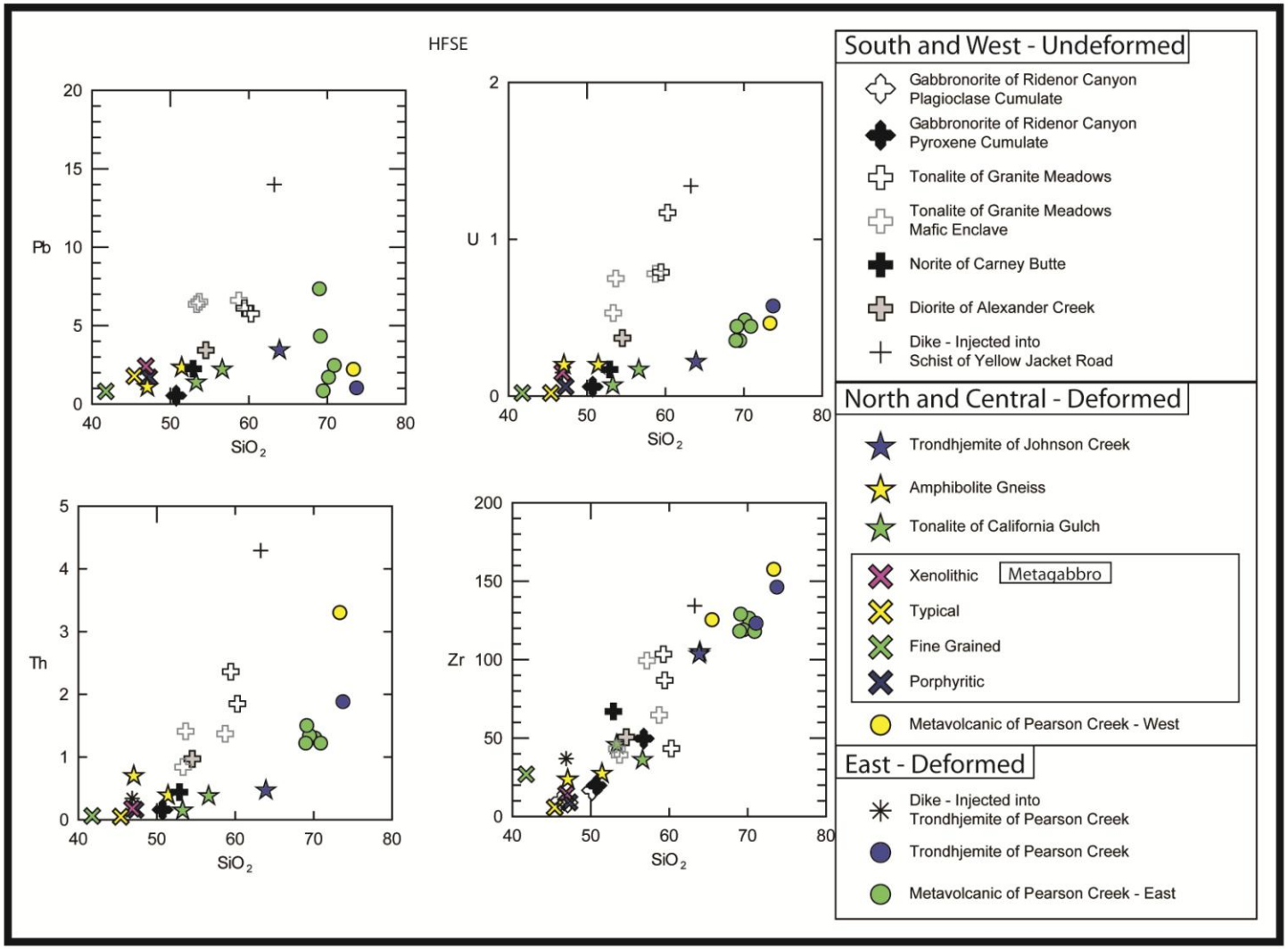

Figure 25. Whole rock high field strength element Harker diagrams. Note the similarity in trends to the REE Harker diagrams in Figure 23. The undeformed units clearly follow a separate trend than the deformed units in U, Pb, and Th, and Zr content corresponds well to SiO_2 content.

ii. *Whole Rock REE Patterns of Deformed Units*

The chondrite-normalized REE diagrams (Figure 26) of the MHMC units show marked differences between the predeformation units and those emplaced in the post deformational period. The plutonic units which were emplaced prior to the end of deformation (especially in the north and central regions) are characterized by flat REE patterns with a slight depletion in the LREEs relative to the HREEs. The exception is the Trondhjemite of Johnson Creek, which shows a slight enrichment in LREEs relative to the HREEs, although it is still fairly flat.

Of the northern plutonic units, only the Metagabbro shows a positive europium anomaly, and only in the typical and porphyritic varieties (Figure 26B). All four of the textures defined by Trauba (1975) were sampled and analyzed. Two were collected in the northern region and two were collected in the central region. Only the 'typical' texture shows minor LREE enrichment. The porphyritic sample shows a significant depletion of the LREEs and a flat profile, with a positive slope. The fine grained and xenolithic samples show a distinctive hump as the LREEs are depleted relative to the HREEs, while the MREEs are the most enriched (Figure 26B).

The Tonalite of California Gulch has a flat REE profile relative to Chondrite with depletion in the LREEs (Figure 26C). The Trondhjemite of Johnson Creek is enriched in LREEs and depleted in HREEs with a slight positive Eu anomaly. It is similar to the REE profiles of the post-deformation plutonic units, but less pronounced. Two samples of the Amphibolite Gneiss were analyzed; one (sample 10BSA-TON-3) shows an REE pattern resembling one of the Tonalite of California Gulch samples. The other sample analysis shows a distinctive HREE depletion and LREE enrichment, more akin to Trondhjemite of Johnson Creek (Figure 26C).

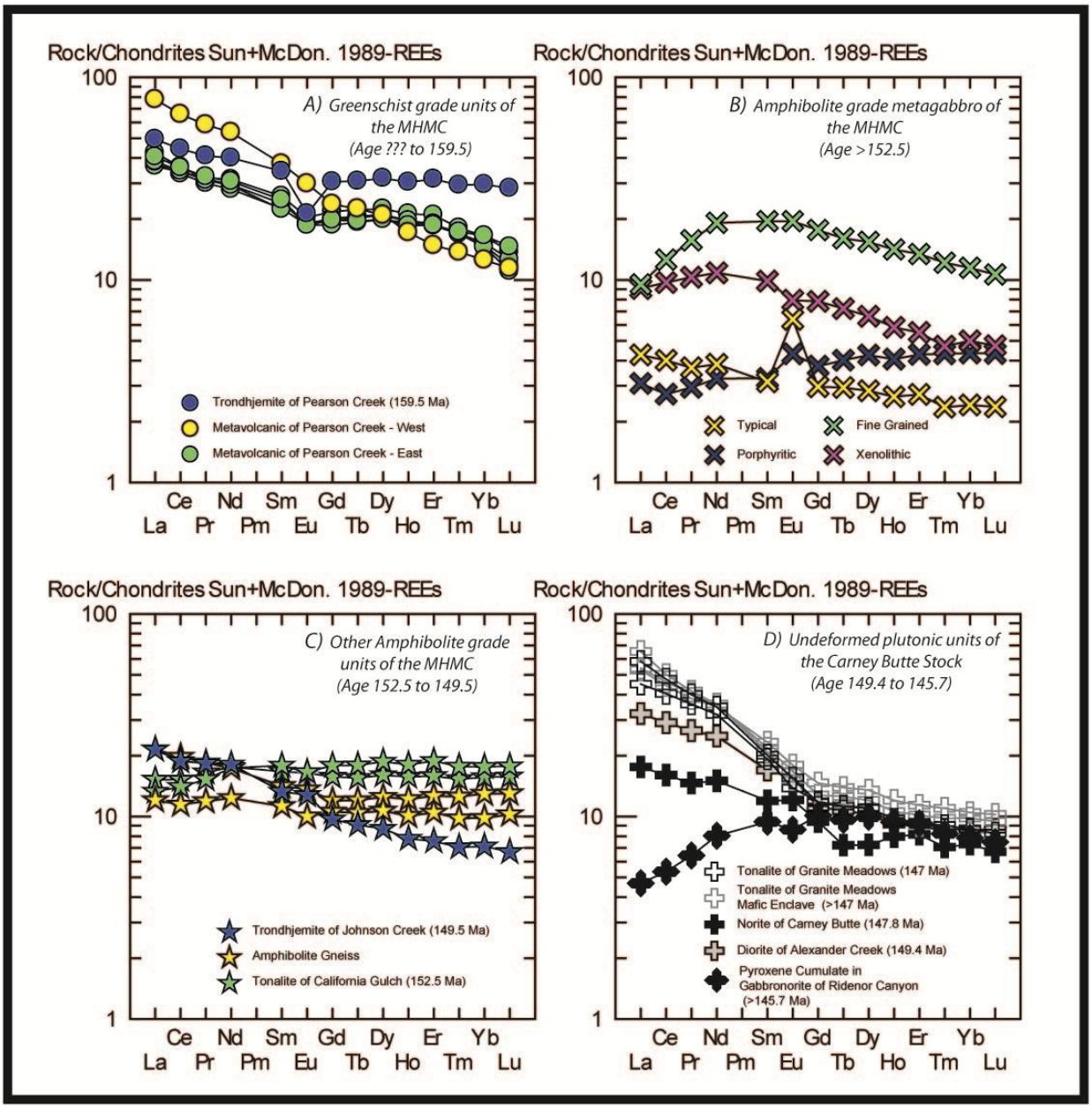

Figure 26. Whole rock chondrite normalized REE spider diagrams for the major units of the MHMC. A) Deformed amphibolite facies plutonic units: the Tonalite of California Gulch, the Trondhjemite of Pearson Creek, and the Amphibolite Gneiss. The Amphibolite Gneiss was included here because of its geochemical similarity to the Tonalite of California Gulch. B) This contains the greenschist facies Trondhjemite of Pearson Creek and Pearson Creek Keratophyre as well as the amphibolite facies Pearson Creek Keratophyre. C) This contains the four varieties of the Metagabbro (all amphibolite facies). D) This contains the undeformed plutonic units of the MHMC: The Diorite of Alexander Creek, the Norite of Carney Butte, The Tonalite of Granite Meadows (and analyses from several mafic enclaves contained therein), and the Gabbronorite of Ridenor Canyon. The Gabbro-norite is the only LREE depleted REE series because the only such analyses performed was on the pyroxene cumulate variety.

The Pearson Creek Keratophyre was sampled both in the Pearson Creek exposure and the central MHMC exposure (sample 10BSA-UMV-1). The samples taken along Pearson Creek show nearly indistinguishable REE patterns with LREE enrichment, a slight negative Eu anomaly (negative), and a humped HREE profile with greater depletion in the heaviest REEs (Figure 26A). The keratophyre sample from the central MHMC region is more enriched in the LREEs, has no Eu anomaly, and has little to no HREE hump (Figure 26A). It is similar to the eastern keratophyre in its REE concentrations and LREE/HREE.

The Trondhjemite of Pearson Creek shows a distinct negative Eu anomaly, a flat profile overall, a very slight enrichment in LREEs relative to HREEs, and a high REE content overall (Figure 26A). Two deformed dikes were also analyzed; one cuts the Trondhjemite of Pearson Creek and the other cuts into the metasediment in the extreme southwest. The Pearson Creek dike is flat in profile with a slight positive Eu anomaly and enrichment in LREEs relative to HREEs. The southwestern dike shows a very distinctive depletion in HREEs, enrichment in LREEs, and a very small positive Eu anomaly, resembling the Tonalite of Granite Meadows (see below) more than any other unit.

iii. *Whole Rock REE Patterns of the Carney Butte Stock*

The undeformed plutons of the MHMC share similar REE patterns (Figure 26D). The Diorite of Alexander Creek is enriched in LREEs, depleted in HREEs, and has a slight positive Eu anomaly. The Norite of Carney Butte also shows LREE enrichment and HREE depletion, but its LREEs have a shallower slope, and its HREEs have a slight hump to their profile. Five samples from the Tonalite of Granite Meadows were analyzed for REEs, two from the pluton itself and three from small mafic enclaves within the pluton. While they all showed enrichment in the LREE and no Eu anomaly, the enclaves show slightly less HREE depletion than the main

intusive body. REEs from one cumulate sample from the Gabbronorite of Ridenor Canyon shows a depletion in LREEs relative to the HREEs with a slight hump of MREE enrichment, and a slight negative Eu anomaly.

iv. *Whole Rock Trace Element Patterns of Deformed Units*

The trace element data are displayed using a N-MORB normalized spider diagram (Figure 27). The Pearson Creek Keratophyre has a consistent pattern for all of the samples from the exposure along Pearson Creek with a smooth pattern with depletion in Ti, P, and K, and enrichment in Cs, Ba, Th, Pb (for half of the samples), and U (Figure 27A). More variation in the pattern occurs with distance from the intruding trondhjemite. As this distance increases, Ba and Sr become enriched while the magnitude of the enrichment in Pb and depletion in K increases. The sample from the westernmost exposure of the keratophyre has a similar pattern overall, but is more enriched in all the trace elements plotted from Pr to Cs, with the exceptions of U and Pb. It has troughs at Ti and P. The Trondhjemite of Pearson Creek is enriched in trace elements relative to N-MORB, and shows depletion in Ti and P as well as a small depletion relative to the overall trend in K. It is strongly enriched in Cs and enriched in Ba, Th, and U (Figure 27A).

The Trondhjemite of Johnson Creek is enriched in all the LILEs analyzed with peaks at Pb, Sr, a tiny one at Zr and a low at Ti (Figure 27C). It is significantly depleted in the HREEs relative to N-MORB. The trondhjemite is strikingly similar to the profiles of the undeformed units and also somewhat similar to the profile of the mafic dike in the Trondhjemite of Pearson Creek (Figure 27A).

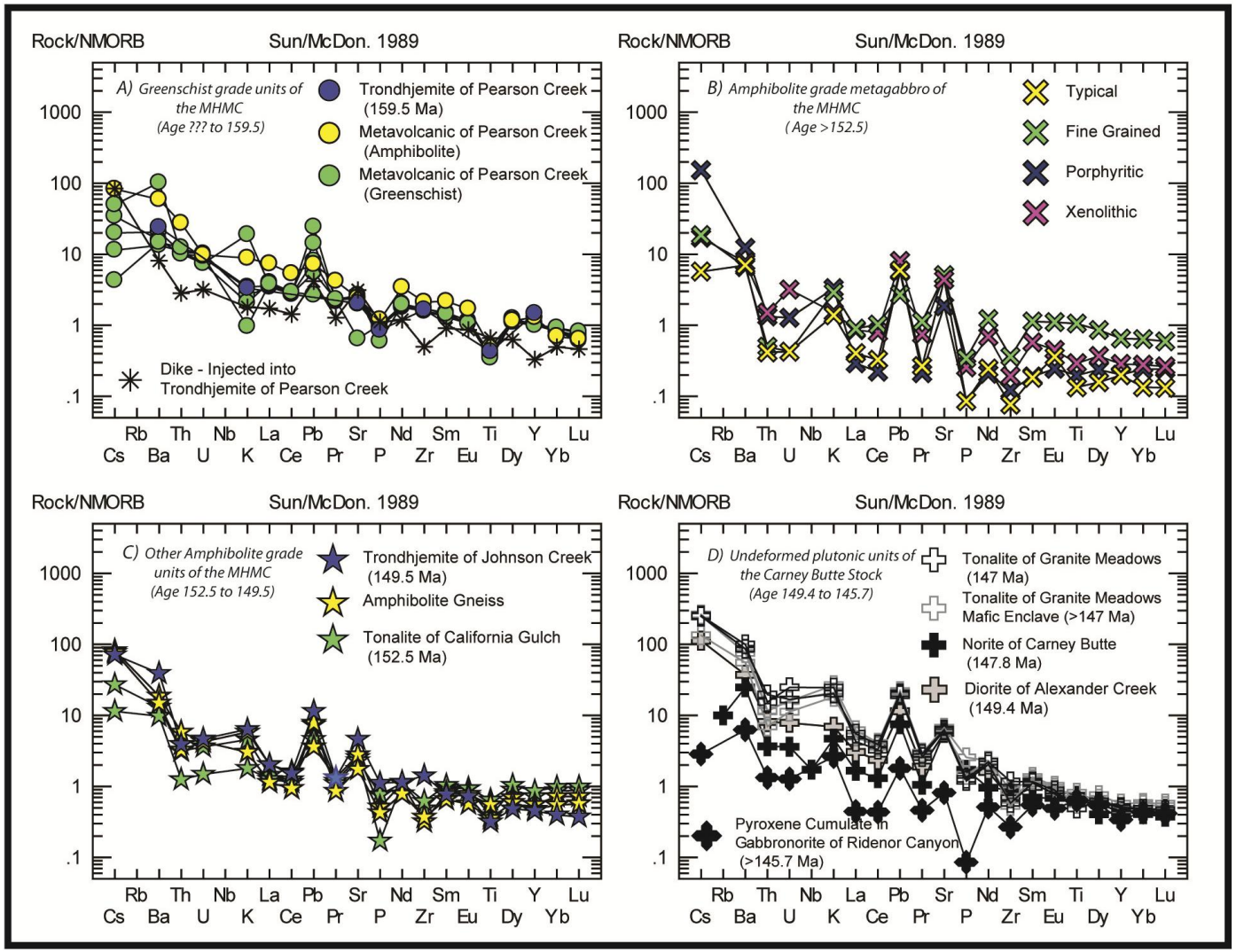

Figure 27. Whole rock N-MORB normalized trace element spider diagrams for the primary units of the MHMC. A) Greenschist facies Trondhjemite of Pearson Creek and Pearson Creek Keratophyre, amphibolite facies Pearson Creek Keratophyre, and an analysis of the dike which intrudes the Trondhjemite. B) Four varieties of the Metagabbro (all amphibolite facies). C) Deformed amphibolite facies plutonic units from the the MHMC. D) Undeformed plutonic units of the MHMC.

The four varieties of the Metagabbroic unit are distinct from each other. Trauba's (1975) 'typical' Metagabbro is depleted in the plotted trace elements relative to N-MORB with peaks at Pb, Sr, Ba, Cs, and K, that exceed N-MORB (Figure 27B). A small peak at Eu does not exceed N-MORB, and there are small troughs at Zr and P. The overall patterns are fairly flat.

The fine grained Metagabbro is the least depleted of the Metagabbro variations relative to N-MORB; in fact, it is the most consistently close to N-MORB of any unit in the MHMC. All of its large-ion lithophile elements (LILEs) are enriched and have peaks (Figure 27B) with a small peak at Pb. It is depleted in Th and U (both relative to N-MORB and as troughs) as well as P and Zr. The overall trend shows a depletion of Dy, Y, Yb, and Lu.

The porphyritic Metagabbro is enriched in all of the LILEs and Pb (Figure 27B). Cesium is particularly enriched. Uranium and Th are equivalent to N-MORB while everything else is depleted; the most compatible elements are flat and do not exceed 0.25 of N-MORB. There are minor troughs at P and Zr.

The xenolithic textured Metagabbro shows enrichment peaks at Pb and Sr (Figure 27B). There are depletion troughs at P, Zr, and a very small one at Ti. This is also depleted in the more compatible elements relative to N-MORB.

The Tonalite of California Gulch plots close to N-MORB with an overall profile that is flat (Figure 27C) and is the second closest to M-MORB of the MHMC. It has peaks at Pb, Sr, Cs, Ba, and a small peak at K. It has weak lows at Zr, Ti, and P. The other sample from this tonalite had a noisier signal with more pronounced lows at Zr, Ti, and P and more pronounced peaks at Pb and Sr. It was also uniformly more enriched in K, U, Th, and Cs.

Finally, the Amphibolite Gneiss has a smooth profile with its HREE's depleted relative to N-MORB and peaks at Pb, Sr, Nd, K, Ba, and Cs. It also has lows at Ti (minor), Zr, and P. This

profile is similar to those of the Tonalite of California Gulch as well as the porphyritic and xenolithic Metagabbro samples, although the amphibolite has higher Th, U, and Cs than the either the tonalite or xenolithic Metagabbro (Figure 27C).

v. *Whole Rock Trace Element Profiles of Undeformed Units*

The undeformed units have similar trace element spider diagrams. The Diorite of Alexander Creek, Norite of Carney Butte, and Tonalite of Granite Meadows all show similar overall profiles with enrichment in the LILEs as well as Pb, Sr and the other high field strength elements (HFSE, see Figure 27D). Both the tonalite and the diorite are depleted in Zr, and the norite is lower in Cs. All three are (in terms of REEs) depleted in Dy through Lu relative to N-MORB. Both pluton and mafic enclave samples of the Tonalite of Granite Meadows were analyzed. The enclave samples were close to the plutonic signatures but more strongly depleted in Th and without depletion in Ti; one also lacked a depletion in P. A complete data was obtained for one pyroxene cumulate sample from the Gabbronorite of Ridenor Canyon with peaks at Ba, K, and Pb, and depletion in everything from La to Lu (relative to N-MORB). The cumulate is more depleted in Cs through K than the other undeformed units. Acceptable Nb data was collected from two of the undeformed units via X-ray fluorescence. The Norite of Carney Butte (sample 08MH03) has an Nb content of 4.00 ppm and the Tonalite of Granite Meadows (sample 10BSA-TGM-1) has a content of 5.40 ppm. This is similar to the Nb content of the granodiorite in the SW outlier reported by Vallier (1995).

The dike intruding the Trondhjemite of Pearson Creek has a flat profile overall with peaks at Pb and Sr as well as lows at Zr and Y. It is enriched in the most incompatible LILE's and depleted in the HREEs. The tonalite dike in the Schist of Yellow Jacket Road has a strong peak at Pb, a lesser peak at Sr, and barely distinguishable peaks at Nd and K. It is enriched

relative to N-MORB in all the non HREE elements and depleted in the HREEs, with a low at Ti. The tonalite dike's overall profile is a steep, smooth curve toward Cs. Its N-MORB normalized trace element profile is nearly identical to that of the Tonalite of Granite Meadows.

3h. Zircon rare earth element results

In addition to U-Pb isotope data, partial REE data for each zircon grain was collected (Tables 9 and 10; Figure 28, which is normalized to Chondrite). Trace element data for Hf, Th, U, and Y of the analyzed zircons was also collected (Tables 9 and 10). The Trondhjemite of Pearson Creek has a tightly grouped REE pattern with the consistently highest REE content in the MHMC. The Tonalite of California Gulch is the second youngest unit and the bulk of the grains analyzed had the second highest REE content. The third and youngest of the deformed units, the Trondhjemite of Johnson Creek, has much less spread in the REE contents, but has the same range as the bulk of the grains in the Tonalite of California Gulch. The oldest of the post-deformational plutons, the Diorite of Alexander Creek, contains zircons of significantly lower REE content than its temporal predecessor. The next pluton to crystallize, the Norite of Carney Butte, is more enriched than the Diorite of Alexander Creek and is similar to the Trondhjemite of Johnson Creek in REE magnitude. The REE range of the Tonalite of Granite Meadows is similar to that of the Norite of Carney Butte and will be explored in more detail below. The range of REE values from the Gabbronorite of Ridenor Canyon (also explored below) is as complex as the magma body is heterogeneous. The xenocrystic older population of zircons has an HREE range matching the Trondhjemite of Johnson Creek, but a LREE that fits poorly within the wide range of the Tonalite of California Gulch, of the deformed units. The younger population of zircons in the gabbronorite does not fit well with any other unit in the MHMC or

Carney Butte Stock as they are depleted in both LREEs and MREEs. The baddeleyites analyzed are, of course, not comparable, but are plotted and reported.

The Ce values of the analyzed units all range from 0-21ppm including outliers except for the Trondhjemite of Pearson Creek, which contains values ranging from 55 ppm to 216 ppm with a single outlier of 12 ppm. This outlier is the only zircon grain to lack a high Y content (1466 versus a range from 7100 to 16300 ppm) or total REE content (866 ppm versus 5100 ppm to 9700 ppm), and is excluded from the mean weighted average of sample MTJ because of a very discordant age of 335 Ma.

Table 9. Rare earth element and selected trace element compositions of zircons from three deformed plutons in the MHMC. Modeled REE values were calculated with coefficients from Sano *et al.* (2002). REE and trace element compositions are recorded in ppm.

Trondhjemite of Pearson Creek												
Spot #	1	2	3	4	5	6	7	8	9	10	11	12
La	209.94	72.45	25.53	25.63	15.20	25.28	45.56	47.82	21.26	16.89	31.19	33.22
Ce	215.53	394.38	602.50	454.78	278.14	152.93	433.40	266.35	221.53	508.37	209.39	34.17
Nd	98.15	187.33	136.46	57.68	50.36	65.29	142.33	115.03	32.19	75.81	80.45	5.00
Sm	31.15	50.88	47.14	25.39	21.22	20.23	40.60	33.45	13.26	29.22	23.42	2.04
Eu	3.16	6.34	5.07	2.27	2.06	1.55	1.90	2.77	1.01	2.09	1.52	0.72
Gd	34.48	53.67	51.98	33.19	25.58	24.13	45.88	38.55	17.80	35.57	26.88	3.25
Dy	24.91	36.42	34.87	24.33	18.60	17.70	33.88	28.04	14.86	25.90	21.28	3.11
Er	14.93	21.43	20.62	14.51	11.19	12.00	21.00	17.33	9.42	15.80	13.32	1.81
Yb	11.42	16.10	15.35	10.88	8.68	9.27	16.16	13.12	7.54	12.08	10.38	1.57
La (ppm)	0.31	0.11	0.04	0.04	0.02	0.04	0.07	0.07	0.03	0.03	0.05	0.05
Ce (ppm)	77.59	141.98	216.90	163.72	100.13	55.06	156.02	95.89	79.75	183.01	75.38	12.30
Nd (ppm)	7.56	14.42	10.51	4.44	3.88	5.03	10.96	8.86	2.48	5.84	6.19	0.39
Sm (ppm)	24.92	40.70	37.72	20.32	16.98	16.19	32.48	26.76	10.61	23.37	18.73	1.63
Eu (ppm)	3.85	7.73	6.18	2.77	2.51	1.89	2.32	3.37	1.23	2.55	1.86	0.87
Gd (ppm)	275.84	429.37	415.82	265.55	204.61	193.01	367.02	308.42	142.42	284.59	215.07	26.00
Dy (ppm)	1143.50	1671.74	1600.67	1116.70	853.90	812.60	1555.22	1287.17	682.10	1188.62	976.96	142.68
Er (ppm)	2029.91	2914.86	2803.98	1973.98	1522.01	1631.64	2856.44	2356.99	1280.77	2149.31	1811.61	246.47
Yb (ppm)	3163.18	4459.62	4250.93	3014.14	2403.67	2567.23	4475.18	3633.74	2087.33	3346.41	2875.51	435.54
Lu (ppm)	n.d.	n.d.	n.d.	n.d.	n.d.	n.d.	n.d.	n.d.	n.d.	n.d.	n.d.	n.d.
ΣREE (ppm)	6726.66	9680.53	9342.75	6561.66	5107.71	5282.67	9455.71	7721.27	4286.72	7183.72	5981.36	865.94
Hf (ppm)	8049.33	8290.79	7990.84	9282.75	8038.94	9936.17	9784.98	9294.01	10279.01	9264.47	10718.58	10337.00
Th (ppm)	338.76	499.39	1486.90	1287.16	729.26	279.72	550.09	427.39	324.77	1155.82	325.23	49.56
U (ppm)	409.65	516.76	1136.72	1050.45	697.29	398.48	670.99	510.40	512.62	1052.44	450.05	498.84
Y (ppm)	11356.41	16315.35	15821.01	11242.31	8560.25	9049.84	16306.99	13306.16	7128.90	12237.28	10359.98	1466.56
Th/U	0.83	0.97	1.31	1.23	1.05	0.70	0.82	0.84	0.63	1.10	0.72	0.10
Yb/Gd	11.47	10.39	10.22	11.35	11.75	13.30	12.19	11.78	14.66	11.76	13.37	16.75
Sm/La	79.15	374.50	984.72	528.40	744.47	426.93	475.24	373.03	332.70	922.41	400.37	32.74
Dy+Er+Yb	6336.59	9046.22	8655.58	6104.83	4779.58	5011.47	8886.84	7277.90	4050.20	6684.34	5664.08	824.69

Table 9, continued. Rare earth element and selected trace element compositions of zircons from three deformed plutons in the MHMC. Modeled REE values were calculated with coefficients from Sano *et al.* (2002). REE and trace element compositions are recorded in ppm.

	Tonalite of California Gulch												
Spot #	1	1.2	2	3	4	5	6	7	8	9	10	11	12
La	15.57	11.46	8.54	8.38	6.93	10.32	10.82	13.98	17.01	10.85	12.30	12.65	11.08
Ce	6.83	58.87	2.41	14.41	8.18	20.86	5.32	9.52	10.03	11.40	1.96	8.46	7.47
Nd	9.63	6.21	0.22	3.33	1.52	5.97	1.82	5.35	2.39	11.36	0.18	11.83	6.80
Sm	2.00	1.76	0.12	1.10	0.60	1.48	0.52	1.47	0.81	2.49	0.05	2.35	1.74
Eu	0.73	0.61	0.06	0.40	0.24	0.67	0.24	0.46	0.36	0.67	0.04	0.77	0.50
Gd	1.94	2.93	0.12	1.56	0.80	2.15	0.66	1.64	1.06	2.56	0.07	2.29	1.64
Dy	1.51	2.97	0.16	1.72	0.83	2.57	0.71	1.18	1.21	1.84	0.09	1.61	1.15
Er	1.22	3.00	0.14	1.73	0.86	2.78	0.76	0.95	1.38	1.44	0.08	1.22	0.90
Yb	1.47	3.87	0.21	2.05	1.11	3.38	1.07	1.06	1.90	1.56	0.14	1.31	1.00
La (ppm)	0.02	0.02	0.01	0.01	0.01	0.02	0.02	0.02	0.03	0.02	0.02	0.02	0.02
Ce (ppm)	2.46	21.19	0.87	5.19	2.95	7.51	1.91	3.43	3.61	4.10	0.71	3.04	2.69
Nd (ppm)	0.74	0.48	0.02	0.26	0.12	0.46	0.14	0.41	0.18	0.87	0.01	0.91	0.52
Sm (ppm)	1.60	1.41	0.09	0.88	0.48	1.18	0.42	1.18	0.65	1.99	0.04	1.88	1.39
Eu (ppm)	0.89	0.75	0.07	0.49	0.30	0.82	0.30	0.57	0.44	0.82	0.05	0.95	0.61
Gd (ppm)	15.56	23.43	0.98	12.44	6.40	17.21	5.32	13.12	8.48	20.50	0.57	18.34	13.10
Dy (ppm)	69.20	136.52	7.15	78.77	38.23	118.13	32.38	54.14	55.64	84.52	3.93	74.00	52.94
Er (ppm)	166.55	408.49	19.30	235.43	116.42	378.02	102.79	129.79	188.10	195.23	11.35	166.04	123.04
Yb (ppm)	406.25	1072.90	57.80	567.34	308.17	936.49	297.29	294.53	526.73	433.06	38.28	362.11	277.05
Lu (ppm)	n.d.	n.d.	n.d.	n.d.	n.d.	n.d.	n.d.	n.d.	n.d.	n.d.	n.d.	n.d.	n.d.
ΣREE (ppm)	663.27	1665.18	86.30	900.82	473.06	1459.84	440.56	497.19	783.86	741.11	54.95	627.30	471.37
Hf (ppm)	10061.30	14303.41	9482.03	10077.49	9919.32	8405.47	8728.33	12430.72	9349.67	11288.89	9525.94	9540.67	10228.30
Th (ppm)	26.34	390.02	3.17	50.48	21.46	78.72	10.09	47.06	23.43	63.42	31.05	36.44	33.53
U (ppm)	65.64	947.81	16.79	201.55	103.76	176.75	44.15	124.47	99.77	172.93	142.22	94.27	92.44
Y (ppm)	861.13	2219.68	96.31	1227.00	606.68	1969.06	508.42	714.42	935.18	1070.62	57.05	917.79	702.25
Th/U	0.40	0.41	0.19	0.25	0.21	0.45	0.23	0.38	0.23	0.37	0.22	0.39	0.36
Yb/Gd	26.11	45.79	58.81	45.59	48.18	54.41	55.91	22.44	62.11	21.13	67.75	19.74	21.14
Sm/La	68.55	81.80	7.28	70.03	45.86	76.32	25.62	56.10	25.41	122.18	2.07	99.16	83.61
Dy+Er+Yb	642.00	1617.91	84.25	881.54	462.82	1432.64	432.46	478.46	770.48	712.81	53.55	602.16	453.03

Table 9, continued. Rare earth element and selected trace element compositions of zircons from three deformed plutons in the MHMC. Modeled REE values were calculated with coefficients from Sano *et al.* (2002). REE and trace element compositions are recorded in ppm.

	Trondhjemite of Johnson Creek											
Spot #	1	2	3	4	5	6	7	8	9	10	11	12
La	9.24	10.07	6.77	17.73	10.95	15.24	16.16	15.59	11.81	9.65	8.09	14.02
Ce	26.86	37.84	8.57	19.09	13.64	23.57	12.94	26.36	10.69	17.23	28.55	22.37
Nd	5.85	6.10	1.86	4.56	3.34	4.05	3.47	4.85	2.46	3.43	4.90	3.56
Sm	2.08	2.63	0.64	1.29	1.10	1.39	1.29	1.47	0.81	1.32	1.82	1.30
Eu	0.87	1.33	0.36	0.68	0.52	0.78	0.65	0.79	0.44	0.67	0.93	0.68
Gd	2.50	3.23	0.71	1.58	1.19	1.78	1.56	1.98	0.94	1.49	2.34	1.75
Dy	1.94	2.43	0.58	1.23	1.00	1.51	1.30	1.64	0.73	1.21	1.82	1.36
Er	1.64	1.82	0.49	1.04	0.89	1.24	1.11	1.32	0.63	0.97	1.39	1.09
Yb	1.88	2.00	0.68	1.29	1.16	1.45	1.32	1.54	0.81	1.17	1.62	1.26
La (ppm)	0.01	0.02	0.01	0.03	0.02	0.02	0.02	0.02	0.02	0.01	0.01	0.02
Ce (ppm)	9.67	13.62	3.09	6.87	4.91	8.48	4.66	9.49	3.85	6.20	10.28	8.05
Nd (ppm)	0.45	0.47	0.14	0.35	0.26	0.31	0.27	0.37	0.19	0.26	0.38	0.27
Sm (ppm)	1.66	2.11	0.51	1.04	0.88	1.11	1.03	1.18	0.65	1.06	1.46	1.04
Eu (ppm)	1.07	1.63	0.44	0.83	0.64	0.95	0.80	0.96	0.54	0.82	1.13	0.83
Gd (ppm)	20.02	25.85	5.68	12.66	9.52	14.24	12.52	15.81	7.49	11.89	18.70	14.01
Dy (ppm)	88.91	111.56	26.53	56.42	45.68	69.32	59.54	75.09	33.35	55.61	83.49	62.30
Er (ppm)	223.10	246.85	66.16	141.39	120.56	168.96	150.46	179.05	85.90	131.48	189.11	148.45
Yb (ppm)	520.73	554.38	187.47	356.12	320.61	402.10	365.38	425.55	223.33	323.06	449.48	349.30
Lu (ppm)	n.d.	n.d.	n.d.	n.d.	n.d.	n.d.	n.d.	n.d.	n.d.	n.d.	n.d.	n.d.
ΣREE (ppm)	865.61	956.49	290.04	575.71	503.07	665.50	594.67	707.53	355.31	530.41	754.03	584.27
Hf (ppm)	10559.12	10612.90	11966.40	11071.68	11227.98	10087.84	9726.90	10399.94	10395.22	10112.25	10350.88	9890.04
Th (ppm)	35.07	56.38	8.99	23.94	17.87	27.78	15.08	33.30	11.56	21.91	37.96	25.26
U (ppm)	99.13	149.68	40.42	82.15	69.10	96.53	48.99	107.42	47.39	73.73	115.24	82.21
Y (ppm)	1268.01	1447.22	374.86	801.58	661.90	970.64	832.75	1047.31	520.78	738.17	1107.22	868.70
Th/U	0.35	0.38	0.22	0.29	0.26	0.29	0.31	0.31	0.24	0.30	0.33	0.31
Yb/Gd	26.01	21.45	33.01	28.14	33.69	28.23	29.19	26.92	29.80	27.16	24.04	24.92
Sm/La	119.81	139.47	50.48	38.94	53.42	48.50	42.54	50.40	36.54	72.93	120.14	49.49
Dy+Er+Yb	832.73	912.80	280.17	553.94	486.85	640.38	575.38	679.69	342.57	510.15	722.08	560.04

Table 10. REE and selected trace element compositions of zircons from the four undeformed plutons composing the Carney Butte Stock of the MHMC. Modeled REE values were calculated with coefficients from Sano et al. (2002). REE and trace element compositions are recorded in ppm.

Diorite of Alexander Creek							
Spot #	1.1	2.1	3.1	4.1	5.1	6.1	7.1
La	9.66	7.21	11.70	17.70	14.56	20.41	16.14
Ce	5.18	9.87	6.25	6.24	6.16	13.81	14.90
Nd	0.77	2.13	1.28	1.19	1.14	12.32	11.37
Sm	0.26	0.55	0.23	0.22	0.19	1.51	2.03
Eu	0.16	0.36	0.17	0.15	0.15	0.74	0.86
Gd	0.21	0.54	0.19	0.20	0.26	1.01	1.27
Dy	0.16	0.36	0.18	0.16	0.19	0.57	0.69
Er	0.13	0.27	0.15	0.12	0.16	0.39	0.48
Yb	0.20	0.33	0.24	0.18	0.24	0.48	0.55
La (ppm)	0.01	0.01	0.02	0.03	0.02	0.03	0.02
Ce (ppm)	1.86	3.55	2.25	2.25	2.22	4.97	5.36
Nd (ppm)	0.06	0.16	0.10	0.09	0.09	0.95	0.88
Sm (ppm)	0.21	0.44	0.19	0.17	0.15	1.21	1.62
Eu (ppm)	0.20	0.44	0.20	0.19	0.19	0.90	1.05
Gd (ppm)	1.66	4.31	1.50	1.58	2.06	8.12	10.15
Dy (ppm)	7.30	16.53	8.15	7.22	8.86	26.05	31.87
Er (ppm)	17.94	36.13	20.54	16.56	22.44	53.55	65.30
Yb (ppm)	55.47	92.74	66.53	49.36	66.52	133.17	152.55
Lu (ppm)	n.d.	n.d.	n.d.	n.d.	n.d.	n.d.	n.d.
ΣREE	84.71	154.33	99.47	77.45	102.55	228.96	268.82
Hf (ppm)	9770.20	8934.54	9913.81	8977.27	10145.44	8678.17	8737.19
Th (ppm)	25.62	30.50	18.36	27.99	65.25	25.87	25.99
U (ppm)	96.97	64.76	68.83	87.88	256.34	55.55	52.00
Y (ppm)	95.79	192.19	106.90	90.66	119.03	298.85	377.15
Th/U	0.26	0.47	0.27	0.32	0.25	0.47	0.50
Yb/Gd	33.39	21.49	44.44	31.21	32.24	16.40	15.02
Sm/La	14.22	40.98	10.67	6.54	6.92	39.54	67.01
Dy+Er+Yb	80.71	145.40	95.22	73.14	97.82	212.78	249.73

Table 10, continued. REE and selected trace element compositions of zircons from the four undeformed plutons composing the Carney Butte Stock of the MHMC.

Norite of Carney Butte												
Spot #	1	2	3	4	5	6	7	8	9	10	11	12
La	8.77	8.37	8.41	21.80	6.71	3.38	7.04	16.54	6.66	65.86	19.38	19.59
Ce	16.53	15.55	13.15	15.05	12.82	9.96	12.17	22.48	12.91	11.80	16.28	14.06
Nd	17.23	17.23	11.66	16.60	11.10	3.08	11.72	22.50	10.79	8.09	17.79	16.26
Sm	3.15	3.15	2.09	2.79	2.10	1.00	2.19	3.81	2.02	1.81	2.64	2.39
Eu	1.17	1.08	1.00	1.07	0.91	0.61	0.95	1.43	0.92	0.82	1.18	1.02
Gd	2.37	2.25	1.52	1.88	1.52	0.79	1.47	3.27	1.62	1.33	1.91	1.63
Dy	1.47	1.32	0.84	1.17	0.81	0.49	0.83	2.44	0.94	0.82	1.23	1.04
Er	0.90	0.87	0.53	0.94	0.52	0.32	0.53	1.66	0.61	0.52	0.80	0.83
Yb	0.85	0.83	0.55	1.06	0.55	0.35	0.55	1.53	0.62	0.52	0.82	0.97
La (ppm)	0.01	0.01	0.01	0.03	0.01	0.01	0.01	0.02	0.01	0.10	0.03	0.03
Ce (ppm)	5.95	5.60	4.74	5.42	4.62	3.58	4.38	8.09	4.65	4.25	5.86	5.06
Nd (ppm)	1.33	1.33	0.90	1.28	0.85	0.24	0.90	1.73	0.83	0.62	1.37	1.25
Sm (ppm)	2.52	2.52	1.67	2.23	1.68	0.80	1.75	3.05	1.62	1.45	2.11	1.92
Eu (ppm)	1.43	1.31	1.23	1.31	1.12	0.74	1.16	1.75	1.12	1.01	1.44	1.24
Gd (ppm)	18.99	18.00	12.14	15.04	12.15	6.32	11.79	26.14	12.96	10.63	15.32	13.04
Dy (ppm)	67.53	60.62	38.63	53.74	37.29	22.52	38.12	111.77	42.92	37.77	56.31	47.82
Er (ppm)	122.23	118.69	72.47	128.06	71.33	43.51	71.85	225.31	82.76	70.23	109.42	113.10
Yb (ppm)	234.80	230.03	153.24	292.53	151.59	97.25	151.44	423.71	172.29	142.92	228.52	269.33
Lu (ppm)	46.89	46.21	32.14	65.38	32.26	21.35	33.15	84.80	35.80	29.84	48.30	61.69
ΣREE	501.68	484.32	317.15	565.01	312.91	196.32	314.56	886.39	354.95	298.81	468.67	514.48
Hf (ppm)	8571.11	8495.57	8213.84	8058.50	8410.58	7709.84	8442.48	8556.03	8752.30	7967.18	8322.53	8124.43
Th (ppm)	n.d.	n.d.	n.d.	n.d.	n.d.	n.d.	n.d.	n.d.	n.d.	n.d.	n.d.	n.d.
U (ppm)	n.d.	n.d.	n.d.	n.d.	n.d.	n.d.	n.d.	n.d.	n.d.	n.d.	n.d.	n.d.
Y (ppm)	688.03	648.76	411.89	629.89	407.87	235.87	400.78	1221.19	464.87	390.32	604.93	567.71
Th/U	n.d.	n.d.	n.d.	n.d.	n.d.	n.d.	n.d.	n.d.	n.d.	n.d.	n.d.	n.d.
Yb/Gd	12.36	12.78	12.63	19.45	12.48	15.40	12.85	16.21	13.29	13.44	14.92	20.66
Sm/La	191.68	200.92	132.28	68.16	166.95	157.25	166.03	122.90	161.98	14.67	72.55	65.21
Dy+Er+Yb	424.56	409.34	264.34	474.33	260.21	163.28	261.41	760.80	297.96	250.91	394.25	430.26

Table 10, continued. REE and selected trace element compositions of zircons from the four undeformed plutons composing the Carney Butte Stock of the MHMC. The ages listed are $^{206}Pb/^{238}U$ ages of the individual grains to which they correspond.

	Tonalite of Granite Meadows												
	Population 1								Population 2				
Spot #	1.1	10.1	11.1	12.1	6.1	8.1	9.1	3.1	13.1	2.1	4.1	5.1	7.1
La	13.10	283.28	12.60	14.29	10.76	14.16	13.44	11.93	17.08	14.89	13.09	9.46	10.96
Ce	47.88	33.49	21.48	47.20	28.39	31.06	23.12	25.00	41.31	39.10	44.88	41.05	44.60
Nd	4.94	13.75	5.08	4.37	4.06	7.67	7.70	9.58	17.46	26.88	14.73	26.25	23.01
Sm	1.67	1.60	1.08	1.43	1.06	1.71	1.51	1.61	3.73	5.63	3.20	4.59	5.41
Eu	0.74	0.62	0.49	0.68	0.44	0.61	0.55	0.66	0.75	0.91	0.78	0.85	0.89
Gd	1.52	1.11	0.87	1.42	0.95	1.18	1.06	1.10	2.61	3.83	2.52	3.21	3.93
Dy	1.19	0.64	0.57	1.14	0.65	0.75	0.66	0.66	1.49	2.27	1.47	1.73	2.20
Er	0.96	0.50	0.41	0.91	0.50	0.57	0.47	0.48	0.98	1.29	1.03	1.08	1.33
Yb	1.32	0.62	0.52	1.24	0.64	0.76	0.58	0.64	0.99	1.08	1.10	0.99	1.13
La (ppm)	0.02	0.42	0.02	0.02	0.02	0.02	0.02	0.02	0.03	0.02	0.02	0.01	0.02
Ce (ppm)	17.24	12.06	7.73	16.99	10.22	11.18	8.32	9.00	14.87	14.07	16.16	14.78	16.06
Nd (ppm)	0.38	1.06	0.39	0.34	0.31	0.59	0.59	0.74	1.34	2.07	1.13	2.02	1.77
Sm (ppm)	1.34	1.28	0.86	1.14	0.85	1.36	1.21	1.29	2.98	4.51	2.56	3.67	4.33
Eu (ppm)	0.91	0.75	0.60	0.83	0.54	0.74	0.67	0.81	0.92	1.11	0.95	1.03	1.09
Gd (ppm)	12.16	8.88	6.96	11.38	7.58	9.40	8.50	8.79	20.89	30.63	20.15	25.72	31.48
Dy (ppm)	54.47	29.47	26.36	52.30	29.71	34.24	30.26	30.22	68.48	104.28	67.51	79.35	100.89
Er (ppm)	131.14	67.61	55.67	123.99	67.72	78.06	64.00	64.77	133.80	174.98	140.49	146.75	180.56
Yb (ppm)	364.83	170.81	144.88	343.03	178.27	211.33	160.68	176.20	273.38	297.92	304.08	274.29	313.53
Lu (ppm)	n.d.	n.d.	n.d.	n.d.	n.d.	n.d.	n.d.	n.d.	n.d.	n.d.	n.d.	n.d.	n.d.
ΣREE	582.48	292.34	243.48	550.03	295.22	346.94	274.26	291.84	516.70	629.59	553.05	547.63	649.72
Hf (ppm)	16508.84	10962.35	11146.53	15627.83	12534.83	12216.78	11345.54	12172.47	10425.15	9654.64	11820.21	10383.71	10756.72
Th (ppm)	390.58	291.15	188.49	369.69	224.52	152.32	236.70	210.33	102.97	74.98	123.89	90.62	99.34
U (ppm)	1703.51	557.67	345.37	1697.90	407.99	263.04	430.14	382.90	163.21	124.83	202.80	142.68	163.33
Y (ppm)	715.89	386.58	320.19	693.67	379.96	441.38	368.25	362.42	799.17	1019.54	823.31	879.88	1056.39
Th/U	0.23	0.52	0.55	0.22	0.55	0.58	0.55	0.55	0.63	0.60	0.61	0.64	0.61
Yb/Gd	30.01	19.24	20.81	30.14	23.52	22.48	18.90	20.03	13.09	9.73	15.09	10.67	9.96
Sm/La	68.12	3.01	45.67	53.30	52.53	64.27	59.85	71.89	116.51	201.65	130.29	258.59	263.24
Dy+Er+Yb	550.44	267.89	226.91	519.32	275.70	323.64	254.94	271.19	475.66	577.18	512.08	500.40	594.98
Age (Ma)	146.50	141.60	142.80	141.00	146.20	148.60	144.50	147.80	143.40	147.80	148.40	144.70	150.60
Age error	0.50	0.80	1.20	0.50	1.00	1.30	1.00	1.10	1.60	1.90	1.50	1.70	1.70

Table 10, continued. REE and selected trace element compositions of zircons from the four undeformed plutons composing the Carney Butte Stock of the MHMC. The ages listed are $^{206}Pb/^{238}U$ ages of the individual grains to which they correspond.

Gabbronorite of Ridenor Canyon											
	Older			Younger					Baddeleyite		
Spot #	2.1	4.1	5.1	1.1	10.1	11.1	3.1	6.1	8.1	9.1	12.1
La	23.61	13.66	37.33	23.90	23.04	11.48	22.34	10.56	373.22	174.67	326.15
Ce	1.79	3.32	4.64	0.79	5.01	4.45	2.13	2.26	2.88	2.37	14.05
Nd	2.46	3.44	16.57	0.79	3.56	4.03	2.32	1.82	2.64	1.86	4.51
Sm	0.52	1.10	2.69	0.21	1.20	1.12	0.53	0.44	0.39	0.38	1.00
Eu	0.33	0.86	1.31	0.10	0.59	0.50	0.37	0.22	0.23	0.29	0.47
Gd	0.67	2.08	2.10	0.21	1.89	2.38	0.87	0.66	0.32	0.48	1.08
Dy	0.64	1.68	1.57	0.21	1.57	2.14	0.88	1.05	0.24	0.45	0.63
Er	0.57	1.28	1.21	0.24	1.12	1.46	0.80	1.23	0.24	0.42	0.47
Yb	0.69	1.45	1.47	0.36	1.03	1.31	1.01	1.55	0.32	0.49	0.50
La (ppm)	0.04	0.02	0.06	0.04	0.03	0.02	0.03	0.02	0.56	0.26	0.49
Ce (ppm)	0.64	1.20	1.67	0.28	1.80	1.60	0.77	0.81	1.04	0.85	5.06
Nd (ppm)	0.19	0.27	1.28	0.06	0.27	0.31	0.18	0.14	0.20	0.14	0.35
Sm (ppm)	0.42	0.88	2.15	0.17	0.96	0.89	0.42	0.35	0.31	0.30	0.80
Eu (ppm)	0.40	1.05	1.59	0.12	0.72	0.60	0.45	0.27	0.28	0.35	0.57
Gd (ppm)	5.36	16.62	16.82	1.65	15.08	19.07	7.00	5.29	2.56	3.85	8.61
Dy (ppm)	29.49	77.29	72.13	9.78	72.02	98.21	40.30	48.14	10.96	20.55	28.77
Er (ppm)	77.65	173.66	165.03	32.12	151.92	198.69	108.80	167.80	32.49	56.88	64.18
Yb (ppm)	191.64	401.78	408.12	100.55	286.63	361.68	279.61	429.75	88.62	136.29	137.18
Lu (ppm)	n.d.	n.d.	n.d.	n.d.	n.d.	n.d.	n.d.	n.d.	n.d.	n.d.	n.d.
ΣREE	305.83	672.76	668.84	144.77	529.44	681.07	437.56	652.57	137.02	219.48	246.01
Hf (ppm)	5162.34	5658.85	6267.59	6474.29	5518.02	6772.30	5429.16	6813.95	3156.34	2862.66	3253.47
Th (ppm)	209.08	733.59	415.00	34.74	1180.47	1072.14	317.20	246.98	64.68	155.46	11.60
U (ppm)	798.27	1504.48	987.00	172.94	2869.57	2170.66	992.51	965.16	254.12	493.99	33.08
Y (ppm)	389.65	932.81	833.83	149.95	816.29	1086.32	544.07	803.74	181.09	315.77	451.73
Th/U	0.26	0.49	0.42	0.20	0.41	0.49	0.32	0.26	0.25	0.31	0.35
Yb/Gd	35.76	24.18	24.27	60.91	19.01	18.97	39.97	81.31	34.62	35.42	15.93
Sm/La	11.77	42.90	38.44	4.63	27.81	51.95	12.55	22.31	0.56	1.16	1.63
Dy+Er+Yb	298.78	652.73	645.28	142.45	510.57	658.58	428.71	645.69	132.07	213.71	230.13
Age (Ma)	150.20	149.80	151.10	147.50	146.00	145.50	145.50	144.80			
Age error	0.80	0.60	0.70	1.70	0.40	0.50	0.70	0.70			

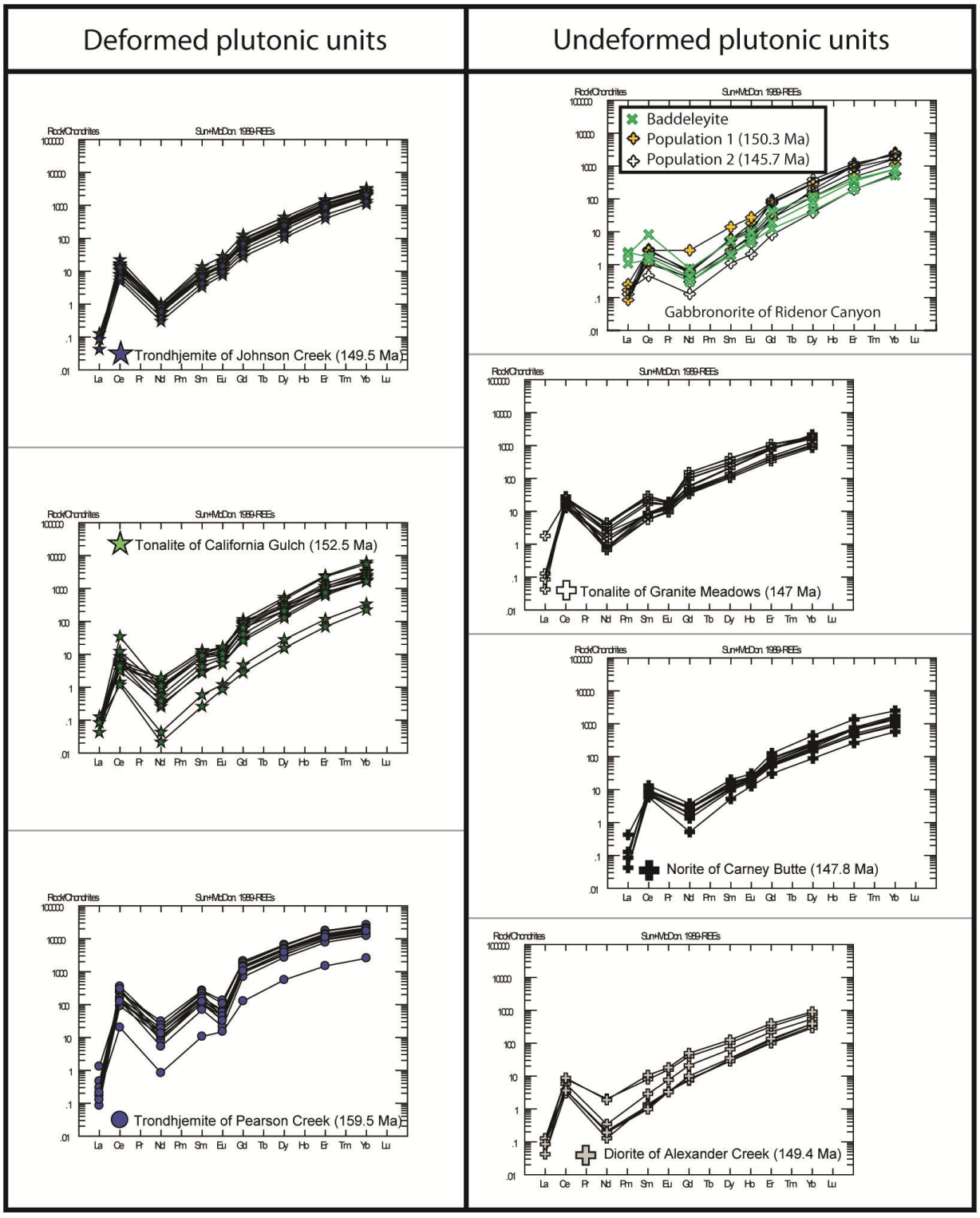

Figure 28. REE Spider diagrams from the zircons of the seven plutonic units analyzed, deformed (left) and undeformed (right).

The magnitude of the Eu anomalies of the zircons in the MHMC and Carney Butte Stock decreases from the oldest deformed unit to the youngest deformed unit. After deformation, the magnitude of the negative anomaly begins to grow, only to be reduced again in the Gabbronorite of Ridenor Canyon. This relationship is independent of the final mineralogy of the pluton.

The Tonalite of Granite Meadows shows a variation in zircon chemistry that is found in the cathodoluminescence (CL) images (Figure 16; Appendix C). The CL images range from very dark to very light with bright rims. The darker population is also more enriched in Th, U, and Hf while the lighter population is more enriched in Y, Yb, Er, Dy, Gd, Eu, Sm, Nd, and Ce. This chemical bimodality is evident in all of the analyzed zircons.

3i. Structure

The majority of structural data is measured from foliation planes in the deformed plutonic rocks, the keratophyre unit, or the metasedimentary unit. Other features such as small shear zones and dikes were also measured (Figure 29, Table 11). Significant folding was observed in the Schist of Yellowjacket Road and the Amphibolite Gneiss at outcrop scale. Medium scale (up to tens of feet in amplitude) folding with occasional isoclinal crenulation folding was found in the Schist of Yellow Jacket Road, especially in proximity to its contact with the Diorite of Alexander Creek. Open to gentle folds were found in the Amphibolite Gneiss along Stanley Creek. In general, the easternmost exposures have principle compressive stress vectors that are shallowly dipping (to the modern NW), and the other deformed units of the MHMC generally have steeply dipping compressive stress vectors (to the modern N by NW). These findings are comparable to those of Trauba (1975) and Avé Lallemant (1995).

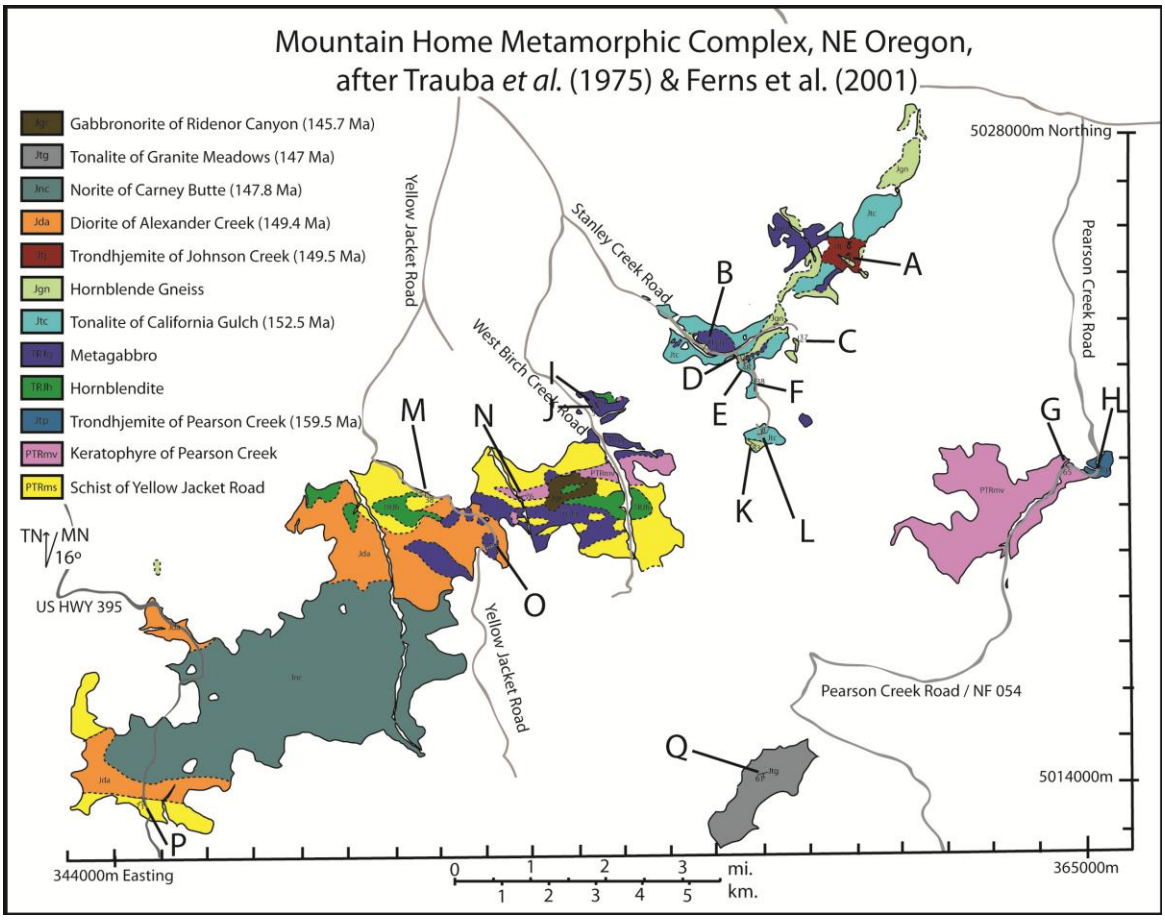

Figure 29. Structural analysis site locations used in this study of the MHMC. Site H (b) is on a Shear zone and H (a) is on a dike; the rest are foliation planes. See corresponding Table 10 for dip and dip direction values as well as any corresponding linear measurements.

Table 11. Structural analysis measurements taken in this study of the MHMC. Site letters correspond with the map in Figure 29. All lineations are mineral lineations (amphibole).

Map Label	Unit	Description	Dip	Dip Direction	Linear Feature	Trend	Plunge
A	Trondhjemite of Johnson Creek	Foliation	75	285			
B (a)	Amphibolite Gneiss	Foliation	14	198	Lineation	327	1
B (b)	Amphibolite Gneiss	Foliation	21	122	Lineation	187	21
C	Amphibolite Gneiss	Foliation	37	6			
D	Amphibolite Gneiss	Foliation	38	160			
E	Amphibolite Gneiss	Foliation	48	145			
F	Tonalite of California Gulch	Foliation	38	14			
G	Keratophyre of Pearson Creek (Grn)	Foliation	65	138			
H (a)	Dike	Dike	85	113			
H (b)	Trondhjemite of Pearson Creek	Shear Zone	45	237			
I	Metagabbro - Typical	Foliation	41	60	Lineation	140	9
J	Metagabbro - Typical	Foliation	57	234	Lineation	140	9
K	Amphibolite Gneiss	Foliation	83	212	Lineation	183	74
L	Tonalite of California Gulch	Foliation	87	352			
M	Schist of Yellowjacket Road	Foliation	38	179			
N (a)	Keratophyre of Pearson Creek (Amph)	Foliation	76	250			
N (b)	Keratophyre of Pearson Creek (Amph)	Foliation	53	172	Lineation	171	52
O	Metagabbro - Fine Grained	Foliation	69	183			
P	Foliated Dike in Schist	Foliation	71	253			
Q	Tonalite of Granite Meadows - Enclave	Foliation	61	166			

4. DISCUSSION

4a. Hafnium analysis of the MHMC

The results of the Hf zircon analysis provide insight into the origins of the MHMC. A negative εHf_i value reflects contributions from old, continental crust and a positive value suggests derivation from depleted mantle source. The εHf_i isotope values for the zircons of the MHMC range from +16.3 to +4.2, with a 2σ mean weighted average of +10.33 +/- 0.46 (Tables 2 and 4, Figure 30). The εHf_i values of the MHMC are different than the +9.5 to +5 values of the Baker terrane, but overlap with the +14 to +9 values of individual plutons in the Wallowa terrane (Schwartz, personal communication, values are 2σ weighted averages).

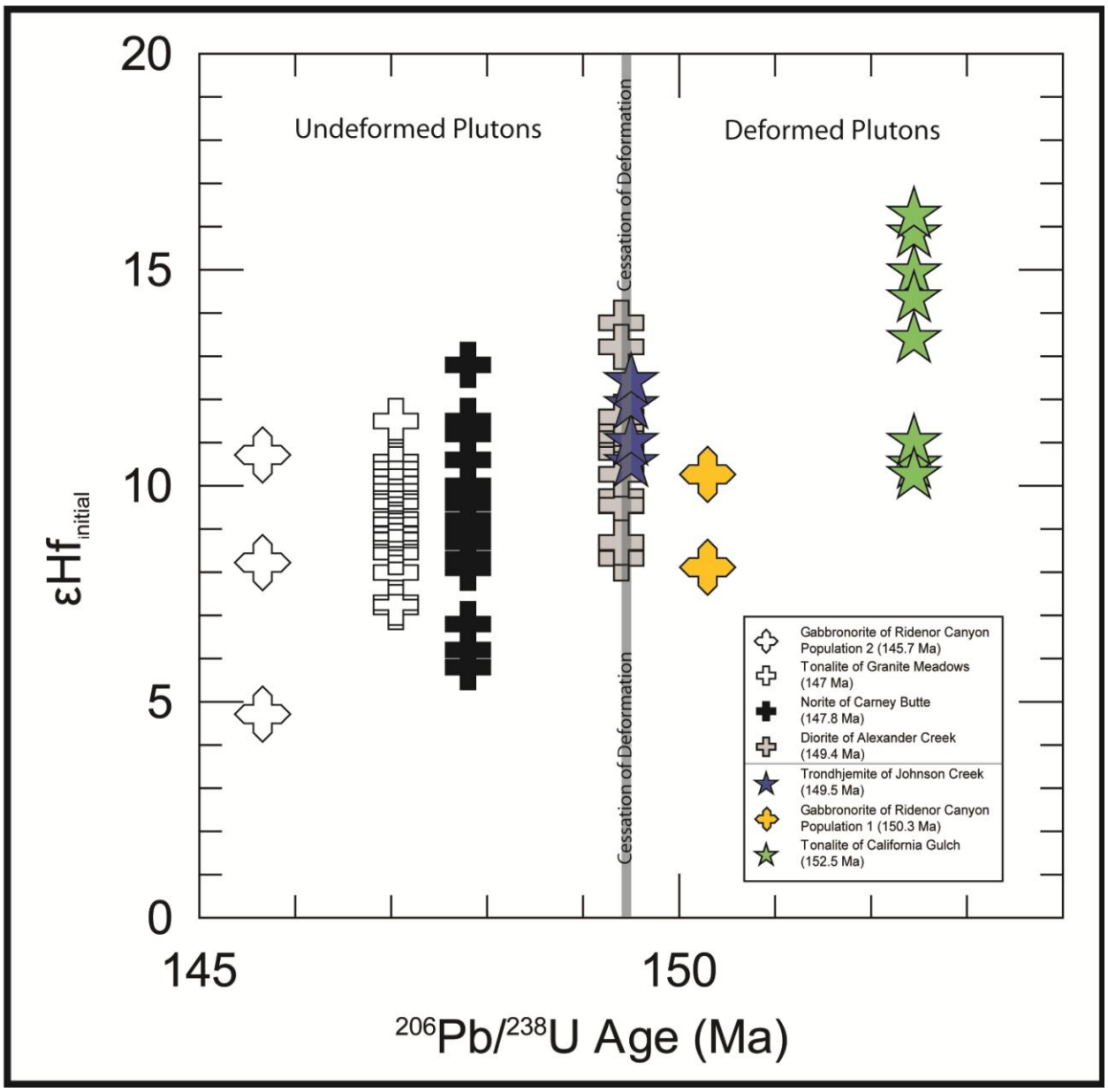

Figure 30. εHf_i plotted against $^{206}Pb/^{238}U$ age. Only analyses which produced both acceptable $^{206}Pb/^{238}U$ and eHfi data are included.

4b. Major and trace element geochemistry

Geochemical signatures vary across the MHMC and correlate with specific age ranges and degrees of metamorphism. The old (>159 Ma), greenschist facies, deformed units in the eastern section of the MHMC are felsic; the middle-age (as young as 149.5 Ma), amphibolite facies, deformed units of the north and central regions are mafic; the young (145.7 to 149.5 Ma), undeformed units to the south and central are intermediate to mafic in composition. In terms of N-MORB normalized trace element profile, all units show positive Th, U, and Ba anomalies, and negative P and Ti (and Nb where data is available) anomalies, consistent with derivation in a subduction zone environment or from interaction with crust formed in a subduction zone environment.

Some previous geochemical characterization has been performed in the Dixie Butte complex of the adjacent Baker terrane. Middle Jurassic (162-157 Ma) gabbros, diorites, and trondhjemites in the Dixie Butte complex are characterized by flat to slightly enriched light rare earth element (REE) abundances, low Sr (<400) and low Sr/Y values (<40). Late Jurassic (148-145 Ma) tonalites and dacites are characterized by depleted heavy REE abundances with steep LREE profiles, high Sr (>600 ppm) and high Sr/Y values (>40) (Schwartz *et al*., 2011b). Geochemical signatures of the plutons of the MHMC and those of the Dixie Butte complex are compared here to determine whether geochemical characteristics may provide a link between the MHMC and the Baker terrane.

i**.** *Deformed Units of the MHMC*

The Pearson Creek Trondhjemite is chemically distinctive, with the highest SiO_2 and Na_2O_3 and lowest MgO content in the MHMC. Relative to chondrite, the Trondhjemite of

Pearson Creek has a slightly LREE enriched flat profile, indicating little REE fractionation occurred to this melt. The presence of a negative Eu anomaly may indicate that plagioclase feldspar fractionated out of the melt. The laterally adjacent, greenschist facies, eastern exposure of the Pearson Creek Keratophyre also shows some enrichment in the LREEs as well as an unusual depletion relative to chondrite in the three heaviest HREEs. Similar geochemical studies of plutons in the nearby Baker terrane and in plutons stitching the Baker/Wallowa terrane boundary have not produced similar results.

The centrally located, amphibolite facies exposure of the Pearson Creek Keratophyre is more LREE enriched and slightly more HREE depleted than its greenschist equivalent. It also lacks the slight negative Eu anomaly found in the greenschist keratophyre. Although this outcrop has undergone a higher grade of metamorphism, major element composition does not differ greatly between the eastern greenschist-facies exposure and the central amphibolite-facies exposure. In terms of major elements, only two of the most mobile elements, K_2O and Na_2O, show minor differences between the two outcrops, indicating that while there has been some elemental mobility resulting from metamorphism, it has not been of great magnitude.

The Amphibolite Gneiss samples analyzed are chemically very similar to the Tonalite of California Gulch and exhibit a flat REE pattern. The N-MORB normalized trace element profile shows peaks at Ba, La, Pb, Sr, and Eu as well as either enrichment or depletion in Th and Zr. This chemical similarity may indicate that the tonalite could be the protolith for the Amphibolite Gneiss in the southern half of the northern region; however the Schist of Yellow Jacket Road is another potential protolith and has not been chemically characterized.

The Tonalite of California Gulch has the most positive εHf_i value (13 ± 1.3) and is therefore the most primitive in magmatic origin. For both samples analyzed, its chondrite normalized REE pattern is mostly flat with a slight LREE depletion and its N-MORB normalized trace element spider diagram is flat and close to N-MORB. The zircons analyzed were geochemically consistent with the whole rock geochemistry. The trace element spider profiles of the Tonalite of California Culch show a marked dissimilarity to the profiles of the plutons of the Dixie Butte complex in the Baker terrane.

The Trondhjemite of Johnson Creek has a chondrite normalized spider profile depleted in the HREEs relative to LREEs , as well as a LILE enriched N-MORB normalized spider profile. It also has the second most positive average εHf_i (11.47 ± 0.64). Whereas the Trondhjemite of Johnson Creek's chondrite normalized REE profile is somewhat similar to those of the Dixie Butte meta-andesite and some samples of the Dixie Summit gabbro, its trace element profile is distinct from that of plutons in the Dixie Butte complex,

The 'typical' variety of the Metagabbro shows a positive Eu anomaly and LREE enrichment. The Chondrite normalized REE pattern is flat overall and is similar to that of the 'porphyritic' textured sample, although the porphyritic sample has a much smaller positive Eu anomaly and shows a distinct depletion in all the LREEs. The typical and porphyritic variants have the lowest overall REE content in the entire MHMC.

Both the fine grained and xenolithic variants of the Metagabbro have similar Chondrite normalized REE patterns, characterized by LREE depletion and a humped profile. The fine grained texture is chemically closest to N-MORB and is significantly more mafic in major and trace element geochemistry than the 'typical' Metagabbro.

The combined implications of these profiles are that all parts of the Metagabbro, while somewhat heterogeneous across the exposures in texture and chemistry, are most likely derived from primitive sources, as indicated by their flat or LREE depleted Chondrite normalized REE profiles and flat N-MORB normalized trace element profiles. The textural variations Trauba (1975) described correspond to somewhat striking differences in chemistry across the exposure areas, suggesting that this is not one unit, but several different units that appear similar. They were later subjected to the same metamorphism and deformation conditions, which compounds the complexity, and further research is needed to clarify this issue.

The largely flat chondrite normalized REE profiles and the N-MORB normalized trace element spider profiles of many of the deformed plutons in the MHMC including the Tonalite of California Gulch, the Trondhjemite of Johnson Creek, and the Amphibolite Gneiss bear little chemical similarity to the plutons of the Dixie Butte complex in the Baker terrane.

ii. *The Undeformed Plutons of the MHMC*

The undeformed units of the MHMC (the Diorite of Alexander Creek, the Norite of Carney Butte , and the Tonalite of Granite Meadows) are chemically similar in terms of N-MORB normalized trace element profile and in most Harker diagrams. These undeformed plutons show enriched LREE patterns and depleted, flat HREE patterns. The N-MORB normalized spider diagrams generally show LILE enrichment and peaks at Pb, Sr, and Nd as well as troughs at Th, Nb, P, and Zr. In the LREEs, the undeformed units form a separate fractionation trend from that of the deformed units; however this is not true with respect to HREEs. In the high field strength element Harker diagrams (specifically U, Pb, and Th), the undeformed units form a separate trend from the deformed units; however, this may be due more

to their different silica range than to a separate fractionation trend. In Zr and V Harker space, the undeformed units plot along trend, supporting their major element classification.

The Gabbronorite of Ridenor Canyon is an exception to the chemical trends described for most of the undeformed plutons of the MHMC. The gabbronorite is distinctly heterogeneous, with two outcrops of coarse grained pyroxene cumulates and the other two being plagioclase cumulates. The REE pattern for the single pyroxene cumulate analyzed exhibits LREE depletion and the slight humped profile expected of a rock composed almost entirely of pyroxene. In the V Harker diagram, the cumulate is semi-linear but very high and not correlating with the overall trend of the MHMC. However, the V content supports its mafic nature, as does the low Zr content. The high V is likely due to incorporation into oxides, pyroxenes, and amphibole. The lateral, mineralogical, and chemical heterogeneity combined with its tendency to crop out poorly implies that the Gabbronorite of Ridenor Canyon may not be a single pluton. This would explain why the pyroxene cumulate fits poorly with the geochemical trends of the undeformed plutons in the MHMC in Harker diagram space, why its N-MORB normalized trace element pattern and chondrite normalized REE pattern are more similar to the Metagabbro than to undeformed plutons of the MHMC, and why there are two clearly distinguishable age populations of zircons that span the end of the MHMC's deformational event.

When compared to the geochemically characterized Dixie Butte complex in the Baker terrane, the undeformed units of the MHMC are geochemically distinct. In chondrite normalized REE space, they are both HREE depleted and LREE enriched with a significant slope (with the exception of the Gabbronorite of Ridenor Canyon), but the slope found in the plutons of the MHMC is much less steep and the magnitude of the LREE enrichment is less as well. In N-MORB normalized trace element space the MHMC and the Dixie Butte complex also differ

substantially; the undeformed plutons of the MHMC are less enriched in the LILEs and less depleted in the elements Ti through Lu than the plutons of the Dixie Butte complex.

4c. Zircon geochemistry

The zircons analyzed from the deformed and undeformed plutonic suites showed fairly consistent REE patterns (Figure 26), with moderate slopes, positive Ce anomalies, and Eu anomalies ranging from nonexistent to minor negative. The zircon analysis from the Tonalite of Granite Meadows shows a curious chemical bimodality. One group is REE enriched and shows a negative Eu anomaly (but is lower in U), and the other group is REE depleted and shows a positive Eu anomaly (but is higher in U). The Trondhjemite of Pearson Creek is generally an order of magnitude higher in every element analyzed than any other unit in the MHMC. The high REE content of this unit is what made it impossible to accurately measure its εHf value.

4d. Metamorphism in the MHMC

Metamorphism in the MHMC is medium to high grade, reaching amphibolite facies in its main exposure and greenschist facies in its eastern exposure. The Schist of Yellow Jacket Road is a clear-cut example of garnet zone metamorphism in the central MHMC, with a mineral assemblage of quartz+plagioclase+biotite+muscovite±garnet±graphite. Trauba (1975) also found substantial local staurolite as well as select localities that contained sillimanite. The Schist of Yellow Jacket Road contains rotated pre to syn-tectonic garnets acting as strain markers in some regions as well. The presence of staurolite in the Schist of Yellow Jacket Road is diagnostic of the area having locally reached amphibolite facies.

The Keratophyre of Pearson Creek further demonstrates the extent of metamorphism in the MHMC: the eastern exposure contains quartz+chlorite+sodic

plagioclase+muscovite±biotite±hornblende±sphene (Trauba also found epidote and established the plagioclase to be albite), whereas the central exposure of the keratophyre also contains garnet and staurolite (much like the nearby Schist of Yellow Jacket Road), but lacks epidote and chlorite. The mineral assemblage of the eastern exposure indicates that it may have experienced metamorphism of no higher facies than greenschist, although further work P-T work would need to be done to support this conclusion. The presence of diagnostic minerals such as garnet and staurolite indicate that the central exposure experienced conditions more favorable to the growth of amphibolite facies minerals. In the Amphibolite Gneiss the presence of metamorphic garnet associated with leucosomes primarily composed of plagioclase may reflect partial melting and growth of peritectic garnet. However, the bulk of the unit is composed of hornblende and plagioclase of varying composition (An_{70} or less, Trauba, 1975) and with some sodic rim growth. The presence of small pockets containing tremolite and actinolite consistent with a lower grade of metamorphism may reflect retrograde metamorphism or possibly the local preservation of prograde mineral assemblages.

4e. Magmatism and deformation in the MHMC and the BMP

Based on the results of U-Pb zircon geochronology, magmatism in the MHMC occurred continuously from ca. 152-145 Ma. In contrast, three pulses of magmatism have been identified in the central BMP: 111-124 Ma, 141-148 Ma, and 154-162 Ma (Schwartz *et al*., 2011b). No evidence of magmatism from 154-148 Ma in the central BMP has been identified, a time frame during which magmatism was frequent in the MHMC.

However, Pb/U ages of plutons in the western Klamath Mountains indicate fairly continuous magmatism from ~150-136 Ma, a timeframe that overlaps that of the MHMC (Allen

and Barnes, 2006). Specifically, the magmatic pulse associated with the Western Klamath episode (pluton ages ranging from ~154-147 Ma) (Irwin and Wooden, 1999) correlate with the 152-145 Ma magmatism of the MHMC. The magmatic pulse associated with the Rattlesnake Creek episode in the Klamaths (pluton ages ranging from ~ 164-155 Ma) overlaps with the emplacement of the oldest dated unit in the MHMC, the Trondjhemite of Pearson Creek (~159.5 Ma) Taken together, the timing of magmatism in the MHMC overlaps with the timing of magmatism in the Klamath Mountains, but contrasts with that of the central BMP, indicating that the MHMC may have originated as part of the western Klamath Mountain province.

U-Pb geochronology in the deformed and undeformed plutonic suites indicate that a major deformational event accompanied by moderate to high grade metamorphism occurred between ~150-148 Ma. This timing of deformation does not match any of the proposed models for deformation in the BMP. Other workers have constrained the ages of deformation resulting from the formation of the two nearest terrane/subterrane boundaries in the BMP; the Wallowa-Baker terrane boundary contractional deformational event has been constrained to 159-157 Ma (based on detrital zircons, LaMaskin, 2009, and zircons from post-kinematic fault stitching plutons, Schwartz *et al.* 2011a) and the Bourne-Greenhorn subterrane boundary is similarly constrained to between 159 and 154 Ma (Schwartz *et al.*, 2011b). The deformational event with the most similar timing in the Cordillera is that of the Nevadan orogeny initially proposed by Harper and Wright (1984) and revised by Chamberlain *et al.* (2006; 153 to 150 Ma) in relation to the Klamath Mountains to the south.

The timing of deformation and magmatism, combined with the moderate to high grade metamorphism that occurred in the MHMC, indicates that the MHMC does not share the same geologic history as the central BMP. Instead, the MHMC may be a new island arc terrane that

amalgamated onto the BMP in the Late Jurassic, with associated deformation occurring at the same time as the Nevadan deformation. An alternative hypothesis is that the MHMC may have originated as part of the Klamath Mountains province to the south, with which the MHMC shares similar timing of magmatism and deformation as well as lithology, and been translated northeastward during the Late Cretaceous.

5. CONCLUSIONS

The geologic history of the MHMC fits poorly with the known history of the rest of the BMP. The major metamorphic event and the corresponding deformation was regionally amphibolite facies, significantly higher grade than any other regional scale metamorphism in the BMP. This metamorphic event ended between 147.3 and 151.1Ma, which coincides with the 147 to 150 Ma Nevadan Orogeny of the Klamath Mountains (Wright and Fahan, 1988) but not with any known BMP event or deformation model. Magmatism in the MHMC occurred continuously from 152-145 Ma, whereas no magmatism is known to have occurred in the central BMP during an overlapping time period of 154-148 Ma. The εHf_i range (+16.3 to +6.5, predeformation and +13.8 to +5.8, postdeformation) of the MHMC's plutons is greater than that of the Baker Terrane. Cumulatively, these results imply that the MHMC is not part of the Wallowa or Baker terranes, but is an independent island arc terrane and may possibly be linked to the Nevadan orogeny of the Klamath Mountains. To further substantiate this possibility, more study of the area would be necessary. The metasedimentary unit as well as the predeformational units in particular still need to be better understood, especially the ages of emplacement for the plutonic units, the ages of metamorphic mineral growth for the metasedimentary unit (as well as the Amphibolite Gneiss), and the geochemistry of all the MHMC units. The P-T path for the main body of the MHMC also needs to be established. Future research into the connection between the MHMC, the Carney Butte Stock, and their outlier to the southwest would also be needed to fully define the role of the MHMC in the geologic history of the Western North American Cordillera.

6. REFERENCES

Allen, C.M., and Barnes, C.G., 2006, Ages and some cryptic sources of Mesozoic plutonic rocks in the Klamath Mountains, California and Oregon, *in* Snoke, A.W., and Barnes, C.G., eds., Geological Studies in the Klamath Mountains Province, California and Oregon: A volume in honor of William P. Irwin, Volume 410, Geological Society of America, p. 223-245.

Ashley, R.P., 1995, Petrology and deformation history of the Burnt River Schist and associated plutonic rocks in the Burnt River Canyon area, northeastern Oregon, *in* Vallier, T.L., and Brooks, H.C., eds., Geology of the Blue Mountains Region of Oregon, Idaho, and Washington: Petrology and Tectonic Evolution of Pre-Tertiary Rocks of the Blue Mountains Region: U.S. Geological Survey Professional Paper 1438, p. 457-495.

Avé Lallemant, H.G., 1995, Pre-Cretaceous tectonic evolution of the Blue Mountains Province, northeastern Oregon: U. S. Geological Survey Professional Paper 1438, p.271-304.

Barnes, C.G., Snoke, A.W., Harper, G.D., Frost, C.D., McFadden, R.R., Bushey, J.C., and Barnes, M.A.W., 2006, Arc plutonism following regional thrusting: Petrology and Geochemistry of syn- and post-Nevadan plutons in the Siskiyou Mountains, Klamath Mountains province, California, *in* Snoke, A.W., and Barnes, C.G., eds., Geological Studies in the Klamath Mountains Province, California and Oregon: A Volume in Honor of William P. Irwin: Geological Society of America Special Paper 410, p. 357-376.

Belousova, E.A., Griffin, W.L., and O'Reilly, S.Y., 2006, Zircon Crystal Morphology, Trace Element Signatures and Hf Isotope Composition as a Tool for Petrogenetic Modeling: Examples From Eastern Australia Granitoids, Journal of Petrology, vol. 47, p. 329-353.

Bishop, E.M., 1995a, High-pressure, low-temperature schistose rocks of the Baker terrane, northeastern Oregon, *in* Vallier, T.L., and Brooks, H.C., eds., Geology of the Blue Mountains Region of Oregon, Idaho and Washington: Petrology and Tectonic Evolution of Pre-Tertiary Rocks of the Blue Mountains Region: U.S. Geological Survey Professional Paper 1438, p. 211-245.

Brooks, H.C., and Vallier, T.L., 1978, Mesozoic rocks and tectonic evolution of eastern Oregon and western Idaho, *in* Howell, D.G., and McDougall, K.A., eds., Mesozoic Paleogeography of the Western United States: Los Angles, Pacific Section, Society of Economic Paleontologists and Minerologists, p. 133-145.

Barnes, C.G., eds., Geological studies in the Klamath Mountains Province, California and Oregon: a volume in honor of William Pl Irwin: Geological Society of America Special Paper 410, p. 317-332.

Coleman, R.G., Manning, C.E., Mortimer, N., Donato, M.M., and Hill., 1988, Tectonic and regional metamorphic framework of the Klamath Mountains and adjacent Coast Ranges, California and Oregon, *in* Ernst, W.G., ed., Metamorphism and Crustal Evolution of the Western United States—Rubey volume 7: Englewood Clifs, New Jersey, Prentice Hall, p. 1059-1097.

Condie, K.C., and Chomiac, B., 1996, Continental Accretion: Contrasting Mesozoic and Early Proterozoic tectonic regimes in North America: Tectonophysics, vol. 265, p. 101-126.

Corfu, F., Hanchar, J.M., Hoskin, P.W.O., & Kinny, P., 2003. Atlas of zircon textures, in Hanchar, J.M., Hoskin, P.W.O., & Kinny, P.W.O., eds., Zircon. Reviews in Minerology and Geochemistry, vol. 53, p. 469-499.

de Witt, M.J., 1998, On Archean granites, greenstones, cratons and tectonics: does the evidence demand a verdict? : Precambrian Research, vol. 91, p. 181-226.

DeBari, S.M. and Sleep, N.H., 1991, High-MG, Low-AL bulk composition of the Talkeetna island-arc, Alaska- Implications for primary magmas and the nature of arc crust: Geological Society of America Bulletin, vol. 103(1), p. 37-47.

Dhuime, B., Hawkesworth, C., Cawood, P., 2011, When Continents Formed. Science, v. 331, pp. 154-155.

Dorsey, R.J., and LaMaskin, T.A., 2007, Stratigraphic record of Triassic-Jurassic collisional tectonics in the Blue Mountains Province, Northeastern Oregon: American Journal of Science, vol. 307, p. 1167-1193.

Ferns, M.L., and Brooks, H.C., 1995, The Bourne and Greenhorn subterranes of the Baker terrane, northeastern Oregon: Implications for the evolution of the Blue Mountains island-arc system *in* Vallier, T.L. and Brooks, H.C., ed., Geology of the Blue Mountains Region of Oregon, Idaho, and Washington: Petrology and Tectonic Evolution of Pre-Tertiary Rocks of the Blue Mountains Region: U.S. Geological Survey Professional Paper 1438, p. 331-358.

Ferns, M.L., Maden, I.P., and Taubeneck, W.H., 2001, Reconnaissance Geologic Map of the La Grande 30x60 Minute Quadrangle, Baker, Grant, Umatilla, and Union Counties, Oregon: Oregon Department of Geology and Mineral Industries Reconnaissance Map Series RMS-1, map scale 1:24,000, 52 p.

Follo, M.F., 1994, Sedimentology and stratigraphy of the Martin Bridge Limestone and Hurwal Formation (Upper Triassic to Lower Jurassic) from the Wallowa Terrane, Oregon, *in* Vallier,

T.L., and Brooks, H.C., eds., Geology of the Blue Mountains Region in Oregon, Idaho, and Washington: Stratigraphy, physiography, and mineral resources: Reston, Virginia, U.S. Geological Survey Professional Paper 1439, p. 1-27.

Frost, B.R., Barnes, C.G., Collins, W.J., Arculus, R.J., Ellis, D.J., and Frost, C.D., 2001, A geochemical classification for granitic rocks: Journal of Petrology, v. 42, p. 2033-2048, doi: 10.1093/petrology/42.11.2033.

Getty, S.R., Selverstone, J., Wernicke, B.P., Jacobsen, S.B., Aliberti, E., Lux, D.R., 1993, Sm-Nd dating of multiple garnet growth events in an arc-continent collision zone, northwestern U.S. Cordillera: Contributions to Mineralogy and Petrology, no. 115, p. 45-57.

Hacker, B.R., Donato, M.M., Barnes, C.G., McWilliams, M.O., and Ernst, W.G., 1995, Timescales of Orogeny; Jurassic construction of the Klamath Mountains: Tectonics, v. 14, p. 677-703, doi: 10.1029/94TC02454.

Harper, G.D., and Wright, J.E., 1984, Middle to Late Jurassic tectonic evolution of the Klamath Mountains, California-Oregon: Tectonics, v. 3, p. 759-772, doi: 10.1029/TC003i007p00759.

Jarvis, I., and Jarvis, K.E., 1992, Plasma spectrometry in the Earth Sciences: techniques, applications and future trends: Chemical Geology, v. 95, p. 1-33.

Johnson, K., Barnes, C.G., and Miller, C.A., 1997, Petrology, geochemistry, and genesis of high-Al tonalite and trondhjemites of the Cornucopia Stock, Blue Mountains, northeastern Oregon: Journal of Petrology, v. 38, no. 11, p. 1585-1611.

Johnson, K., and Schwartz, J.J., 2009, Overview of Jurassic—Cretaceous magmatism in the Blue Mountains Province (NE Oregon & W Idaho): Insights from new Pb/U (SHRIMP-RG) age determinations: Geological Society of America Abstracts with Programs, v. 41, no. 7, p. 182.

Johnson, K., Schwartz, J.J., Richter, M.E., Downing, J., Barnes, M.A., and Wooden, J.L., 2012, The Fish Lake Complex, NE Oregon: Estimating melt compositions using clinopyroxene trace element data from a cumulate-rich pluton: Geological Society of America Abstracts with Programs, v. 44, no. 6, p. 94.

Johnson, K., Schwartz, J.J., Wooden, J.L., O'Driscoll, L.J., and Jeffcoat, C.R., 2011, The Wallowa Batholith: New Pb/U (SHRIMP-RG) ages place constraints on arc magmatism and crustal thickening in the Blue Mountains province, NE Oregon: Geological Society of America Abstracts with Programs, v. 43, no. 4, p. 5.

Kinny P.D., and Maas, R., 2003, Lu–Hf and Sm–Nd isotope systems in zircon: Reviews in Mineralogy and Geochemistry, v. 53, p. 327-341.

Kurz, G.A., Schmitz, M.D., Northrup, C.J., and Vallier, T.L., 2012. U-Pb geochronology and geochemistry of intrusive rocks from the Cougar Creek Complex, Wallowa arc terrane, Blue Mountains Province, Oregon-Idaho; Geological Society of America Bulletin, v. 124, no. 9-10.

LaMaskin, T.A., Schwartz, J.J., Dorsey, R.J., Snoke, A.W., Johnson, K., Vervoort, J.D., 2009, Mesozoic sedimentation, magmatism, and tectonics in the Blue Mountains Province, northeastern Oregon, in O'Connor, J.E., Dorsey, R.J., and Madin, I.P., eds., Volcanics to Vineyards: Geologic Field Trips through the Dynamic Landscape of the Pacific Northwest: Geological Society of America Field Guide 15, p. 1-17.

LaMaskin, T.A., Vervoort, J.D., Dorsey, R.J., and Wright, J.E., 2011 Early Mesozoic paleogeography and tectonic evolution of the western United States: Insights from detrital zircon U-Pb geochronology, Blue Mountains Province, northeastern Oregon: Geological Society of America Bulletin, v. 123, p. 1939-1965, doi: 10.1130/B30260.1.

Mailloux J.M., Starns, E.C., Snoke, A.W., and Frost, C.D., 2009, An isotopic study of the Burnt River Schist: Implications for the development of the composite Baker terrane, Blue Mountains Province, NE Oregon: Geological Society of America Abstracts with Programs, v. 41, no. 7, p. 441.

Nir-El, Y., & Lavi, N., 1998, Measurement of the half-life of ^{176}Lu: Applied Radiation and Isotopes, v. 49, p. 1653-1655.

Parker, K.O., Schwartz, J.J., Johnson, K., and Anonymous, 2008, Petrology and age of Dixie Butte plutonic rocks, Blue Mountains, NE Oregon: Geological Society of America Abstracts with Programs, v. 40, no. 6, p. 154-155.

Patchett, P.J., & Tatsumoto, M., 1980, Hafnium isotope variations in oceanic basalts: Geophysical Research Letters, v. 7, p. 1077-1080.

Patchett, P.J., and Tatsumoto, M., 1980a, A routine high-precision method for Lu-Hf isotope geochemistry and chronology: Contributions to Mineralogy and Petrology, v. 69, p. 33-47.

Patchett, P.J., 1983, Importance of the Lu-Hf isotopic system in studies of planetary chronology and chemical evolution: Geochimica et Cosmochimica Acta, v. 47, p. 81-91.

Petcovic, H.L., and Grunder, A.L., 2003, Partial melting of tonalite at the margins of a Columbia River Basalt Group Dike, Wallowa Mountains, northeastern Oregon: Journal of Petrology, v. 44, n. 12, p. 2287-2312.

Sano, Y., Terada, K., Fukuoka, T., 2002, High mass resolution ion microprobe analysis of rare earth elements in silicate glass, apatite and zircon: lack of matrix dependency: Chemical Geology, v. 184, p. 217-230.

Scherer, E., Munker, C., Mezger, K., 2001, Calibration of the Lutetium-Hafnium Clock: Science, v. 239, p. 683-687.

Schwartz, J.J., and Johnson, K., 2009, Origin of paired Late Jurassic high and low Sr/Y magmatic belts in the Blue Mountains Province, NE Oregon: Geological Society of America Abstracts with Programs, v. 41, no.7, p. 182.

Schwartz, J.J., Snoke, A.W., Frost, C.D., Barnes, C.G., Gromet, L.P., and Johnson, K., 2010, Analysis of the Wallowa-Baker terrane boundary: Implications for tectonic accretion in the Blue Mountains province, northeastern Oregon: Geological Society of America Bulletin, v. 122, no. ¾, p. 517-536.

Schwartz , J.J., Johnson, K., Miranda, E.A., and Wooden, J.L., 2011b, The generation of high Sr/Y plutons following Late Jurassic arc-arc collision, Blue Mountains province, NE Oregon: Lithos, v. 126, p. 22-41.

Schwartz , J.J., Snoke, A.W., Cordey, F., Johnson, K., Frost, C.D., Barnes, C.G., LaMaskin, T.A., Wooden, J.L., 2011a, Late Jurassic magmatism, metamorphism and deformation in the Blue Mountains province, northeast Oregon: Geological Society of America Bulletin 123, p. 2083-2111.

Selverstone, J., Wernicke, B.P., Aliberti, E.A., 1992, Intracontinental subduction and hinged unroofing along the Salmon River Suture Zone, West Central Idaho: Tectonics, v. 11, no. 1, p. 124-144.

Sguigna, A. P., Larabee, A. J., Waddington J. C., 1982, The half-life of ^{176}Lu by a γ–γ coincidence measurement: Canadian Journal of Physics, v. 60, p. 361-364.

Siivola, J, and Schmid, R. A systematic nomenclature for metamorphic rocks: 12. List of mineral abbreviations. Recommendations by the IUGS Subcommission on the Systematics of Metamorphic Rocks. *Recommendations*, web version of 01.02.2007.

Snee, L.W., Lund, K., Sutter, J.F., Balcer, D.E., Evans, K.V., 1995, An 40Ar/39Ar Chronicle of the tectonic development of the Salmon River Suture Zone, Western Idaho: U.S. Geological Survey Professional Paper 1438, p. 359-414.

Snoke, A.W., and Barnes, C.G., 2006 The development of tectonic concepts for the Klamath Mountains province, California and Oregon, *in* Snoke, A.W., and Barnes, C.G., eds., Geological Studies in the Klamath Mountains Province, California and Oregon: A Volume in Honor of William P. Irwin: Geological Society of America Special Paper 410, p. 1-29.

Stacey, J.S., and Kramers, J.D., 1975, Approximation of terrestrial lead isotope evolution by a two stage model: Earth and Planetary Science Letters, v. 26, p. 207-221, doi: 10.1016/0012-821X(75)90088-6.

Tatsumoto, M., Unruh, D.M. Patchett, P. J., 1981, U-Pb and Lu-Hf systematics of Antarctic meteorites: Memoirs of the National Institute of Polar Research, Special Issue No. 20, p.237.

Taylor and McLennan, 1995, The geochemical evolution of the continental crust: Reviews of Geophysics, vol. 33 (2), p. 241-265.

Trauba, W.C., 1975, Petrography of Pre-Tertiary Rocks of the Blue Mountains, Umatilla County, Northeast Oregon [Masters Thesis]: Oregon State University, 188 p.

Tumpane, K.P., 2010, Age and isotopic investigations of the Olds Ferry terrane and its relations to other terrenes of the Blue Mountains Province, eastern Oregon and west-central Idaho: [M.S. Thesis], Boise State University, Boise, Idaho., 201 p.

Unruh, D.M., Lund, K., Kuntz, M.A., and Snee, L.W., 2008, Uranium-Lead Zircon Ages and Sr, Nd, and Pb Isotope Geochemistry of Selected Plutonic Rocks from Western Idaho: U.S. Geological Survey Open-File Report 1142, 37p.

Vallier, T.L., 1995, Petrology of pre-Tertiary igneous rocks in the Blue Mountains region of Oregon, Idaho, and Washington; implications for the geologic evolution of a complex island arc, *in* Vallier, T.L., and Brooks, H.C., eds., Geology of the Blue Mountains Region of Oregon, Idaho and Washington: Petrology and Tectonic Evolution of Pre-Tertiary Rocks of the Blue Mountains Region: U.S. Geological Survey Professional Paper 1438, p. 125-209.

Vallier, T.L., Brooks, H.C., and Thayer, T.P., 1977 Paleozoic rocks of eastern Oregon and western Idaho: Los Angeles, California, Pacific Section, Society of Economic Paleontologists and Mineralogists, p. 455-466.

Vervoort, J.D., Patchett, P.J., Söderlund, U., Baker, M., 2004, Isotopic composition of Yb and the determination of Lu concentrations and Lu/Hf ratios by isotope dilution using MC-ICPMS: Geochemistry, Geophysics, Geosystems, v. 5, p. 15.

Walker, N.W., 1995, Tectonic implications of U-Pb zircon ages of the Canyon Mountain Complex, Sparta complex, and related metaplutonic rocks of the Baker terrane, northeastern Oregon, chap. 6 *of* Vallier, T.L., and Brooks, H.C., eds., Geology of the Blue Mountains region of Oregon, Idaho, and Washington: Petrology and tectonic evolution of pre-Tertiary rocks of the Blue Mountains region: U.S. Geological Survey Professional Paper 1438, p. 247-269.

Walker, N.W., 1989. Early Cretaceous initiation of post-tectonic plutonism and the age of the Connor Creek Fault, northeastern Oregon. Geological Society of America Abstracts with Programs 21, 155.

White, D.L., and Vallier, T.L., 1994, Geologic evolution of the Pittsbug Landing area, Snake River Canyon, Oregon and Idaho, *in* Vallier, T.L., and Brooks, H.C., eds., Stratigraphy,

Physiography, and Mineral Resources of the Blue Mountains Region: U.S. Geological Survey, Reston, VA, Volume Professional Paper 1439, p. 55-74.

Wilson, D., and Cox, A., 1980, Paleomagnetic evidence for tectonic rotation of Jurassic plutons in Blue Mountains, eastern Oregon: Journal of Geophysical Research, v. 85, p. 3681–3689.

Wright, J.E., and Fahan, M.R., 1988, An Expanded view of Jurassic Orogenesis in the Western United States Cordillera: Middle Jurassic (pre-Nevadan) regional metamorphism and thrust faulting within an active arc environment, Klamath Mountains, California: Geological Society of America Bulletin, v. 100, p. 859-876.

Zen, E., 1985, Implications of magmatic Epidote-bearing plutons on crustal evolution in the accreted terranes of northwestern North America: Geology, v. 13, p. 266-269.

Appendix A

All images are of thin sections (10µm sample thickness) taken using the standard settings of a petrographic microscope. They were taken at the 4x magnification setting unless otherwise marked. A table of sample collection coordinates is included at the end of this Appendix.

a. Schist of Yellow Jacket Road

i. Garnet Bearing Variety

The garnet-bearing variety of the Schist of Yellow Jacket Road is a strongly schistose rock primarily composed of quartz, biotite, and garnet porphyroblasts. The garnets found at this outcrop generally do not exceed 2mm (usually closer to 1mm) in diameter and the state of the inclusions within varies with location and proximity to dikes or faults. Amphibole is present locally, but again this varies with proximity to faults.

Sample 08MH02 shows garnet porphryblasts (>1mm diameter). The garnets present are largely euhedral with few inclusions (quartz, plagioclase, biotite, and opaques). These garnets grew pretectonically or syntectonically and grew in two stages. The garnets often show signs of sigmoidal rotation.

Sample SYR-5 has slightly more quartz relative to biotite than is usual at this outcrop. Garnets are also smaller and a bit less copious. Opaques occur as laths parallel to foliation here and this sample also contains lenses of deformed quartz clots. What are most distinctive in this sample are the garnets, specifically their inclusions. These inclusion clouds are radial in form and several clearly parallel the chemically defined growth sector boundaries (Stowell et al, 2011). This may reflect the boundary between sectors as a low point in thermodynamic barriers to crystal growth, leading to inclusions being grown over faster at those points. It was collected along a small fault near SYR-4.

Sample SYR-6 was taken along a much less fissile zone and contains very little garnet for the area. It has two variations in the same sampling area; one quartz dominated and the other more biotite rich. Garnets are partially resorbed when present and even those are fractured. There is also a small amount of amphibole present.

Sample SYR-7 was taken near a pair of shear zone bounded pods of bluish, amphibole rich metamorphic or possibly metaigneous derived material. The sample itself shows little sign of the unit's general schistosity. It contains up to 20% (modal mineralogy) amphibole content and contains little, if any, plagioclase. Garnet is present, but complex. Some garnets show signs of post-tectonic growth such as overgrowth of the matrix, others are clearly three stage. Both the garnets and the amphiboles contain copious inclusions and may have undergone metasomatic growth.

Sample SYR-8 was taken from a shear bounded zone of schistose quartzite in the Yellow Jacket Schist. It contains no plagioclase. The garnets are well preserved and have relatively few inclusions. The inclusions they do contain are found in tracks, implying that these garnets were syn- or post-tectonic. They are also oblong in shape and have clearly been rotated, although pressure shadows are not as distinct as they could be. The matrix contains distinct crenulation folding, which (combined with the rotation and unusual crystalline habit of the garnets) implies that these underwent a second and lesser deformational event.

Sample SYR-9 was taken from an obviously folded zone. It contains a significant modal component of muscovite and amphibole in addition to the Quartz, biotite, and garnet that make up the bulk of the unit. This unit also contains oblong one stage (no zonation) syn- or post-tectonic (containing overgrown and rotated inclusion tracks) garnets. These garnets, however, show clear signs of later stage resorption. The amphiboles in this sample contain proportionally fewer inclusions. The most strikingly unique trait of this sample is its strong crenulation folding.

Sample BSA-10-SYR-5
Schist of Yellowjacket Road - Garnet with radiating inclusions

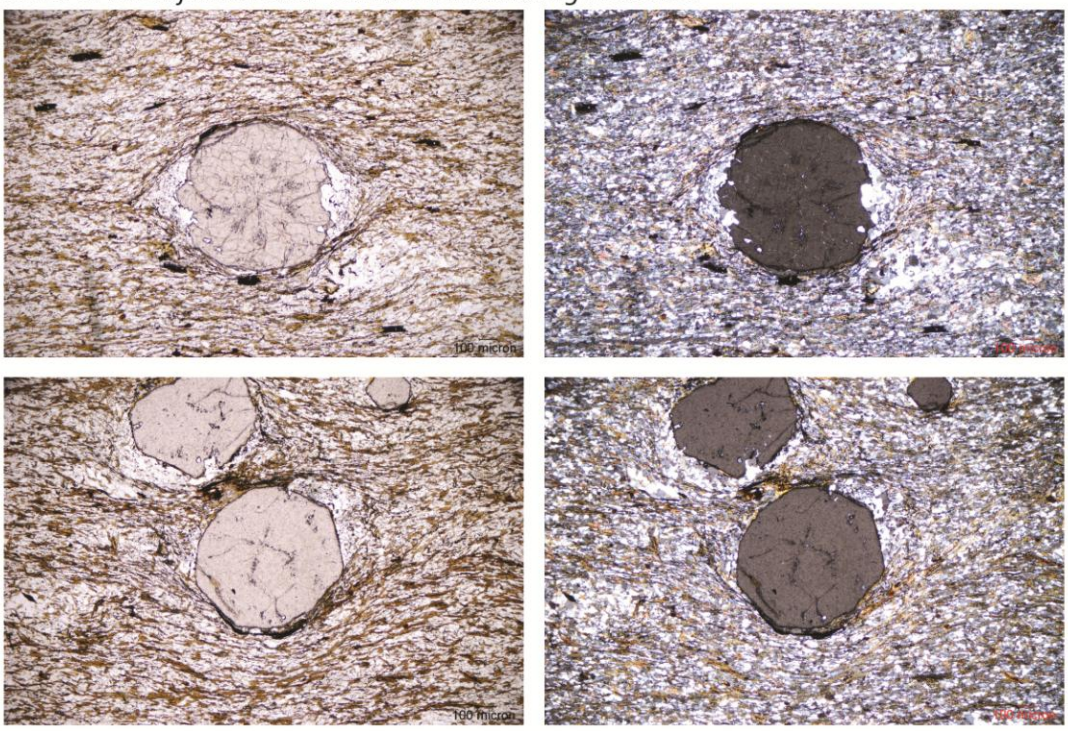

Sample 08MH02
Schist of Yellowjacket Road - Showing typical euhedral garnet

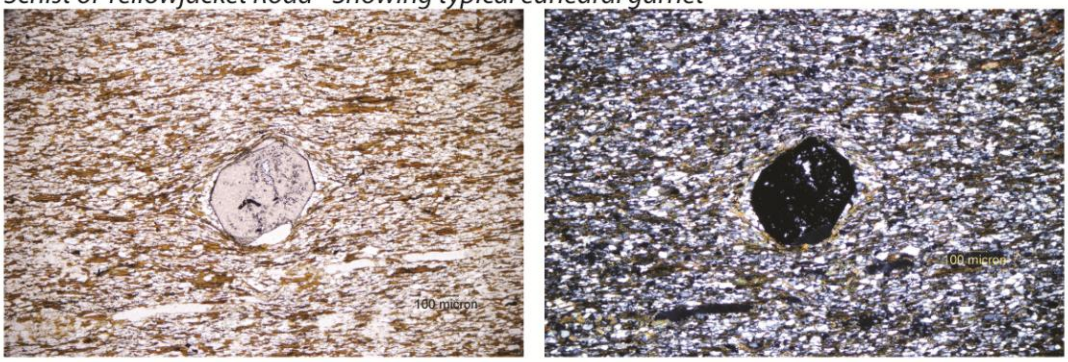

Figure 1A. Samples SYR-5 and 08MH02. The top pair of images of SYR-5 display the radiating inclusion pattern well; the lower pair displays the possible sector zoning from center to tip.

Sample BSA-10-SYR-7
Schist of Yellowjacket Road - Complex garnet and amphibole near intrusive dike

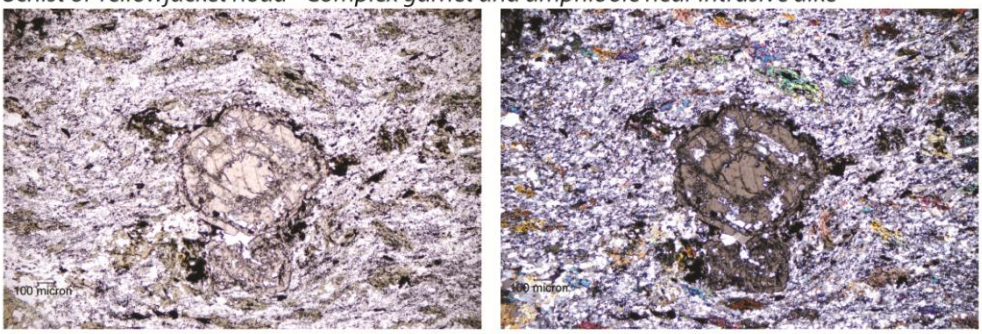

Sample BSA-10-SYR-8
Schist of Yellowjacket Road - Syndeformationa garnet and crenulation folding

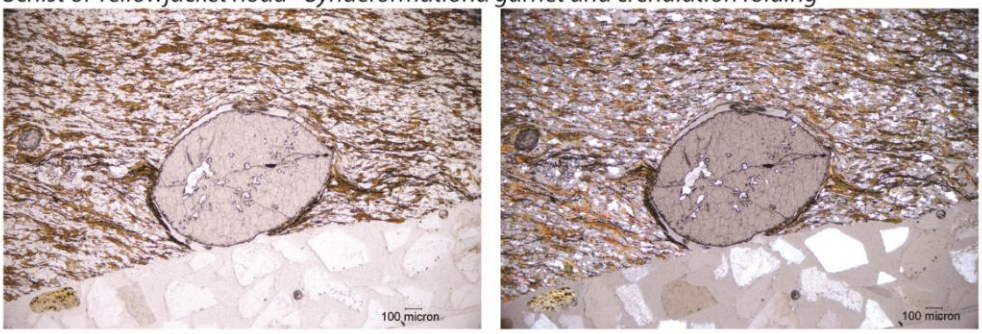

Sample BSA-10-SYR-9
Schist of Yellowjacket Road - Crenulation folding, Amphibole, and Garnet (Garnet image is 10x)

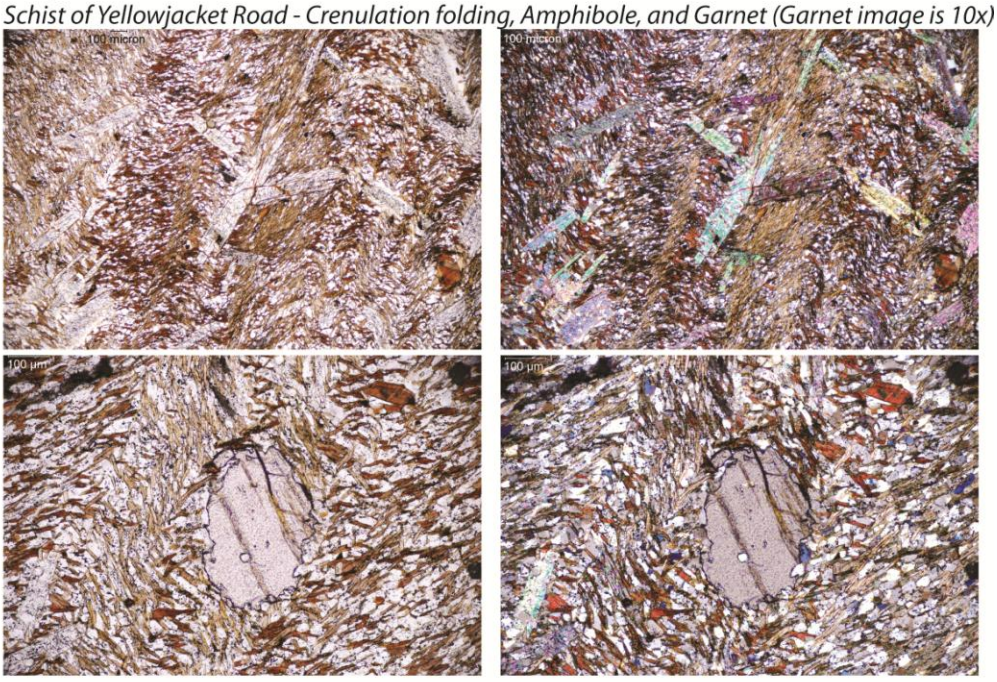

Figure 2A. Samples SYR-7, SYR-8, and SYR-9. Sample SYR-7 shows an unusual extra inclusion defined growth zone in garnet as well as amphibole. SYR-8 shows an unusually oblate garnet displaying linear inclusion tracks. Sample SYR-9 shows more significant crenulation folding as well as amphibole growth which crosses both foliation and crenulations.

ii. Hornblende Bearing Variety

The hornblende-bearing variety of the Schist of Yellow Jacket Road is less schistose than the garnet bearing variation and primarily composed of quartz, amphibole, plagioclase, chlorite, and opaques. All three samples of this variety were found to the south and southwest of the Gabbronorite of Ridenor Canyon and had been mapped by previous workers as hornfelsed keratophyre. This rock is indeed rich in hornblende porphyroblasts, but they are primarily found as rotated clumps and schistosity defining matrix material. The matrix, too, is dissimilar to the keratophyre. It is not a fine grained groundmass, but a coarser grained metasedimentary matrix of quartz and (limited, but variable) plagioclase between layers of schstosity defining amphiboles. Textural evidence implies that chlorite is a retrograde metamorphic mineral path and it is the only mica found in this area of the Schist of Yellow Jacket Road.

Sample PCSS-1 is very much representative of this variety of the unit. The matrix is a fine to medium grained mix of quartz and plagioclase interspersed with layers of schistosity defining amphibole. The porphyroblasts are rotated clumps of coarser grained amphiboles.

Sample PCSS-3 is similar to PCSS-1; a schistose quartz, plagioclase, and amphibole matrix with larger rotated amphibole and amphibole clump porphyroblasts. Differentiating this sample from the others is the increased chlorite content and the matrix amphiboles; which are euhedral needles in this sample. This sample also contains more clearly defined opaque rich zones, often corresponding with amphibole. Distinct for this sample is the presence of chlorite without amphibole cores or inclusions and following foliation. This may imply that this region of the Schist of Yellow Jacket road may have undergone a period of lower grade metamorphic mineral growth postdating the peak (amphibolite grade) metamorphic event experienced by the bulk of the MHMC. This might also explain previous workers diagnosis of the area as a hornfelsed unit.

Sample PCSS-4 shows a quartz, plagioclase, amphibole matrix schist with rotated amphibole porphyroblasts. This sample is both the least altered/overprinted and contains the least plagioclase. It contains the highest birefringence amphibole as well.

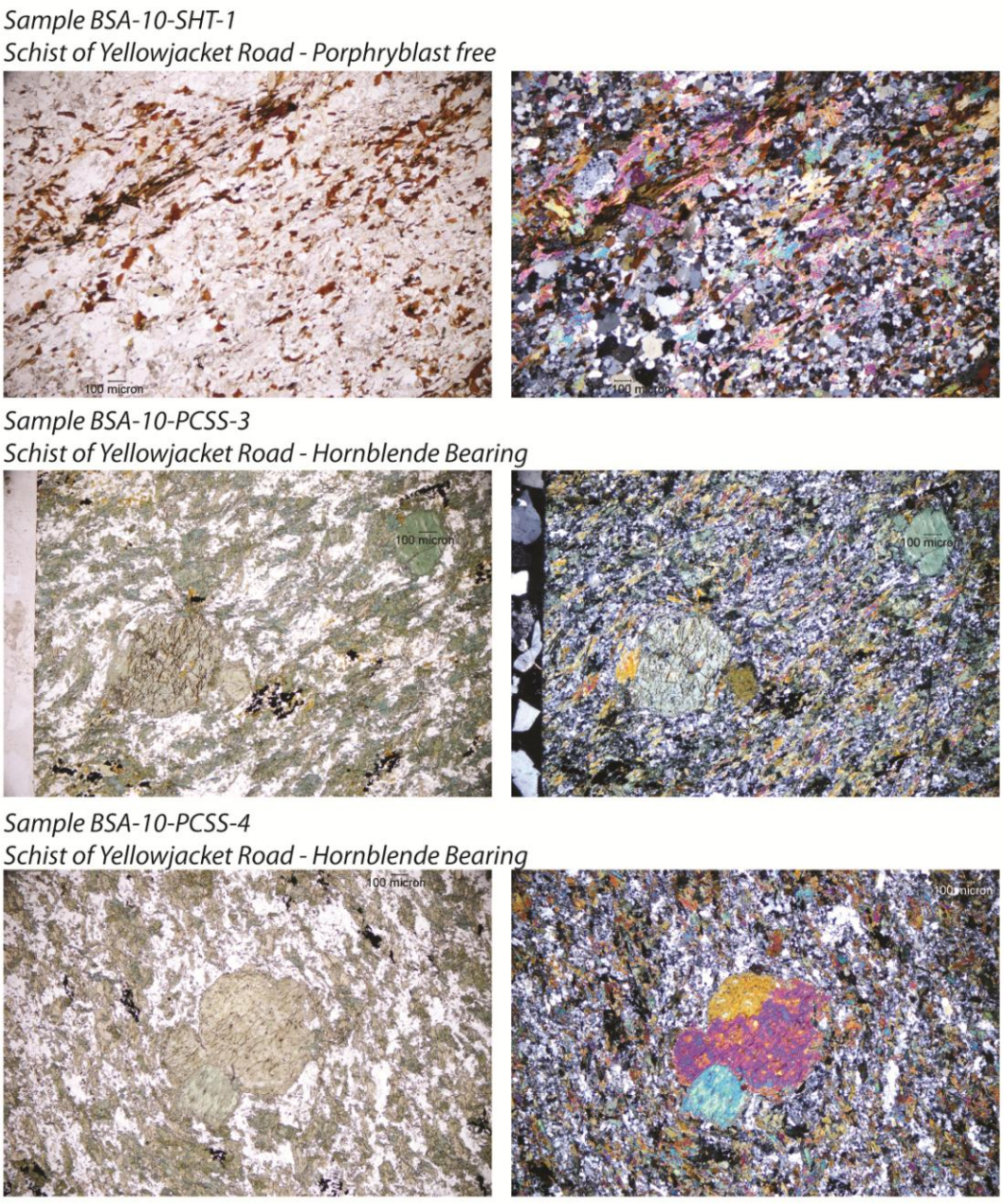

Figure 3A. Samples SHT-1, PCSS-3, and PCSS-4. Sample SHT-1 simply displays the nature of the (here graphitic) Schist in locations lacking porphryblasts (a minority in the MHMC), in this location it contains both muscovite and biotite. Samples PCSS-3 and PCSS-4 display the metasedimentary unit in its strongly hornblende defined variety; with hornblendes of variable levels of chloritization defining foliation around rotated amphibole clots and grains.

iii. Neither Hornblende Nor Garnet Bearing Variety

Sample SHT-1 is the only sample of the Schist of Yellow Jacket Road collected from the region due east of the Gabbronorite of Ridenor Canyon. It is also the only one to lack porphyroblasts of some kind. This sample is primarily composed of quartz, biotite, and muscovite. It is clearly a fine grained schistose rock. While garnets are lacking in this sample, it is relevant that they were observed (but unsampled) across West Birch Creek (to the east) indicating that they are still in the area.

b. Serpentinized Peridotite

Sample MGB-6 is the only sample taken of the serpentinized peridotite which is found throughout the MHMC, usually as float of unknown origin. Trauba reported a sizable body of fault bounded peridotite in the northern area of the MHMC, but as it wasn't found in this study this sample was taken from a small (0.5m by 15cm) slice found in place in the Metagabbro at the northern edge of the central area of the MHMC. It is a strongly fractured, strongly altered sample of serpentine, secondary quartz, altering clinopyroxene, opaques, and other clay minerals. If any olivine is preserved in this sample it is indistinguishable amongst the alteration.

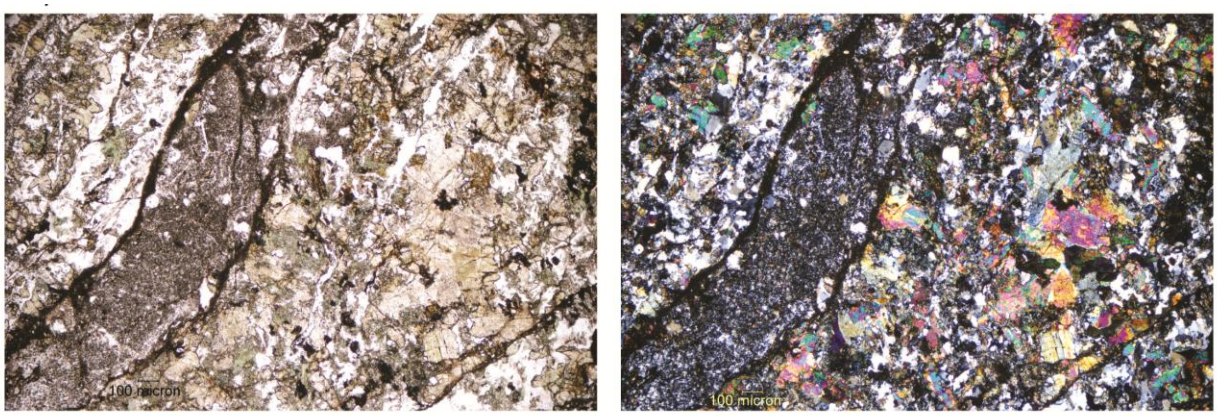

Figure 4A. Sample MGB-6. This sample shows the degree of alteration common in the serpentinized peridotite as this study found it throughout the MHMC area.

c. Pearson Creek Keratophyre

i. Eastern Exposure

The eastern exposure of the Pearson Creek Keratophyre is the largest single greenschist grade unit in the MHMC. Its groundmass is aphanitic and quartz dominated. It often contains substantial chlorite. Phenocrysts are common and usually found in clumps of plagioclase, amphibole, or euhedral rhombohedral opaques. Both plagioclase and amphibole are usually altered, although the amphibole is often almost altered away. The exposure varies texturally from massive to foliated with location. When foliation is present it is usually defined by muscovite, and when muscovite is absent it is defined by finer grained zones of quartz. Occasionally a sigmoidally rotated porphyroblast is found within a foliation. Clots of even finer grained glassy material are found throughout the exposure. The unit also contains a small amount of what is most likely cordierite, although this study was unable to identify it definitively. Both sphene and zircon are present as well, but zircon is not ubiquitous and its presence seems to vary with location. The southernmost sampling location (PCS-7) was unusual in that it contained round clasts of undulatory blue quartz which appear to be uniquely less deformed than the other quartz in the unit. It also contains radiating clumps of well formed biotite blades and no muscovite in a sample containing substantial schistosity. This end of the exposure may have undergone retrograde metasomatism or some other form of low pressure retrograde metamorphic growth.

Sample BSA-10-PCS-4
Keratophyre of Pearson Creek - Eastern Region - Northernmost sample

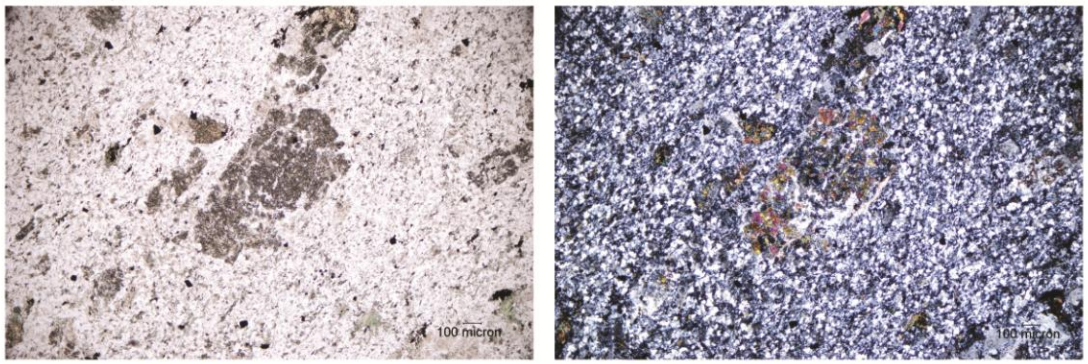

Sample BSA-10-PCS-6
Keratophyre of Pearson Creek - Eastern Region - Middle of exposure

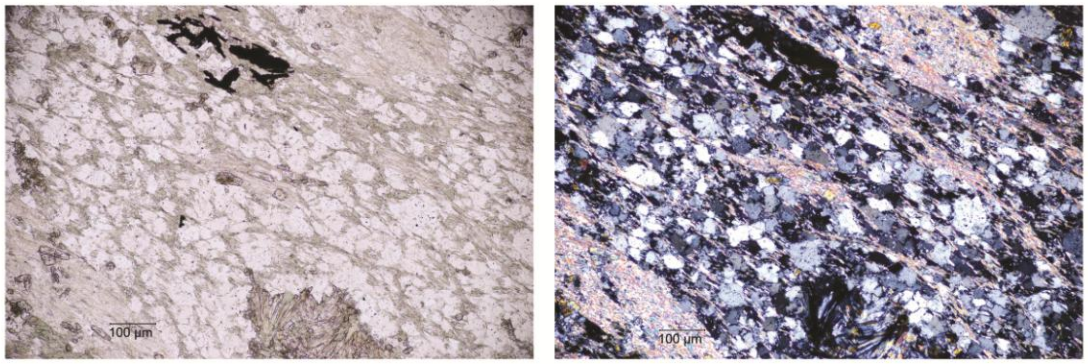

Sample BSA-10-PCS-7
Keratophyre of Pearson Creek - Eastern Region - Southernmost sample

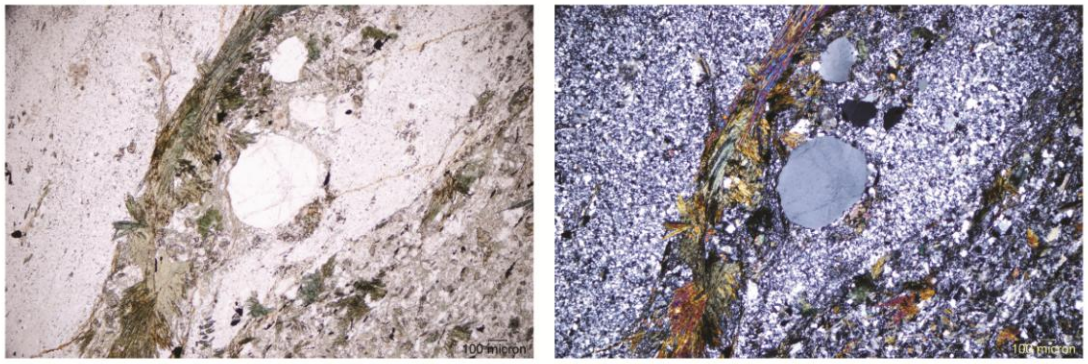

Figure 5A. Samples PCS-4, PCS-6, & PCS-7. These samples represent the units exposure from north to south along Pearson creek. They display the greenschist grade metamorphic growth of minerals such as chlorite and muscovite as well as the preservation of extrusive textures such as groundmass in both the more blocky (PCS-4) and more schistose (PCS-6) areas of the exposure. Sample PCS-7 displays unusual (and unusually undeformed) spheres of blue quartz as well as a little bit of the biotite, which is found in this sample growing in radiating clumps.

ii. Central Exposure

The central MHMC exposure of the Pearson Creek Keratophyre is texturally very similar to the eastern exposure while being mineralogically distinct. It has the same fine grained groundmass with some phenocrysts present. In this area, however, the unit lacks chlorite and muscovite entirely. Two areas of this version of the keratophyre were sampled; one west of the Gabbronorite of Ridenor Canyon (UMV-1, UMV-2, and UMV-3), and the other was an in place xenolith near the contact between the hornblendite and the metagabbro in the northmost part of the West Birch Creek exposures of the MHMC. The xenolith is unusually high in plagioclase feldspars (up to 10% modal mineralogy) which are present as euhedral (although undulose) needles which define foliation. The groundmass is well preserved as are the glassy tephra. Amphibole is also present. The westernmost part of the central keratophyre contains a clear groundmass, but it is less well preserved than the other areas of the unit. Plagioclase is present and altered, but not undulose. Biotite is common throughout the rock and defines foliation where present. Phenocrysts are generally better preserved than in the eastern exposure and quartz (phenocryst or groundmass) is often quite undulose, possibly even to the point of demonstrating dynamic recrystalization. Sample UMV-3 was taken in a more foliated location and it is not only an L>S tectonite but also contains pre- or syn-tectonic garnets and staurolites and ribbons of quartz showing clear evidence of dynamic recrystalization (bulging and flattening). This area also contains substantial biotite showing crenulation folding amidst the ubiquitous foliation. Some of the staurolites contain sizable opaque cores. The garnets are generally one stage, but at least one may be two stage.

Sample BSA-10-UMV-1
Keratophyre of Pearson Creek - Central Region

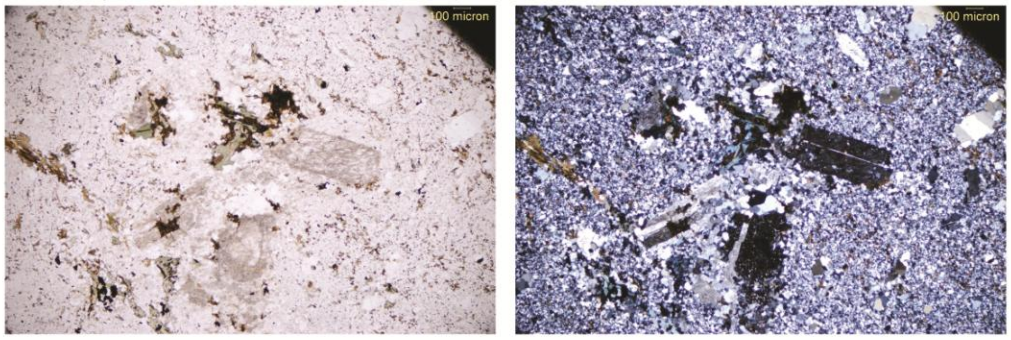

Sample BSA-10-UMV-3
Keratophyre of Pearson Creek - Central Region

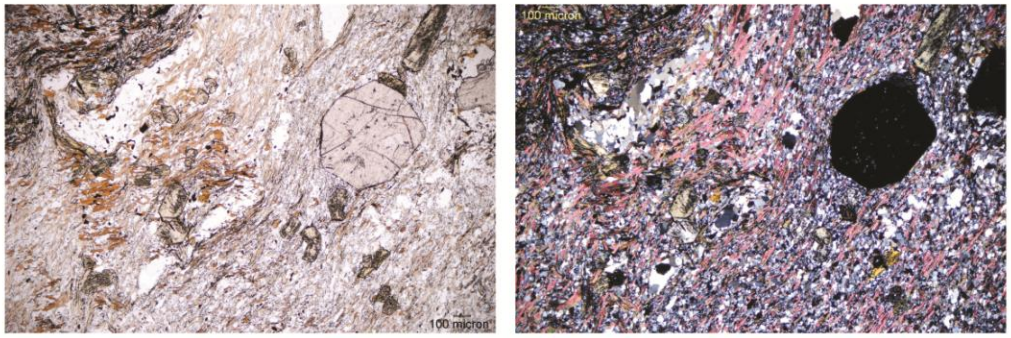

Sample BSA-10-MGB-5
Keratophyre of Pearson Creek - North Central Region

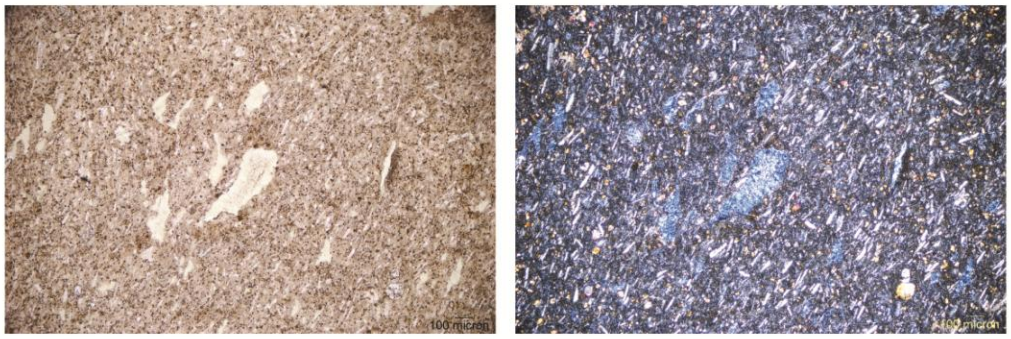

Figure 6A. Samples UMV-1, UMV-2, & MGB-5. Sample UMV-1 shows the texture and composition of the Pearson Creek Keratophyre in the central region; greenschist minerals are rare or absent, biotite is present, and the texture of the volcanic groundmass is preserved (even if the grain size is slightly increased). The volcanic texture is preserved but it is not easily confused with any other unit. Sample UMV-3 shows this unit in a more schistose (L>S tectonite) form with biotite, muscovite, staurolite, and garnet. Sample MGB-5 was sampled from near the metagabbro-hornblendite/pyroxenite contact in along west birch creek and it still displays the volcanic texture, sans greenschist facies metamorphic minerals.

d. Trondhjemite of Pearson Creek

i. Pluton

The Trondhjemite of Pearson Creek is the only plutonic unit in the eastern exposure of the MHMC. It is mineralogically dominated by plagioclase followed by quartz. These two minerals made up 80 to 95% of the unit prior to alteration. Minor minerals consist of hornblende, biotite, and some opaques. This unit shows very little foliation in hand sample, but shows evidence of deformation in thin section. Quartz has clearly undergone dynamic recrystalization (evidence of flattening, bulging, and subgrain development is present) and plagioclase feldspar exists as unaltered rims surrounding sericite cores (likely the result of microfracturing prior to later crystal growth). Less clearly developed crystals exhibit vermicular intergrowths of quartz in the plagioclase feldspar. Amphibole can reach 15% of the rock (modal) and is often found in association with opaques. These hornblendes are generally euhedral, prismatic, and blue-green in plain polarized light. Biotite is sparse and well formed. The combination of secondary chlorite (replacing mafic minerals), secondary plagioclase growth, and secondary epidote growth (reported by trauba as a minor mineral component, not identified in this study) firmly establishes this unit as having undergone greenschist grade metamorphic conditions and mineral growth.

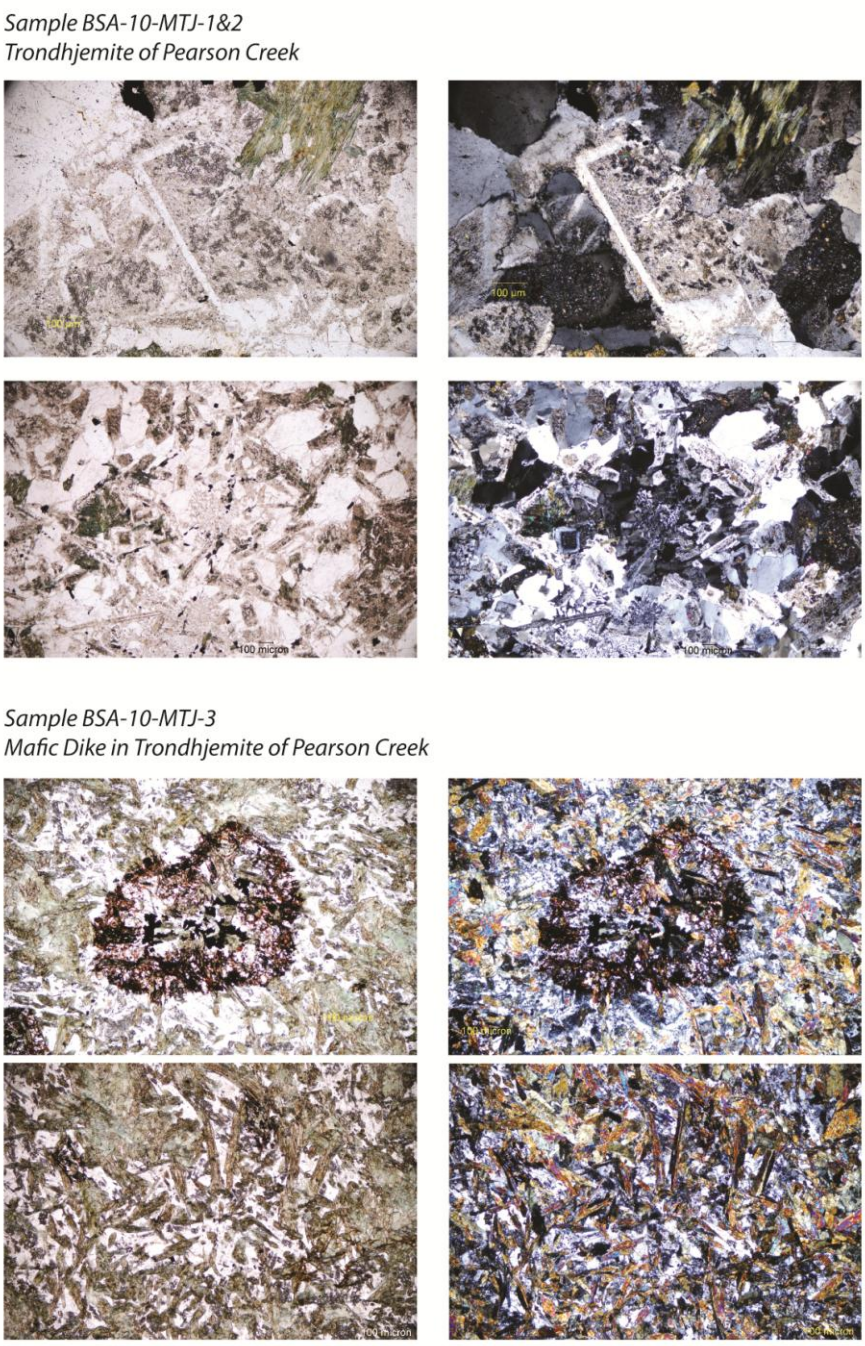

Figure 7A. Thin section photomicrographs of samples MTJ-1/MTJ-2 and MTJ-3. The top pair of images from sample MTJ-2 further illustrate the later growth of plagioclase over microfractured (and later altered) core material. The second pair of images further illustrates the wormlike intergrowth of quartz and plagioclase common in this unit. Both show the chlorite (and possibly some epidote) which later grew in this unit. Sample MTJ-3 shows both the opaque cored bull's-eye structures distinctive of this mafic dike (upper pair of images) and the typical mesh of needlelike amphiboles (and now, metamorphic chlorite) which make up this unit.

ii. Mafic Dike

This amphibole-rich deformed dike of uncertain provenance intrudes the Trondhjemite of Pearson Creek. It doesn't exceed 2m in thickness but is nontrivial compared to the small exposure of the trondhjemite it intrudes. This dike is mineralogically dominated by blue-green prismatic amphiboles with embayed ends and no preferred orientation. While some of the amphibole needles are bent to accommodate deformation, most of the deformation has been accommodated by the interstitial quartz and plagioclase feldspar, which are both undulose, small, and inclusion (as well as alteration) rich. There are some small orthopyroxenes preserved in this dike as well as opaque blebs surrounded by halo like rings of isotropic rusty material laced with more amphibole and quartz. Although nonfoliated, the unit is clearly deformed and the presence of chloritization of the mafic minerals combined with likely metamorphic plagioclase growth (plagioclase and quartz are very similar to those in the Trondhjemite of Pearson creek) implies that this dike was intruded prior to the greenschist grade metamorphism of them both.

e. Hornblendite

i. Hornblendite (North-East)

The hornblendite found in this study is close to that reported by previous workers (hornblende dominated with lesser quartz and biotite, secondary chlorite and opaques, and alteration white mica). Samples WBC-4a and WBC-4b were collected in the north most edge of the central region of the MHMC, near the contact with the metagabbro. Mineralogically speaking, while this rock does reach 45% amphibole (with as much as 35% amphibole derived chlorite) in this area it never approaches Trauba's (1975)reported 90% hornblende content. Also significant is the variable amount of preserved clinopyroxene (ranging from ~1 % to 25% modal mineralogy), often as cores in hornblende. Both quartz and plagioclase are present and demonstrate significant dynamic recrystalization; plagioclase is both undulose and contains significant deformation twinning while quartz shows flattening, bulging, and subgrain formation. Grain size varies from medium for the amphiboles to fine grained for the 'interstitial' quartz and feldspars. The mineralogy and texture make it likely that this is an igneous cumulate which has undergone significant (likely amphibolite grade) metamorphism.

ii. Pyroxenite (East-Central)

Samples from the area east of the Gabbronorite of Ridenor Canyon (PYX-1, GNR-1/GNR-2, and GNR-4) are pyroxene cumulates and texturally distinct from the other hornblendite sampling site. In the samples from this area the 'hornblendite' unit is really a pyroxenite containing up to 80% megacrystic clinopyroxenes near West Birch Creek (sample PYX-1) and orthopyroxene closer to the Gabbronorite of Ridenor Canyon (samples GNR-1/GNR-2 and GNR-4). Amphibole is present across the exposure, but doesn't exceed 15%. Both the pyroxenes and amphiboles that make up this unit are unoriented and contain many (often euhedral) inclusions of other pyroxenes, opaques, or micaceous alteration products. When

quartz is found in this version of the unit it is undulose, indicating deformation. This is supported by fracturing in the amphibole grains, although it is not as common in the pyroxenes.

Sample BSA-10-GNR-4
Pyroxenite/Hornblendite - Pyroxene Dominated

Sample BSA-10-PYX-1
Pyroxenite/Hornblendite - Pyroxene Dominated

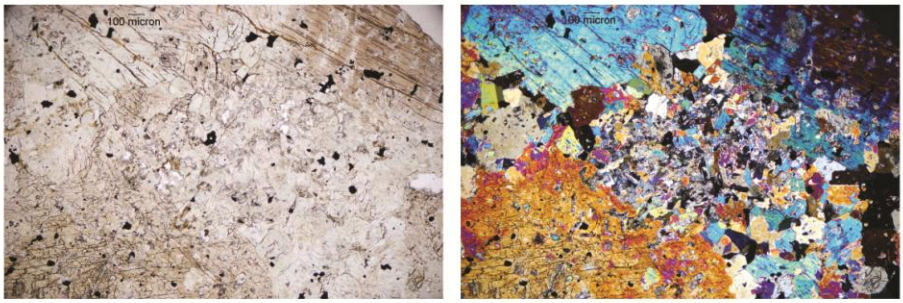

Sample BSA-10-WBC-4a
Pyroxenite/Hornblendite - Amphibole Dominated

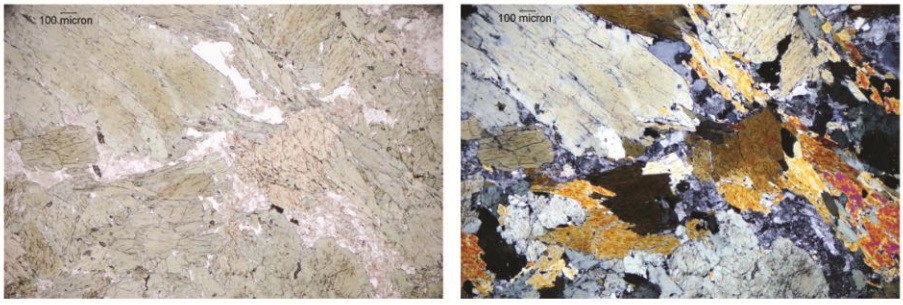

Figure 8A. Samples GNR-4, PYX-1, & WBC-4a. The top pair of images (GNR-4) illustrate a very coarse grained (almost megacrystic), Orthopyroxene and amphibole dominated variation of the Pyroxenite/Hornblendite. This is a relatively quick growing cumulate and the only Pyroxenite/Hornblendite sample to be geochemically analyzed. The middle pair of images (PYX-1) is from the same stretch of exposures as the first and, while it is texturally almost identical, it is clinopyroxene bearing rather than orthopyroxene bearing. The bottom pair of images (WBC-4a) represents a more medium grained, non-cumulate texture. This version of the rock is much more mineralogically varied, containing not only amphibole (sometimes cored by clinopyroxene) and its weathering products, but also minor quartz, plagioclase, and possibly the occasional rare orthopyroxene. Quartz and plagioclase display the effects of dynamic recrystalization, and appear to have accommodated most of the deformation in the unit as minerals like hornblende and pyroxenes are undeformed.

f. Metagabbro

i. Typical Texture

This variety of the metagabbro was sampled south of the Ridenor Canyon pluton, and it is strongly plagioclase dominant. The remaining 20% on the rock is composed mostly of clinopyroxene and amphibole as well as alteration products. Microtextural evidence of deformation is present, primarily as undulosity in the plagioclase. Samples were also taken near the contact with the hornblendite at the northernmost exposure on West Birch Creek. These were more complexly deformed and contained quartz and amphibole (rather than amphibole and clinopyroxene). In this area quartz was dynamically recrystallized and amphibole was microfractured. Plagioclase in this area contained microfractured (and sericitized) cores, undulose extinction, deformation twinning, and (in some locations) stretched into cigar shapes in hand sample.

Sample BSA-10-MGB-4
Metagabbro - Typical

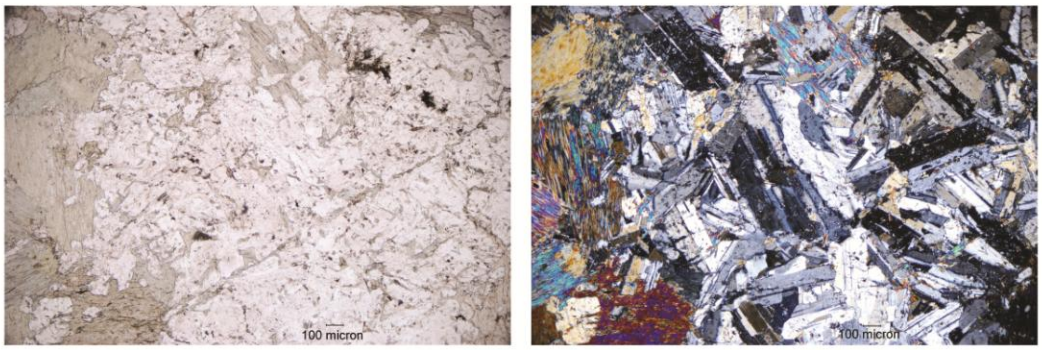

Sample BSA-10-WBC-2
Metagabbro - Typical - near contact with Hornblendite/Pyroxenite

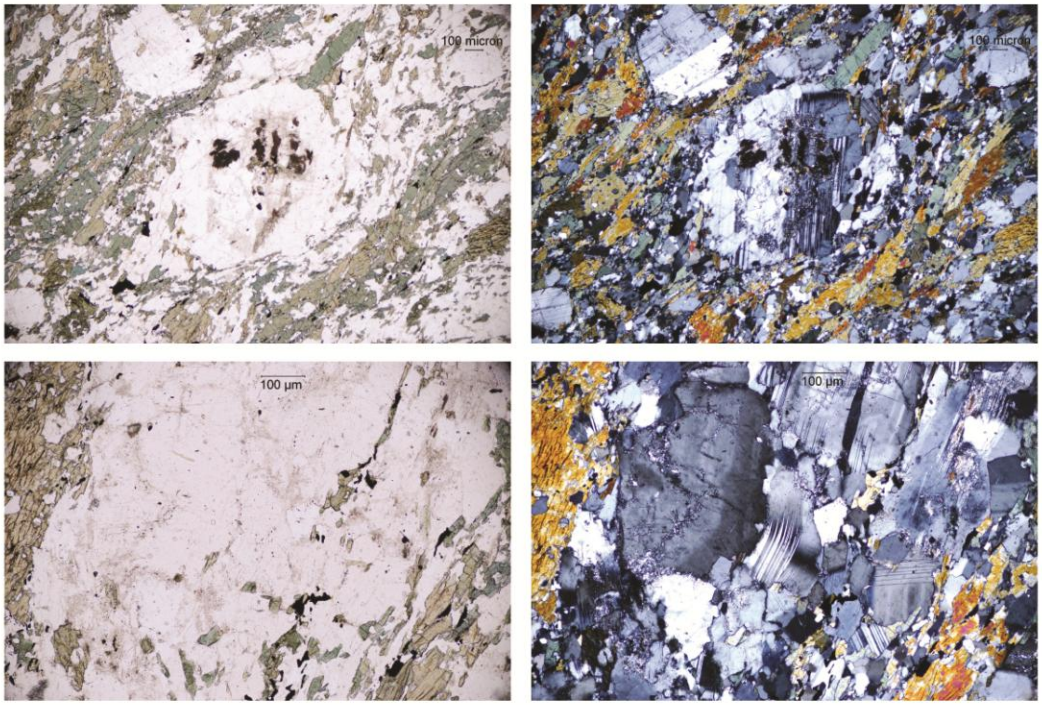

Figure 9A. Samples MGB-4 and WBC-2. The top pair of images (MGB-4) represent the consistent nature of the 'Typical' Metagabbro; medium grained, deformed, mineralogically dominated by plagioclase feldspar, amphibole, and (depending on location) clinopyroxene. Deformation is best observed in the plagioclase, usually as undulosity and deformation twinning. The other four images are from the metagabbro as it is found near the contact with the pyroxenite/hornblendite at the northern edge of West Birch creek. The metagabbro in this area is even more strongly deformed and contains an anomalously high quartz content (<10% modal). In these thin sections (and even in hand specimen) plagioclase can be seen deforming ductily, it also shows deformation twinning, undulose extinction, and late growth over microfractured cores. Amphibole is also fractured and deformed.

ii. Fine Grained Texture

The fine-grained textural variation of the metagabbro was sampled from a map scale xenolith, or at least engulfed in place portion, surrounded by the Diorite of Alexander Creek. It is dominated by stubby, fine grained, pleochroic green amphibole. The rest of the rock is made up primarily of anhedral, deformed plagioclase, a substantial population of possibly late stage opaques, and alteration products (for images see main body of thesis).

iii. Porphyritic Texture

The porphyritic variation is only known to outcrop in one location in the MHMC: a 0.5 km long sliver south of the Trondhjemite of Johnson Creek. This rock is dominated by a matrix of fine grained plagioclase and amphibole surrounding coarse grained plagioclase. The large plagioclase grains largely display undulose extinction and/or deformation twinning. Depending on location, biotite may also be present as well as quartz and sometimes significant alteration products. The occasional presence of biotite may imply that this rock is more akin to the Tonalite of California gulch than to the other metagabbroic rocks.

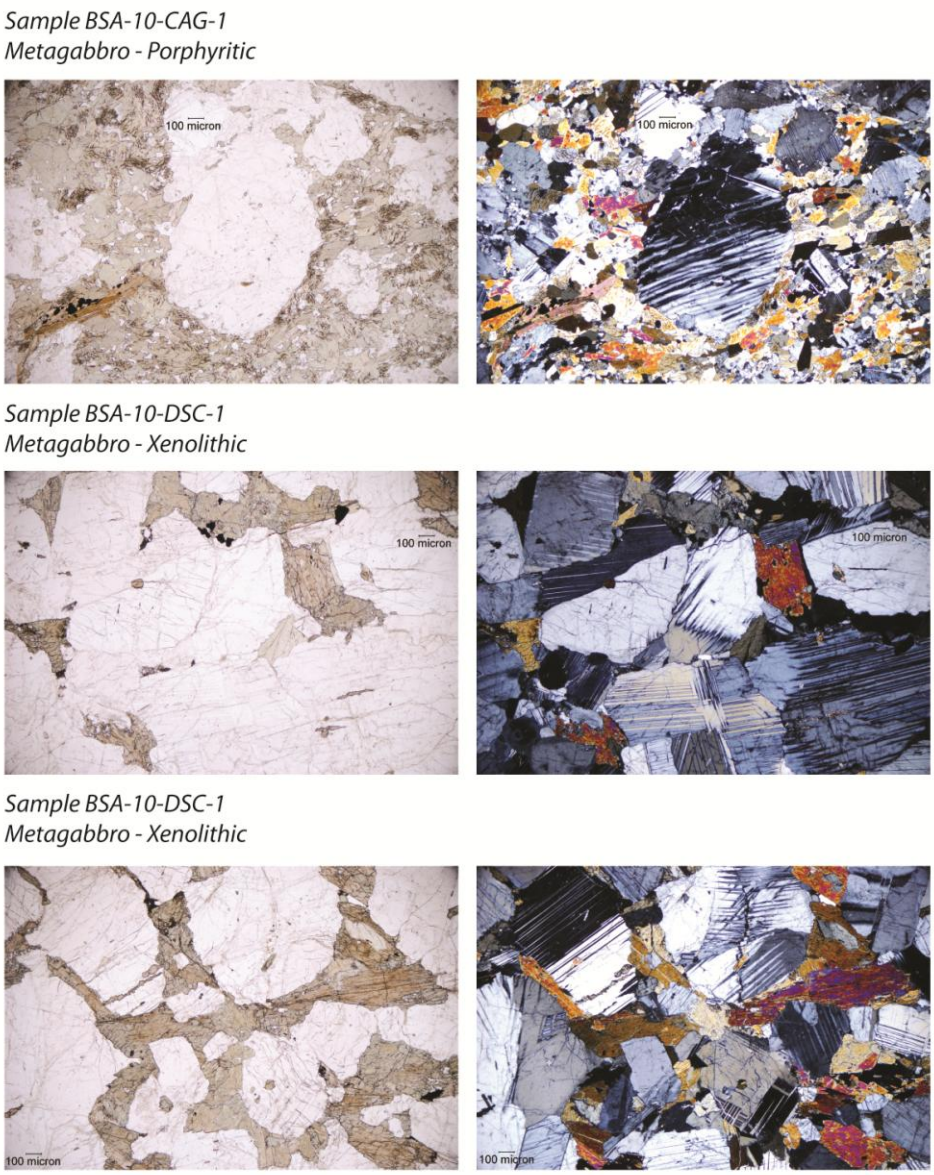

Figure 10A. Samples CAG-1 and DSC-1. The top pair of images (CAG-1) represents the 'porphyritic' metagabbro. This texturally distinctive sub unit is composed of coarse grained plagioclase phenocrysts (often deformed, with undulose extinction and deformation twinning) in a fine grained amphibole (and possibly some orthopyroxene) groundmass. Unique (and also throwing doubt on this rocks grouping with the metagabbro) is the presence of up to 15% (Modal) quartz and the presence of minor (1 to 2% modal) biotite. The middle and bottom images further represent the 'xenolithic' metagabbro (DSC-1). It too is a plagioclase and amphibole dominated rock containing a small amount of quartz. Texturally it is unusual among the metagabbros, with coarse grained, deformed plagioclase grains amongst finer grained amphiboles (albeit not enough so as to be classified as porphyritic). The quartz is finer grained and most likely metamorphic in origin.

iv. Xenolithic Texture (North)

There are only two locations in the MHMC which contain >50% metagabbro xenoliths: one in the Tonalite of California Gulch (sampled in this study) and the other in the Diorite of Alexander Creek. The metagabbro xenoliths analyzed for this study are dominated by medium to coarse grained plagioclase grains which exhibit significant deformation twinning and a lesser, but still substantial, amount of undulose extinction. Some plagioclase grains also show zonation. Amphibole is a lesser constituent of the rock and does exhibit some simple twinning. Quartz is present in small quantities (>3% modal mineralogy) and exhibits flattening and grain boundary migration.

g. Tonalite of California Gulch

The Tonalite of California Gulch makes up a large portion of the northern MHMC. It is easily distinguishable from the metagabbro by the presence of a significant amount of quartz and a minor (but consistently present) amount of biotite. In this study it was sampled in its westernmost and southernmost outcrops. Plagioclase dominates this rock and it shows deformation twinning and undulose extinction as well as later resorption by quartz. Quartz also demonstrates flattening and bulging indicating dynamic recrystalization. The amphibole is also deformed and microfractured. Rarely amphibole can be observed to have grown around the embayed core of earlier amphibole grains, indicating multiple periods of amphibole growth. Biotite can approach 10% (modal mineralogy) and can be found containing amphibole grains. Opaques also make up a minor (<5%) part of this rock and range from (sometimes euhedral) cores in amphiboles and biotite to resorbed inclusions in quartz. Clinopyroxene is sometimes present in this unit, but it is uncommon.

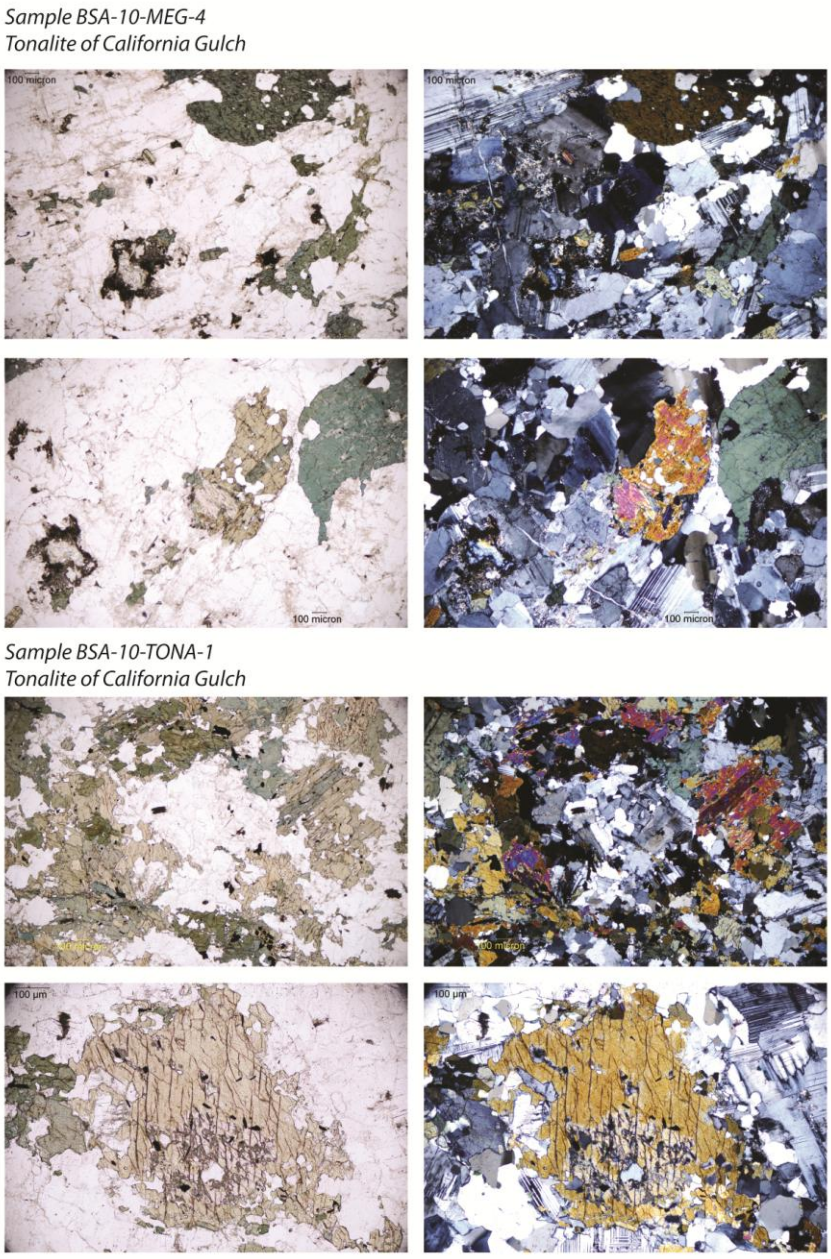

Figure 11A. Samples MEG-4 and TONA-1. The top four (MEG-4) are from the exposure along Merle Gulch (southern end of its exposure). The top two show quartz and plagioclase displaying flattening and bulging as well as some undulose extinction (respectively). The lower two show more deformation of quartz as well as a clinopyroxene cored brown amphibole (likely igneous) as well as a green amphibole (likely metamorphic). The lower four (TONA-1) are from the western-most exposure of the unit. The upper pair shows a finer grained region of the rock showing both dynamically recrystallized plagioclase (and a little quartz) and fracturing in both green and brown amphiboles. The bottom pair (10x images) neatly displays the likely two stages of igneous amphibole growth with brown amphibole containing a core of embayed, earlier brown amphibole.

h. Amphibolite Gneiss

The unit mapped as amphibolite gneiss ranges from an amphibolite schist to a migmatite across the southern half of its main exposure. The bulk of the unit is found in the northern part of the MHMC and most of the sampling of the unit was done within the southern half of this area. The migmatitic samples from this study are most easily identified by the sizable, largely resorbed, garnets surrounded by quartz and plagioclase leucosomes. The surrounding rock is substantially deformed (from outcrop to microstructure scales) and generally composed of quartz, plagioclase, and amphibole. All matrix rock is coarser grained than the leucosomes, but less so than the garnet blasts. Other migmatite grade areas contain alternating layers of more schistose material and more melt material; this can be mistaken for the injection of the nearby Tonalite of California Gulch, but generally clinopyroxene is more plentiful than in the tonalite and biotite is entirely absent. In another relatively high grade area orthopyroxene is present rather than clinopyroxene. All of the higher grade areas of this unit contain significant amphibole and plagioclase (undulose extinction, deformation twinning, etc.), and some quartz. The lower grade exposures of this unit are more similar to a further metamorphosed Schist of Yellow Jacket Road, with copious quartz and plagioclase, sometimes biotite, and sometimes resorbed garnet. In this case, however, amphibole is much more common than biotite (it defines schistosity) and garnet is less common. Evidence of deformation and metamorphism are very common throughout the unit.

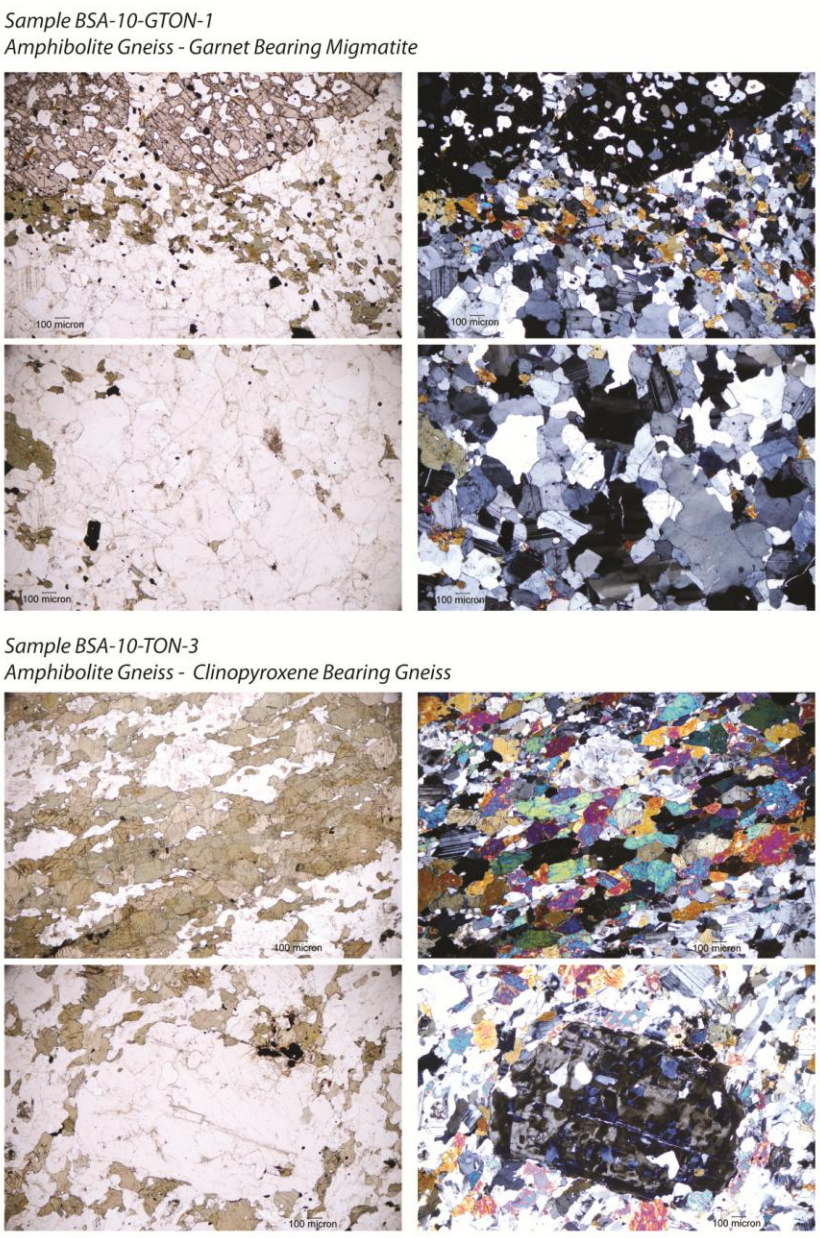

Figure 12A. Samples GTON-1 and TON-3. The top two images of GTON-1 display the inclusion laced garnets surrounded by quartz and plagioclase leucosomes as well as the hornblende that is also common throughout the rock. The lower two images show the somewhat coarser deformed quartz that makes up much of the non-leucosomal matrix rock. The lower four images (from sample TON-3) show composition and texture of a higher grade gneissic version of this unit. The more mafic gneissic bands (upper pair of images)show significant clinopyroxene and amphibole content (20% & 30% modal, respectively) as well as deformed quartz and plagioclase. The more felsic bands (lower pair of images) show at most 10% of either amphibole or clinopyroxene, but are also more likely to contain coarse grained, undulose, plagioclase phenocrysts.

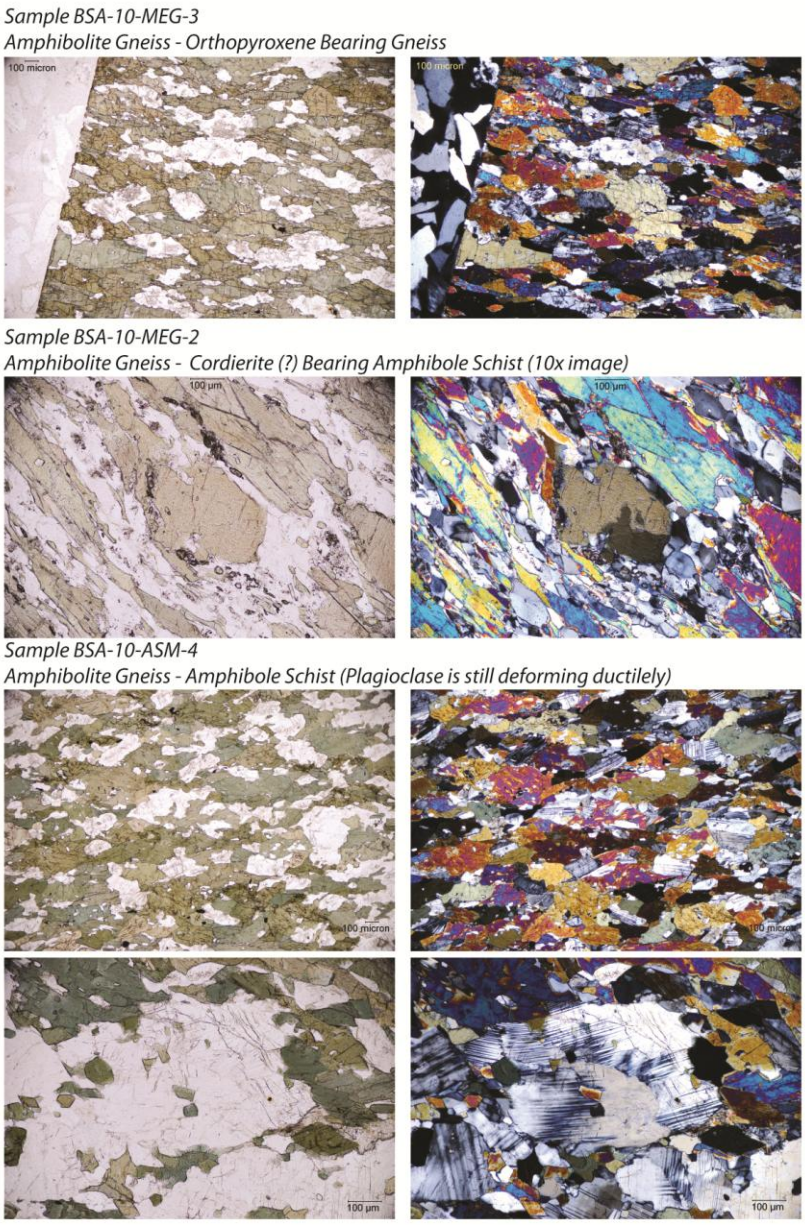

Figure 13A. Samples MEG-3, MEG-2, and ASM-4. The top pair of images (MEG-3) shows another mafic band in the gneissic version of this unit. In this case it is clearly orthopyroxene bearing (although no more than 5% modal orthopyroxene was observed) in addition to the amphibole, plagioclase, and quartz which are ubiquitous in this grade of the amphibolite gneiss. The middle pair of images (MEG-2) represent another relatively mid-grade rock showing banding/schistosity defined by amphibole with very high birefringence, deformed quartz and plagioclase, and what is very likely cordierite (center of image, surrounded on three sides by zircon grains and the associated radiation damage halos). The bottom four images (ASM-4) are from a unit which is clearly an amphibole schist (lower grade, upper image), but still high enough grade to contain ductily deformed plagioclase grains (lower image, 10x magnification).

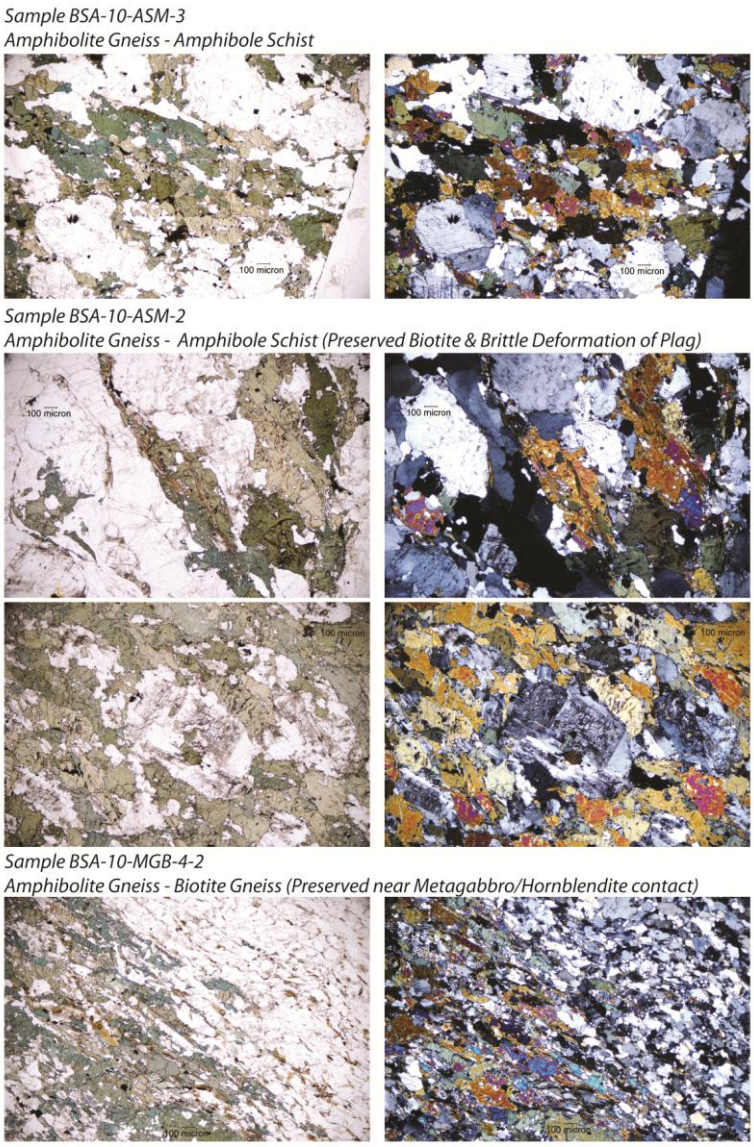

Figure 14A. Samples ASM-3, ASM-2, and MGB-4-2. The top pair of images(ASM-3) display a let lower grade of amphibole schist with many more inclusions and a greater variation in grain size, but still displaying dynamic recrystalization in the plagioclase (deformation twinning and undulosity) and fracturing in the amphiboles. The middle four images (ASM-2) display the now amphibolite schist showing both preserved biotite (as inclusions in amphibole, upper pair of images) and brittily deformed plagioclase (microfractured cores, lower pair of images). The bottom pair of images (MGB-4-2) are unusual among the samples of the amphibolite gneiss; it is texturally gneissic, but is a quartz and plagioclase dominated rock containing significant biotite (~12% modal) and chlorite (<5% modal) with lesser amphibole. This is likely due to its unusual source; it was incorporated as a xenolith into the metagabbro near the metagabbro-pyroxene/hornblendite contact, and is very likely not representing an equilibrium composition.

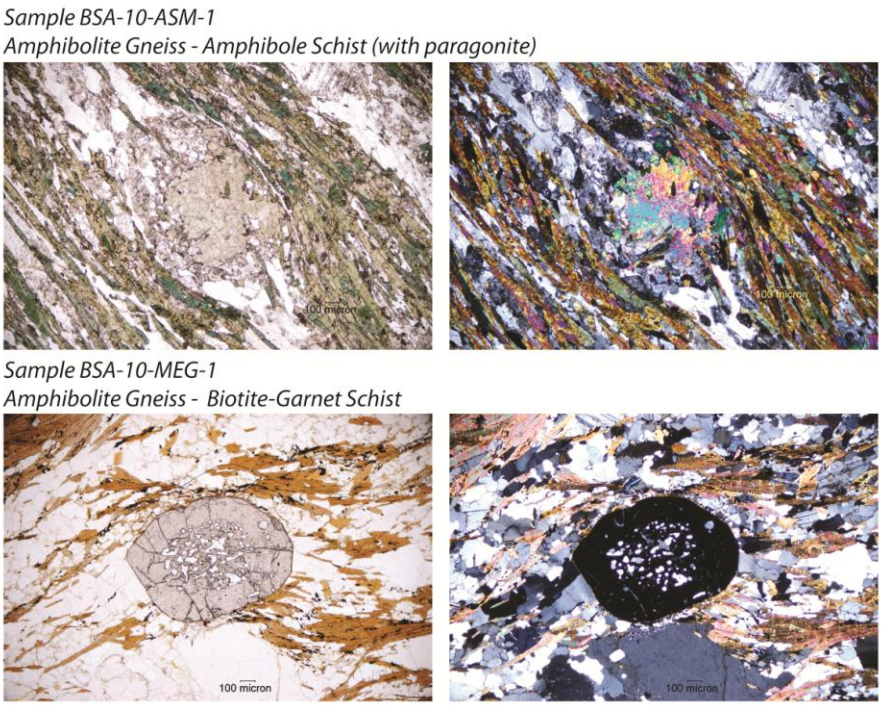

Figure 15A. Samples ASM-1 and MEG-1. The top pair (ASM-1) represent the amphibolite gneiss at the lower end of its, still amphibolite grade, spectrum. In this case the rock is an amphibole bearing biotite schist containing retrograde paragonite filled rotated porphyroblasts (likely after garnet). This rock bears a strong resemblance to the Schist of Yellowjacket road, but the absence of the porphyroblasts hints at the possibility of post-deformational metamorphic activity in the area—perhaps hydrothermal activity related to the post-deformational plutonism of the Carney Butte Stock. The bottom pair of images (MEG-1) shows 'amphibolite gneiss' which is nearly indistinguishable from the Schist of Yellowjacket road; Plagioclase+Quartz+Biotite+Garnet. Differences include the presence of minor undulose extinction in plagioclase, much less garnet rotation (which also do not include tracks of the matrix material), and an absence of any crenulation folding.

i. Trondhjemite of Johnson Creek

This deformed unit is dominated by plagioclase and quartz and contains minor amphibole, biotite, and opaques. Quartz shows significant dynamic recrystalization as do the feldspars (altered cores likely resulting from microfracturing). Amphiboles are generally subhedral and fractured as well as having some simple twinning. Opaques are predominantly associated with clots of amphibole and biotite. Biotite is often deformed and in some cases acts as a shear sense indicator.

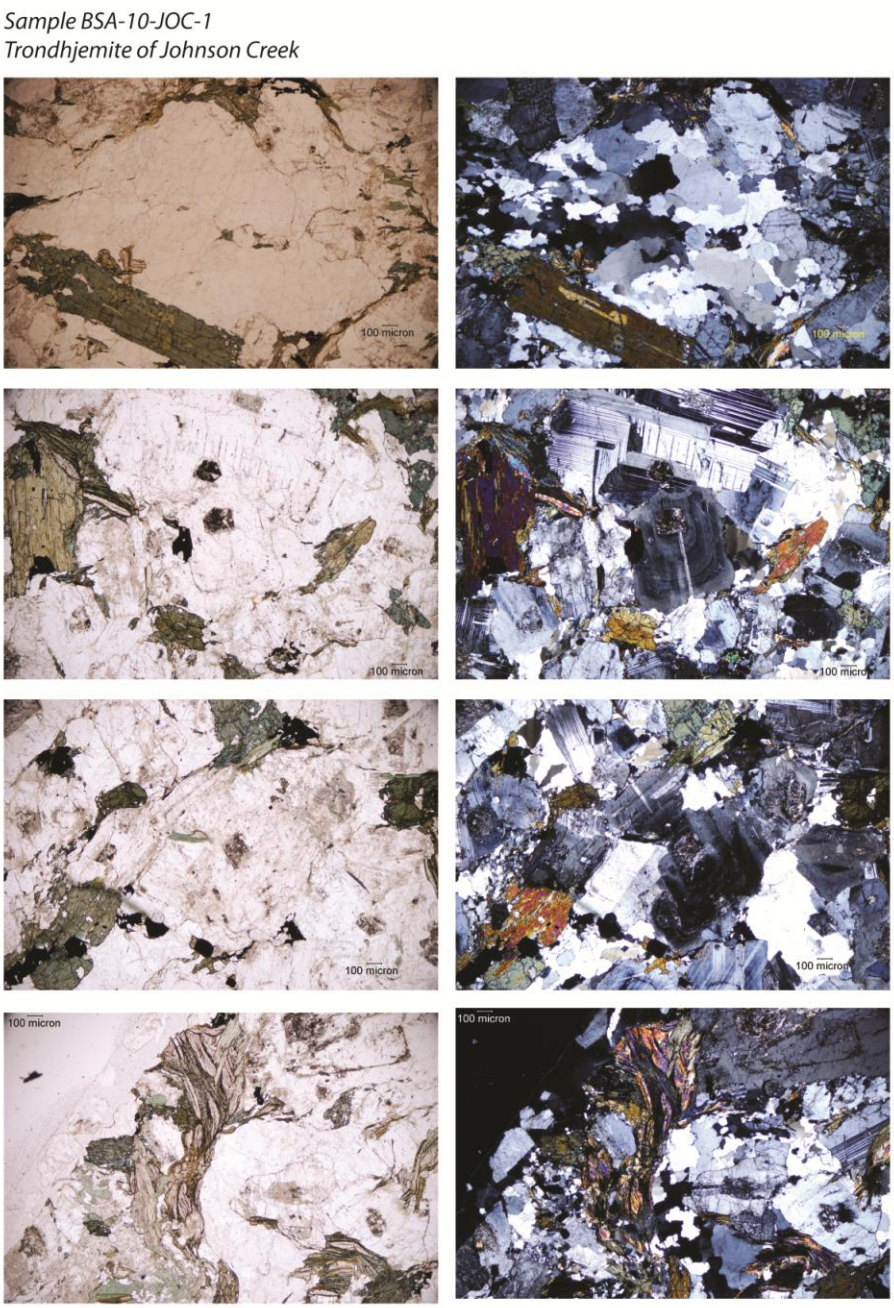

Figure 16A. Sample JOC-1. These eight images further document the deformed nature of the Trondhjemite of Johnson creek; the top two show dynamic recrystalization in quartz as well as a coarse grained subhedral green amphibole, the second two show a plagioclase displaying a microfractured core surrounded by significant oscillatory zonation and some small deformation twinning. The third pair of images from the top is centered on a similar large, zoned plagioclase but also shows a smaller plagioclase (upper left quadrant of image) displaying ductile deformation as well. The bottom pair of images shows significant deformation of both biotite and a ribbon of dynamically recrystallized quartz.

j. Diorite of Alexander Creek

This unit is a deeply weathered, undeformed, augite and biotite bearing diorite. Although it's original mineralogy was dominated by plagioclase followed by amphibole and quartz, the effect of significant alteration often makes the true mineralogy difficult to discern. It contains two generations of plagioclase; the older generation is coarser grained, zoned and even shows some evidence of deformation (undulatory extinction and even a little deformation twinning), while the younger generation is interstitial, unzoned, and completely undeformed. Biotite is generally coarse grained. Clinopyroxene occurs as cores in hornblende. Quartz is interstitial and displays minor undulatory extinction. The deformed early plagioclase is especially interesting and likely indicates that this unit's crystallization period spanned the end of tectonic deformation in the MHMC.

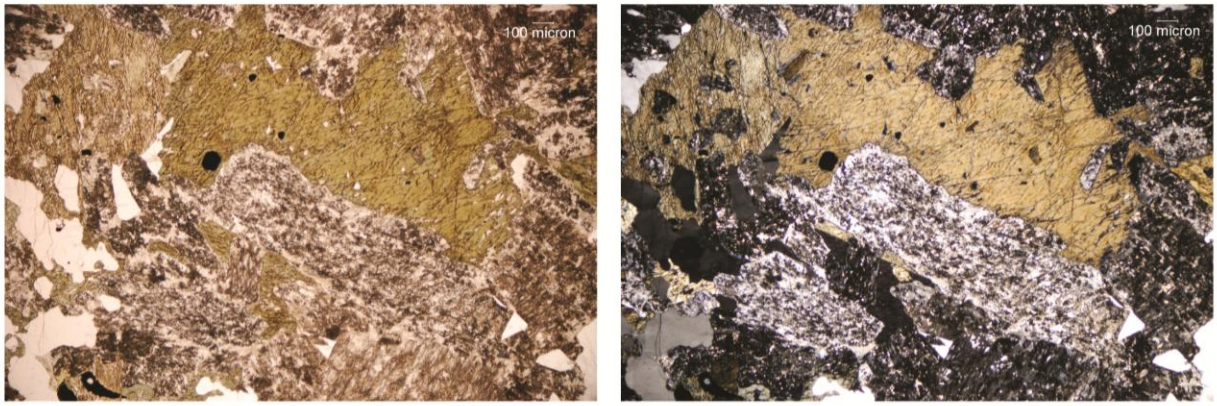

Figure 17A. Sample DAC-1b. This unit is well displayed in the main body of the thesis but this image is included to show the significant degree of alteration more commonly encountered in the unit. The top half of the image is dominated by a low birefringence amphibole, but most of the other minerals present are the remnants of plagioclase (since altered to clays).

k. Norite of Carney Butte

This unit is a less weathered, but similarly undeformed, biotite bearing norite. Unlike the Diorite of Alexander Creek, this unit shows very little weathering and contains both orthopyroxene and clinopyroxene. While it does contain plagioclase showing what may be deformation twinning, there is no evidence of an early growth population of feldspars. The pyroxenes, amphibole, and opaques all show signs of resorption and no signs of major strain accommodation. The late stage quartz is also unstrained.

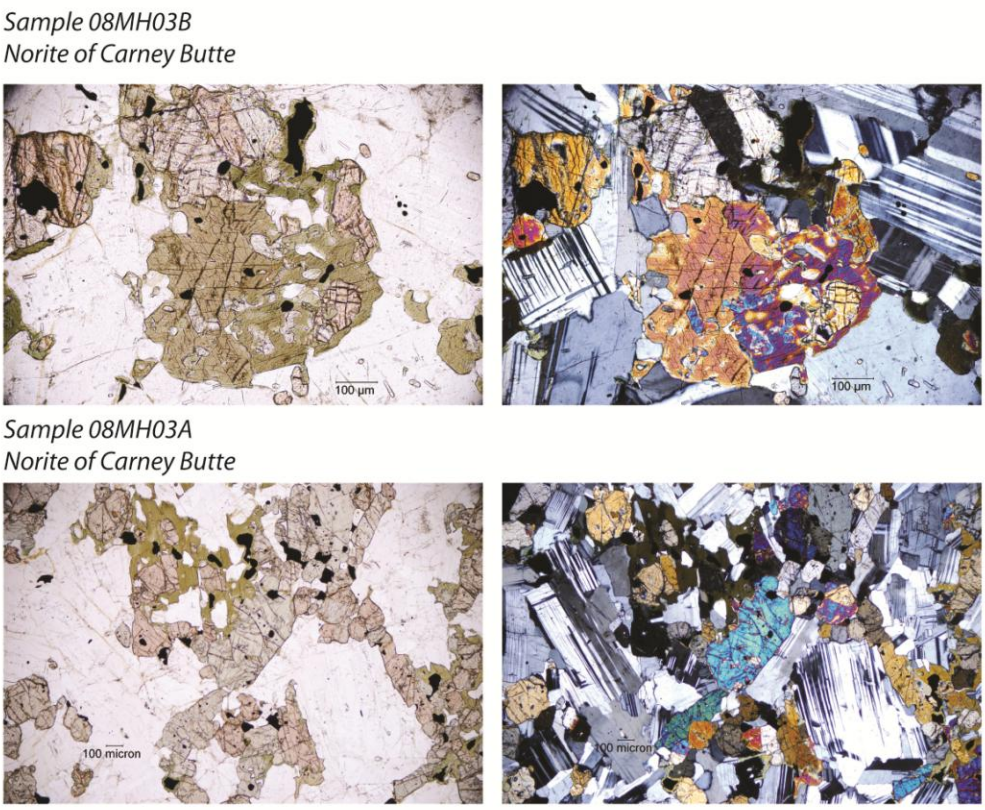

Figure 18A. Samples 08MH03B and 08MH03A. The top pair of images (08MH03B) shows both the unaltered nature of the unit as well as the presence of both resorbed clinopyroxene and resorbed orthopyroxene inside a coarser grained amphibole. It also shows a small amount of deformation twinning (left-hand side). The bottom pair of images (08MH03A) shows the pyroxenes as seen when they are spread through the matrix rather than in a clump with the amphibole.

l. Tonalite of Granite Meadows

This unit is a coarse grained biotite, hornblende, and orthoclase bearing tonalite. The main body of the pluton outcrops in the Granite Meadows area, but dikes of anomalously potassic tonalite (the presence of orthoclase varies with location) are found throughout the south-central area of the MHMC. Mafic enclaves have only been found in the pluton's main body. Although the unit's mineralogy is consistent throughout the main body, the proportion of these minerals varies somewhat (see table below). The Tonalite of Granite Meadows is texturally complex; its plagioclase component includes coarse grains which display some undulose extinction along with what may be deformation twinning as well as zonation (usually defined by inclusion rings) and microfractured cores, but it also includes a component of undeformed plagioclase. It contains microfractured amphibole, but also large clots of undeformed biotite. The orthoclase and quartz present display little to no deformation either. Thin section level cross cutting relationships support the order of crystallization presented below, but may allow for a second, post-biotite, period of plagioclase growth. The presence of more refractory, more structurally resistant deformed minerals which crystallized prior to less structurally resistant, undeformed minerals implies some sort of deformation was active during crystallization of this pluton. Given that previous workers found evidence of a small, late stage deformational event in the southern MHMC (Ave Lallemant's D4 deformational event, 1995) in the area of one of the anomalously potassic dikes associated with the Tonalite of Granite Meadows supports the existence of such a later deformational event.

The mafic enclaves found in the Tonalite of Granite Meadows are clearly visible in hand sample. They are also finer grained than the pluton at large and contain more amphibole (biotite content remains constant, although finer grained) and less orthoclase. Clinopyroxene is present as well, although it is always either in association with or coring, amphibole. This is the only pyroxene found in this unit. Chlorite is also found in these enclaves, always as an alteration product of a more mafic mineral (usually amphibole). The amphiboles themselves are browner in plain polarized light than those of the main pluton, which are more greenish.

Potassic dikes interpreted as related to this unit were sampled along Highway 395, where they intrude the Schist of Yellowjacket Road south of the Diorite of Alexander Creek. This dike is clearly incorporating the surrounding schist and includes substantial quartz and garnet content. The dike is also quite weathered. Some plagioclase, white mica, and possibly orthoclase is present. Altered biotite is also a minor constituent of the dike. A second potassic dike was sampled on the lower slopes of Table Mountain, where it intrudes the amphibole bearing variant of the Schist of Yellowjacket Road. Dikes in this area are dominated by plagioclase, quartz, some orthoclase, and amphibole. Plagioclase is both coarse and fined grained. The coarse grains are sometimes undulose and zoned (very similar to those in the main pluton of the Tonalite of Granite Meadows). Amphibole often displays simple twinning and is euhedral. Quartz is undulose, both it and orthoclase are always fine grained. A mineral that may be cordierite was found in this dike, but this could not be verified.

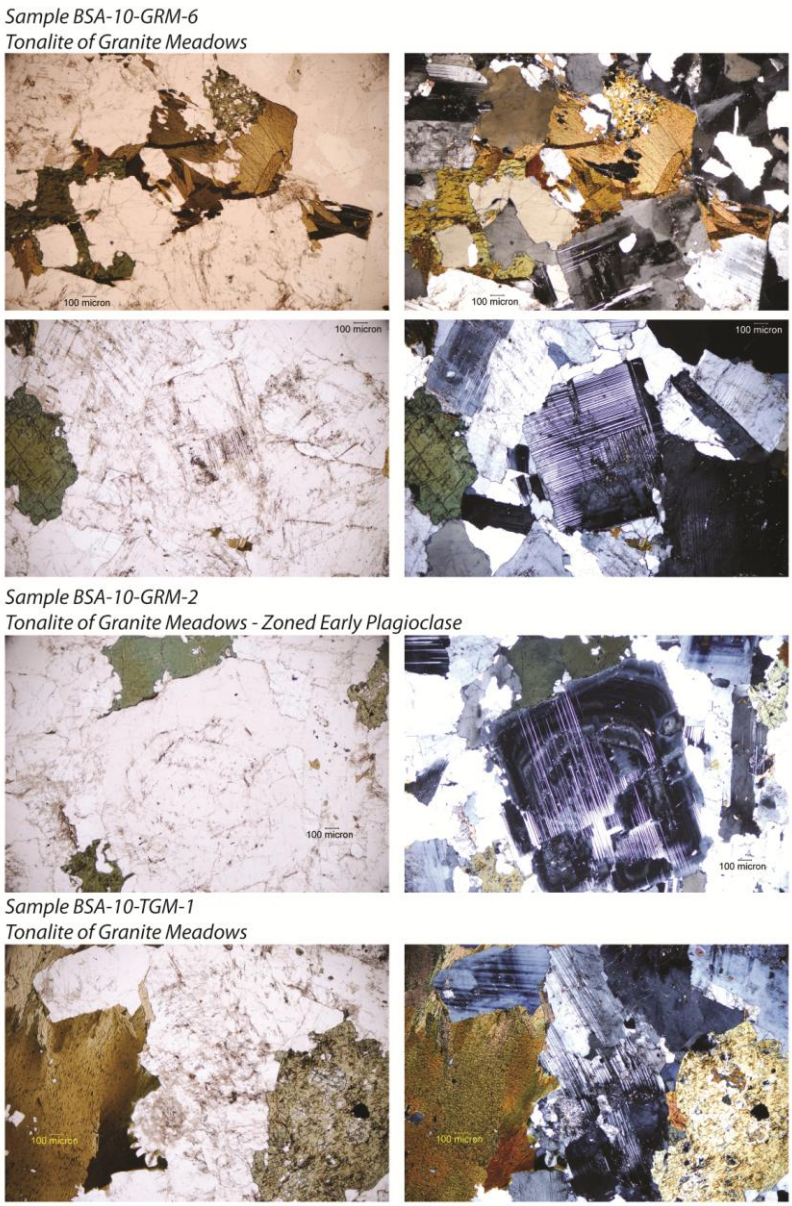

Figure 19A. Samples GRM-6, GRM-2, and TGM-1. The top four images (GRM-6) represent the general texture of this unit: coarse grained, plagioclase dominant, with interstitial quartz, biotite and amphibole in clumps. Larger, earlier, sometimes zoned, deformed plagioclase (upper left and lower center of image) and some alteration of biotite and amphibole is visible. The lower pair of images from this sample focuses on a large plagioclase displaying a small amount of deformation. It also shows one of the units orthoclase grains in contact with one of the smaller, late plagioclase grains in the left-central area of the image. The next pair of images (GRM-2) shows a zoned, early plagioclase even more clearly. The final pair of images (TGM-1) shows plagioclase with undulose extinction (upper left), undeformed biotite (left), a fractured amphibole (lower right), and a plagioclase showing deformation twinning with some ductile deformation and vermicular intergrowth of plagioclase and quartz.

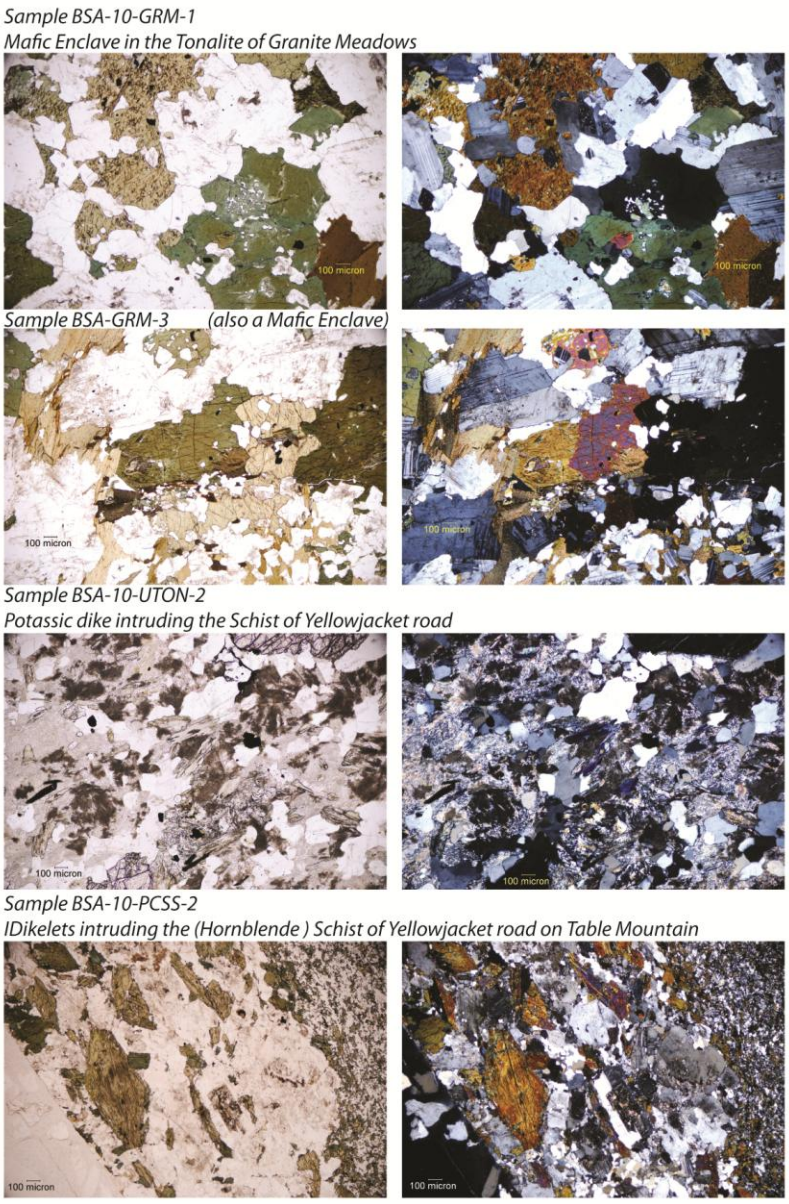

Figure 20A. Samples GRM-1, GRM-3, UTON-2, and PCSS-2. The first pair of images (GRM-1) display the typical nature of the mafic enclaves, very similar to the greater pluton, but for the increased presence of biotite, fractured amphibole, and chlorite. The second pair of images shows a small, nearly resorbed clinopyroxene core in the amphibole at the center of the image. The third pair of images (UTON-2) represents a dike of similarly potassic intrusive material in the Schist of Yellow Jacket road near the intrusion of the Diorite of Alexander Creek. The bottom image (PCSS-2) represents the orthoclase bearing dikelets found intruding the hornblende bearing variant of the Schist of Yellow Jacket road on the lower slopes of Table Mountain. This image clearly shows both euhedral amphibole (left center of image) and subhedral orthoclase with a core of what may be microfractured and altered plagioclase. Quartz and plagioclase are also common in these dikes.

m. Gabbronorite of Ridenor Canyon

The Gabbronorite of Ridenor Canyon is exposed over a small area in the central area of the MHMC. It consists of a handful of low outcrops. The only outcrops analyzed from the true Ridenor Canyon are two plagioclase cumulates (based on geochemistry). One location is fine grained and may represent a relatively quick cooling outer margin of the unit (Figure 15 of Thesis). The other location contains a country rock xenolith, but is overall coarser grained. Both contain subhedral to euhedral plagioclase (the coarse grained sample shows some deformation twinning) and resorbed amphibole (usually the remnant of needles). The fine grained sample clearly contains both orthopyroxene (often with opaques as cores) and clinopyroxene. Alteration in this unit is generally to chlorite. Pyroxenes are less common, but still present near the edges of the pluton.

Sample BSA-10-GNR-5

Figure 21A. Sample GNR-5. Sample GNR-3 is sufficiently imaged in the main body of the thesis; all of these images are of sample GNR-5. The dark spaces in the left-hand one-third of these photomicrographs are due to user error (misaligned condenser lens in the petrographic microscope), that portion of the image should be disregarded. The top two images show primarily plagioclase, a couple of which display some deformation twinning, but most of which do not. There is no pyroxene in this thin section. The center image is sample GNR-5 in the outcrop. The bottom two images further display plagioclase and amphibole in this rock as well as one of the significant opaques which are found throughout the unit.

Appendix B

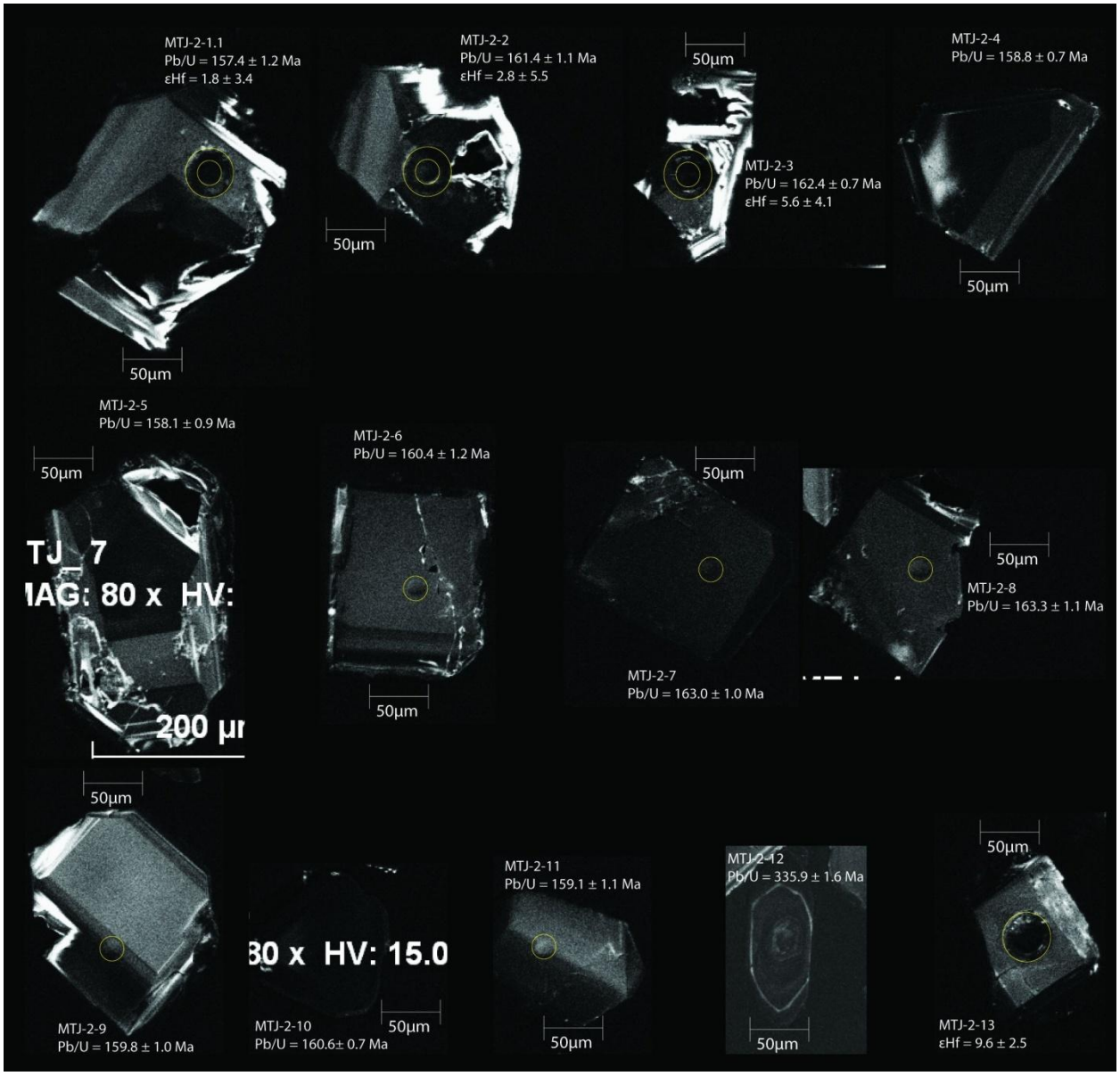

Figure 1B. Cathodoluminescence images of the zircons from the Trondhjemite of Pearson Creek.

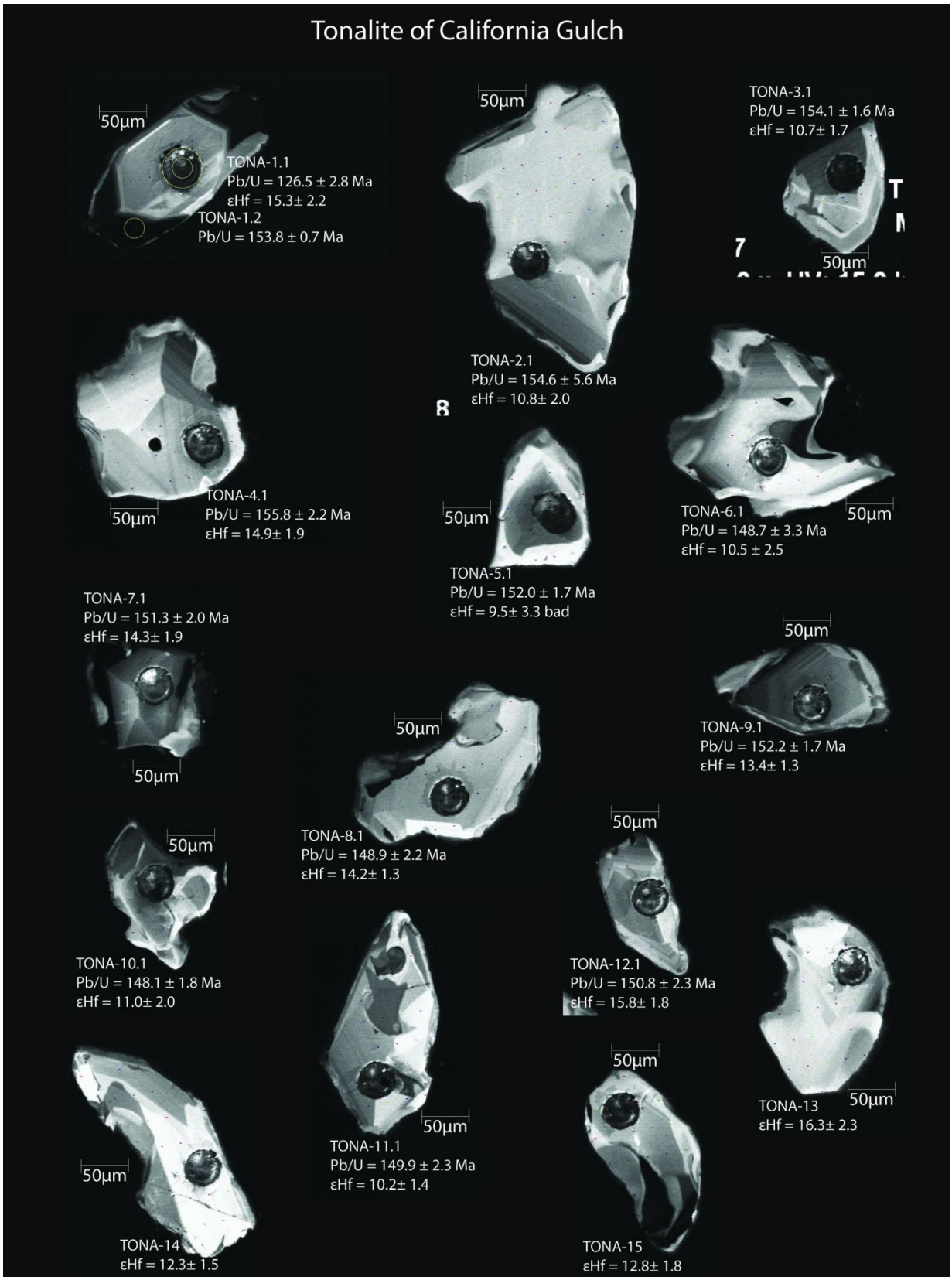

Figure 2B. Cathodoluminescence images of the zircons from the Tonalite of California Gulch.

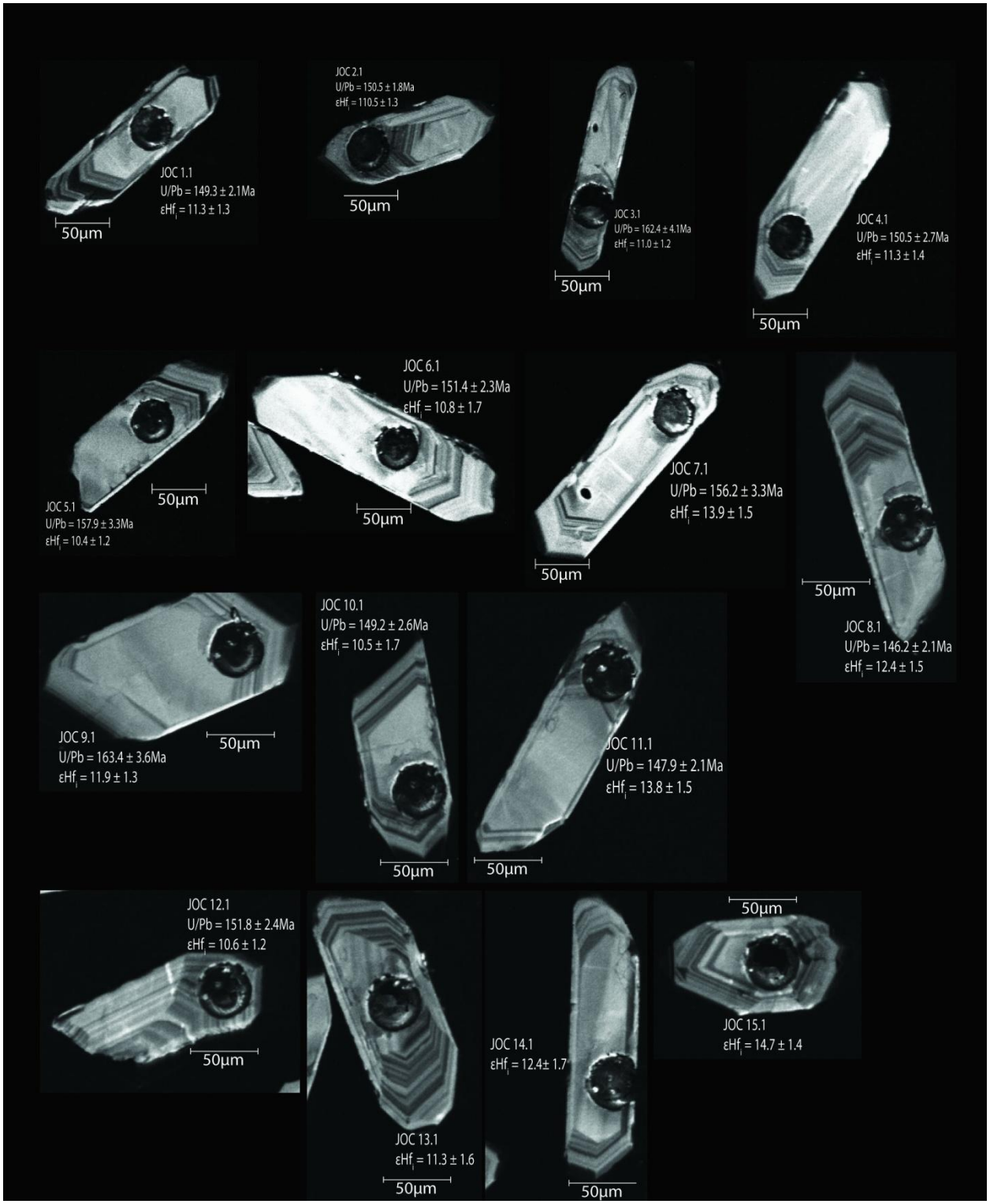

Figure 3B. Cathodoluminescence images of the zircons from the Trondhjemite of Johnson Creek.

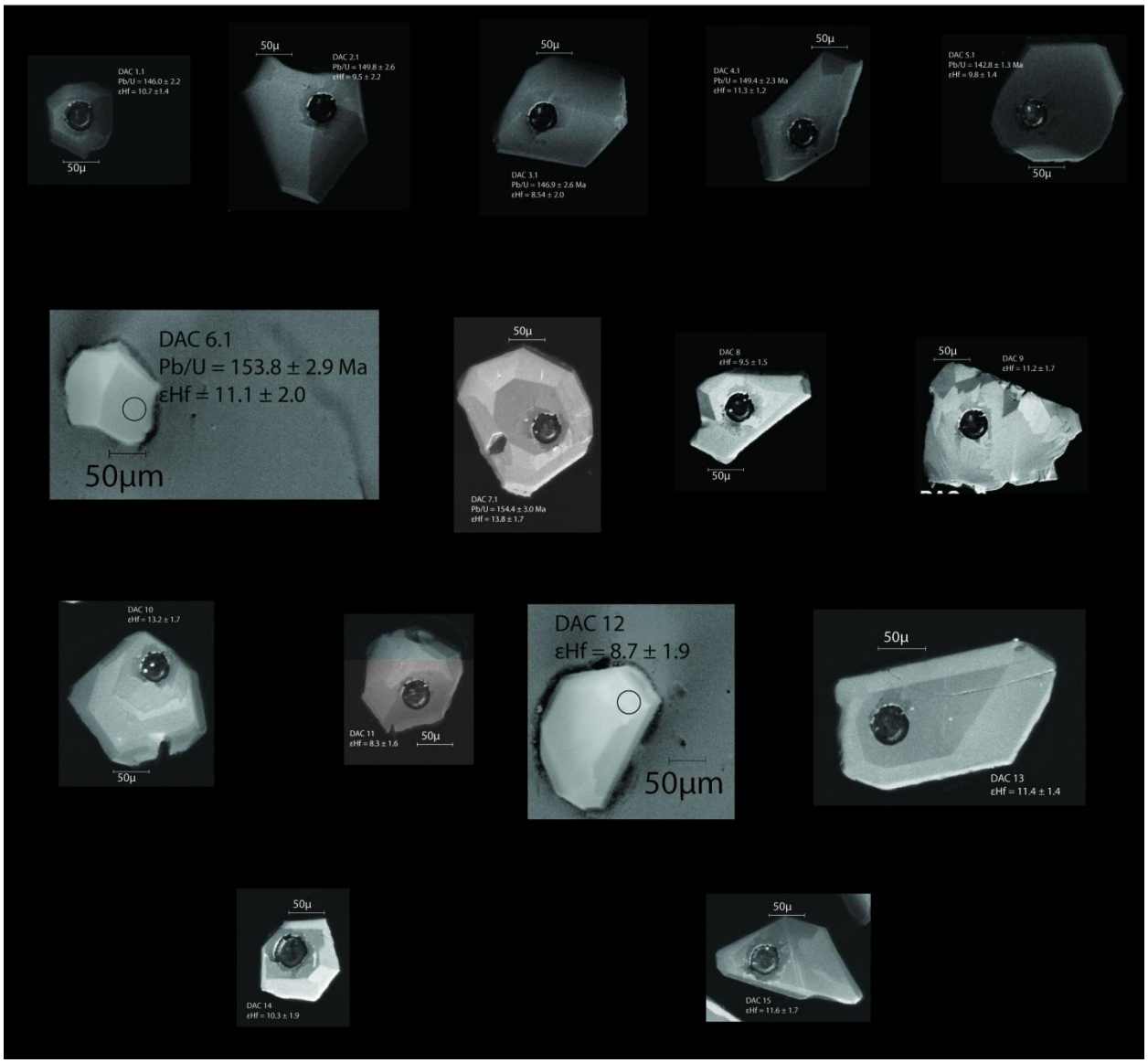

Figure 4B. Cathodoluminescence images of the zircons from the Diorite of Alexander Creek.

Figure 5B. Cathodoluminescence images of the zircons from the Norite of Carney Butte.

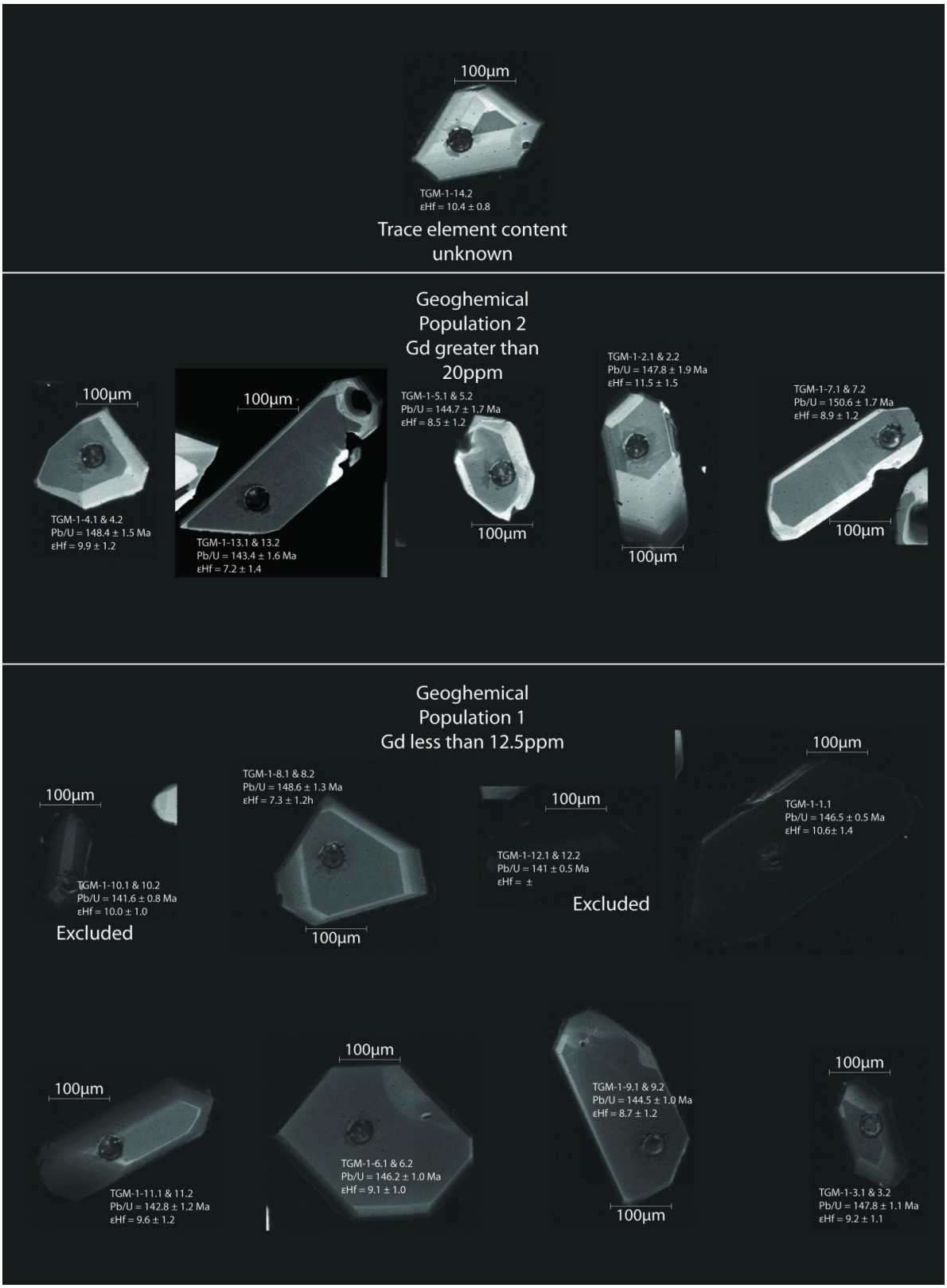

Figure 6B. Cathodoluminescence images of the zircons from the Tonalite of Granite Meadows. Separated based on trace element content.

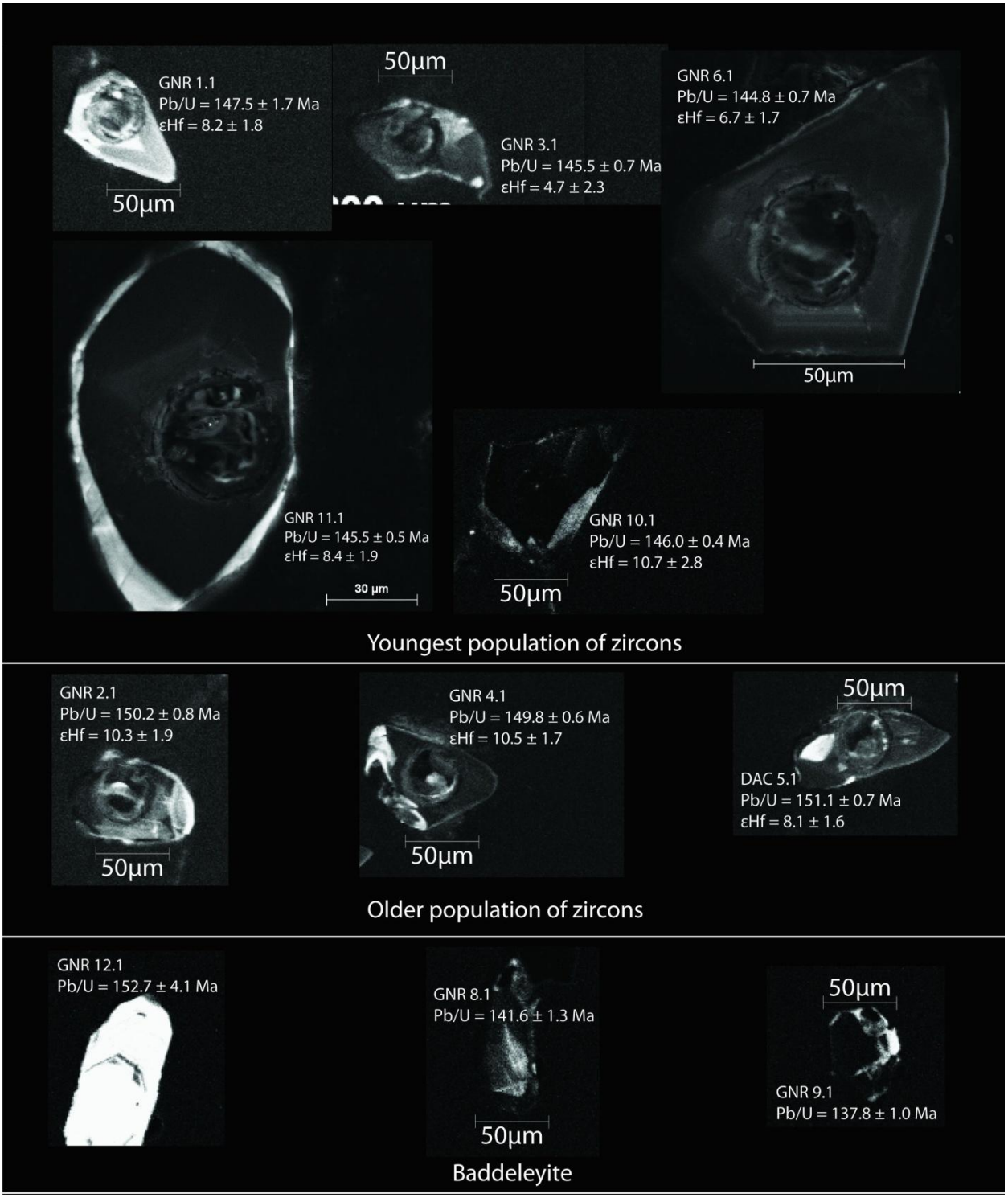

Figure 7B. Cathodoluminescence images of the zircons from the Gabbronorite of Ridenor Canyon. Separated into the younger population, the older population, and the baddeleyite population.

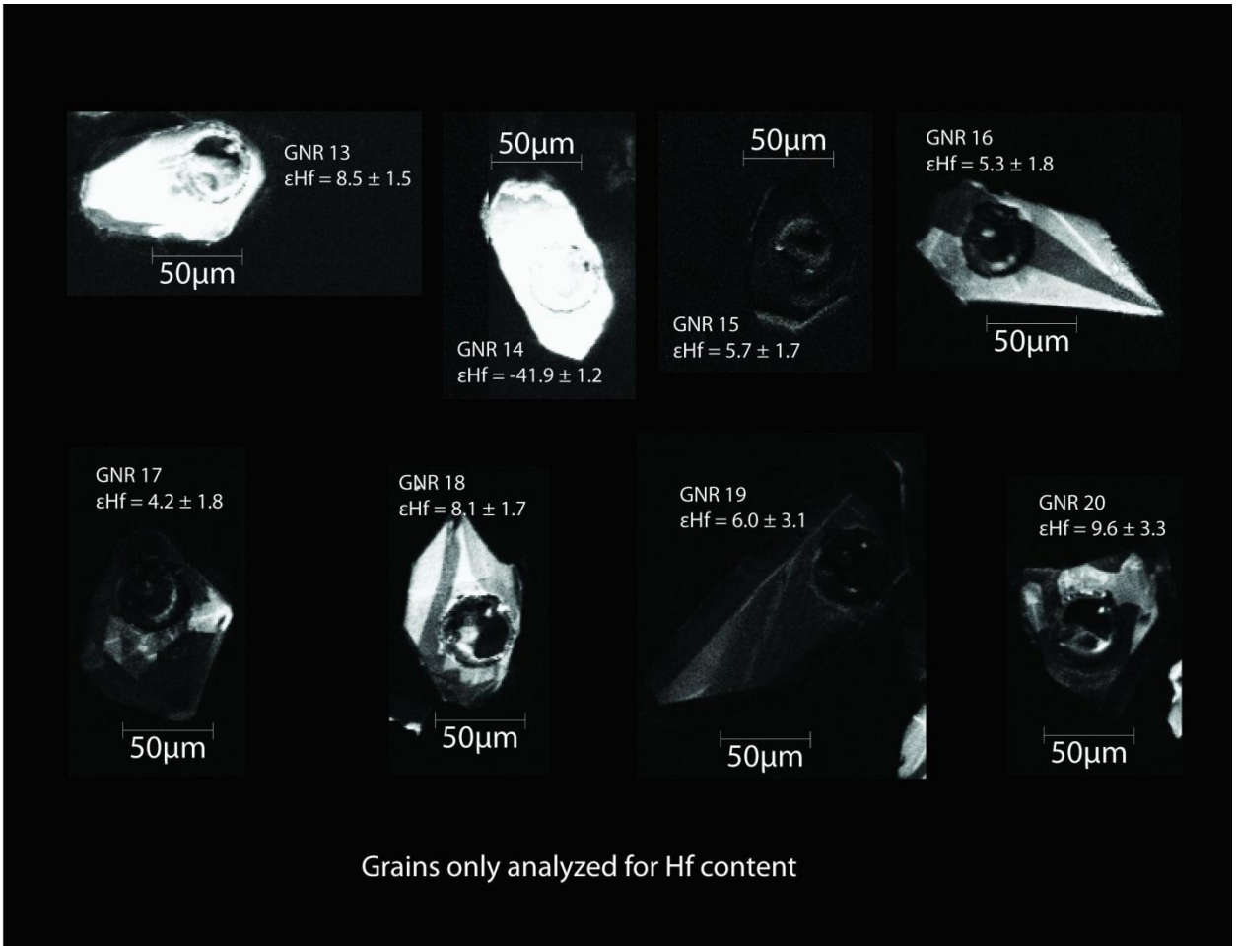

Figure 7B, Continued. Cathodoluminescence images of the zircons from the Gabbronorite of Ridenor Canyon. These grains were not analyzed using the SHRIMP-RG so there is no trace element data or isotopic ages for them, the εHf_i values given were calculated under the assumption that they are the same age as the younger population of zircons in the unit.

Appendix C

Table 1C. Additional εHf_i Correction Data

Sample	Lu	Hf	ε (t=0)	2 σ error	t (Ga)	2 σ error	Tcr (2)	176Lu/177Hf	180/177	% corr
Trondhjemite of Pearson Creek										
MTJ-2-1		8049.33	-0.63653	3.46553	0.1613	0.0012	0.9875229	75.025	1.88643	67
MTJ-2-2		8290.79	0.671889	5.44583	0.1613	0.0012	0.9342108	75.025	1.88653	73
MTJ-2-3		7990.84	3.253355	4.03133	0.1613	0.0012	0.780609	75.025	1.88667	70
MTJ-2-13			7.001786	2.40465	0.1613	0.0012	0.5566383	75.025	1.8866	63
Tonalite of California Gulch										
TONA 1.1_2		10061.30	12.05863	2.19248	0.1527	0.0012	0.2357165	14.025	1.88611	26
TONA 2.1_2		9482.03	7.638312	1.9803	0.1527	0.0012	0.479096	15.025	1.88613	22
TONA 3.1_2		10077.49	7.496862	1.62668	0.1527	0.0012	0.4890194	16.025	1.88651	25
TONA 4.1_2		9919.32	11.63428	1.83885	0.1527	0.0012	0.2534833	17.025	1.88642	13
TONA 5.1_2		8405.47	6.612798	3.25336	0.1527	0.0012	0.5489267	18.025		41
TONA 6.1_2		8728.33	7.249324	2.47538	0.1527	0.0012	0.4994023	19.025	1.88655	20
TONA 7.1_2		12430.72	11.03312	1.83885	0.1527	0.0012	0.286608	20.025	1.88696	13
TONA 8.1_2		9349.67	10.96239	1.27305	0.1527	0.0012	0.2957665	22.025	1.8861	22
TONA 9.1_2		11288.89	10.11369	1.62668	0.1527	0.0012	0.3383311	23.025	1.88648	15
TONA 10.1_2		9525.94	7.673674	1.90958	0.1527	0.0012	0.4702443	24.025	1.8863	8
TONA 11.1_2		9540.67	7.001786	1.4145	0.1527	0.0012	0.5123928	26.025	1.8865	18
TONA 12.1_2		10228.30	12.51834	1.76813	0.1527	0.0012	0.2035511	28.025	1.8862	12
TONA 13_2			13.01342	2.2632	0.1527	0.0012	0.178907	21.025	1.88655	17
TONA 14_2			9.088177	1.48523	0.1527	0.0012	0.3984297		1.88628	21
TONA 15_2			9.583252	1.76813	0.1527	0.0012	0.3730399	27.025	1.88643	24
Trondhjemite of Johnson Creek										
JOC 1.1_2		10559.12	8.16875	1.20233	0.1495	0.0017	0.4506159	45.025	1.88653	24
JOC 2.1_2		10612.90	7.355411	1.27305	0.1495	0.0017	0.4932924	46.025	1.88642	20
JOC 3.1_2		11966.40	7.850487	1.1316	0.1495	0.0017	0.4662043	47.025	1.88653	19
JOC 4.1_2		11071.68	8.133388	1.34378	0.1495	0.0017	0.4523757	48.025	1.88686	24
JOC 5.1_2		11227.98	7.320049	1.1316	0.1495	0.0017	0.4987486	49.025	1.88668	25
JOC 6.1_2		10087.84	7.744399	1.6974	0.1495	0.0017	0.4752485	50.025	1.88674	25
JOC 7.1_2		9726.90	10.75022	1.4145	0.1495	0.0017	0.306527		1.88644	22
JOC-8.1_2		10399.94	9.264989	1.48523	0.1495	0.0017	0.3901018	52.025	1.88679	24
JOC-9.1_2		10395.22	8.699188	1.20233	0.1495	0.0017	0.419044	53.025	1.88646	19
JOC-10.1_2		10112.25	7.390774	1.62668	0.1495	0.0017	0.4932334	54.025	1.88666	23
JOC-11.1_2		10350.88	10.60877	1.48523	0.1495	0.0017	0.3141001	55.025	1.88645	21
JOC-12.1_2		9890.04	7.532224	1.1316	0.1495	0.0017	0.4865002	56.025	1.88637	25
JOC-13_2			8.133388	1.55595	0.1495	0.0017	0.4524093	57.025	1.88695	23
JOC-14_2			9.264989	1.62668	0.1495	0.0017	0.388102	58.025	1.88642	20
JOC-15_2			11.59892	1.34378	0.1495	0.0017	0.261104	59.025	1.88671	24

Sample	Lu	Hf	e(0)	2 σ error	t(Ga)	2 σ error	Tcr (2)	176Lu/177Hf	180/177	% corr
Diorite of Alexander Creek										
DAC 1.1_2		9770.20	7.567587	1.34378	0.1455	0.004	0.4745905	60.025	1.88674	5
DAC 2.1_2		8934.54	6.329897	2.12175	0.1455	0.004	0.5430064	61.025	1.88658	6
DAC 3.1_2		9913.81	5.339746	1.90958	0.1455	0.004	0.5970189	63.025	1.88694	4
DAC 4.1_2		8977.27	8.098025	1.1316	0.1455	0.004	0.4447986		1.88636	4
DAC 5.1_2		10145.44	6.542073	1.34378	0.1455	0.004	0.5306287	66.025	1.88658	4
DAC 6.1_2		8678.17	7.88585	1.90958	0.1455	0.004	0.4576198	67.025	1.88667	7
DAC 7.1_2		8737.19	10.60877	1.62668	0.1455	0.004	0.3084637	72.025	1.8867	11
DAC 8_2			6.36526	1.4145	0.1455	0.004	0.5414042	62.025	1.88656	6
DAC 9_2			7.956575	1.62668	0.1455	0.004	0.4529416	64.025	1.88654	5
DAC 12_2			5.481196	1.76813	0.1455	0.004	0.5894456	68.025	1.88677	5
DAC 10_2			10.0076	1.62668	0.1455	0.004	0.3394598	69.025	1.8862	5
DAC 11_2			5.12757	1.48523	0.1455	0.004	0.6093924	70.025	1.88658	6
DAC 13_2			8.239475	1.27305	0.1455	0.004	0.437714	73.025	1.8866	6
DAC 14_2			7.107873	1.76813	0.1455	0.004	0.5023614	74.025	1.8865	12
DAC 15_2			8.380925	1.62668	0.1455	0.004	0.428899	75.025	1.88634	3
Norite of Carney Butte										
08MH03 2	46.21	8495.57	6.646975	3.25699	148					16
08MH03 3	32.14	8213.84	3.615511	5.20094	148					11
08MH03 4	65.38	8058.50	6.54754	2.68179	148					26
08MH03 5	32.26	8410.58	5.432722	3.41274	148					11
08MH03 6	21.35	7709.84	7.954074	3.28409	148					9
08MH03 7	33.15	8442.48	5.729681	4.09855	148					11
08MH03 8	84.80	8556.03	5.76699	3.26442	148					22
08MH03 10	29.84	7967.18	2.583339	4.22707	148					16
08MH03 11	48.30	8322.53	3.039806	3.34237	148					17
08MH03 12	61.69	8124.43	8.302097	3.97576	148					16
08MH03 13			5.987034	3.25328	148					15
08MH03 14			9.56153	4.44011	148					16
08MH03 15			7.385971	3.73094	148					8
08MH03 16			6.76459	5.53753	148					12
08MH03 17			5.15824	4.5169	148					16
08MH03 18			4.871652	4.21919	148					12
Tonalite of Granite Meadows										
TGM-1.1		16508.84	7.390774	1.34378	0.1456	0.0015	0.4866848	0.025	1.88655	13
TGM-2.2		9654.64	8.345563	1.4145	0.1456	0.0015	0.4341439	1.025	1.88659	13
TGM-3.2		12172.47	6.046997	1.06088	0.1456	0.0015	0.5597786	2.025	1.88671	9
TGM-4.2		11820.21	6.718885	1.1316	0.1456	0.0015	0.5241292	3.025	1.88664	13
TGM-5.2		10383.71	5.304383	1.1316	0.1456	0.0015	0.6020453	5.025	1.88652	14
TGM-6.2		12534.83	5.940909	0.91943	0.1456	0.0015	0.5667724	6.025	1.88666	13
TGM-7.2		10756.72	5.764096	1.1316	0.1456	0.0015	0.5774026	7.025	1.88703	16
TGM-8.2		12216.78	4.137419	1.20233	0.1456	0.0015	0.6659635	8.025	1.88686	12
TGM-9.2		11345.54	5.587284	1.20233	0.1456	0.0015	0.5862546	10.025	1.88687	13
TGM-10.2		10962.35	6.860336	0.99015	0.1456	0.0015	0.5140769	11.025	1.8869	6
TGM-11.2		11146.53	6.471347	1.20233	0.1456	0.0015	0.5372123		1.88679	12
TGM-13.2		10425.15	4.031331	1.34378	0.1456	0.0015	0.6717798	13.025	1.88665	14
TGM-14.2			7.213961	0.77798	0.1456	0.0015	0.4960611	4.025	1.88664	12
TGM-15.2			4.809307	0.99015	0.1456	0.0015	0.6274514	9.025	1.88667	8

Sample	Lu	Hf	e(0)	2 σ error	t(Ga)	2 σ error	Tcr (2)	176Lu/ 177Hf	180/177	% corr
Gabbro-norite of Ridenor Canyon										
Age Population 1										
GNR 2.1_2		5162.34	7.178599	1.90958	0.1456	0.0005	0.5024587	30.025	1.88629	18
GNR 4.1_2		5658.85	7.496862	1.6974	0.1456	0.0005	0.4884227	32.025	1.88631	24
GNR 5.1_2		6267.59	5.056845	1.55595	0.1456	0.0005	0.6211011	33.025	1.88615	20
Age Population 2										
GNR 1.1_2		6474.29	5.056845	1.76813	0.1456	0.0005	0.6150721	29.025	1.88618	10
GNR 3.1_2		5429.16	1.626678	2.2632	0.1456	0.0005	0.8078009	31.025	1.88647	19
GNR 6.1_2		6813.95	3.642343	1.6974	0.1456	0.0005	0.7005116	35.025	1.88653	26
GNR 10.1_2		5518.02	7.567587	2.829	0.1456	0.0005	0.478027	37.025	1.8858	13
GNR 11.1_2		6772.30	5.304383	1.90958	0.1456	0.0005	0.6075275		1.88612	22
Age unknown										
GNR 13_2			5.304383	1.48523	0.1456	0.0005	0.601778	34.025	1.88673	10
GNR 14_2			-45.0519	1.20233	0.1456	0.0005	3.3058354	36.025		13
GNR 15_2			2.687554	1.6974	0.1456	0.0005	0.7532013	39.025	1.88633	25
GNR 16_2			2.192478	1.76813	0.1456	0.0005	0.7743433	40.025	1.88689	14
GNR 17_2			1.131602	1.76813	0.1456	0.0005	0.8357304	41.025	1.88641	20
GNR 18_2			4.915395	1.6974	0.1456	0.0005	0.6228663	42.025	1.88609	8
GNR 19_2			2.899729	3.1119	0.1456	0.0005	0.7367505	43.025	1.88607	15
GNR 20_2			6.471347	3.25336	0.1456	0.0005	0.540285	44.025	1.88629	15

Analysis with % correction values greater than 23 are in blue and should be considered unreliable.
If other values greatly exceed range (ex εHfi=-41 in spot GNR 14_2) they are also in blue and unreliable.